MICROEVOLUTION IN COCCOLITHOPHORES:

EXAMPLES FROM THE PALEOCENE – EOCENE

by

DAVID BORD

A dissertation submitted to the

Graduate School-New Brunswick

Rutgers, The State University of New Jersey

In partial fulfillment of the requirements

For the degree of

Doctor of Philosophy

Graduate Program in Geological Sciences

Written under the direction of

Marie-Pierre Aubry

And approved by

_____

_____

_____

_____

New Brunswick, New Jersey

October 2013

ABSTRACT OF THE DISSERTATION

MICROEVOLUTION IN COCCOLITHOPHORES:

EXAMPLES FROM THE PALEOCENE – EOCENE

by

DAVID BORD

Dissertation Director:

Marie-Pierre Aubry

Morphologic variability is a major theme in microevolutionary studies. Variations provide the raw material from which opportunities for selection are generated, leading to speciation. Three modes of evolution have been described from the paleontological record— Gradualism (gradual evolution implying continuous changes over a long time span), Punctuated Equilibrium (stable morphologies evolving through abrupt jumps), and Punctuated Anagenesis (gradual shifts between stable morphologies). There are only a handful of papers that illustrate unambiguously these models, and none involved the coccolithophores. The latter are, however, an ideal taxonomic group for evolutionary studies, with rapid generational turnovers, high morphological diversity and abundance, and long fossil record.

I present three tests in this dissertation. In the first study, I test the significance of morphological variability in the species *Ellipsolithus macellus* in terms of genetic

versus phenotypic expression, represented by, respectively, cryptic speciation versus adaptation to oligotrophication of the early Paleocene (Danian) Ocean.

In the second study, I test for gradualism versus stasis in the short lived (370 kyr) early Eocene species *Heliodiscoaster mahmoudii*, and show that morphological fixation was achieved after 83 kyr (20% of the range of the species).

In the third study, I first follow up on the previous study to confirm morphologic fixation in two other species that are part of the early Eocene *Tribrachiatus* lineage, *T. bramlettei* being ancestral to *T. contortus*. I then test for abrupt versus gradual morphological change during the evolutionary divergence of T. contortus from T. bramlettei. I show that speciation in this lineage follows the model of Punctuated Gradualism, or Punctuated Anagenesis. The *T. bramlettei*-*T. contortus* transition occurs over 73 kyr during which high morphologic variability occurs and after which the *T. contortus* morphology is fixated. Prior to the transition the T. bramlettei morphology was also fixated.

This thesis unambiguously illustrates examples of Punctuated Anagenesis in the Coccolithophores. Stasis (low morphologic variability) is the primary mode that characterizes species during most of their life span. Speciation events are short episodes of high morphologic variability (25% higher than during stasis) during which morphologic fixation of the new species is progressively achieved.

Acknowledgements

The person who deserves the most appreciation is my wonderful wife Stefanie. She has, from the very beginning, endured this journey with me; she provided endless encouragement, reassurance, and confidence; she gave me the mental strength I needed to finish this work. I am grateful to my family for their endless support, even at times when there seemed to be no end in sight. To my fellow graduate students, I am thankful for the many hours of thoughtful discourse. I would like to thank the many students who called "the green building" home, in particular Morgan Schaller, Huapei Wang, Weimin Si, Ashley Harris, Kelsey Bitting and Lauren Neitzke Adamo.

Preliminary results for the majority of this work were presented at several conferences, including INA in Lyon (2008), Microfossils II (2009), CBEP (2011), Microfossils III (2013). I am also grateful to several colleagues for helpful discussion and suggestions. In particular, Luc Beaufort, for his valuable recommendations and for the unique opportunity he gave me to work on an S.E.M.

Finally, I give special thanks to my advisor Professor Marie-Pierre Aubry, without whose constant guidance and encouragement I would not have finished this dissertation. Much of the content of this thesis came as result of lengthy, and enjoyable conversations.

Table of Contents

List of Figures

Chapter 2

Chapter 3

Chapter 4

List of Tables

Chapter 2

Chapter 3

Chapter 4

List of Plates

Chapter 2

Chapter 3

Chapter 4

Chapter 1

Introduction to the Dissertation

1.1 Objective

The focus of this dissertation is the study of the modalities of the speciation process as expressed through the changing morphologies of an important group of eukaryotic, unicellular organisms, known as *coccolithophores*, with the goal of determining the microevolutionary patterns that underlie their evolution. The essential question of the tempo and mode of evolution is still unclear and the discussion about which of the known modes of evolution dominates the fossil record is still lively. The three modes considered to date are Phyletic Gradualism (which is directional), Punctuated Equilibrium (which implies stasis) and Punctuated Gradualism (which has been assimilated with the random walk). In recent years updated models of speciation have been developed (Hunt, 2006, 2007, 2008, 2010, 2012) with tests of the rates and amounts of variance required for these models to occur. This has ignited renewed interest in the study of microevolutionary processes during speciation among marine protists (e.g., Alizon et al., 2008, Hull and Norris 2009, Hunt 2012). Many studies are based on a combination of genetic analysis and comparison between taxa exhibiting similar morphologies. However, in order to accurately capture patterns of evolution and apply speciation models, high resolution and comprehensive morphometric analyses are required. This is the basis of the work presented here.

1.2 The coccolithophores

Coccolithophorids are unicellular eukaryotes (protists) of the Division Haptophyta which includes nearly 200 living species and thousands of extinct ones. They are broadly distributed and highly diversified in the modern ocean (Okada, 1973; Young, 2003). Thought to have evolved in the Late Triassic (Bown, 2004), they secrete an exoskeleton of calcium carbonate (coccosphere).

Coccospheres are composed of tiny mineralized organic scales (coccoliths). A coccolith is constructed of modified rhombohedral crystals, each called an element. Elements are arranged in interlocking cycles. Taxonomic classification at the species level and higher are based on the morphostructure of coccolith (structure and shape) (Aubry, 1998, 2013-2014).

Coccolithophores are prolific in the modern ocean, found globally, inhabiting nearly all marine habitats from polar to equatorial regions and spreading across the ocean from epicontinental margins to mid-ocean gyres. They are one of the most productive calcifiers and play a major role in the biological pump transferring inorganic carbon from the ocean surface to the ocean floor, a role they have held since at least the Early Cretaceous.

Studies of living coccolithophores have revealed a complex diploid-haploid life cycle, in addition many species produce extremely different coccoliths (hetero-coccoliths and holococcolith) during each stage. Recent molecular studies (Thompson et al., 2012; Hagino, 2012) have demonstrated that coccolithophores may not be strictly autotroph i.e.,

relying on mutualistic symbiosis. This supports earlier observations of mixotrophic behavior by cultured cells (e.g., Parke and Adams, 1960) and also the suggestion by Aubry (2009, 2013) that coccoliths evolved as a means to support their mixotrophic physiology. Upon cell death the coccospheres disarticulate and sink to the ocean floor either within fecal pellets (Honjo, 1976) or as part of aggregates called marine snow. In this way they form a continuous and largely uninterrupted fossil record on the ocean floor, which is ideal for evolutionary studies.

1.4 Methodology

This is the first time that a comprehensive microevolutionary study is undertaken for the coccolithophores. As indicated above, comprehensive morphometric analyses are required for microevolutionary studies, which implies that techniques appropriate to the study of coccolithophores are needed.

A combination of traditional morphometrics (measurements of length, width, diameter and angles) and of geometric morphometric techniques (coordinate-point extended eigenshape analysis - CP-EES) was used to document morphologic variability and speciation. The latter technique has been applied to evolutionary studies in the planktonic foraminifera. These techniques require the analysis of large databases of measurements. They are as follows:

- 882 combined specimens of *E. macellus*, *Gaarderia* and *Umbellosphaera;* 522 photographs of *E. macellus* (Chapter 2)
- 794 specimens of *H. mahmoudii*, 2,382 photographs (Chapter 3), and
- 2719 specimens of *Tribrachiatus*; 13,000 photographs (Chapter 4).

1.4 **Achievements**

Contrary to some claims (e.g., Raffi et al., 2008; Monechi et al., 2013) there are few unambiguous lineages between coccolithophores species recorded in Cenozoic sediments. By this I mean that co-occurrences over a thin stratigraphic interval of taxa with similar morphologies is highly insufficient to imply an ancestor-descendant relationship between them, as too commonly accepted (e.g., Ciummelli and Raffi, 2013 for the most recent example). A firm lineage is one that can be documented by the occurrence of countless intermediate morphologies between the ancestral form and the descendant taxon over a well-delineated stratigraphic interval. The best, and perhaps only, known lineage based on this definition is the early Eocene *Tribrachiatus* lineage which was first reported on by Romein (1979), and which has been the object of some attention in recent years (Raffi et al., 2005) although no attempt was made at characterizing the two prominent speciation events along this lineage. This lineage is the object of the fourth chapter in this dissertation.

Although lineages are not easily determined among coccolithophores, some species show clear morphologic changes through time. One of these is the earliest Eocene species *Heliodiscoaster mahmoudii*. Despite its short life span of ~370 kyr this characteristic species shows high morphologic variability associated with its First Appearance Datum and lasting for ~80 kyr. I explore this variability in Chapter 3.

Even though the earliest stage of speciation is undocumented in the fossil record of *H. mahmoudii*, the patterns of variability associated with this speciation event compares well

with those described in the *Tribrachiatus bramlettei–T. contortus* evolutionary transition. The patterns presented by the two coccolithophore species also compare well with speciation events described in other planktonic unicellular eukaryotes, and in particular the planktonic foraminifera. A seminal study was that by Malmgren et al. (1983) who described speciation in the *Globorotalia plesiotumida – G. tumida* lineage as representing a "compromise" between Gradualism and Punctuated Equilibrium, for which they adopted the term *Punctuated Gradualism*, later renamed *Punctuated Anagenesis*, whereby speciation consists in a relatively long interval of high morphological variation between two phases of morphologic fixation (the first corresponding to the parent species, the second to the daughter species). My records here fit well the model of Punctuated Anagenesis, and I predict from my preliminary measurements of specimens in the evolutionary transition from *Tribrachiatus contortus* to *T. orthostylus* that the whole *Tribrachiatus* lineage is a case of *Punctuated Anagenesis*.

The early Paleogene Period was selected for this work as it represents a critical time of evolution following the Cretaceous/Paleogene mass extinction (~66 Ma; Kuiper et al., 2008). This is a period of increasing diversification with major radiations occurring in both the planktonic foraminifera (appearance of muricate and truly spinose forms) and in the coccolithophore (radiation in the Discoasterales) in response to changes in the early Paleocene ocean to more oligotrophic conditions (Boersma et al., 1987; Coxall et al., 2006.). In addition, the early Paleogene is marked by a major warming event, the Paleocene Eocene Thermal Maximum (PETM), and shorter subsequent events (hyperthermals) that may have perturbed the marine environment and functioned as a

forcing agent in microplankton evolution. The documentation of the biotic forcing on speciation would have been an interesting part of this dissertation, but the temporal demands of data collection and statistical analyses have not permitted me to address satisfactorily this question in this memoir. At a first glance, based on the work of Cramer et al. (2003, 2011), Raffi et al. (2005), Westerhold et al. (2009) and Lourens et al. (2005) there would seem to little relation between speciation and environmental forcing. This, however, will be further discussed during the thesis defense.

I approached the question of abiotic forcing in a different manner. I attempted to decipher a possible relationship between the Danian evolution (~62 Ma) of *Ellipsolithus macellus* and contemporary initiation of oligotrophication of the Paleocene ocean. This is the object of Chapter 2 of this work. My approach has been that small morphologic differences between two coccoliths may not represent pseudo-cryptic speciation as generally assumed (in which the two cryptic species possess different genotypes), but may express phenotypic differences (in which the two coccoliths reflect dimorphic composition of the coccosphere, that is of the envelope of coccoliths that surrounds the living cell). I did this by comparing morphologic variations in *E. macellus* with the morphologic differences among coccoliths found in the coccospheres of living species (of *Gaarderia* and *Umbellosphaera)*, and assumed to represent adaptation to mixotrophy (Aubry, 2009). I have not been able to resolve this question, but I have raised here an important question on the significance of small morphological differences; I have also shown, as an unexpected result of the study, that living coccolithophores may follow different adaptive morphologic paths to fulfill the same physiological requirements.

In summary, my long interest in evolutionary processes has been fulfilled by my demonstration that speciation in the coccolithophores occurs through Punctuated Anagenesis. Of course I have demonstrated this for only two taxa, but the constancy of morphotypes (species) through long time spans indicates that this modality is likely the rule in the group. This, and the demonstration of Punctuated Anagenesis in the planktonic foraminifera (Malmgren et al., 1983; Hull and Norris, 2009) suggest that speciation among unicellular eukaryotes follows this modality. The interval of high morphological variability that accompanies speciation is very short, and may not be recovered in paleontological records that are less continuous than the deep sea record, such as the marginal and continental records. Thus, it may be that the patterns of Punctuated Equilibrium described for organisms living on land or in shallow water simply represent the incomplete record of Punctuated Anagenesis.

Note: In the course of preparation of this thesis, I have also been involved in studies of macroevolutionary processes with my advisor, Dr. Marie-Pierre Aubry. These have resulted in several publications and presentations at conferences. These publications and abstracts are given in full at the end of this dissertation.

1.4 References

Alizon, S., Kučera, M., and Jansen, V.A.A., 2008, Competition between cryptic species explains variations in rates of lineage evolution.: Proceedings of the National Academy of Science, v. 105, no. 34, p. 12382–12386

Aubry, M.-P., Lucas, S.G., and Berggren, W.A., 1998, Late Paleocene-early Ecocene Climatic and Biotic Events in the Marine and Terrestrial Records: Columbia University Press.

Aubry, M.-P., 2009, A sea of lilliputians: Palaeogeography, Palaeoclimatology, Palaeoecology, v. 284, no. 1, p. 88–113.

Aubry, M.-P., 2013. Cenozoic coccolithophores: Syracosphaerales, Part 1, Volume E. New York: Micropaleontology Press. Atlas of Micropaleontology series, pp. xxx.

Aubry, M.-P., Cenozoic coccolithophores: Discoasterales. New York: Micropaleontology Press. Atlas of Micropaleontology series, 3 volumes, (in press).

Boersma, A., Premoli Silva, I., and Shackleton, N., 1987. Atlantic Eocene planktonic foraminiferal paleohydrographic indicators and stable isotope paleoceanography. Paleoceanogra- phy, 2, 287-331.

Bown, P.R., Lees, J.A., and Young, J.R., 2004, Calcareous nannoplankton evolution and diversity through time:, p. 481–508.

Ciummelli, M., and Raffi, I., 2013, New data on the stratigraphic distribution of the nannofossil genus Catinaster and on evolutionary relationships among its species: Journal of Micropalaeontology, v. 32, no. 2, p. 197–205

Cramer, B.S., Wright, J.D., Kent, D.V., and Aubry, M.-P., 2003, Orbital climate forcing of δ13C excursions in the late Paleocene–early Eocene (chrons C24n–C25n): Paleoceanography, v. 18, no. 4, p. 1097.

Cramer, B.S., Miller, K.G., Barrett, P.J., and Wright, J.D., 2011, Late Cretaceous–Neogene trends in deep ocean temperature and continental ice volume: Reconciling records of benthic foraminiferal geochemistry (δ18O and Mg/Ca) with sea level history: Journal of Geophysical Research, v. 116, no. C12.

Coxall, H. K., D'Hondt, S., and Zachos, J. C., 2006. Pelagic evolution and environmental recovery after the Cretaceous- Paleogene mass extinction. Geology, 34 (4), 297-300.

Hagino, K., and Kawachi, M., 2013, Symbiotic relationship between *Braarudosphaera bigelowii* and cyanobacteria.

Honjo, S., 1976, Coccoliths: production, transportation and sedimentation: Marine Micropaleontology, v. 1, p. 65–79.

Hull, P.M., and Norris, R.D., 2009, Evidence for abrupt speciation in a classic case of gradual evolution.: Proceedings of the National Academy of Science, v. 106, no. 50, p. 21224–21229

Hunt, G., 2006, Fitting and comparing models of phyletic evolution: random walks and beyond: Paleobiology, v. 32, no. 4, p. 578–601.

Hunt, G., 2007, The relative importance of directional change, random walks, and stasis in the evolution of fossil lineages: Proceedings of the National Academy of Science, v. 104, no. 47, p. 18404–18408.

Hunt, G., 2008, Gradual or pulsed evolution: when should punctuational explanations be preferred?: Journal Information, v. 34, no. 3.

Hunt, G., 2010, Evolution in Fossil Lineages: Paleontology and The Origin of Species: The American Naturalist, v. 176, no. S1, p. S61–S76, doi: 10.1086/657057.

Hunt, G., 2012, Measuring rates of phenotypic evolution and the inseparability of tempo and mode: Paleobiology, v. 38, no. 3, p. 351–373, doi: 10.5061/dryad.c1m60s84.

Kuiper, K.F., Deino, A., Hilgen, F.J., Krijgsman, W., Renne, P.R., and Wijbrans, J.R., 2008, Synchronizing rock clocks of Earth history: Science, v. 320, p. 500–504.

Lourens, L.J., Sluijs, A., Kroon, D., Zachos, J.C., Thomas, E., Röhl, U., Bowles, J., and Raffi, I., 2005, Astronomical pacing of late Palaeocene to early Eocene global warming events: Nature, v. 435, no. 7045, p. 1083–1087.

Malmgren, B.A., Berggren, W.A., and Lohmann, G., 1983, Evidence for punctuated gradualism in the Late Neogene Globorotalia tumida lineage of planktonic foraminifera: Paleobiology, v. 9, no. 4, p. 377–389.

Monechi, S., Reale, V., Bernaola, G., and Balestra, B., 2013, The Danian/Selandian boundary at Site 1262 (South Atlantic) and in the Tethyan region: Biomagnetostratigraphy, evolutionary trends in fasciculiths and environmental effects of the Latest Danian Event: Marine Micropaleontology, v. 98, no. C, p. 28–40.

Okada, H., and Honjo, S., 1973, The distribution of oceanic coccolithophorids in the Pacific: Deep Sea Research and Oceanographic Abstracts, v. 20, no. 4, p. 355–364, IN3–IN4, 365–374.

Parke, M., and Adams, I., 1960. The motile (Crystallolithus hyalinus Gaarder & Markali) and non-motile phases in the life history of Coccolithus pelagicus (Wallich) Schiller. Journal of the Marine Biological Association of the United Kingdom, 39, pp 263-274.

Raffi, I., Backman, J., and Pälike, H., 2005, Changes in calcareous nannofossil assemblages across the Paleocene/Eocene transition from the paleo-equatorial Pacific Ocean: Palaeogeography, Palaeoclimatology, Palaeoecology, v. 226, no. 1-2, p. 93–126.

Raffi, I., Backman, J., Zachos, J.C., and Sluijs, A., 2009, The response of calcareous nannofossil assemblages to the Paleocene Eocene Thermal Maximum at the Walvis Ridge in the South Atlantic: Marine Micropaleontology, v. 70, no. 3-4, p. 201–212.

Romein, A.J.T., 1979, Lineages in early Paleogene calcareous nannoplankton: Utrecht Micropaleontological Bulletins, v. 22.

Thompson, A.W., Foster, R.A., Krupke, A., Carter, B.J., Musat, N., Vaulot, D., Kuypers, M.M.M., and Zehr, J.P., 2012, Unicellular Cyanobacterium Symbiotic with a Single-Celled Eukaryotic Alga: Science (New York, NY), v. 337, no. 6101, p. 1546–1550

Westerhold, T., Röhl, U., Mccarren, H.K., and Zachos, J.C., 2009, Latest on the absolute age of the Paleocene–Eocene Thermal Maximum (PETM): New insights from exact stratigraphic position of key ash layers +19 and −17: Earth and Planetary Science Letters, v. 287, no. 3-4, p. 412–419.

Young, J.R., and Association, I.N., 2003, A guide to extant coccolithophore taxonomy: Journal of Nannoplankton Research: Special Issue 1.

Chapter 2

Morphologic variability in the coccolithophore *Ellipsolithus macellus*: Phenotypic or genotypic differences?

2.1. Abstract

Through quantitative analysis I compare the coccoliths of the early Paleogene species *Ellipsolithus macellus* with those of the living species of *Gaarderia* and *Umbellosphaera* to determine the significance of two distinct morphotypes of the extinct species. My objective is to determine whether the two morphotypes are akin to the differentiated coccoliths that occur on the coccospheres of the two living taxa, in which case they may represent an early adaptation to mixotrophic behavior in the middle Danian Ocean, ~ 1 Myr prior to widespread adaptation to increasing oligotrophy by the calcareous plankton. *Ellipsolithus macellus* morphotype (B) exhibits lesser ellipticity than morphotype A, which is also a marked difference between the microliths and the macroliths in both *Gaarderia* and *Umbellosphaera*. However the differences between the latter are much greater than between the two morphotypes of *Ellipsolithus*, which renders my data inconclusive. An alternative interpretation is that the two morphotypes represent pseudo-cryptic species, which would imply that cryptic speciation occurred shortly after the evolutionary appearance of the genus *Ellipsolithus*. However, the two morphotypes differ only by their ellipticity, and without differences in size as reported between well-documented pseudo-cryptic species. This study shows the difficulty is interpreting taxonomic differences in extinct taxa, and offers an alternative to cryptic speciation. My study is inconclusive with regard to one explanation or the other with regard to *E. macellus*, but it has enabled me to demonstrate that the microliths and

macroliths of *Gaarderia* and *Umbellosphaera* are functionally adapted to mixotrophy, and that the two genera have followed slightly different adaptive morphologies.

2.2. Introduction

The Danian was a critical time for the evolution of calcareous plankton following the decimation by the Cretaceous/Paleogene boundary event (~66 Ma; Kuiper et al., 2008). The most prominent events in its re-diversification were the appearance of a group of muricate planktonic foraminifera (*Acarinina*, *Morozovella*) at ~62 Ma and the initiation of the radiation of the Discoasterales at ~ 62.13 Ma, corresponding to the "first radiation of the fasciculiths" (figure, 1; Aubry and Bord, 2012.). The proposed forcing agent in both radiations was the development of oligotrophic conditions in the early Paleocene ocean (Boersma et al., 1987; Coxall et al., 2006). The muricate walls were instrumental for the acquisition of photosymbiotic capabilities by the otherwise heterotrophic planktonic foraminifera (Berggren and Norris, 1997), whereas a notable increase in total coccolith surface facilitated food capture and perhaps also symbiotic activities in the coccolithophores (Aubry et al., 2012; for a review of the role of coccoliths see Aubry, 2009 and 2013). The first clear relationships between diversification and oligotrophy are seen in 62.60 Myr old records, but it is possible that other, more subtle morphological adaptations to increasing oligotrophy occurred earlier. Among such possibilities is the appearance of the coccolithophore genus *Ellipsolithus* at ~63.25 Ma, the younger of two genera in the Family Ellipsolithaceae Aubry 2013 of the Order Biscutales Aubry 2013. This taxon, which ranges from early Paleocene through early Eocene (63.25 to ~54 Ma), is known only from its coccoliths, based on which five species have been described to date. Its oldest species *Ellipsolithus macellus* is distinctive in being elliptical to long-

elliptical, with a central area that occupies half of the coccolith. Intraspecific variability involves size and general shape, but no previous attempt has been made at characterizing it through morphometric analysis, possibly because the taxon is generally uncommon. *Ellipsolithus* coccoliths are strongly reminiscent of the coccoliths secreted by species in two living genera, *Gaarderia* and *Umbellosphaera*, although there are demonstrably no phylogenetic relationships between them and *Ellipsolithus* (the former belong to the Order Syracosphaerales). The (spirothecate) coccosphere in these living taxa is unusual in consisting of coccoliths whose size and shape change from the inner side of the coccosphere to the outer side, with internal microliths and external macroliths. This construction has been proposed to represent adaptative morphology to mixotrophic behavior (Aubry, 2009). In this light and considering the morphologic variability in *E. macellus*, the possibility arises that the coccosphere of *E. macellus* may have been spirothecate. In this paper I take advantage of the exceptional abundance (up to 30%) of *E. macellus* in early Paleocene (Danian) assemblages recovered from the Qreiya section in Upper Egypt to conducting a comparative morphometric analysis of the coccoliths of *E. macellus* with *Gaarderia corolla* and *Umbellosphaera* spp. with the objective of testing whether shape variability in *E. macellus* may be linked to a phenotypic character rather than a genotypic one.

2.3. Taxonomic Background

Coccolithophores (5-20 μm on average) are photosynthetic, marine protists. The single cell is surrounded by a calcitic shell (the coccosphere) that is formed piecemeal by skeletal pieces (coccoliths) which are secreted within or outside the cell during, respectively, the diploid and haploid stages of the life cycle of the organism (with a few

exceptions). The latter are referred to as holococcoliths, the former as heterococcoliths. Heterococcoliths (the kind of coccoliths studied herein) show a considerable variety of size, shape, structure and ornamentation that are determinant for taxonomic identification, and their morphologic transformation through time reflects the phylogenetic history of the taxonomic groups to which they belong (Romein, 1979). Except for the highly derived ones (e.g., discoasters) a coccolith is comprised of two parts, a marginal area (or margin) surrounding a central area. Both are formed of strongly modified rhombohedrons of calcite referred to as elements. The general crystallographic orientation of the elements of the margin differs markedly from that of the elements of the central area. The boundary between the two is readily identified in scanning electron micrographs of coccoliths (of *Gaarderia* and *Umbellosphaera* herein). In light microscopy, the boundary is inferred from the extinction patterns produced by coccoliths (*Ellipsolithus macellus* herein) in cross polarized light, with a marked change in the direction of the extinction lines at contact between margin and central area.

2.3.1. Ellipsolithus macellus (Bramlette and Sullivan) *Sullivan 1964*

Ellipsolithus macellus is known only from its very characteristic coccoliths described as being long elliptical, nearly flat, with a depressed central area, and 9-15 μm long. The original illustrations of the species (Bramlette and Sullivan, 1961, pl. 7, Figs. 11, 12) consist of two specimens with noticeably different shapes. The holotype (op. cit., Fig. 14) exhibits an elongate shape, with the two edges parallel to the main axis of the ellipse. The central area is large and the boundary between central area and margin is concentric with the edge of the coccolith (i.e, the width of the margin does not change). The other

specimen is more elliptical; the central area is smaller; and the boundary between the central area and the margin is not concentric with the edge of the coccolith. These two morphologies, occasionally illustrated in the literature (Aubry, in press), were recovered from the Danian interval under study (Plates 1 and 2). I refer to them as morphotype A (the holotype) and B.

2.3.2. Genus Gaarderia Kleijne 1993 (*Family Syracosphaeraceae* Lemmerman 1908).

In the living monospecific genus *Gaarderia* the coccosphere (8 to 15 μm in diameter) is spherical to oval. The coccoliths (microliths) closer to the cell surface are small (~2-3 μm) and cup-like (Pl. 3, Fig. 3). The external coccoliths (macroliths) are considerably larger (>5 μm) and, except for a narrow central depression, they are convex distally. Microliths and macroliths differ by exhibiting different proportions between margin and central area. The central area of the microliths, occupied by a grill, is large whereas the margin is very narrow. The macroliths show opposite characters, with a narrow central area and a flaring margin. The non-overlapping microliths are densely packed, forming an inner layer of saucer-like coccoliths opened to the outside. In contrast, the macroliths are imbricate, the margins of adjacent coccoliths overlapping to form a continuous, regular exotheca.

2.3.3. Genus *Umbellosphaera* Paasche in Markali and Paasche 1955 emend. Gaarder in Heimdal and Gaarder 1981 *(Family Umbellosphaeraceae).*

In the genus *Umbellosphaera* (2 species, at least 4 morphotypes, each possibly a pseudo-cryptic species) the small cell (6-10 μm in diameter) is surrounded by a coccosphere (10-

20 µm) formed by coccoliths (length: 4.4 –11.5µm) roughly arranged in a spiral fashion (as in *Gaarderia*; the coccosphere is named a spirotheca for this reason; Aubry, 2009; Pl. 3, Figs. 2-6). The inner coccoliths, at the contact with the cell, are small, with a large central area and a very narrow margin. The outer coccoliths are much larger; their central area is small and they exhibit a broad margin that confers the macroliths a funnel shape. The outermost coccoliths are so large that a few of them are sufficient to encapsulate all other coccoliths around the cell (pl. 3, Fig. 7).

2.4. Material And Methods

2.4.1. Material

The coccoliths of *Ellipsolithus* analyzed in this study are from the lower Paleocene (Danian; *Ellipsolithus macellus* Zone of Martini 1971 [NP4; subzone NP4a of Aubry and Salem, 2013]) Dakhla Shale Formation exposed in the lower part of the Qreiya section (26° 21'N, 33° 01' E) located at the southeastern end of Gebel Abu Had in the Egyptian Eastern Desert (Fig. 1). Described by Aubry et al. (2012) the section corresponds to Qreiya 1 of Sprong et al. (2009; see Aubry and Salem, 2013), it consists of homogeneous laminated shales of middle to outer neritic origin (Speijer, 2003). The section was qualitatively and quantitatively analyzed for biostratigraphic purposes (Rodriguez and Aubry, 2008). *Ellipsolithus* coccoliths are generally abundant in an ~20 m-thick interval between the base of the section at level -16 and level +3.2 m, then drop sharply in abundance (from 40 % to <10%) between this level and level +5 m (Fig. 2). Five levels with greatest abundance and best preservation of *Ellipsolithus* coccoliths were selected for morphometric analysis. The 5.2 m interval studied here is located between the lowest occurrence (LO) of *E. macellus*, which is at an unknown distance below the base of the

section, and the LO of the "first appearance of the fasciculiths" at ~8.4 m (Aubry et al., 2012). Its duration is <0.5 Myr, between 63.25 Ma (First appearance Datum [FAD] of *E. macellus* and 62.13 Ma (First radiation of the fasciculiths; time scale of Gradstein et al., 2012).

The coccoliths of *Gaarderia* and *Umbellosphaera* were measured from published SEM micrographs of (mostly) living coccospheres and (a few) isolated coccoliths from ocean sediment traps, all compiled in Aubry (2013). The two species of *Umbellosphaera* were treated as a single taxon. Microliths and macroliths were measured as distinct groups for both genera. Full references concerning the measured specimens analyzed in this study are given in Aubry (2013, Appendix 2).

2.4.2. Sample preparation

Smear slides were prepared from each selected stratigraphic level. This process entailed the scraping and crushing of sediment onto a coverslip. Water was added to disaggregate the shale. The mixture was spread across the coverslip to produce a series of evenly spaced ribs. After quick drying on a hot plate the coverslip was mounted on a slide using Norland Optical Adhesive 61. The adhesive, which hardened under an ultraviolet lamp (360 nanometer wavelength), causes no harm to the coccoliths.

2.4.3. Morphometric Analysis

The samples were studied using a Zeiss Axioplan2 photomicroscope at 1600X magnification, under polarized light. They were systematically scanned along parallel

transects until ~100 unbroken coccoliths of *Ellipsolithus macellus* were photographed in each sample. A total of 522 specimens were measured. The measurements were made along the major (long) and minor (short) axes of the coccoliths (Fig. 4), and included the total width and length of the coccoliths and of their central area. The width of the margin along the major and minor axis was arithmetically determined.

Measurements were conducted in similar fashion for the coccoliths of *Gaarderia* and *Umbellosphaera* spp. Most measured coccoliths occur *in situ* on both well-preserved and collapsed coccospheres. Because coccoliths overlap strongly in coccospheres, not all coccoliths visible on a photograph could be reliably measured. Also, not all coccoliths were oriented in a manner favorable for measurement. One hundred and thirty coccoliths of *Gaarderia* and two hundred and thirty coccoliths of *Umbellosphaera* were measured.

Histograms and scatterplots were first established for preliminary analyses of the data (Fig. 5). Bins for histograms were set at 0.5 μm. Since sample sizes for the three genera are different, density histograms were used for comparing the relative frequencies of their distributions. Overlying each histogram is a frequency density polygon, a smooth function describing the relative frequency of the distribution. The measurements along the major and minor axes were plotted for the total coccolith length and width, the central area length and width, and the width of the margin. The same plots were constructed for *Gaarderia* and *Umbellosphaera*. Graphs constructed in Rstudio using the *ggplot2* package (Wickham, 2009)

Secondary analysis of the data focused on variations in 1) the marginal widths along the major and minor axes. The marginal width (e) along the major axis was calculated by subtracting the length of the central area (c) and from the total length (a) of the coccolith (Fig. 4). The marginal width (f) along the minor axis was calculated by subtracting the width of the central area (d) from the total width (b) of the coccolith (Fig. 4); 2) the ratio f/e of the marginal widths; 3) the total surface area of coccolith, (SAT μm^2), 4) the surface area of the central area (SACA μm^2), 5) surface area of the margin (SAM, μm^2), 6) the ratio SACA /SAM between these areas; and 7) the ellipticity (f). These parameters are similar to those measured by Bornemann and Mutterlose (2006) in their size analysis of *Biscutum constans* and *Watznaueria barnesiae,* which share similar morphology (elliptical coccoliths with a margin and central area) to *Ellipsolithus*, *Gaarderia* and *Umbellosphaera.*

Ellipticity refers to the amount of deviation from a circle, also known as flattening; a circle has an ellipticity of 0 (zero). Ellipticity was calculated using the following equation:

$$\text{Ellipticity } (f) \ = \ \frac{a-b}{a}$$

Ellipticity was calculated for both the whole coccolith and the central area.

The area of the whole coccolith was calculated using the following equation:

$$\text{SAT} = \ \text{Area of Outer Ellipse} \ = \ \pi \frac{ab}{4}$$

The area of the central area was calculated using the following equation:

$$\text{SACA} = \ \text{Area of Inner Ellipse} \ = \ \pi \frac{cd}{4}$$

The marginal area is calculated by subtracting the area of the central area from the total area (SAM = SAT – SACA). The ratio SACA/SAM describes how the central area and the margin vary as a function of the variations in the total size of the coccolith.

Data transformation (log10) was performed to normalize the sizes of coccoliths of three taxa, which differ by several magnitudes (within coccospheres and between species). This allows for proper statistical testing through multivariate analysis of variance (MANOVA) and pairwise tests of significance using Hotelling's T^2 test. The multivariate allometric test found in the PAST statistical software was run to analyze allometry and describe how the morphology of coccoliths in *Gaarderia* and *Umbellosphaera* change around their respective coccospheres and to describe the similarities and differences between the different groups. Finally, A multigroup discriminant analysis known as a canonical variates analysis (CVA) was conducted to simplify and describe the differences between groups. This method is similar to a principle component analysis, where the greatest amount of variance between individual specimens is found in the least number of orthogonal axes. However, CVA differs in that it finds the maximum variance to discriminate between pre-assigned groups. The first canonical variates (CV) axis describes the maximum difference between groups and is the direction in which groups are most effectively discriminated. Each sequential axis describes lower variance. It is important to note that since CV's are rotated and scaled axes, distances on them are not comparable to original distances. All computations were performed using the PAST software v. 2.17c (Hammer et al., 2009), and Rstudio with packages *MASS* (Venables, 2012) and *psych* (Revelle, 2013).

2.5. Results

The measured and calculated values for the variable described above are given in Table 1. The important features are described below starting with the living species as a reference and then proceeding to *Ellipsolithus*.

2.5.1. Size and shape variability of Gaarderia

The total length of *Gaarderia* coccoliths shows a wide bimodal and positively skewed frequency distribution with a spread from 1.08 to 8.55 μm. A similar pattern is seen in the total coccolith width (range: 5.85 μm, Fig. 5b) and in the widths of the margin along both the major and minor axes (range: 4.90 μm and 4.78 μm, respectively, Fig. 5e, f). In contrast, the length and width of the central area exhibit frequencies that are symmetrically distributed with narrow spreads (range: 2.6 μm and 1.65 μm, respectively; see caption Fig. 5c, d).

Bimodality in the size and shape distribution is caused by the microliths and macroliths (Fig. 6a, b, e, f), as seen in the frequency distributions of length and width. Both the microliths and macroliths show a symmetric distribution. For microliths the distributions are wide with a strong peak at the mean value. They decay rapidly, are fat-tailed, and have two smaller peaks at either end of the distribution. In macroliths the distributions are wider (range micro, and macro, respectively, Fig. 6 a, b), fat-tailed and with weaker peaks. The frequency distributions show significant overlap between at least the 75%-percentile of the microliths and the 25%-percentile of the macroliths. The distributions of the margin widths differ only for the microliths, which are positively skewed.

Although, the sizes of the central area as a whole are unimodal (Fig 3c, d), the distribution peaks for the micro- and macroliths differ slightly along the length (means = 1.8-2.5 μm for the length of the central area; 0.99–0.92 μm for its width; Fig. 6 c, d). This implies that the shape of the central area varies little between the microliths and macroliths.

The scatterplots in Fig. 7 show a strong linear correlation between the total length and width in both the micro- and macroliths (Table 2). Pearson correlation coefficients are high in both groups ($r = 0.93$ for microliths, and $r = 0.89$ for macroliths). The length and width of the central area in the microliths are strongly correlated ($r = 0.87$). The slope of the linear regression line in the central area is significantly lower in the macroliths than in the microliths (Fig. 7b). Together with a lower correlation coefficient ($r = 0.59$) and the lower correlation of determination value of the linear regression function ($r^2 = 0.35$), this suggests a weaker length to width relationship in the central area of the macroliths than in the microliths ($r^2 = 0.75$). In contrast, the total length and the total width are strongly correlated in the microliths and the macroliths ($r^2 = 0.87$ and $r^2=0.79$, respectively). The major and minor widths (e and f) of the margin also show high linear correlation in both micro- and macroliths ($r = 0.80$ and 0.81, respectively), but slightly lower slopes ($r^2 =$ 0.65 and 0.65) than for the total length and width.

2.5.2. Size and Shape variability of Umbellosphaera

In *Umbellosphaera* the distribution of total length is symmetric and very widespread (range: 10.19 µm, Fig 3a) with a small peak and fat tails. The distribution of the total width is similar to that of the total length with regards to spread and symmetry except that the distribution is flat (range: 9.63 µm, kurtosis = 2.77, Fig 3b). This applies also to the widths along the major and minor axes, whose distributions are broadly spread (range: 9.05 and 8.05 µm, respectively, Fig 3 d, e) flat (kurtosis = 2.91 and 2.63, respectively) and fat-tailed. In contrast, the length and width of the central area exhibit narrow unimodal distributions (range: 4.31µm and 2.17 µm, respectively, see caption Fig. 5c, d).

A deconstruction of the collective relative frequencies for the total length and width, and of the major and minor widths of the margin in both the micro- and macroliths reveals the composition of the total distribution (Fig. 8a, b, e, f,). The tail ends of the total distribution are formed by the microliths and macroliths, solely. Between the 25%-percentile and the 75%-percentile, the intermediate coccoliths (I-liths) overlap the micro- and macroliths, peaking between about half way between the other two coccolith types. Deconstruction of the total relative frequencies for the length and width of the central area reveals little difference between the three (micro-, I, and macro-) coccoliths: they exhibit completely overlapping symmetric distributions with similar means (mean lengths: 1.41 - 1.45 µm, and means widths: 0.84 - 0.96 µm, Fig. 8c, d, Table 1).

For all the measured parameters, the central area excepted microliths have a wide, positively skewed and slightly bimodal distribution (Fig. 8, Table 1), and the macroliths

have a very broad, symmetric, and fat-tailed distribution. The shape of the distribution of the I-liths is very similar to that of the macroliths, except for the width of the margin along the major axis, which shows flattening.

Scatterplots show strong length to width correlation for all three coccolith types (r =0.90, 0.93, and 0.91, respectively, Fig. 9a). In addition, the regression line shows good fit (r^2 = 0.81, 0.86, and 0.83, respectively). The correlation between length and width in the central area for micro- and I- liths are only slightly lower (r= 0.82 and 0.79, respectively) than for total length and width. In contrast the correlation between these variables is much lower (r= 0.5) in the macroliths. Lowering in slope between microliths to macroliths with decreasing regression (r^2=0.64, 0.62, and 0.26, respectively) suggests weakening in length to width correlations for the central area from microliths to macroliths. The major and minor widths of the margin also a show strong positive correlation in the three coccolith types (Fig. 9c). Linear fit decreases from highest in the I-liths (r^2= 0.89), to intermediate in microliths (r^2 = 077) and lowest in the macroliths (r^2 = 0.62). This implies that microliths and I-liths show a positive correlation with low variability between the major and minor widths of the margin. As size increases from the I-liths to the macroliths there is a decrease in the r^2 values, implying a slight increase in variability. This suggests a positive relationship: when coccolith size increases shape variability also increases.

2.5.3. Size and Shape variability of Ellipsolithus

All the measured variables for the coccoliths of *Ellipsolithus* show unimodal normal distributions with narrow spreads, the total length having a slightly broader spread than the other variables (Fig.3a-d, Table 1).

The two morphotypes, A and B, overlap heavily in all variables (Fig. 10 a-d). All distributions for morphotype A are normal and unimodal with well-behaved tails. In morphotype B the distributions for total length, total width, and length and width of the central area are slightly broader and flatter. The only difference between the two morphotypes concerns the width of the margin along the minor axis, which shows a wider positive skewed distribution and a lower peak.

The scatterplot in Fig. 11a for total length and total width shows that both morphotypes have positive linear correlation ($r = 0.85$, $r = 0.88$), although the slope for morphotype A is lower. For the length and width of the central area, morphotype A groups tightly with lower correlation ($r = 0.76$, Fig. 11b) than for total length and width. For morphotype B correlation and regression also show a lower fit ($r = 0.75$, $r^2 = 0.55$) for length and width of the central area compared to total length and width. This suggests that there is a positive, low variability correlation between the length and width of the central area in morphotype A, whereas the correlation is weaker in morphotype B. In this morphotype there is more variability in size along the width of the central area than along the length (Fig. 11b). For the major and minor widths of the margin both morphotypes show positive correlation (Fig. 11c) although the correlation in morphotype B is stronger

(r=0.90) than in morphotype A (r = 0.72). This suggests that there is greater variability along the minor axis in morphotype B.

2.6. Discussion

2.6.1. Within-group comparison

A multivariate analysis of variance (MANOVA) performed on the log transformed (Fig. 12) dataset for *Ellipsolithus* shows that there are significant differences between the five samples (Wilk's λ = 0.892, F=2.5, and $p<0.0001$). A summary of the analysis of variance model by ANOVA (Bralower, 1996) reveals that the statistically significant differences only concern the central area, significant p-values occurring on its length are statistically significant ($p< 0.001$), the ellipticity of the central area, is significant ($p = 0.001$), and the surface area of the central area (SACA), being marginally significant ($p=0.01$). There were no other significant differences in the other variables ($p>0.05$). A MANOVA performed on the variables of the two morphotypes (A and B) indicates statistically significant differences between the two (Wilk's λ = 0.735, F=30.9, and $p<0.0001$). A summary by ANOVA indicates that differences between morphotype A and B are found in the total width, the width of the central area, and the minor width of the margin, being highly significant ($p<0.001$). Differences concerning the length of the central area are marginally significant ($p=0.01$) and differences regarding the total length, the margin width along the major axis and SACA are not significant ($p>0.05$). Frequency distributions of the log-transformed data for the different variables imply that, as a whole, the dimensions of *Ellipsolithus* are rather homogenous between samples suggesting the absence of any directional trend (Fig. 12). This further implies that the morphology of *E. macellus* was fixed over the interval of time (<0.5 Myr) represented by this section.

However, a post hoc pairwise comparison among the pairs of samples and morphotypes indicate significant differences ($p < 0.05$) between morphotypes A and B that are therefore regarded as discrete entities.
(Table 3).

The performed multivariate allometric test computes a coefficient α from the loadings on the first principal component analysis (PCA) axis. A coefficient $\alpha = 1$ describes isometry. Isometry is inferred for variables when $\alpha = 1$ is within the 95% confidence interval (Fig. 13). In *Ellipsolithus,* the total length and width exhibit near isometric (coefficient $\alpha =$ 0.94 and 1.00, respectively); total length showing a trace of negative allometry. The length of the central area has negative allometry (coefficient $\alpha = 0.76$), whereas the width of the central area demonstrates isometry. Both major and minor widths of the margin show positive allometry (coefficient $\alpha = 1.18$ and 1.1, respectively). Thus, as size increases, 1) the proportions of total length and width increase uniformly, though, perhaps slightly less along the total length; 2) the margin increases proportionally along both axes; 3) the length of the central area does not change proportionally, decreasing while the width of the central area increases uniformly; and 4) both total ellipticity and central ellipticity decrease with size (Fig.11a). A major difference in the proportions of shape change between morphotypes A and B in *E. macellus* is found with the total width and the width of the central area, as the size of the coccolith increases morphotype B experiences positive allometry while morphotype A displays negative allometry (Fig. 13a). There is strong positive correlation between the surface area of the margin (SAM) and the surface area of the central area (SACA), this supports that growth in both regions

is isometric (Fig. 14a). Interestingly, no correlation is found in morphotype A between SAM and the total ellipticity (Fig. 14b), as well as between the SACA and the ellipticity of the central area (Fig. 14c). Thus, an increase in the surface area within these regions does not affect their ellipticity in morphotype A. In contrast, the slight negative correlation present in morphotype B implies that size in this morphotype does affect ellipticity (Fig. 14b, c). Lastly, there is a slight positive relationship in morphotype A between the SACA and the total ellipticity, whereas in morphotype B there is a negative correlation. This suggests that ellipticity in *Ellipsolithus* is affected more by changes in the SACA and than by the widths of the margin.

The same multivariate allometric test was conducted on the coccoliths of *Gaarderia* and *Umbellosphaera* to characterize changes in their morphology as coccolith size changes. In *Gaarderia,* both the total length and width display near isometric (coefficient $\alpha = 0.93$ and 1.07, respectively). The central area shows negative allometry along both the length and width (coefficient $\alpha = 0.49$ and 0.18, respectively). Conversely, the width of the margin displays positive allometry along both the major and minor axes (coefficient $\alpha =$ 1.4 and 1.8 respectively). Thus, as the coccoliths increase in size 1) their total length and width display an inverse correlation, the length decreasing proportionally to the increase in width; 2) the length and width of the central area decreases proportionally to one another; 3) the width of the margin increases along the major and minor axes; and 4) the total ellipticity and central ellipticity decreases. Size and shape change differs between the micro- and macroliths. In microliths most of the shape change is nearly isometric along the total length and total width and also on the widths of the margin. However, the

shape of the central area and the margin show an inverse relationship: the length and width of the central area decrease proportionally whereas the widths of the margin increase (Fig. 13b). In macroliths, isometry occurs only along the total length. The total width increases with size. As in microliths the relationship between the size of the central area and the size of the margin is inverse. Correlation between SAM and SACA is positive; both the microliths and macroliths show clear separation (Fig. 15a). Correlation between SAM and total ellipticity is weak, although the slope of the regression line suggests some negative relationship (Fig. 15b). Therefore, an increase in the surface area of the margin slightly affects ellipticity in both coccolith types. This is different for the relationship between SACA and central ellipticity. These variables show no correlation in microliths but are weakly correlated in macroliths (Fig. 15c). This demonstrates that ellipticity of the central area does not change in microliths, but decreases in macroliths as the surface area of the central area increases. Lastly, the relationship between SACA and total ellipticity shows opposite relationships between coccolith types, being negative in macroliths and positive in microliths (Fig. 15d). This implies that 1) total ellipticity is slightly affected by changes in size of the central area in both microliths and macroliths; 2) microliths become more elliptical as the central area increases in size, and 3) the ellipticity of macroliths decreases as the size of the central area increases.

In *Umbellosphaera*, the total length and width show a small positive allometry (coefficient $\alpha = 1.07$ and 1.17, respectively). The margin shows a large magnitude of positive allometry (coefficient $\alpha = 1.62$ and 1.62, respectively). The length and width of the central area display a strong negative allometric relationship (coefficient $\alpha = 0.21$ and

0.3 respectively). As the coccolith size increases both the total length and width increase in a non-isometric manner, suggesting disproportionate shape change among the different coccolith types. In microliths and I-liths the central area and the margin show an inverse relationship with regard to size (Fig. 13c). In macroliths change in shape is isometric, however the large magnitudes of the 95% confidence intervals suggest high variability. A positive correlation is found between SAM and SACA (Fig. 16a). The slightly different slopes of the regression lines exhibited by the microliths, macroliths and I-liths are likely due to the different allometry of the central area. Correlation is slightly positive between SAM and total ellipticity in the microliths, whereas correlation is strongly negative in I-liths and macroliths (Fig. 16b). This implies that in microliths, as the margin increases in size the total ellipticity also increases, whereas in I-liths and macroliths the ellipticity decreases as size increases. There is little correlation between SACA and central ellipticity (Fig. 16c). Therefore, ellipticity in the central area is not, or only slightly, affected by size changes. Finally, although SACA does not change by much, a positive correlation between SACA and total ellipticity is present in all three coccolith types (Fig. 16d), which suggests some relationship between total ellipticity and the size of the central area in them all.

2.6.2. Between-Group Comparison

A MANOVA was first performed on the dataset of log-transformed variables to compare the three genera . The different sample sizes between *Ellipsolithus* (n= 522), *Gaarderia* (n =130), and *Umbellosphaera* (n=230) were reduced by treating all specimens of *Ellipsolithus* morphotype B occurring at different stratigraphic levels as one group (n =

87), and treating those of morphotype A as five separate groups, each corresponding to a stratigraphic level (n= 69, 107, 84, 100, 75). *Gaarderia* was divided by lith-type (macroliths n= 58, microliths n= 72). *Umbellosphaera* was also divided by lith-type (macroliths n= 98; I-liths n = 87, microliths n = 48). The MANOVA indicates statistically significant differences between lith-types (Wilk's = 0.22, F = 382.92, and $p<0.0001$). The summary by ANOVA indicates that all differences between variables are highly significant ($p<0.001$), except for the minor/major width ratio (f/e), which is marginally significant ($p=0.01$).

The first two canonical variates (CV) axes account for 97% of the between-group variance, clearly discriminating between the three genera (Fig. 17). *Ellipsolithus* is a very homogenous group, tightly clustered with the two morphotypes fully overlapping. In *Gaarderia,* the two lith-types are quite different for one another, grouping in distinct clusters. The macroliths are well defined and tightly grouped while more variability is displayed by the microliths that are more dispersed. *Umbellosphaera* is surprisingly well defined with a main cluster containing all three lith-types. There is greater spread than in *Gaarderia*, and it is not limited to one lith-type, although the spread is predominantly caused by microliths suggesting some degree of variability. Interestingly, there is an overlap between the microliths of *Umbellosphaera* and of *Gaarderia* indicating similarities between these lith-types. The lack of overlap with *Ellipsolithus* indicates that morphologies are different; however the proximity of the clusters corresponding to the three genera is indicative of a strong morphologic similitude between the three genera.

As CVA describes the between group relationships, it can also describe which variables are related and how. However, I found that this was more easily accomplished through bivariate scatterplots of the transformed data (Figs. 16, 17). *Ellipsolithus*, compared to *Gaarderia* and *Umbellosphaera* varies little in size. Its coccoliths are comparable in size to the macroliths of *Gaarderia* and *Umbellosphaera* (Fig. 18a). The dimensions of its central area, however, are much larger with little spread (Fig. 18 b). In contrast the dimensions of the central areas in *Gaarderia* and *Umbellosphaera* fully overlap. The SAM and SACA show a similar pattern, the variability in the surface area of *Ellipsolithus* being small and correlated to the surface area of the central area (Fig. 19a). Instead, the surface area of *Gaarderia* and *Umbellosphaera* are highly variable with little correlation to changes in SACA. The major and minor widths of the margin of *Ellipsolithus* strongly overlap with those of the macroliths in both *Gaarderia* and *Umbellosphaera* (Fig. 18c). This indicates that the observed variability seen in the margin of *Ellipsolithus* is similar to the variability exhibited by the macroliths of *Gaarderia* and *Umbellosphaera*. Ellipticity is lower (more circular) in the coccoliths of *Gaarderia* and *Umbellosphaera* than in *Ellipsolithus*, but not correlated to the total and central ellipticity (Fig. 18d). *Ellipsolithus* exhibits a positive correlation between the central and total ellipticity, which suggests a stronger link between the shape of central area and the total shape, unlike in *Gaarderia* and *Umbellosphaera.* The relationship between ellipticity and surface area is highly variable in *Gaarderia* and *Umbellosphaera* (Fig. 19b). *Ellipsolithus* exhibits similar variability in ellipticity further supporting the similarities between the coccoliths of *Ellipsolithus* and the macroliths of the other two genera. No relationship is present between SACA and central ellipticity in *Ellipsolithus* but *Gaarderia* and *Umbellosphaera*

show increased variability in central ellipticity (Fig. 19c). Ellipticity, highly variable in the three groups (although less in *Ellipsolithus*) is negatively correlated with SACA in *Umbellosphaera* (Fig. 19d). As the surface of the central area decreases it becomes more circular, this is characteristic and only present in the larger macoliths of *Umbellosphaera.* Finally, in *Gaarderia* and *Umbellosphaera* there is a positive correlation between the ratio SACA /SAM and the total ellipticity (Fig. 40). This ratio describes the observation in *Gaarderia* and *Umbellosphaera* that reduced SACA is associated with increases in the SAM, producing more circular coccoliths. This is not the case in *Ellipsolithus*, which exhibits a remarkable stability of the SACA /SAM ratio, supporting the observation that proportions in this coccolith remains stable regardless of size. However, a distinct character of morphotype B is the slight decrease in ellipticity with increasing size.

2.6.3. Was the coccosphere of Ellipsolithus a spirotheca?

My quantitative analysis shows that the coccoliths of the extinct species *Ellipsolithus macellus* exhibit significantly lower variability than those of the living species *Gaarderia* and *Umbellosphaera***.** Although the morphology of the coccoliths of the three taxa are remarkably similar, they are also distinct in subtle ways. Both morphotypes of *Ellipsolithus* are similar in total size (length and width) to the macroliths of both *Gaarderia* and *Umbellosphaera* (figure 18a). They are also similar with regard to the surface areas of the margin (Figure 18c). In contrast, the central area (length and width) in *Ellipsolithus* is distinctly larger than that found in either micro- or macrolith of *Gaarderia* and *Umbellosphaera* (figure 18b). When comparing the surface area of the central area (SACA; figure 19a), *Ellipsolithus macellus* plots distinctively from the

species of *Gaarderia* and *Umbellosphaera* having a larger SACA and steeper regression. The primary difference between the *Ellipsolithus* morphotypes concerns their ellipticity, morphotype B being more circular than morphotype A. The lith-types of *Gaarderia* and *Umbellosphaera* also differ in their ellipticity. The long- elliptical morphotype A is similar in shape to the microliths of both *Gaarderia* and *Umbellosphaera*. The more circular Morphotype B resembles their macroliths (figure 19d). Interestingly, the ratio of SACA/SAM in both morphotypes reveals very low variability and plots as transitional between microliths and macroliths (figure 20).

Despite these interesting similarities the evidence is insufficiently strong to allow description of morphotypes A and B of *Ellipsolithus* as the counterparts of, respectively, the microliths and macroliths of *Gaarderia* and *Umbellosphaera*. However, as adaptation to mixotrophic physiology (Aubry, 2009; see below), the spirothecas of these two living genera are probably the result of a long evolutionary history and it would not be expected that fully developed spirothecas would be present in the early Paleocene ocean when coccolithophores only began adapting to nascent oligotrophy.

2.6.4. Are morphotypes A and B of Ellipsolithus macellus pseudo-cryptic species?

If morphotypes A and B are not poorly differentiated micro- and macroliths, they may be pseudo-cryptic species. Pseudo-cryptic species are taxa that are morphologically very similar (enough to be confused with one another) although differing by very subtle characters (Amato, 2010). Pseudo-crytpic species were first distinguished on the basis of studies in molecular biology (Saez et al., 2003 in the coccolithophores) and are now

routinely identified based on biometric/morphometric analysis (e.g., Huber et al, 1997; de Vargas et al., 1999 Amato and Montresor, 2008; Morard et al., 2009; Hagino et al., 2009; Amato, 2010; Lundholm et al., 2012). Extant and extinct pseudo-cryptic species of coccolithophores have been differentiated based on size, distinct size categories representing distinct genotypes (e.g., Knappertsbusch et al., 2000; Hagino et al., 2009). Morphotypes A and B occupy the same size ranges, and if size is the primary criterion for differentiation of pseudo-cryptic species, they do not qualify. The two morphotypes differ only by their overall shape, one being consistently more circular than the other. This, alone, would have to be indicative of cryptic speciation.

2.6.5. Description of morphotypes A and B of E. macellus

My data are inconclusive with regard to the status of the two morphotypes of *E. macellus*. I describe them to provide a basis for future studies concerned with this taxon.

Morphotype A (Pl. 1): This is a long-elliptical form. The dimensions (as measured in the Qreiya section) are as follow:

The total length is from 4.55 to 10.35 μm (mean length = 7.67 μm). Total width range from 2.58 to 6.61μm (mean = 4.56 μm). The length of the central area is from 2.63 to 5.74 μm (mean = 4.33 μm). The width of the central area is from 0.93 to 2.54 μm (mean = 1.69 μm). The width of the margin along the major axis is from 1.3 to 5.12 μm (mean = 3.34 μm). The width of the margin along the minor axis ranges from 1.25 to 4.30 μm (mean = 2.96 μm). Total ellipticity ranges from 0.22 to 0.55 (mean total ellipticity = 0.39). Central elliptically range from 0.47 to 0.74 (mean central ellipticity = 0.61).

There are strong positive correlations between the total length and total width (r = 0.85), the length and the width of the central area (r = 0.76), the widths of the margin along the major and minor axis (r= 0.72), and between the SAM and SACA (r= 0.75). There is no correlation between the total ellipticity and the central ellipticity (r= 0.37).

Morphotype B (Pl. 2): This is a broadly elliptical form. Dimensions (as measured in the Qreiya section) are as follow:

The total length is from 4.44 to 11.54 μm (mean length = 7.65 μm). Total width range from 3.32 to 9.05 μm (mean = 5.28 μm). The length of the central area is from 2.46 to 5.54 μm (mean = 4.16 μm). The width of the central area is from 1.06 to 2.9 μm (mean = 1.92 μm). The width of the margin along the major axis is from 1.98 to 6.46 μm (mean = 3.48 μm). The width of the margin along the minor axis ranges from 2.15 to 4.17 μm (mean = 3.37 μm). The total ellipticity ranges from 0.14 to 0.45 (mean total ellipticity = 0.31). The central elliptically ranges from 0.39 to 0.72 (mean central ellipticity = 0.54).

Remarks: Strong positive correlations are found between the measured variables, the total length and total width (r = 0.88), length and width of the central area (r = 0.74), total ellipticity and central ellipticity (r= 0.76), and between the SAM and SACA (r= 0.79). Noteworthy is the extremely strong correlation between the widths of the margin along the major and minor axis (r= 0. 89).

2.6.7. Adaptative morphology of the coccospheres of Umbellosphaera and Gaarderia

Whereas my test that morphotypes of *E. macellus* are the counterparts of the microliths and macroliths of spirotheca living species remains inconclusive, my study has shed further light on a likely role of coccoliths, and revealed slightly different strategies in the two extant genera that secrete them.

To understand the significance of the morphological differences between microliths and macroliths, it is necessary to consider their location on the cells. The microliths are directly in contact with the cell. The combination of a large central area, occupied by a grid, and a narrow margin maximizes the total surface of the cell in contact with the surrounding microliths. The macroliths are large, have a laterally flaring margin shaped like a funnel around the central area. Their central area/margin ratio is much smaller than in microliths, but, their central area is only slightly smaller than that of microliths (see above; Fig. 19). Macroliths considerably increase the diameter of the organism (perhaps by 2 folds) but, more importantly, they increase the surface area in contact with seawater. Ribs, knobs, pustules on their distal surface in some morphotypes only contribute further to increase this contact. In these coccospheres, the interface between cell and seawater is thus mediated by two superposed coccoliths arranged in such a manner that the central area of the macroliths is directed towards the central area of the underlying microliths (e.g., pl. 3, Fig. 1). Therefore the macroliths may be interpreted as serving as collectors of drifting organic particles or, perhaps more likely, as supports for diazotrophic bacteria capable of providing the coccolithophores in oligotrophic waters (where *Gaarderia* and *Umbellosphaera* are most abundant) with the fixed nitrogen that they could not obtain

otherwise. The food particles or the products of bacterial activity may be transferred to the microliths via the central area of the appropriately funnel-shaped macrolith. They may then be "filtered" into the cell through the grid that fills the central area of the microliths. In this perspective, there is a clear functional complementarity between microliths and macroliths. The former are strongly modified so that the margin is as narrow as possible, thereby maximizing exchanges between them and the cell; the macroliths are strongly modified so that the central area is as large as in microliths, but their flaring margin enhances contact with sea water. I interpret this as a complex morphological adaptation to mixotrophy, in agreement with Aubry (2009). Evidence of symbiosis between coccolithophores and bacteria has been shown through molecular studies of *Braarudosphaera bigelowii* (Thompson et al., 2013) whose coccoliths have been proposed as support for bacterial attachment (Aubry, 2013).

If the adaptative morphology to mixotrophy appears to be generally the same in *Gaarderia* and *Umbellosphaera*, this study also shows that it differs in the details between the two genera. In *Gaarderia* the transition from microliths to macroliths is abrupt, with only few intermediate coccoliths, if any. In contrast the transition is progressive in *Umbellosphaera*, where intermediate morphologies between macroliths and microliths occur. This implies that the coccoliths play an important role in regulating the physiology of cells. Rather than simple protective skeletal elements that may also act as ballast or as floating devices (Young, 1987), coccoliths would seem to play a fundamental role in the life of a coccolithophore.

2.7. Conclusions

Using statistical techniques (MANOVA, ANOVA, CVA) I have shown that *Ellipsolithus macellus* includes two morphotypes that differ clearly in ellipticity. I have compared them with the coccoliths that constitute the unusual coccospheres (with spirotheca) of the living species of *Gaarderia* and *Umbellosphaera* to test whether the coccosphere of E. *macellus* may have also been a spirotheca, which would represent an adaptation to mixotrophic physiology in the early Paleocene ocean. I have shown that there is morphologic similarity between morphotype B of *Ellipsolithus* and the macroliths of *Umbellosphaera* and *Gaarderia*, which may imply that the coccosphere of *Ellipsolithus* was a spirotheca, although the evidence is not compelling. The alternative possibility is that the two morphotypes of *E. macellus* represent distinct pseudo-cryptic species. The latter would differ only by ellipticity, and not size which is the primary character that has been used to distinguish pseudo-cryptic taxa among extinct populations. Thus at this time the interpretation of the two morphotypes is ambiguous. Extension of this study over the complete life span of the species may help resolve the uncertainty. Incidentally, I show that the coccospheres of *Umbellosphaera* and *Gaarderia*, although very similar, represent slightly different adaptive morphologies to mixotrophic physiology by these two coccolithophores.

2.7. References

Amato, A., 2010, Species concepts and definitions: reproductive isolation as a tool to reveal species boundaries: The Journal of Plant Reproductive Biology, v. 2, no. 2.

Amato, A., and Montresor, M., 2008, Morphology, phylogeny, and sexual cycle of *Pseudo-nitzschia mannii* sp. nov. (Bacillariophyceae): a pseudo-cryptic species within the *P. pseudodelicatissima* complex: Phycologia, v. 47, no. 5, p. 487–497, doi: 10.2216/07-92.1.

Aubry, M.-P., 2009, A Sea of Lilliputians: Palaeogeography, Palaeoclimatology, Palaeoecology, v. 284, no. 1, p. 88–113.

Aubry, M.-P., Rodriguez, O., Bord, D., Godfrey, L.V., and Knox, R.W.O., 2012, The First Radiation of the Fasciculiths: Morphologic adaptations of the coccolithophores to oligotrophy: Austrian Journal of Earth Sciences, v. 105/1, p. 29–38.

Aubry, M.-P., 2013. *Cenozoic coccolithophores: Syracosphaerales, Part 1, Volume E.* New York: Micropaleontology Press. Atlas of Micropaleontology series, pp. xxx.

Aubry, M.-P., Rodriguez, O., Bord, D., Godfrey, L., Schmitz, B., and Knox, R.W.O., 2012. The first radiation of the fasciculiths: Morphologic adaptations of the coccolithophores to oligotrophy. Austrian Journal of Earth Sciences, v. 105 (1): 29-38.

Aubry, M.-P., and Salem, R., 2013. The Dababiya Corehole: A Window into Paleocene to Early Eocene depositional history in Egypt based on coccolith stratigraphy. In Berggren, W. A., and Ouda, Kh.,(Eds.), *Early Paleogene history of upper Egypt: The Dababiya Corehole*. Stratigraphy, v. 9, nos. 3-4: pp. 287 – 346.

Berggren, W. A., & Norris, R. D., 1997. Biostratigraphy, phylogeny and systematics of Paleocene trochospiral planktic foraminifera. *Micropaleontology*, *43*, i-116.

Boersma, A., Premoli Silva, I., and Shackleton, N., 1987. Atlantic Eocene planktonic foraminiferal paleohydrographic indicators and stable isotope paleoceanography. Paleoceanogra- phy, 2, 287-331.

Bornemann, A., and Mutterlose, J., 2006, Size analyses of the coccolith species Biscutum constans and Watznaueria barnesiae from the Late Albian “Niveau Breistroffer” (SE France): taxonomic and palaeoecological implications: Géobios, v. 39, no. 5, p. 599–615, doi: 10.1016/j.geobios.2005.05.005.

Bralower, T.J., and Parrow, M., 1996, Morphometrics of the Paleocene coccolith genera Cruciplacolithus, Chiasmolithus, and Sullivania: a complex evolutionary history: Paleobiology,, p. 352–385.

Bramlette, M., and Sullivan, F., 1961, Coccolithophorids and related nannoplankton of the early Tertiary in California: Micropaleontology, v. 7, no. 2, p. 129.

Coxall, H. K., D’Hondt, S., and Zachos, J. C., 2006. Pelagic evolution and environmental recovery after the Cretaceous- Paleogene mass extinction. Geology, 34 (4), 297-300.

de Vargas, C., Norris, R.D., Zaninetti, L., Gibb, S.W., and Pawlowski, J., 1999, Molecular evidence of cryptic speciation in planktonic foraminifers and their relation

to oceanic provinces.: Proceedings of the National Academy of Science, v. 96, no. 6, p. 2864–2868,

Gradstein, F.M., Ogg, J.G., and Hilgen, F.J., 2012, On The Geologic Time Scale: Newsletters on Stratigraphy, v. 45, no. 2, p. 171–188.

Hagino, K., Takano, Y., and Horiguchi, T., 2009, Pseudo-cryptic speciation in Braarudosphaera bigelowii (Gran and Braarud) Deflandre: Marine Micropaleontology, v. 72, no. 3-4, p. 210–221,

Hammer, Ø., Harper, D.A.T., Ryan, P.D., 2009. PAST: Paleontological Statistics SoftwarePackage for Education and Data Analysis, Version 1.94. Palaeontol. Electron., 4, p. 9.

Huber, B.T., Bijma, J., and Darling, K., 1997, Cryptic speciation in the living planktonic foraminifer Globigerinella siphonifera (d'Orbigny): Paleobiology,, p. 33–62.

Kleijne, A., 1993. *Morphology, Taxonomy and Distribution of Extant Coccolithophorids (Calcareous Nannoplankton)*. Enschede, The Netherlands: FEBO, 169–226.

Knappertsbusch, M.W., 2000, Morphologic evolution of the coccolithophorid Calcidiscus leptoporus from the Early Miocene to Recent: Journal of Paleontology, v. 74, no. 4, p. 712.

Kuiper, K.F., Deino, A., Hilgen, F.J., Krijgsman, W., Renne, P.R., and Wijbrans, J.R., 2008, Synchronizing rock clocks of Earth history: Science, v. 320, p. 500–504.

Lundholm, N., Bates, S.S., Baugh, K.A., Bill, B.D., Connell, L.B., Léger, C., and Trainer, V.L., 2012, Cryptic and Pseudo-Cryptic Diversity in Diatoms-with Descriptions of Pseudo-Nitzschia Hasleana Sp. Nov. and P. Fryxelliana Sp. Nov.1: Journal of Phycology, v. 48, no. 2, p. 436–454

Morard, R., Quillévéré, F., Escarguel, G., Ujiié, Y., de Garidel-Thoron, T., Norris, R.D., and de Vargas, C., 2009, Morphological recognition of cryptic species in the planktonic foraminifer *Orbulina universa*: Marine Micropaleontology, v. 71, no. 3-4, p. 148–165,

Revelle, W., 2013. psych: Procedures for Personality and Psychological Research, Northwestern University, Evanston, Illinois, USA, http://CRAN.R-project.org/package=psych Version = 1.3.2.

Rodríguez, O. M. and Aubry, M.-P., 2006. Lower to middle (Danian-Selandian) Paleocene calcareous nannofossil stratigraphy of the Qreiya section (Egypt). In Caballero, F., Apellaniz, E., Baceta, J. L., Orue-Etxebarria, X., Payros, A., and Pujalte, V. (ed.s), *Climate and Biota of the Early Paleogene. Abstract volume,* 111. Bilbao: Croman S. A.

Romein, A.J.T., 1979, Lineages in early Paleogene calcareous nannoplankton: Utrecht Micropaleontological Bulletins, v. 22.

RStudio, 2012. RStudio: Integrated development environment for R (Version 0.97.551) [Computer software]. Boston, MA. Available from http://www.rstudio.org/

Sáez, A.G., Probert, I., Geisen, M., Quinn, P.S., Young, J.R., and Medlin, L.K., 2003, Pseudo-cryptic speciation in coccolithophores.: Proceedings of the National Academy of Science, v. 100, no. 12, p. 7163–7168, doi: 10.1073/pnas.1132069100.

Speijer, R. 2003. Danian-Selandian sea-level change and biotic excursion on the southern Tethyan margin (Egypt). In: Wing, S.L., Gingerich, P.D., Schmitz, B. And Thomas E., Eds., Causes and Consequences of globally warm climates in the Early Paleogene, 275-290. Boulder, Colorado, Geological Society of America. Special Paper 369, 275-290.

Sprong, J., Speijer, R. P. and Steurbaut, E., 2009. Biostratigraphy of the Danian/Selandian transition in the southern Tethys. Special reference to the Lowest Occurrence of planktic fora- minifera Igorina albeari. Geologica Acta, 7, 63-77._

Thompson, A.W., Foster, R.A., Krupke, A., Carter, B.J., Musat, N., Vaulot, D., Kuypers, M.M.M., and Zehr, J.P., 2012, Unicellular Cyanobacterium Symbiotic with a Single-Celled Eukaryotic Alga: Science (New York, NY), v. 337, no. 6101, p. 1546–1550

Venables, W. N. & Ripley, B. D., 2002. Modern Applied Statistics with S. Fourth Edition. Springer, New York. ISBN 0-387-95457-0

Wickham, H. 2009. ggplot2, elegant graphics for data analysis. Springer New York,

Young, J.R., 1987, Possible functional interpretations of coccolith morphology: Abhandlungen der Geologischen Bundesanstalt, v. 39, p. 305–313.

2.8. Figure Captions

Figure 1.
Map of Egypt. Qreiya, location of samples.

Figure 2.
The Qreiya section as measured in my study. *Ellipsolithus* coccoliths are generally most abundant in a ~20 m-thick interval between the base of the section at level -16 and level +3.2 m partially represented by the yellow box. Black arrows indicate position of samples selected for this study: Q-2.0, Q-0.8, Q+1.1, Q+2.0, Q+3.2. Figure modified from Aubry et al. 2012

Figure 3.
Temporal distribution of evolutionary events (modified from Aubry and Bord, 2009). Purple bar is range of *Ellipsolithus* macellus (~63.25 Ma to ~54 Ma). First radiation of the fasciculiths (~ 62.13 Ma) yellow bar = range of fasciculiths. Blue bar is the diversification of the spine-bearing planktonic foraminifera *Acarinina* and *Morozovella* (~62.60 Ma). Light blue bar = range of *Umbellosphaera*; light green bar = range of *Gaarderia*. Red line is the Cretaceous/ Paleogene mass extinction; green shading is the Paleocene/Eocene turnover; violet shading is the Eocene/Oligocene turnover. Figure modified from Aubry and Bord, 2009

Figure 4.
Variables measured in this study: (a) length along the major axis = total length, (b) width long the minor axis = total width, (c) length of the central area along the major axis, (d) width of the central area along the minor axis. Calculated variables: (e) width of the margin along the major axis = (a) - (c), (f) width of the margin along the minor axis = (b) - (d).

Figure 5.
Relative frequency distribution with relative density curves for *Gaarderia* (blue), *Umbellosphaera* (green), and *Ellipsolithus* (orange). Measured and calculated variables; (a) total length, (b) total width, (c) length of the central area, (d) width of the central area, (e) width of the margin along the major axis, and (f) minor axis. Dashed vertical lines indicate the position of the mean values. Note: outliers presented in *Gaarderia* and *Umbellosphaera* are due to mislabeled scale bars in reprinted micrographs. Outliers removed from other figures and from statistical analysis. Illustrations show the general shape for each group and indicate the measured variable.

Figure 6.
Relative frequency distributions and relative density curves for the measured and calculated variables of *Gaarderia* deconstructed by the microliths (dark blue) and the macroliths (light blue). Colored illustrations show the general shape for micro- and macroliths and indicate the measured variable. (see figure 1 for description of variables).

Figure 7.

Scatter plots with linear regression lines for the measured and calculated variables of *Gaarderia* lith-types, microliths (inverted triangle, dark blue) and macroliths (triangle, light blue). (a) total length to total width, (b) central length to central width, (c) margin major to minor axis, (d) total ellipticity to central ellipticity,(e) surface area of the margin (SAM) to central surface area (SACA), (f) surface area of the margin (SAM) to margin ratio. See table 2 for linear regression coefficients and line equation. Colored illustrations show the general shape for micro- and macroliths and indicate the measured variable. Grey illustrations show the inferred shapes expected in each plot quadrant. SAM and SACA show strong positively correlation. A steeper correlation in the microliths suggests higher SACA variability than in macroliths. In microliths, no correlations are found between the margin ratio and SAM. Variability along the margins ratio is high in microliths. In macroliths, SAM exhibits high variability.

Figure 8.
Relative frequency distributions and relative density curves for the measured and calculated variables of *Umbellosphaera* deconstructed by microliths (dark green), I-lith (light green), macroliths (medium green). Colored illustrations show the general shape for micro-, I-liths, and macroliths and indicate the measured variable. (see figure 1 for description of variables)

Figure 9.
Scatter plots with linear regression lines for the measured and calculated variables for *Umbellosphaera* lith-types, microliths (inverted triangles, dark green), I-lith (squares, light green), and macroliths (triangles, green). (see Figure 7 for description of bivariate combinations; See table 2 for linear regression and equation). Colored illustrations show the general shape for micro-, I-liths, and macroliths and indicate the measured variable. Grey illustrations show the inferred shapes expected in each plot quadrant. SAM and SACA are positively correlated. SACA has lower variability. Microliths and I-liths show no correlations between the margin ratio and SAM, and a slight positive correlation in macroliths.

Figure 10.
Relative frequency distributions and relative density curves for the measured and calculated variables of *Ellipsolithus* deconstructed by morphotype A. (orange, circles) and B. (yellow, diamonds). Colored illustrations show the general shape for morphotypes A and B. (see figure 1 for description of variables)

Figure 11.
Scatter plots with linear regression lines for the measured and calculated variables for *Ellipsolithus*, morphotype A (circles, yellow) and B (diamonds, orange). (see Figure 7 for description of bivariate combinations; See table 2 for linear regression and equation). Colored illustrations show the general shape for morphotypes A and B. Grey illustrations show the inferred shapes expected in each plot quadrant SAM and SACA are strongly correlated in both morphotypes. No correlation is presented between the margin ratio and SAM.

Figure 12.
Relative frequency distribution with relative density curves for transformed data.

Figure 13.
Multivariate allometric coefficient plot. Dashed horizontal line represents the coefficient $\alpha = 1$. Calculated allometric coefficient are represented by the central tic mark, bars are the 95% confidence intervals. Isometric growth is represented by a coefficient of 1or implied if within confidence interval. (**a)**. *Ellipsolithus*; all (light orange), morphotype A (yellow), morphotype B (gold). (**b)**. *Gaarderia*; all (blue), microliths (dark blue), macroliths (light blue). (**c)**. *Umbellosphaera*; all (dark green), microliths (green), I-liths (light green), macroliths (bright green).

Figure 14.
Scatter plots of transformed data with linear regression lines of *Ellipsolithus*; (a) SAM to SACA, (b) SAM to total ellipticity, (c) SACA to central ellipticity, and (d) SACA to total ellipticity. See caption 8 for description of colors and symbols

Figure 15.
Scatter plots of transformed data with linear regression lines of Gaarderia; a) SAM to SACA, (b) SAM to total ellipticity, (c) SACA to central ellipticity, and (d) SACA to total ellipticity. See caption 4 for description of colors and symbols

Figure 16.
Log-transformed bivariate scatter plots with linear regression line of Umbellosphaera; a) SAM to SACA, (b) SAM to total ellipticity, (c) SACA to central ellipticity, and (d) SACA to total ellipticity. See caption 6 for description of colors and symbols

Figure 17.
Canonical variates analysis on the transformed data. Ordination of coccolith shapes along the first two canonical variates axes. First and second axes describes 97% of the dispersion between the genera. *Ellipsolithus,* orange. (circles = morphotype A, diamonds = morphotype B); *Gaarderia*, blue (inverted triangle = microliths, triangle = macroliths; *Umbellosphaera*, green (inverted triangles = microliths, squares = I- lith, and triangles = macroliths). Superimposed on each group is a calculated 95% confidence ellipse.

Figure 18.
Comparative Bivariate scatter plot analysis of transformed data. *Ellipsolithus,* orange. (circles = morphotype A, diamonds = morphotype B); *Gaarderia*, blue (inverted triangle = microliths, triangle = macroliths; *Umbellosphaera*, green (inverted triangles = microliths, squares = I- lith, and triangles = macroliths).

Figure 19.
Comparative Bivariate scatter plot analysis of transformed data. *Ellipsolithus,* orange. (circles = morphotype A, diamonds = morphotype B); *Gaarderia*, blue (inverted triangle = microliths, triangle = macroliths; *Umbellosphaera*, green (inverted triangles = microliths, squares = I- lith, and triangles = macroliths).

Figure 20.
Comparison of the ratio SACA/SAM to the total ellipticity. *Ellipsolithus,* orange. (circles = morphotype A, diamonds = morphotype B); *Gaarderia*, blue (inverted triangle = microliths, triangle = macroliths; *Umbellosphaera*, green (inverted triangles = microliths, squares = I- lith, and triangles = macroliths).

2.9. Table captions

Table 1.

A list of descriptive statistics for all measured and calculated variables. Mean, standard deviation (stand. dev.), median, minimum (min), maximum (max), range, skewness (skew), kurtosis, and standard error (stand. err.)

Table 2.

Pearson's correlation coefficient (r), Coefficient of determination (r2), and linear regression equation formula

Table 3.

Pairwise comparison (Hotelling's T^2) of Qreiya samples with and *Ellipsolithus* morphotypes.
Significant values at the 5% significance level in bold.

2.10. Plate Captions

Plate 1.

Micrographs of *Ellipsolithus macellus* Morphotype A, transmitted cross-polarized light. 1, 10) Q+3.2; 2, 4, 6, 8, 9, 11 - 15, 20) Q-0.8; 3, 16) Q+1.1; 5, 19) Q+2.0; 7, 17, 18) Q-2.0

Plate 2.

Micrographs of *Ellipsolithus macellus* Morphotype B, transmitted cross-polarized light. **1, 2, 17, 20)** Q-2.0; **3)** Q+1.1; **4 - 8, 11, 13, 14 , 18, 19**) Q-0.8; **9, 10)** Q+2.0; **12)** Q+1.1; **15, 16)** Q+3.2

Plate 3. Scanning electron micrographs.

1) Spirothecate coccosphere of *Gaarderia corolla* (Lecal) Kleijne, 1993. From Aubry, 2009, pl.2, Figs. 4. **2- 5)** Spirothecate coccosphere *Umbellosphaera irregularis* (Kamptner) Paasche in Markali and Paasche 1955 type 1 Kleijne, 1993. From Aubry, 2009, pl.3, Figs. 1- 3, pl.2, Figs. 5. **6)** Spirothecate coccosphere of *Umbellosphaera tenuis* Umbellosphaera tenuis (Kamptner) Paasche in Markali and Paasche 1955 type 4 Kleijne, 1993. From Aubry, 2009, pl.2, Figs. 6

Figure 1.

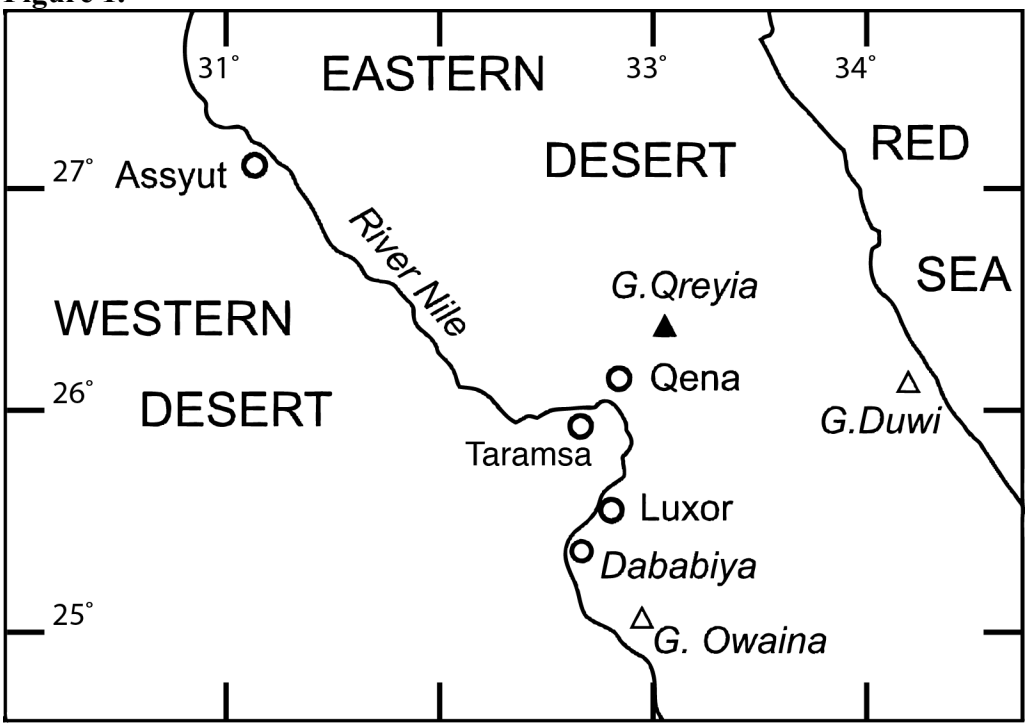
31°
EASTERN
33°
34°
RED
DESERT
27°
Assyut
River Nile
SEA
G.Qreyia
WESTERN
Qena
26°
DESERT
G.Duwi
Taramsa
Luxor
Dababiya
25°
G. Owaina

Figure 2.

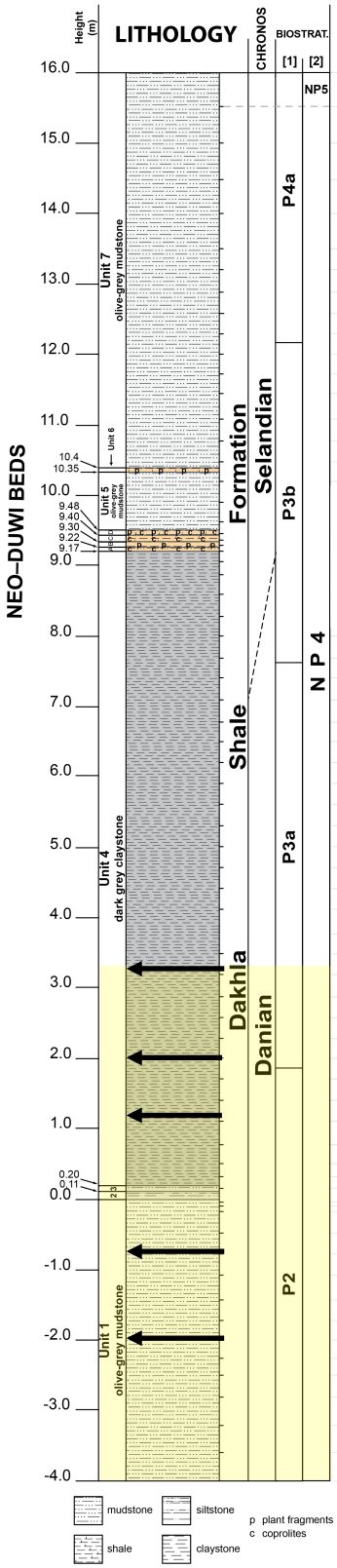
Height (m)
LITHOLOGY
CHRONOS
BIOSTRAT.
[1]
[2]
NP5
P4a
P3b
P3a
P2
N P 4
Selandian
Formation
Shale
Dakhla
Danian
NEO–DUWI BEDS
Unit 7
olive-grey mudstone
Unit 6
Unit 5
olive-grey mudstone
Unit 4
dark grey claystone
Unit 1
olive-grey mudstone
16.0
15.0
14.0
13.0
12.0
11.0
10.4
10.35
10.0
9.48
9.40
9.30
9.22
9.17
9.0
8.0
7.0
6.0
5.0
4.0
3.0
2.0
1.0
0.20
0.11
0.0
-1.0
-2.0
-3.0
-4.0
mudstone
siltstone
shale
claystone
p plant fragments
c coprolites

Figure 3.

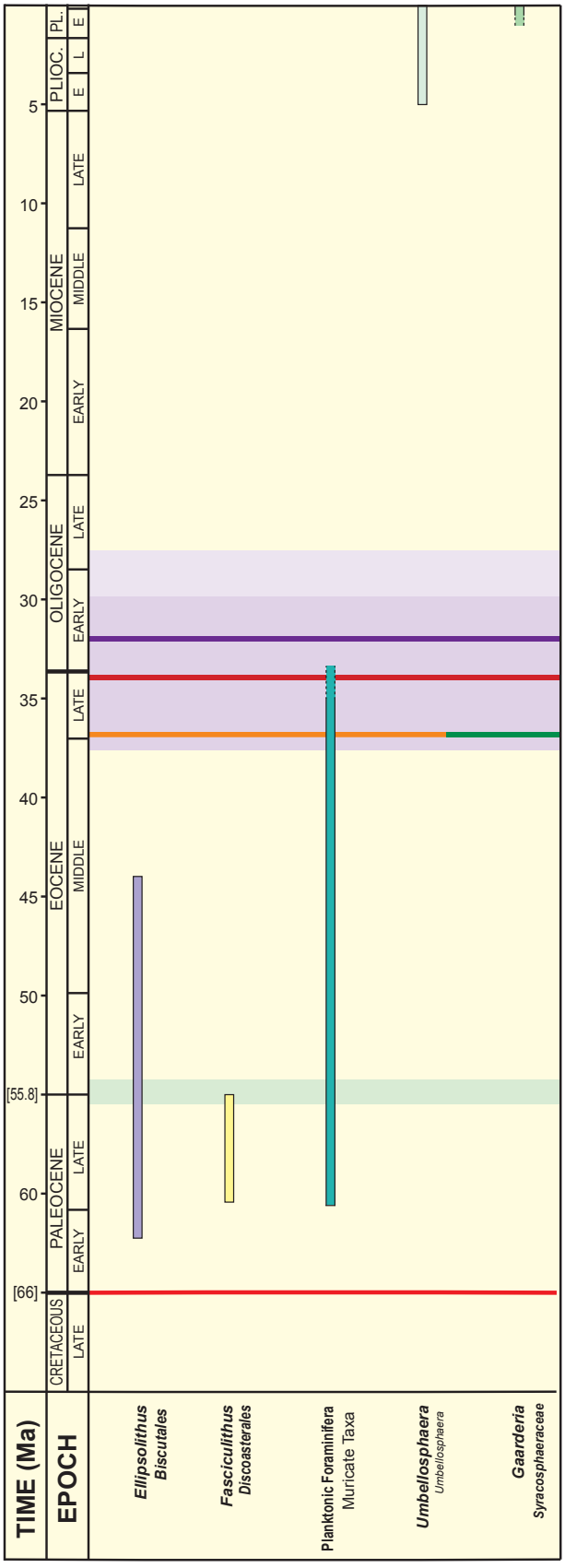
TIME (Ma)
EPOCH
CRETACEOUS
LATE
PALEOCENE
EARLY
LATE
EOCENE
EARLY
MIDDLE
LATE
OLIGOCENE
EARLY
LATE
MIOCENE
EARLY
MIDDLE
LATE
PLIOC.
E
L
PL.
E
5
10
15
20
25
30
35
40
45
50
[55.8]
60
[66]
Ellipsolithus Biscutales
Fasciculithus Discoasterales
Planktonic Foraminifera Muricate Taxa
Umbellosphaera Umbellosphaera
Gaarderia Syracosphaeraceae

Figure 4.

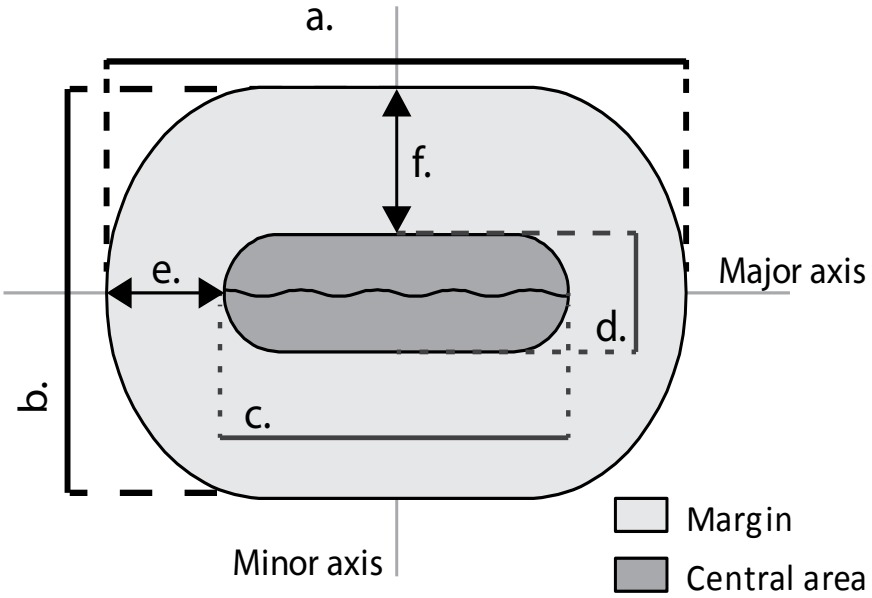

Figure 5.

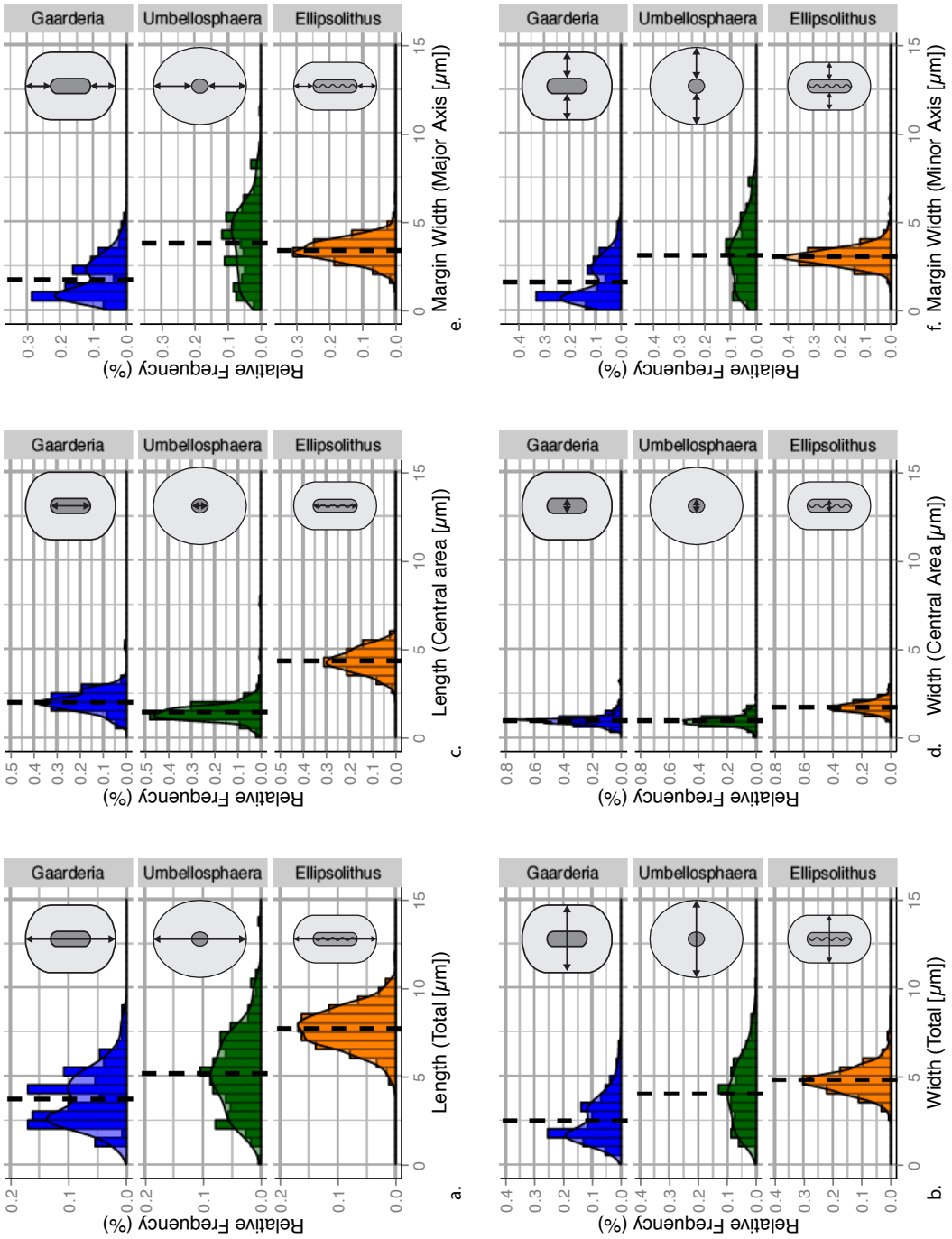
Gaarderia
Umbellosphaera
Ellipsolithus
Relative Frequency (%)
Length (Total [µm])
a.
Width (Total [µm])
b.
Length (Central area [µm])
c.
Width (Central Area [µm])
d.
Margin Width (Major Axis [µm])
e.
Margin Width (Minor Axis [µm])
f.

Figure 6.

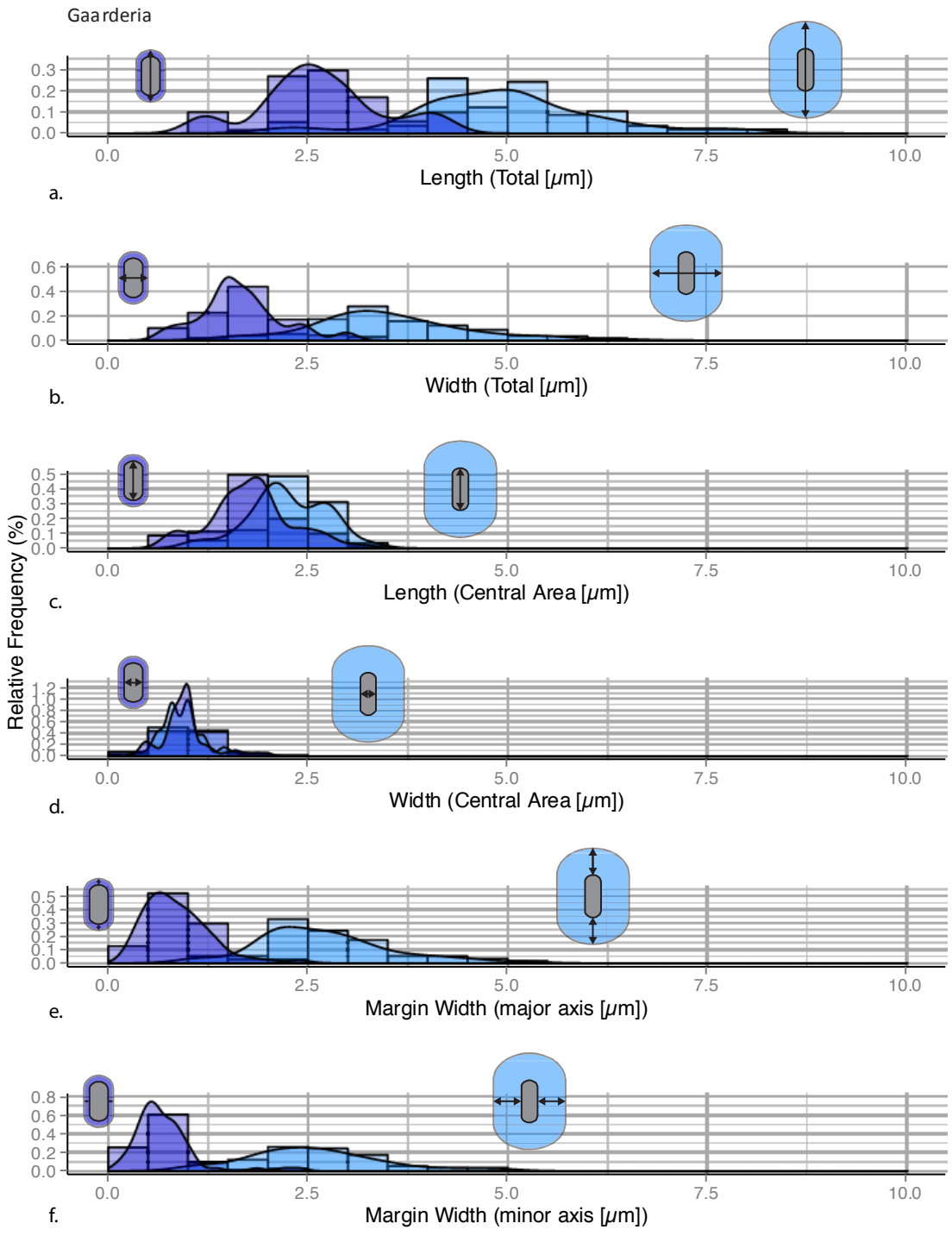
Gaarderia
Relative Frequency (%)
Length (Total [μm])
a.
Width (Total [μm])
b.
Length (Central Area [μm])
c.
Width (Central Area [μm])
d.
Margin Width (major axis [μm])
e.
Margin Width (minor axis [μm])
f.

Figure 7.

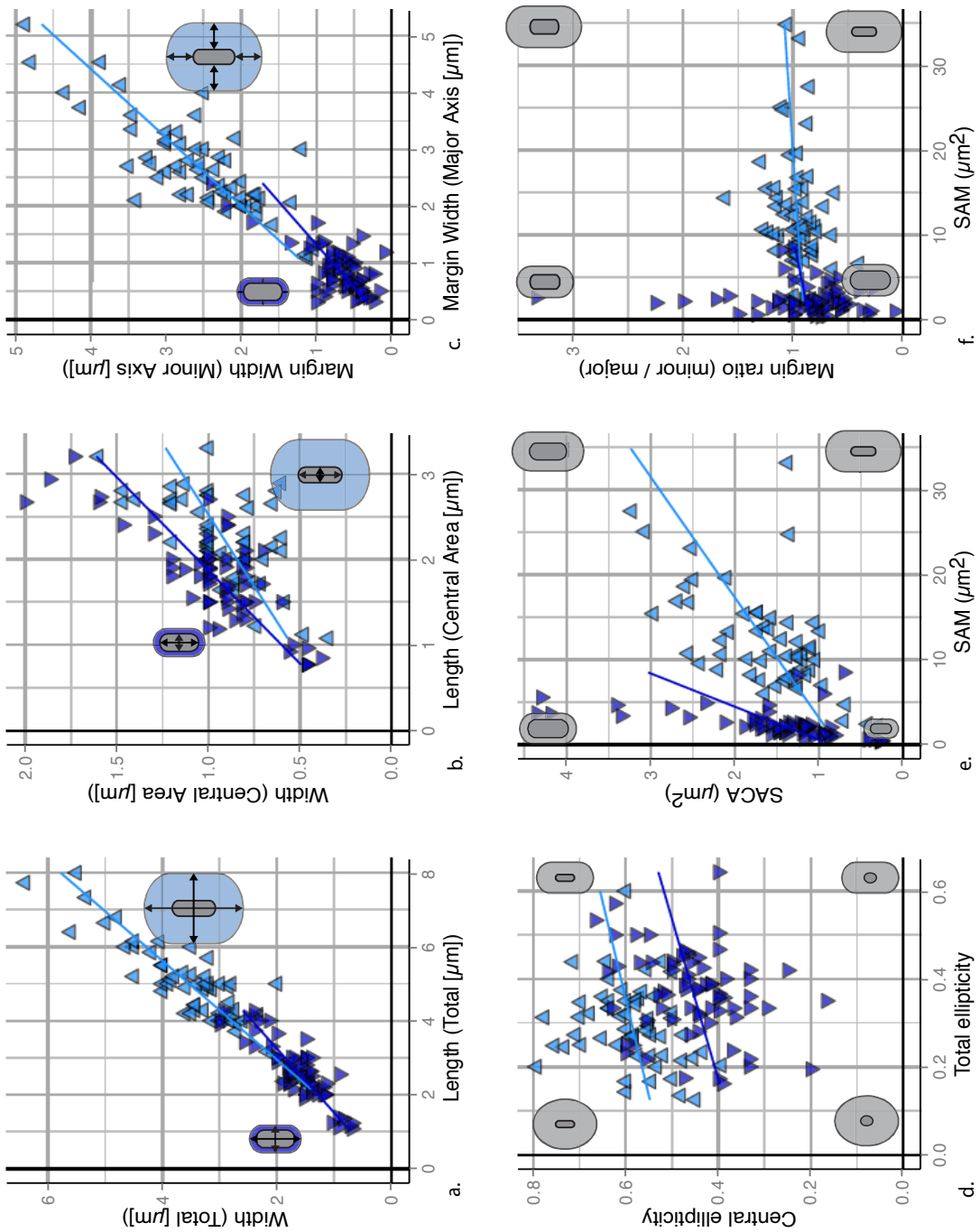
a.
Length (Total [μm])
Width (Total [μm])
b.
Length (Central Area [μm])
Width (Central Area [μm])
c.
Margin Width (Major Axis [μm])
Margin Width (Minor Axis [μm])
d.
Total ellipticity
Central ellipticity
e.
SAM (μm2)
SACA (μm2)
f.
SAM (μm2)
Margin ratio (minor / major)

Figure 8

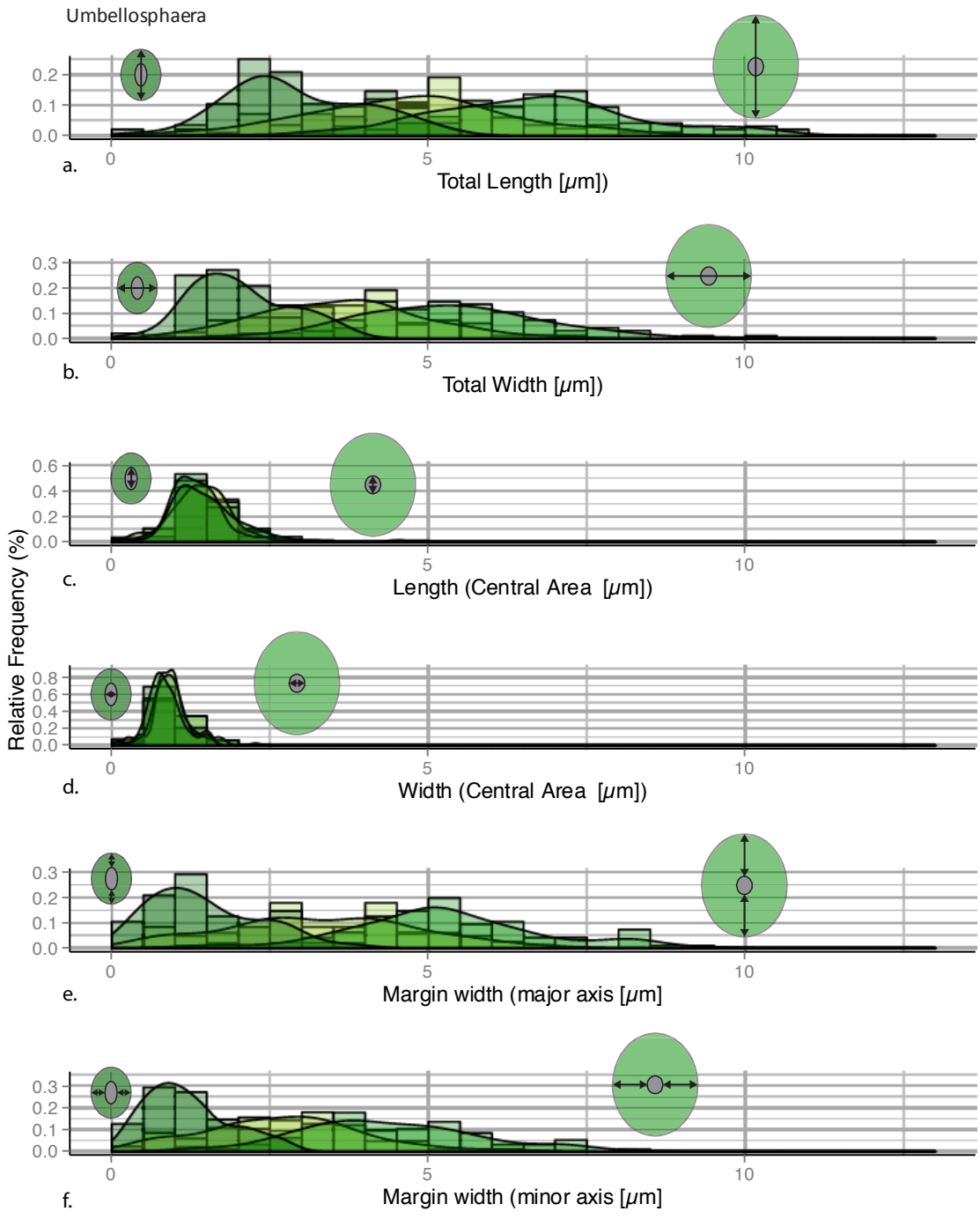
Umbellosphaera
Relative Frequency (%)
a.
Total Length [μm])
b.
Total Width [μm])
c.
Length (Central Area [μm])
d.
Width (Central Area [μm])
e.
Margin width (major axis [μm]
f.
Margin width (minor axis [μm]

Figure 9

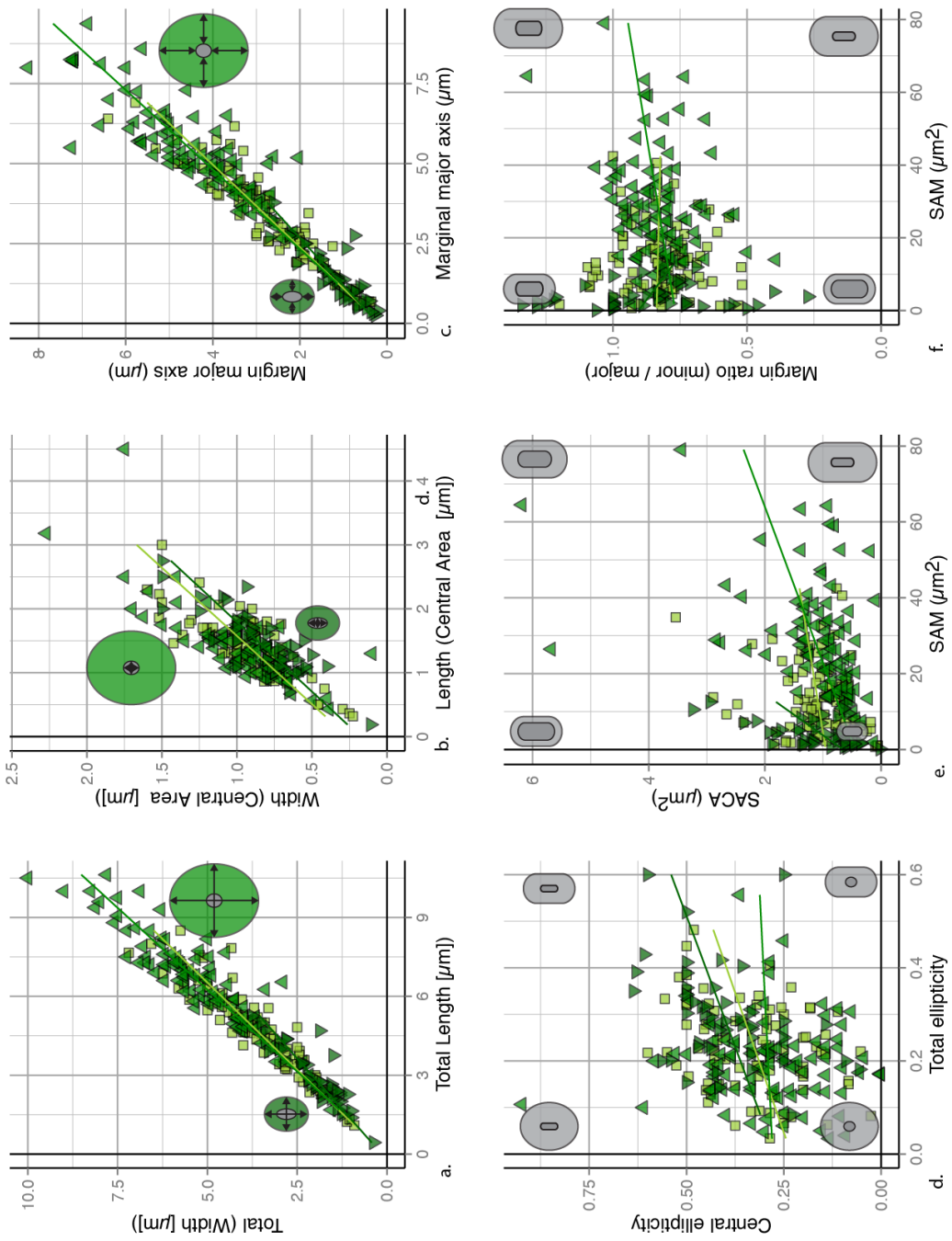
a.
Total Length [µm])
Total (Width [µm])
b.
Length (Central Area [µm])
Width (Central Area [µm])
c.
Marginal major axis (µm)
Margin major axis (µm)
d.
Total ellipticity
Central ellipticity
e.
SAM (µm2)
SACA (µm2)
f.
SAM (µm2)
Margin ratio (minor / major)

Figure 10.

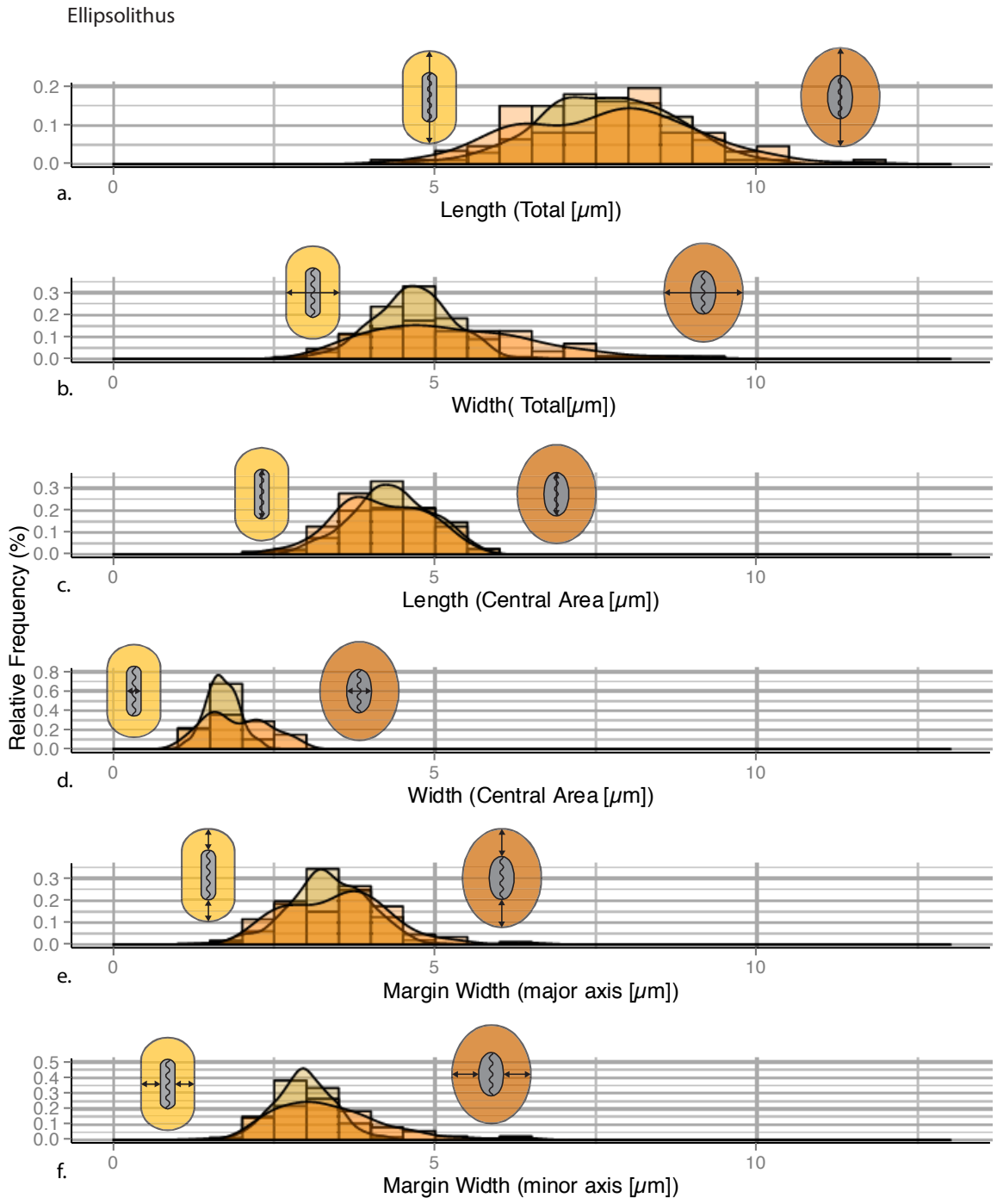
Ellipsolithus
Relative Frequency (%)
a.
Length (Total [μm])
b.
Width(Total[μm])
c.
Length (Central Area [μm])
d.
Width (Central Area [μm])
e.
Margin Width (major axis [μm])
f.
Margin Width (minor axis [μm])

Figure 11

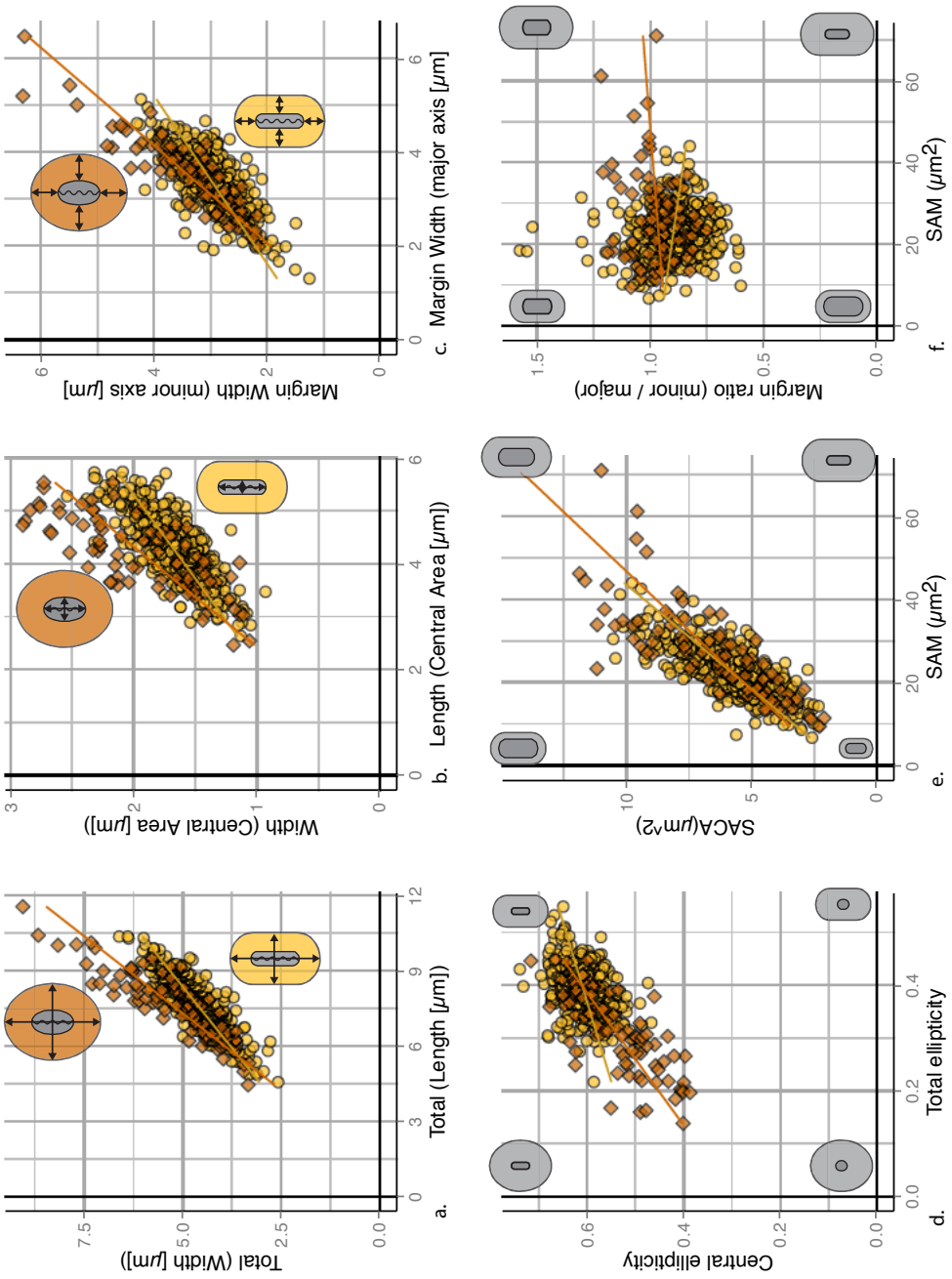
a.
Total (Length [μm])
Total (Width [μm])
b.
Length (Central Area [μm])
Width (Central Area [μm])
c.
Margin Width (major axis [μm])
Margin Width (minor axis [μm])
d.
Total ellipticity
Central ellipticity
e.
SAM (μm2)
SACA(μm^2)
f.
SAM (μm2)
Margin ratio (minor / major)

Figure 12.

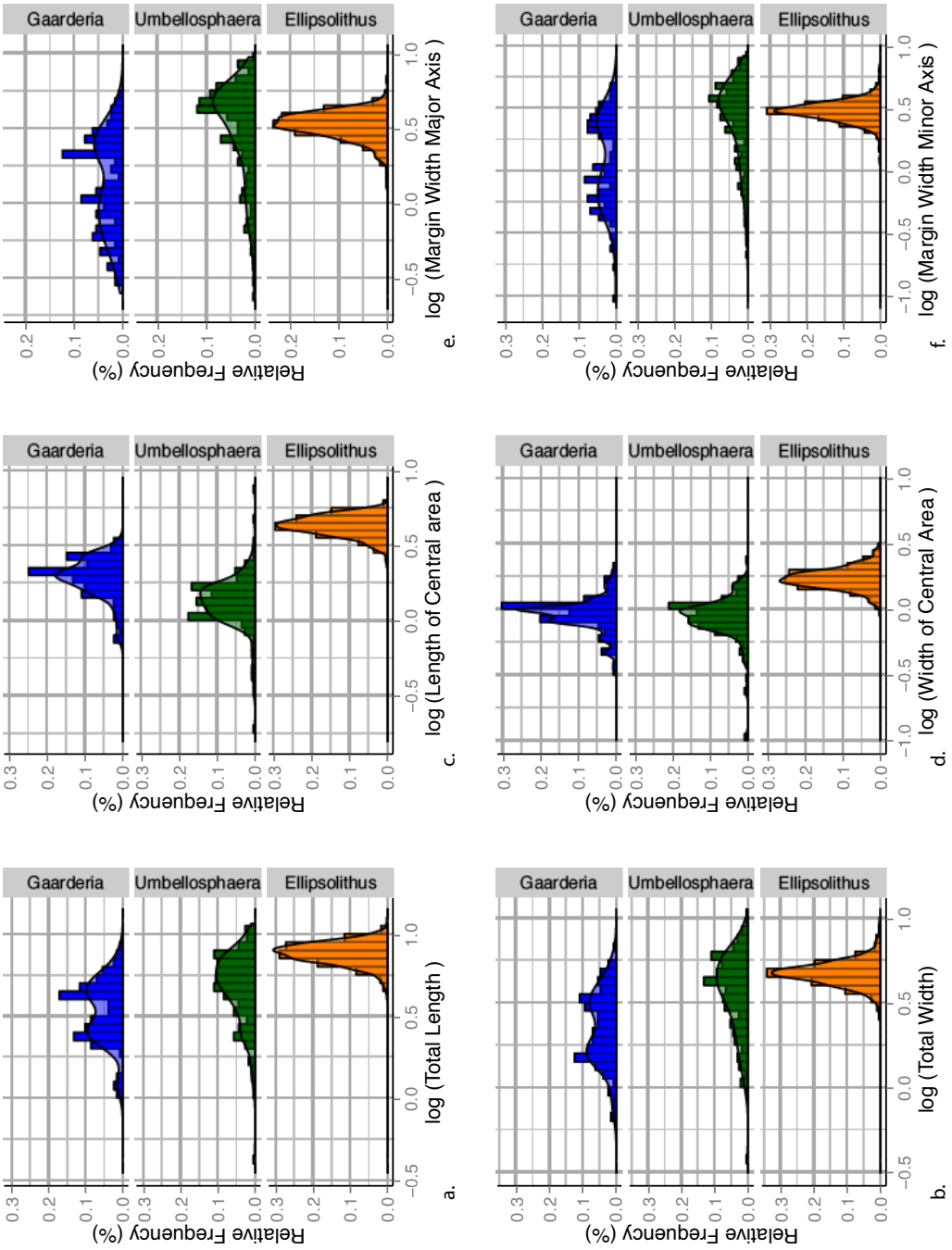
Gaarderia
Umbellosphaera
Ellipsolithus
Relative Frequency (%)
log (Total Length)
a.
log (Total Width)
b.
log (Length of Central area)
c.
log (Width of Central Area)
d.
log (Margin Width Major Axis)
e.
log (Margin Width Minor Axis)
f.

Figure 13.

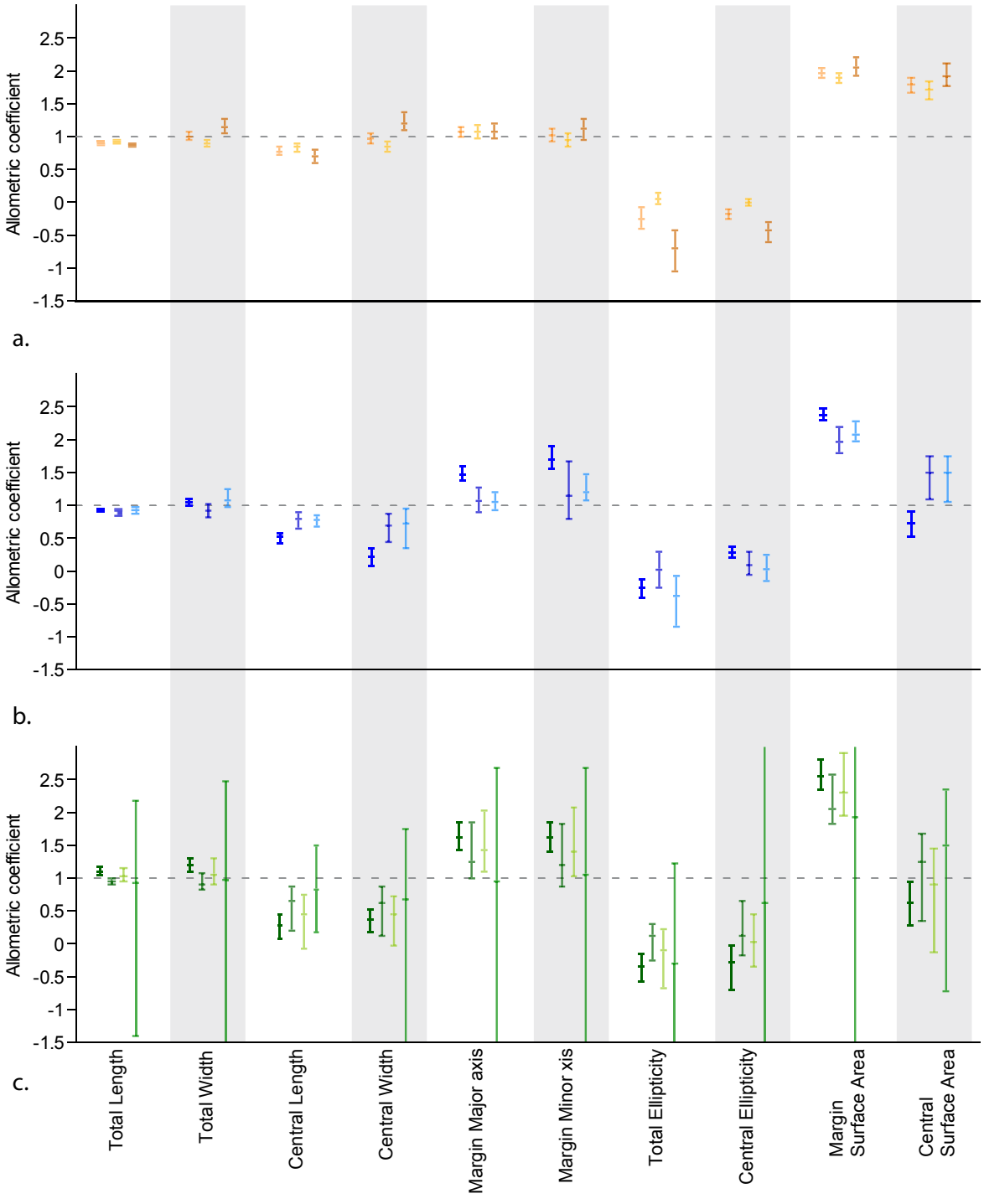
Allometric coefficient
2.5
2
1.5
1
0.5
0
-0.5
-1
-1.5
a.
b.
c.
Total Length
Total Width
Central Length
Central Width
Margin Major axis
Margin Minor xis
Total Ellipticity
Central Ellipticity
Margin Surface Area
Central Surface Area

Figure 14.

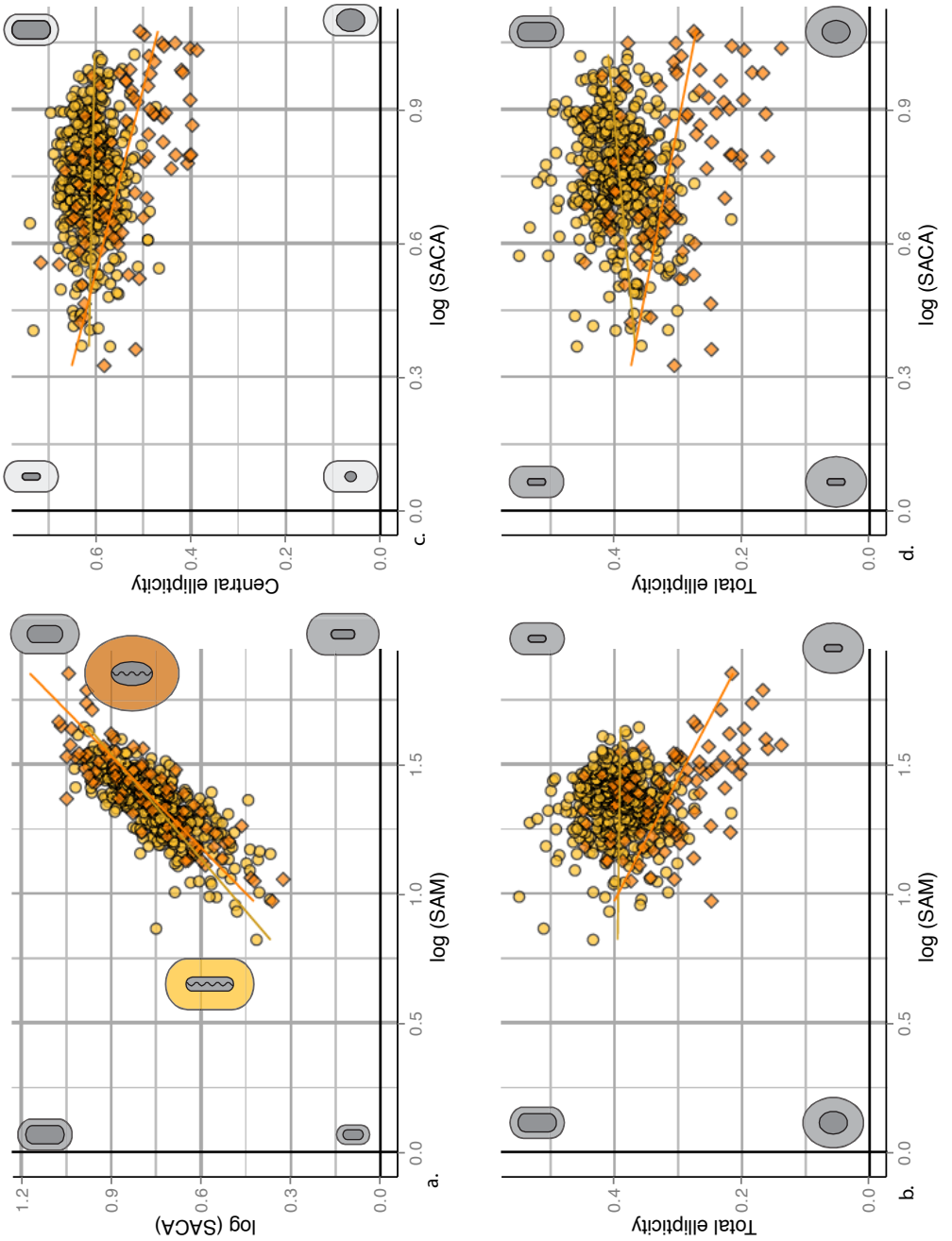
a.
b.
c.
d.
log (SACA)
log (SAM)
Central ellipticity
Total ellipticity
0.0
0.3
0.5
0.6
0.9
1.0
1.2
1.5
0.2
0.4

Figure 15.

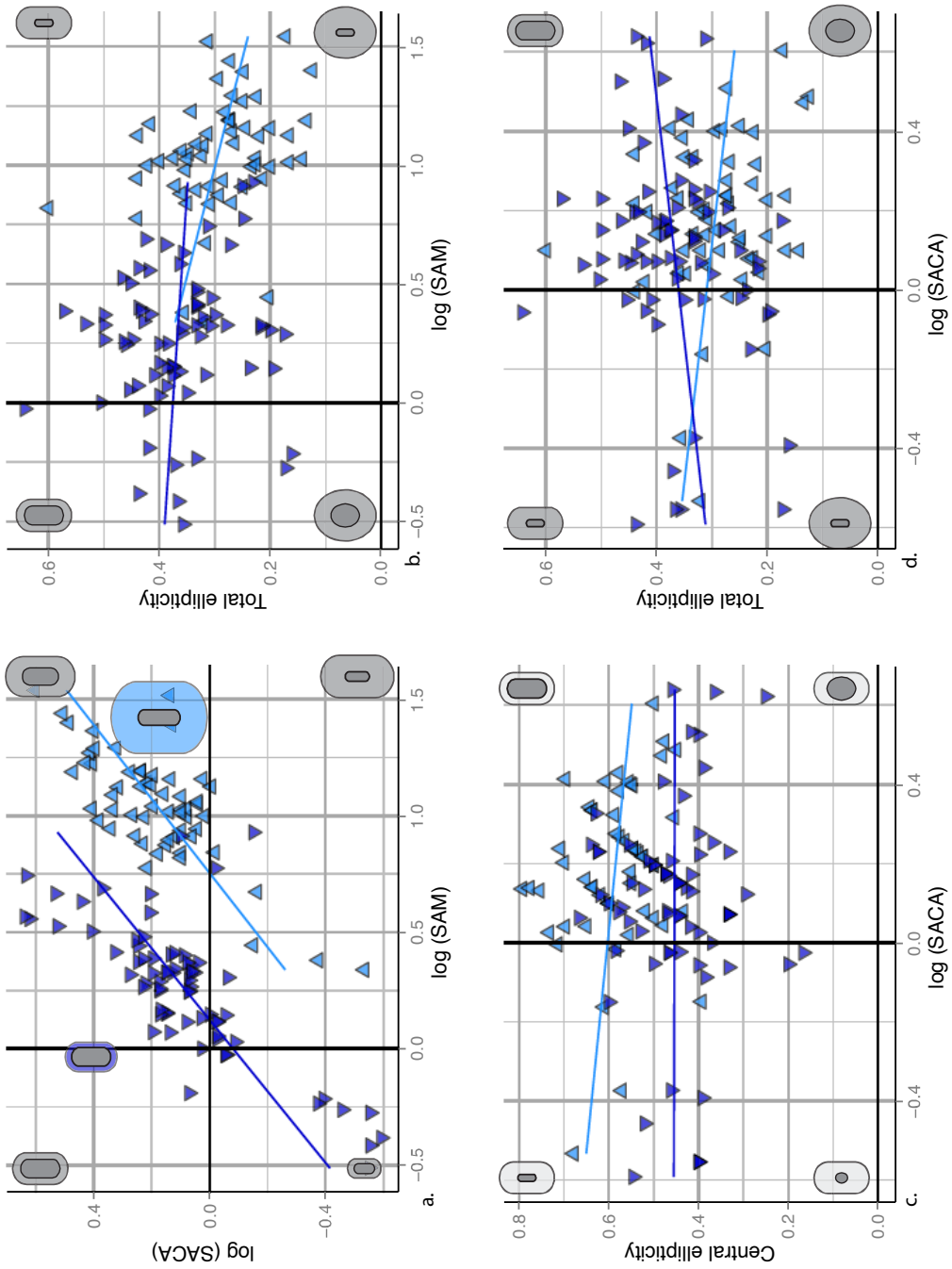
a.
b.
c.
d.
log (SACA)
log (SAM)
Total ellipticity
Central ellipticity
0.4
0.0
−0.4
−0.5
0.0
0.5
1.0
1.5
0.0
0.2
0.4
0.6
0.8

Figure 16.

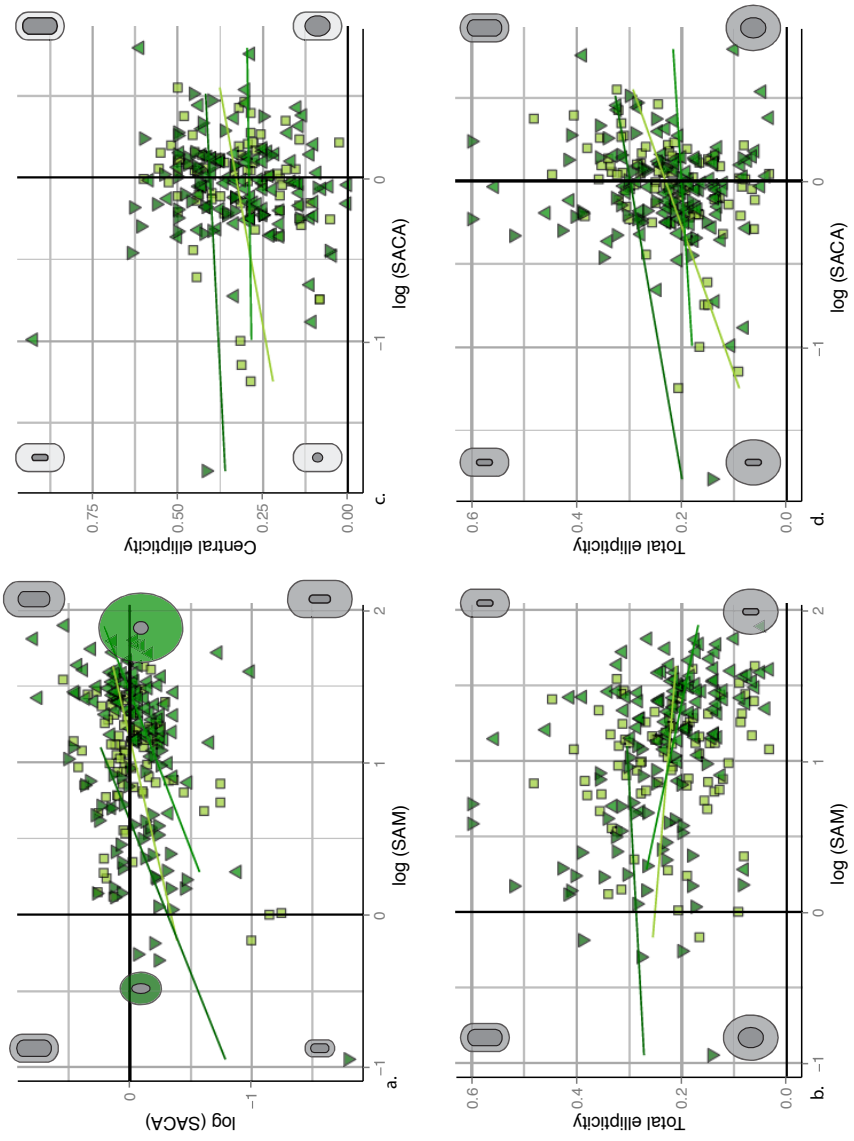
a.
log (SACA)
log (SAM)
b.
Total ellipticity
log (SAM)
c.
Central ellipticity
log (SACA)
d.
Total ellipticity
log (SACA)

Figure 17.

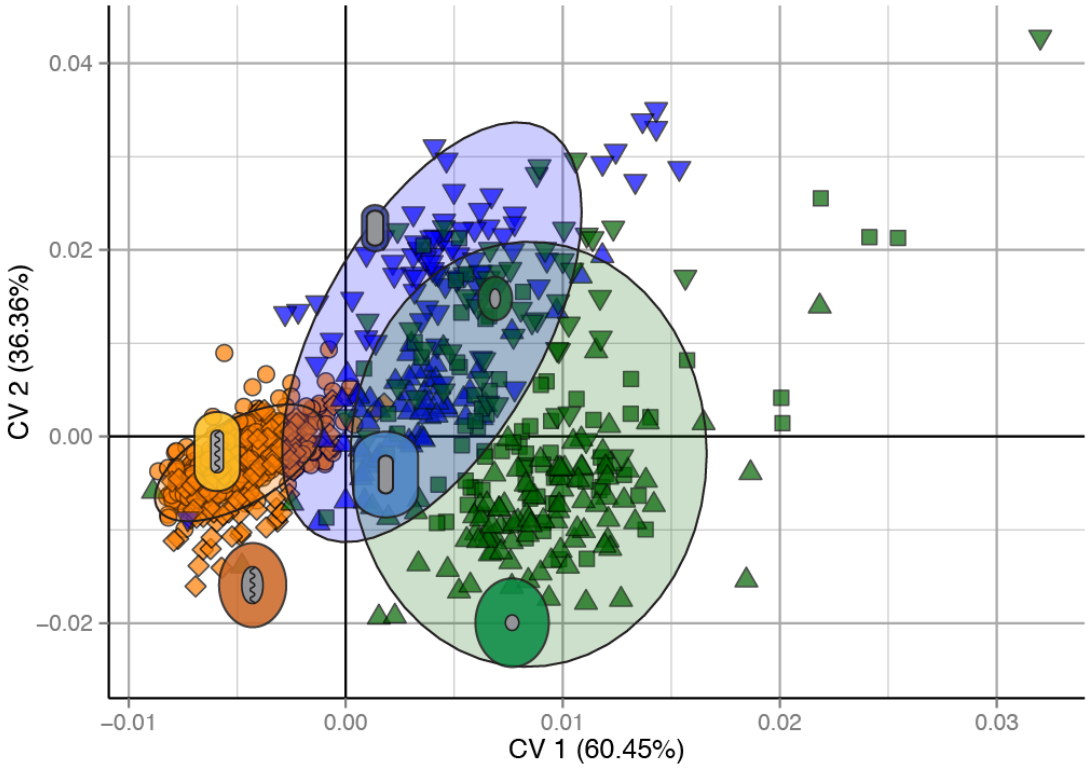

Figure 18.

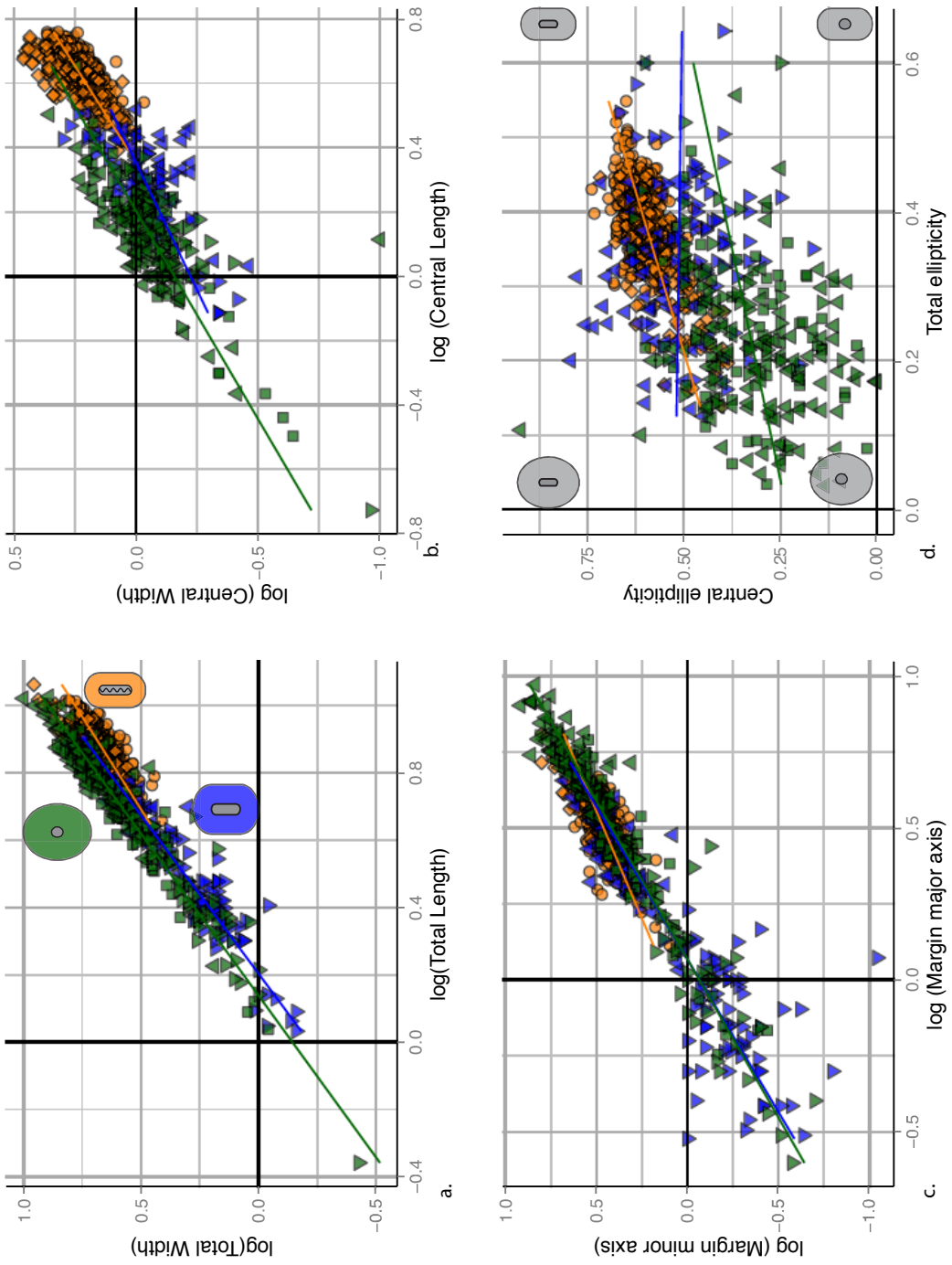
log(Total Width)
log(Total Length)
a.
log (Central Length)
log (Central Width)
b.
log (Margin minor axis)
log (Margin major axis)
c.
Central ellipticity
Total ellipticity
d.

Figure 19.

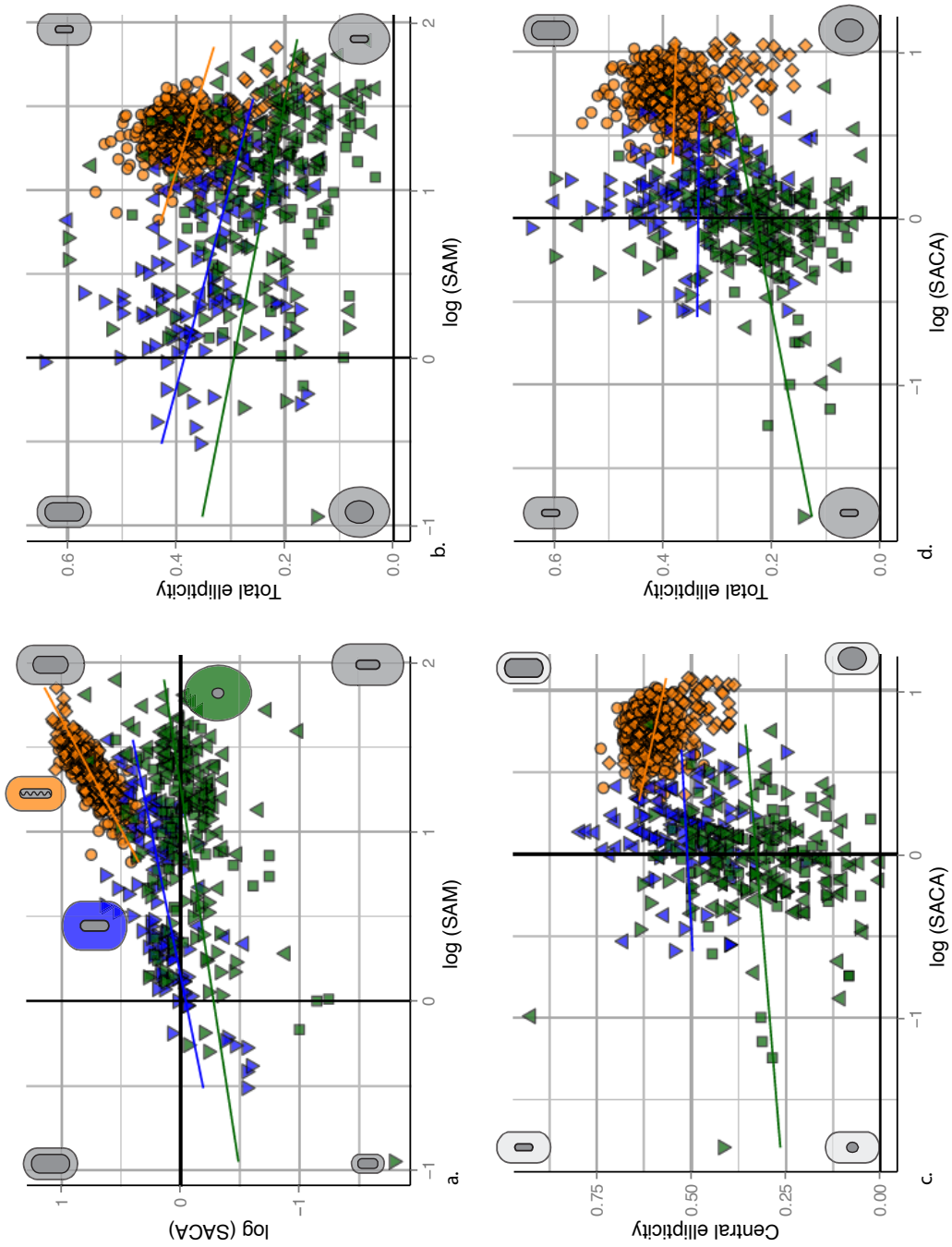
a.
b.
c.
d.
log (SACA)
log (SAM)
Total ellipticity
Central ellipticity

Figure 20.

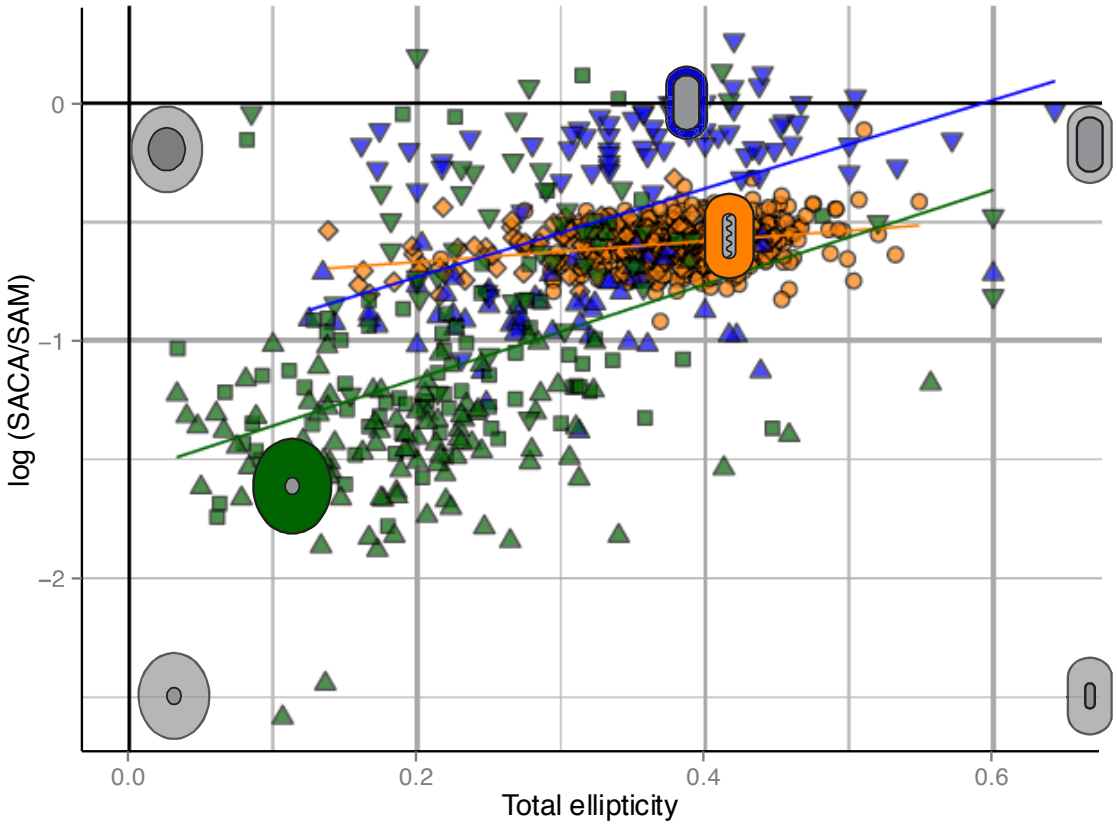

Table 1.

		total length [µm]	total width [µm]	central length [µm]	central width [µm]	margin major axis [µm]	margin minor axis [µm]	total ellipticity	central ellipticity	total aspect ratio	central aspect ratio	margin ratio (minor/major)	total surface area (SAM) [µm^2]	surface area of central surface area (SACA) [µm2]	margin surface area (SAM) [µm2]	SACA/SAM
Ellipsolithus Morphotype A (n = 435)	mean	7.67	4.65	4.33	1.69	3.34	2.96	0.39	0.61	0.61	0.39	0.9	28.46	5.85	22.61	0.26
	stand. dev.	1.05	0.63	0.62	0.26	0.61	0.47	0.05	0.04	0.05	0.04	0.13	7.33	1.6	6.05	0.06
	median	7.69	4.66	4.32	1.68	3.31	2.96	0.39	0.61	0.61	0.39	0.89	28.25	5.65	22.3	0.26
	min	4.55	2.58	2.63	0.93	1.3	1.25	0.22	0.47	0.45	0.26	0.6	9.22	2.33	6.62	0.12
	max	10.35	6.61	5.74	2.54	5.12	4.3	0.55	0.74	0.78	0.53	1.58	53.73	10.53	43.96	0.77
	range	5.8	4.03	3.11	1.61	3.82	3.05	0.33	0.27	0.33	0.27	0.97	44.51	8.2	37.33	0.65
	skew	-0.08	-0.13	-0.07	0.13	-0.19	-0.1	0.01	-0.31	-0.01	0.31	1.15	0.3	0.36	0.3	1.86
	kurtosis	-0.15	0.23	-0.41	0.06	0.09	0.44	0.48	0.39	0.48	0.39	4.29	0.14	-0.13	0.31	12.88
	stand. err.	0.05	0.03	0.03	0.01	0.03	0.02	0	0	0	0	0.01	0.35	0.08	0.29	0
Ellipsolithus Morphotype B (n = 87)	mean	7.65	5.28	4.16	1.92	3.48	3.37	0.31	0.54	0.69	0.46	0.97	32.9	6.46	26.44	0.25
	stand. dev.	1.36	1.26	0.69	0.49	0.82	0.87	0.08	0.08	0.08	0.08	0.11	13.42	2.49	11.35	0.06
	median	7.79	5.05	4.1	1.8	3.56	3.17	0.31	0.55	0.69	0.45	0.97	31.76	6.18	25.27	0.25
	min	4.44	3.32	2.46	1.06	1.98	2.15	0.14	0.39	0.55	0.28	0.73	11.65	2.11	9.35	0.16
	max	11.54	9.05	5.54	2.9	6.46	6.32	0.45	0.72	0.86	0.61	1.22	82.02	11.88	71.01	0.48
	range	7.1	5.73	3.08	1.84	4.48	4.17	0.31	0.33	0.31	0.33	0.48	70.38	9.76	61.66	0.33
	skew	0.1	0.67	-0.08	0.24	0.59	1.12	-0.22	-0.19	0.22	0.19	0.25	0.97	0.39	1.22	0.76
	kurtosis	-0.27	0.06	-0.6	-1.02	0.79	1.47	-0.79	-0.91	-0.79	-0.91	-0.28	1.25	-0.86	2.19	1.8
	stand. err.	0.15	0.13	0.07	0.05	0.09	0.09	0.01	0.01	0.01	0.01	0.01	1.44	0.27	1.22	0.01
Gaarderia microliths (n = 72)	mean	2.73	1.73	1.84	0.99	0.9	0.73	0.37	0.45	0.63	0.55	0.88	4.28	1.6	2.67	0.73
	stand. dev.	1.03	0.77	0.64	0.4	0.51	0.5	0.1	0.1	0.1	0.1	0.47	5.19	1.57	3.76	0.27
	median	2.59	1.6	1.8	0.97	0.8	0.6	0.37	0.44	0.63	0.56	0.81	3.37	1.32	2.05	0.71
	min	1.08	0.69	0.77	0.38	0.3	0.09	0.16	0.17	0.36	0.33	0.08	0.59	0.26	0.31	0.08
	max	8.55	6.55	5.09	3.18	3.45	3.36	0.64	0.67	0.84	0.83	3.33	43.93	12.72	31.21	1.83
	range	7.47	5.85	4.32	2.8	3.15	3.27	0.48	0.5	0.48	0.5	3.26	43.34	12.47	30.9	1.75
	skew	2.4	3.48	1.79	2.66	2.26	2.9	0	-0.16	0	0.16	2.46	6.22	5.07	6.17	0.8
	kurtosis	11.77	19.2	7.46	11.38	7.89	10.73	0.03	0.13	0.03	0.13	9.38	44.5	32	43.44	2.88
	stand. err.	0.12	0.09	0.08	0.05	0.06	0.06	0.01	0.01	0.01	0.01	0.06	0.61	0.19	0.44	0.03
Gaarderia macroliths (n = 58)	mean	4.94	3.49	2.25	0.92	2.7	2.58	0.29	0.59	0.71	0.41	0.97	14.34	1.67	12.67	0.15
	stand. dev.	1.16	0.97	0.48	0.24	0.83	0.85	0.09	0.09	0.09	0.09	0.19	7.2	0.71	6.71	0.05
	median	5	3.41	2.2	0.91	2.62	2.5	0.29	0.58	0.71	0.42	0.96	12.55	1.54	10.84	0.13
	min	2.15	1.46	1.08	0.35	1.08	1.04	0.13	0.39	0.4	0.21	0.4	2.47	0.29	2.18	0.04
	max	8	6.4	3.3	1.6	5.2	4.88	0.6	0.79	0.87	0.61	1.62	38.87	4.02	34.85	0.28
	range	5.85	4.94	2.22	1.25	4.12	3.84	0.47	0.4	0.47	0.4	1.22	36.4	3.73	32.67	0.24
	skew	0.17	0.52	-0.21	0.46	0.69	0.58	0.56	0.29	-0.56	-0.29	0.25	1.25	0.85	1.31	0.6
	kurtosis	0.69	0.56	-0.19	0.4	0.57	0.33	1.06	-0.22	1.06	-0.22	2.1	1.83	0.85	1.92	-0.13
	stand. err.	0.15	0.13	0.06	0.03	0.11	0.11	0.01	0.01	0.01	0.01	0.02	0.95	0.09	0.88	0.01
Umbellosphaera microliths (n=48)	mean	2.92	2.04	1.45	0.84	1.47	1.19	0.29	0.4	0.71	0.6	0.86	5.24	1.04	4.2	0.39
	stand. dev.	1.08	0.77	0.49	0.27	0.86	0.66	0.11	0.13	0.11	0.13	0.23	3.67	0.66	3.31	0.34
	median	2.65	1.89	1.4	0.8	1.29	1.05	0.28	0.42	0.72	0.58	0.83	4.01	0.77	3.23	0.28
	min	0.44	0.38	0.19	0.11	0.25	0.2	0.08	0.06	0.4	0.36	0.27	0.13	0.02	0.11	0.05
	max	5.25	3.75	2.75	1.5	3.78	2.7	0.6	0.64	0.92	0.94	1.34	15.46	3.24	12.52	1.57
	range	4.81	3.38	2.56	1.39	3.53	2.5	0.52	0.58	0.52	0.58	1.07	15.33	3.22	12.4	1.52
	skew	0.26	0.38	0.41	0.42	0.66	0.63	0.93	-0.57	-0.93	0.57	-0.07	0.94	1.4	0.94	1.76
	kurtosis	-0.64	-0.66	0.32	0.78	-0.43	-0.5	1.12	0.2	1.12	0.2	0.03	-0.02	1.83	-0.24	2.53
	stand. err.	0.16	0.11	0.07	0.04	0.12	0.1	0.02	0.02	0.02	0.02	0.03	0.53	0.1	0.48	0.05
Umbellosphaera I- liths (n = 87)	mean	4.7	3.63	1.41	0.92	3.29	2.7	0.23	0.32	0.77	0.68	0.83	14.84	1.1	13.74	0.15
	stand. dev.	1.58	1.29	0.46	0.28	1.49	1.25	0.09	0.13	0.09	0.13	0.14	9.34	0.62	9.22	0.23
	median	4.77	3.67	1.4	0.9	3.23	2.74	0.22	0.31	0.78	0.69	0.83	13.94	1.03	13.02	0.07
	min	1.09	0.91	0.32	0.23	0.57	0.36	0.03	0.03	0.52	0.4	0.52	0.78	0.06	0.68	0.02
	max	8.5	7.19	3	1.6	6.91	6.41	0.48	0.6	0.97	0.97	1.2	43.22	3.53	42.45	1.3
	range	7.41	6.28	2.68	1.37	6.34	6.04	0.45	0.57	0.45	0.57	0.68	42.44	3.48	41.77	1.29
	skew	0.04	0.22	0.19	0.1	0.09	0.32	0.2	-0.08	-0.2	0.08	0.05	0.88	1.23	0.88	3.22
	kurtosis	-0.22	-0.17	0.98	0.5	-0.62	0.05	-0.37	-0.84	-0.37	-0.84	-0.32	0.48	2.52	0.52	10.69
	stand. err.	0.17	0.14	0.05	0.03	0.16	0.14	0.01	0.01	0.01	0.01	0.02	1.02	0.07	1.01	0.02
Umbellosphaera macroliths (n = 98)	mean	6.75	5.38	1.45	0.96	5.29	4.42	0.2	0.3	0.8	0.7	0.83	30.54	1.2	29.34	0.05
	stand. dev.	1.86	1.56	0.82	0.32	1.65	1.46	0.09	0.16	0.09	0.16	0.13	16.67	1.02	16.18	0.04
	median	6.74	5.32	1.33	0.91	5.17	4.24	0.2	0.29	0.8	0.71	0.83	27.92	0.92	26.39	0.04
	min	1.68	1.55	0.43	0.1	1.25	1.16	0.03	0	0.44	0.08	0.39	2.04	0.1	1.91	0
	max	13.5	10	7.5	2.27	11.25	8.25	0.56	0.92	0.97	1	1.32	92.78	6.19	90.12	0.28
	range	11.82	8.45	7.07	2.17	10	7.09	0.52	0.92	0.52	0.92	0.93	90.73	6.08	88.21	0.28
	skew	0.43	0.3	4.75	1.06	0.54	0.32	0.86	1.02	-0.86	-1.02	-0.13	1.17	3	1.15	3.76
	kurtosis	1.09	0.12	30.15	2.68	1.19	-0.25	1.82	2.79	1.82	2.79	2.75	1.69	10.46	1.62	19.26
	stand. err.	0.19	0.16	0.08	0.03	0.17	0.15	0.01	0.02	0.01	0.02	0.01	1.68	0.1	1.63	0

Table 2.

			Total length to Total width	Central length to Central width	Margin major to minor axis	Total ellipticity to central ellipticity	SAM to SACA	Margin ratio to SAM
Ellipsolitus	Morphotype A	*r*	0.854	0.766	0.721	0.373	0.75	0.125
		r^2	0.73	0.586	0.519	0.139	0.562	0.016
		Lin. equ.	Y = 0.7384 + 0.5102 *X	Y = 0.3291 + 0.3146 * X	Y = 1.0938 + 0.5590 * X	Y = 0.4780 + 0.3312 * X	Y = 6.0797 + 2.8249 * X	Y = 0.9579 - 0.0026 * X
	Morphotype B	*r*	0.882	0.744	0.899	0.766	0.797	0.152
		r^2	0.778	0.553	0.808	0.587	0.635	0.023
		Lin. equ.	Y =- 0.9437 + 0.8145 * X	Y =- 0.2752 + 0.5263 * X	Y = 0.0191 + 0.9615 * X	Y = 0.2930 + 0.7963 * X	Y = 1.8286 + 0.1751 * X	Y = 0.9322 + 0.0014 * X
Gaarderia	microliths	r^2	0.865	0.753	0.645	0.14	0.762	0.003
		r	0.93	0.868	0.803	0.375	0.873	0.054
		Lin. equ.	Y =- 0.1601 + 0.6905 * X	Y = 0.0067 + 0.5374 * X	Y = 0.0204 + 0.7954 * X	Y = 0.2971 + 0.4138 * X	Y = 0.6280 + 0.3659 * X	Y = 0.8482 + 0.0161 * X
	macroliths	*r*	0.889	0.59	0.809	0.232	0.666	0.182
		r^2	0.79	0.348	0.654	0.054	0.443	0.033
		Lin. equ.	Y =- 0.1968 + 0.7465 * X	Y = 0.2453 + 0.2991 * X	Y = 0.3433 + 0.8281 * X	Y = 0.5197 + 0.2267 * X	Y = 0.7812 + 0.0704 * X	Y = 0.9022 + 0.0051 * X
Umbellosphaera	microliths	*r*	0.901	0.821	0.877	0.365	0.458	0.148
		r^2	0.812	0.674	0.769	0.133	0.21	0.022
		Lin. equ.	Y = 0.1417 + 0.6485 * X	Y = 0.1764 + 0.4594 * X	Y = 0.2024 + 0.6735 * X	Y = 0.2724 + 0.4448 * X	Y = 0.6575 + 0.0919 * X	Y = 0.9053 - 0.0103 * X
	l-liths	r^2	0.855	0.618	0.859	0.088	0.025	0.
		r	0.925	0.786	0.927	0.297	0.158	0.021
		Lin. equ.	Y = 0.0819 + 0.7538 * X	Y = 0.2614 + 0.4689 * X	Y = 0.1517 + 0.7752 * X	Y = 0.2306 + 0.4163 * X	Y = 0.9526 + 0.0106 * X	Y = 0.8373 - 0.0003 * X
	macroliths	*r*	0.908	0.507	0.801	0.032	0.452	0.263
		r^2	0.825	0.258	0.642	0.001	0.204	0.069
		Lin. equ.	Y = 0.2327 + 0.7624 * X	Y = 0.6694 + 0.1981 * X	Y = 0.6759 + 0.7072 * X	Y = 0.2853 + 0.0561 * X	Y = 0.3595 + 0.0285 * X	Y = 0.7680 + 0.0022 * X

Table 3.

	Q-2.0 A-type	Q-2.0 B-type	Q-0.8 A-type	Q-0.8 B-type	Q+1.1 A-type	Q+1.1 B-type	Q+2.2 A-type	Q+2.2 B-type	Q+3.2 A-type	Q+3.2 B-type
Q-2.0 A-type	0	**0.00741421**	0.562552	**1.88E-05**	0.162742	0.667649	0.0673763	**0.000960749**	0.036775	**0.000120119**
Q-2.0 B-type		0	**0.000930181**	0.395288	**6.59E-09**	0.832441	**4.50E-06**	0.303714	**0.000148666**	0.313861
Q-0.8 A-type			0	**2.16E-07**	**0.00295083**	0.281256	**0.00255848**	**1.43E-06**	0.170135	**5.33E-07**
Q-0.8 B-type				0	**3.44E-11**	0.639288	**8.35E-11**	0.155942	**9.95E-07**	0.0394974
Q+1.1 A-type					0	**0.00851313**	**0.00726755**	**2.87E-10**	**0.00195173**	**9.18E-11**
Q+1.1 B-type						0	**0.00306443**	0.596888	0.204922	0.396612
Q+2.2 A-type							0	**1.94E-09**	**1.57E-05**	**3.28E-07**
Q+2.2 B-type								0	**1.80E-06**	0.0630635
Q+3.2 A-type									0	**3.13E-07**
Q+3.2 B-type										0

Plate Caption

Plate 1

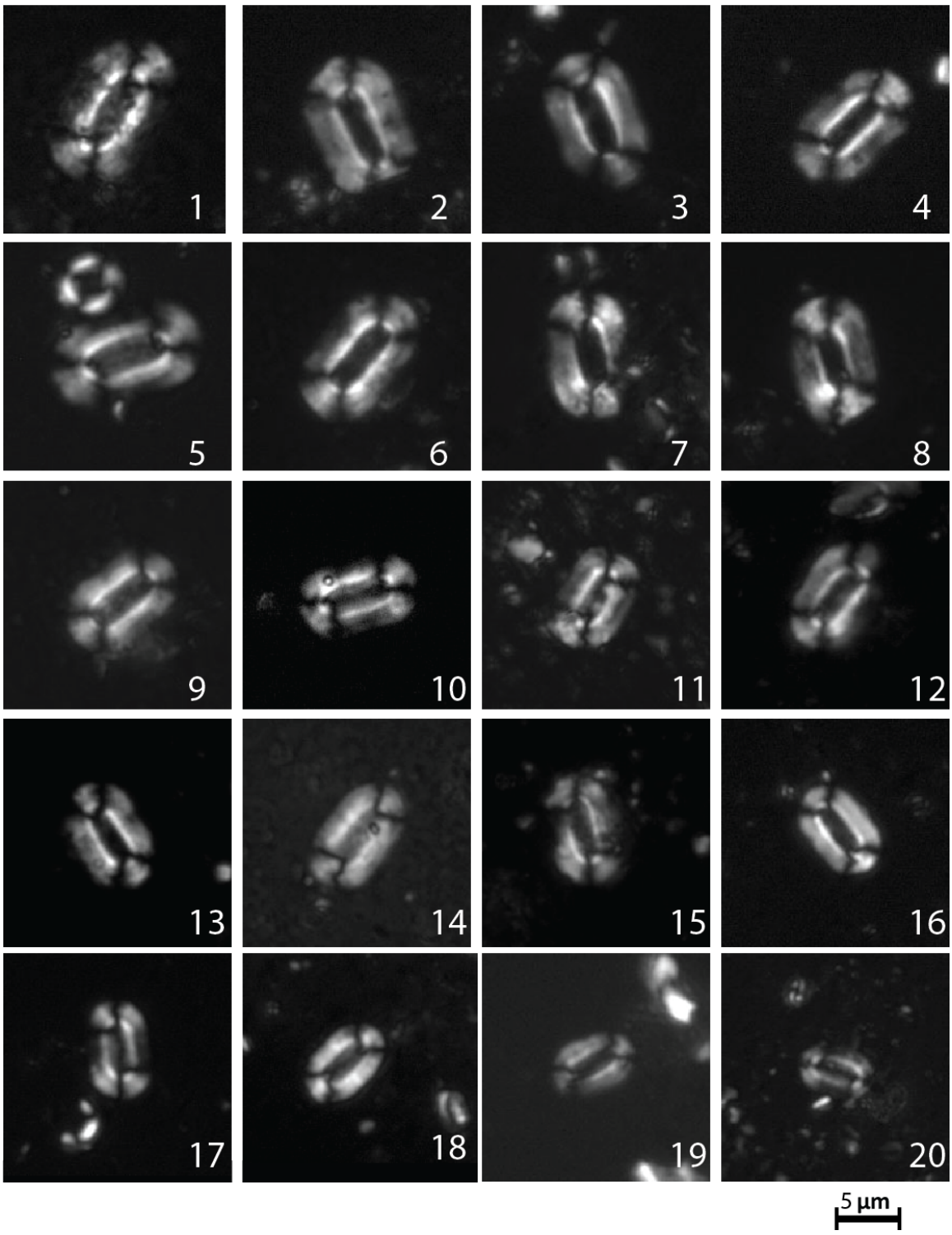

Plate 2

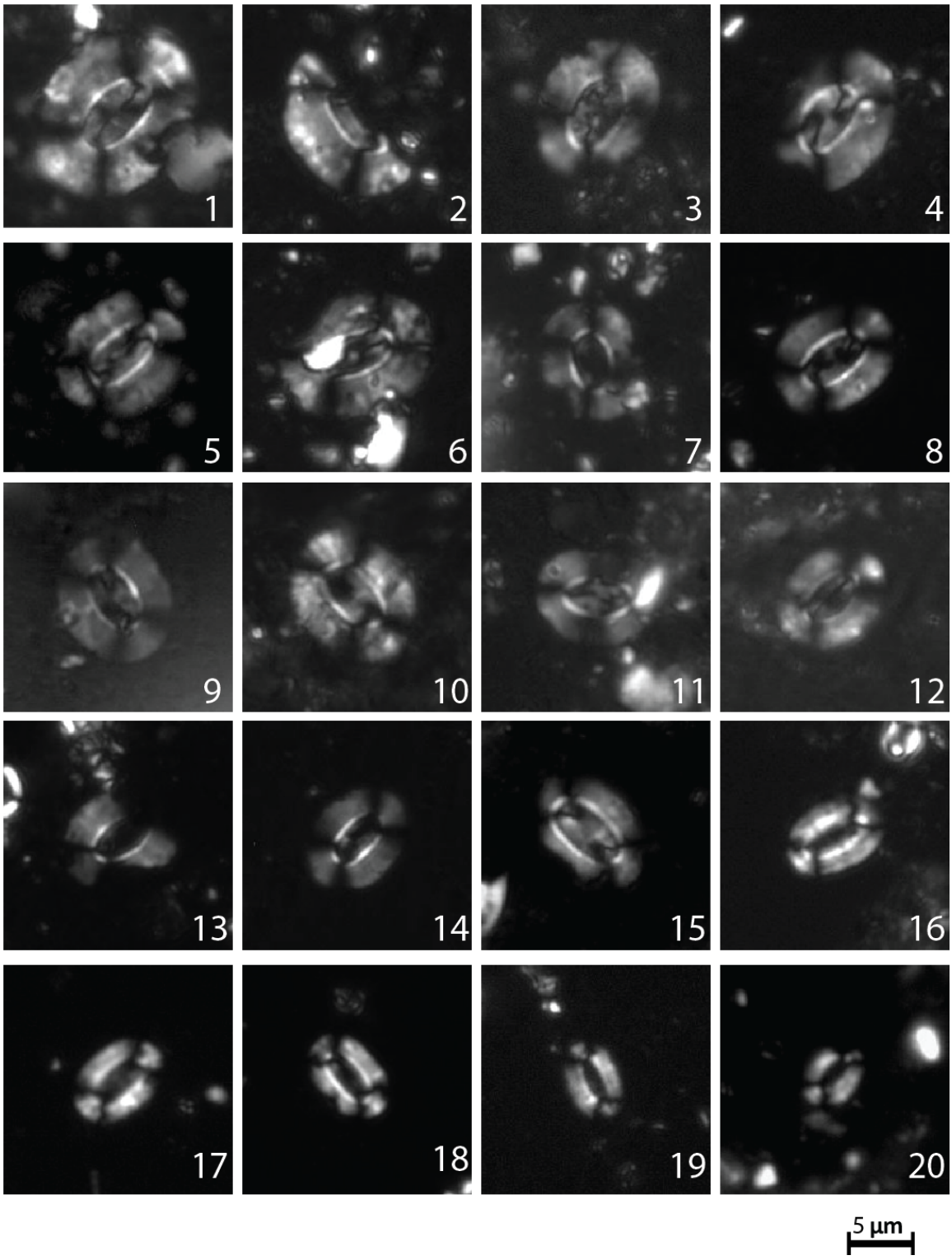

Plate 3

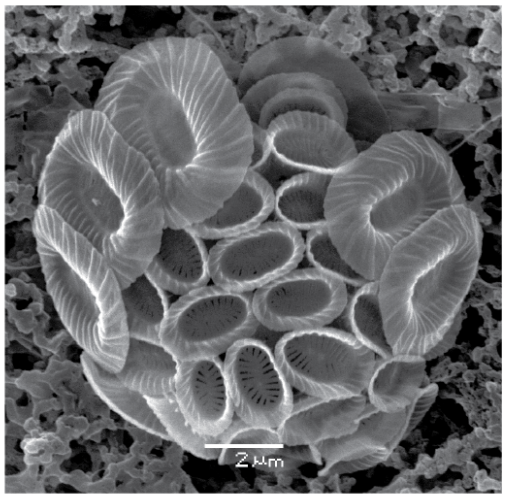

1

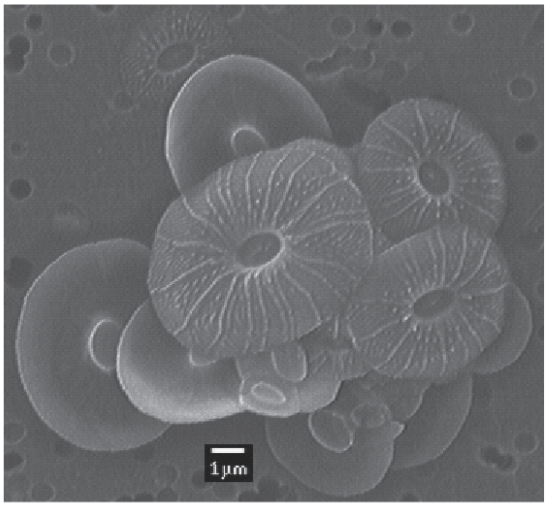

2

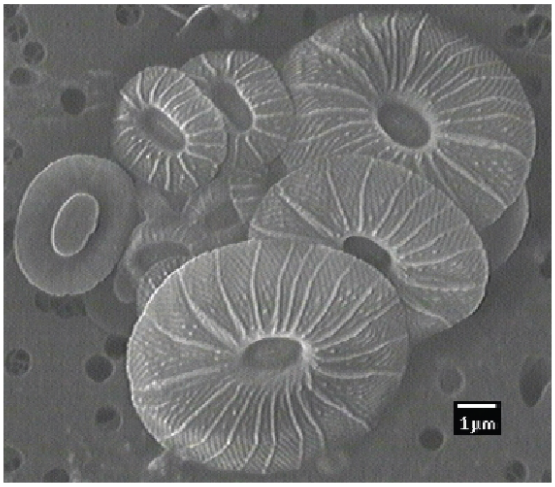

3

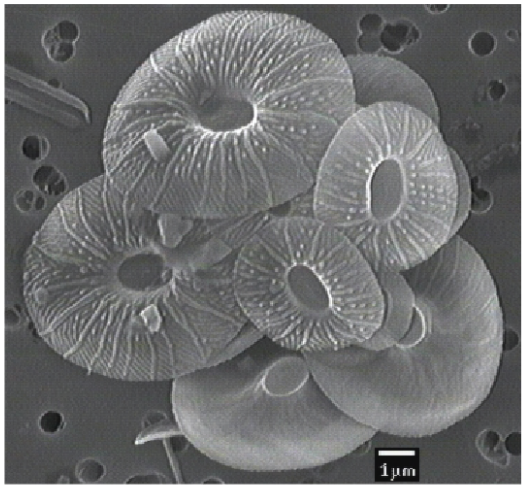

4

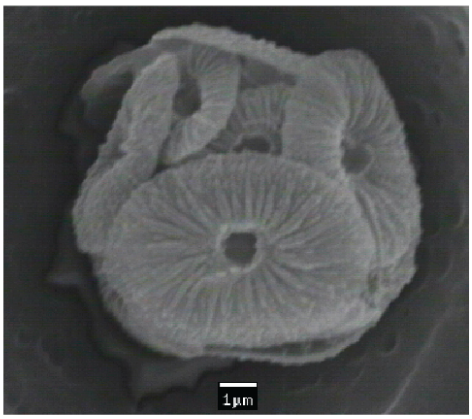

5

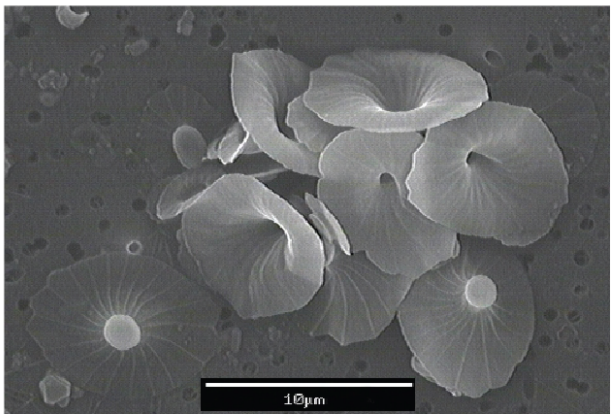

6

Chapter 3

Evolutionary Modality In A Coccolithophore (The Early Eocene *Heliodiscoaster mahmoudii*)

3.1. Abstract:

Based on a multivariate quantitative analysis, I conduct the first high-resolution study of morphologic evolution in a coccolithophore during its life span of 370 kyr. I show that high morphologic variability during the first ~ 83 kyr of this span precedes morphologic stability. This corresponds to morphologic fixation as described in other organisms, more particularly in planktonic eukaryotes, and supports evolution through punctuated equilibrium. The period of high variability is marked by the co-occurrence of typical and atypical forms of the species (the earliest Eocene *Heliodiscoaster mahmoudii*). A morphological continuum occurs between them, but their proportions reverse with time at the same time as variability decreases, implying that the atypical forms carry the variability prior to fixation. I interpret this high variability as a means to adapt rapidly to rapid environmental changes during speciation by increasing the envelope of possible morphologies in successive generations.

3.2. Introduction

Microevolutionary trends during speciation and the subsequent life span of species remains a topic of extreme interest. Numerous studies have attempted to answer the question of the evolutionary rates and modalities in a variety of fossil lineages

(Kellogg, 1975; Kellogg and Hays, 1975; Malmgren and Kennett, 1981; McHargue, 1982; Lazarus 1983 ; Malmgren et al., 1983; Arnold, 1983; Reyment, 1985; Sorhannus et al., 1988; Wei and Kennett, 1988; Lazarus 1995; Malmgren and Kucera 1996; Kučera and Malmgren 1998; Jackson and Cheetham 1999, Benton and Pearson, 2001; Hull and Norris, 2009). These studies have demonstrated that the tempo of speciation in plankton is variable (Fig. 1), with examples of speciation through gradual morphological change (anagenesis), and of relatively rapid change, between relative intervals of stasis (cladogenesis). Consequently, the question of which is the common mode of evolutionary change—gradual vs. punctuated evolution—remains unanswered.

An ideal taxonomic group for evolutionary studies would be an extant planktonic one with an abundant, diverse and geologically long fossil record, characterized by rapid generational turnovers. The coccolithophorids represent such a group. These are marine protists of the Division Haptophyta that secrete an exoskeleton of calcium carbonate (coccosphere) composed of tiny mineralized organic scales (coccoliths). The haploid-diploid life cycle is complex, and the generational turnover is rapid. Asexual reproduction occurs every 12 to 60 hours (Brand, 1994); poorly understood as yet, sexual reproduction (which introduces the mutations that drive evolution) is thought to occur seasonally or yearly (McIntyre and Bé, 1967) or is virally driven (Frada, 2012). In any case, this translates to over 700 generations per year (i.e., 7.0×10^5 kyr), which explains the enormous sedimentary accumulation of deep sea ooze and chalks (Bramlette, 1967). Despite these ideal circumstances, there have been no quantitative tests of microevolutionary processes in the coccolithophores.

I examine here the evolutionary modalities in the short-ranging coccolithophore species *Helio-discoaster mahmoudii* recovered from the Paleocene/Eocene boundary Global Boundary Stratotype Section and Point (GSSP) section at Dababiya, Egypt. I first introduce the morphology and structure of the species. I then analyze the morphological variability of three main morphological characters, and concentrate on that of the proximal knob, which shows the greatest amount of variability. I show that the initial appearance of the species was marked by very high variability that lasted for one fifth of its living range, followed by stasis until its extinction.

3.2.1. Taxonomic background

The holotype of *Helio-discoaster mahmoudii* (Perch-Nielsen, 1981) Aubry n. comb (=*Discoaster mahmoudii* Perch-Nielsen 1981, p. 836, pl. 4 Fig. 1-10) was described from Gebel Taramsa near Qena in the upper Nile Valley (Egypt). This locality is ~70 km north of Dababiya, implying that the specimens studied here are closest to those from the stratotypic area.

3.2.2. Morphology

This is a large (12 - 18 µm) stellate discoaster with 5 to 7 straight, elongate (> 5µm), wedged-shaped rays, each a single crystal (Fig. 3a, plate 1). The rays are joined along about ½ of their length. The free part of each ray tapers to a point. The central disc, formed by the coalescing parts of the rays, is concave on the proximal face, convex on

the distal one (see Fig. 3b, plate 2). A distinctive lobate knob occurs on each face. The proximal knob is high with deep depressions between the narrow lobes. The distal knob is wide and low. The suture between rays differs on each face, being straight and radial on the proximal face and curving clockwise on the distal face.

3.2.3. Morphostructure

Distal face

Each ray has a medial axis (Fig. 4a,b,c). Below the medial plane is a low ridge that runs the length of the free ray. The ridge gradually widens towards the central disc. The rays coalesce distally, each ridge widening to form a low lobe. The lobes coalesce with adjacent lobes over more than half of their length to form the knob. The distal knob is broad with a shallow central depression. The sutures are sigmoidal. The number of lobes corresponds to the number of rays. Each lobe points to the inter-ray region. Variability affects mostly the shape and symmetry of the knob. This variability was not easily quantifiable, although it is a significant taxonomic character.

Proximal face

A narrow ridge rises abruptly above the medial plane of each ray (Fig. 4c). Each ridge represents a free lobe of the knob. The lobes radiate from the center of the discoaster to the inter-ray region (extending slightly beyond it) abruptly decreasing in height. The lobes coalesce into a tall stem with a central depression. Between each lobe is a deep

depression that is delineated by a lobe on one side and the curved suture between adjacent rays on the other. The variability in size and symmetry of the knob is readily quantifiable.

3.3. Methodology

3.3.1. Material

The material studied here is from the Dababiya quarry, Egypt, which is located ~35 km south of Luxor, Upper Egypt and about 85 km from the type locality of Taramsa (Dupuis et al., 2003). The quarry exposes ~120 m of upper Paleocene and lower Eocene Esna shales that were deposited in the southern Tethyan epicontinental margin in outer neritic to upper bathyal depth (150-250 m; Allegret and Ortiz, 2013). The stratigraphy of this succession has been worked out in detail in connection to the definition of the Global Boundary Stratotype Section and Point (GSSP) for the base of the Eocene, which is located 12.57 m above the base of the Esna Shale and is marked by the onset of the carbon isotope excursion (CIE) between 12.57 m and 15 m (Aubry et al., 2007). The measured Eocene section in the quarry is a composite of two main subsections, DBH (in which the GSSP is located) and DBD, which is 400 m further east. The two subsections overlap over 3 m (see below). *Helio-discoaster mahmoudii* was shown to occur over a thin stratigraphic interval. Its lowest occurrence (LO) is just above the CIE at DBH 5.0 m in subsection DBH; its highest occurrence (HO) is at 18 m in subsection DBD, and corresponds approximately with the E2/E3 (=P5b/P6a) biozone boundary (Berggren and Pearson, 2005, Pearson et al., 2006).

The lowest occurrence (LO) of *H. mahmoudii* is well delineated in the DBH section for which smear slides were prepared at 50 cm intervals between DBH 4.5 m and DBH 9 m. Typical, five- and six-rayed morphotypes with the large proximal knob characteristic of the species occur from level DBH 5.4 m to level DBH 9.0 m. These morphotypes are scarce in the oldest level (5.4), but their abundance increases rapidly upwards. Levels DBH 5.14 m and 5.00 m also yielded five- and six- rayed discoasters assignable to *H. mahmoudii*, but with a much less stellate proximal knob (Dupuis et al., 2003). They were regarded as early morphotypes of *H. mahmoudii* (as confirmed in this study). Consequently the LO of *H. mahmoudii* is placed between levels DBH 4.75 and 5.00 in agreement with Dupuis et al. (2003).

The species occurs continuously, albeit in varying abundance, from DBD 0.5 m up to level DBD 10.5 m where it is common. It is extremely rare between DBD 5 m to DBD 8 m and above DBD 9.5 m. Sample DBD 7.5 m was barren. Scarce specimens (no more than 2 specimens/slide) were also recovered from levels DBD 11.5 m and 18 m, but none from DBD 16.5 m. The occurrence of *Heliodiscoaster araneus* at 18 m is indicative of reworking. On this basis, it is reasonable to place the HO of *H. mahmoudii* either at DBD 10.5 or DBD 11.5 (but not at DBD 18 m as shown in Dupuis et al., 2003, Fig. 11).

A total of 17 samples were selected for this study, constituting a 10 m-thick interval with an overlap of 3 m between DBH and DBD. Preservation in most samples was

good, although completely preserved discoasters (i.e., without broken ray tips) were rare.

In Dupuis et al. (2003) a composite of the two sections is constructed based on the correlation between three distinct pink layers. Dupuis et al. (2003) determined that the top of section DBH (9 m) is corresponds to section DBD at 7 m. There is some disagreement with this correlation. A biostratographic study of planktonic foraminiferal by Kh. Ouda (personal communication) correlates the two sections (3 m overlap): 1) DBD 0.0 m (the base of DBD) corresponds to DBH 5.75 m; 2) DBD 1.0 m corresponds to DBH 6.5 m; 3) DBD 2.0 m corresponds DBH 7.5 m; 4) DBD 3.0 m is between levels DBH 8.5 m and DBH 9 m. My quantitative analysis of H. mahmoudii validates the latter composite section (CS; Fig. 5). I determine that DBD 3.0 m is approximately equivalent to DBH 8 m and that the base of DBD (0.0 m) is approximate to level DBH 6 m (since pk2 is not represent in DBD, see Dupuis et al. 2003), and that the top of the DBH (9 m) is approximate to DBD 4 m.

3.3.2. Chronology

The FAD and LAD of *H. mahmoudii* have not been tied to the Integrated Magnetobiostratigraphic time scale (IMBS). Moreover, significant uncertainty remains concerning the age of the Paleocene/Eocene (P/E) boundary and earliest Eocene chronology. Therefore the life span of the species can only be approximated. In the

GSSP section, the LO of the species correlates with the end of the recovery of the CIE, and its highest occurrence with the LO of *Tribrachiatus bramlettei* at level DBD 10.5 m, slightly above the HO of *F. tympaniformis* at level DBD 7 m (Dupuis et al., 2003). Gradstein et al. (2012) place the P/E boundary at 56 Ma. Using a duration of 210 kyr for the CIE, I date the first appearance datum (FAD) of *H. mahmoudii* at 55.79 Ma. I adopt a date of 55.42 Ma for its last appearance datum (LAD), based on the determination of the FAD of *T. bramlettei* in Gradstein et al. (2012). I note their date of 55.64 Ma for the LAD of *F. tympaniformis*, supporting my chronology. I thus calculate a provisional life span of 370 kyr for *H. mahmoudii*. This is in the order of magnitude of the age (400 kyr) that would have been determined counting precessional cycles at Sites 1262 and 550 between the end of the CIE and the FAD of *T. bramlettei* (Westerhold et al., 2009).

3.3.3. Technique

Acquisition of data was undertaken using the complementary techniques of both light microscopy and scanning electron microscopy, as microfossils are 3-dimensional objects. A comprehensive 3-dimensional interpretation of a specimen can be obtained through light microscopy, which reveals information concerning shape, structure, and size. This is the primary method used for taxonomic identification.

Scanning electron microscopy permits detailed examination, particularly with regards to the shape of the sutures between the elements of which the discoaster is made. A limitation of scanning electron microscopy for the study of coccoliths is that usually only

one face is visible (unless the coccolith is oriented in edge view). The morphostructure of *H. mahmoudii* was determined using SEM analysis.

3.3.3.a. Light microscopy

Standard smear slides were prepared for all samples (Bown, 1998). Each sample was examined using a Zeiss Axioplan II photomicroscope at a magnification of ~1600X. A minimum of 50 specimens (± 5) was photographed per level. For levels where *H. mahmoudii* was scarce it was necessary to prepare several smear slides in order to record a sufficient number of specimens. Despite this, a count of 50 specimens was not reachable at all levels. For instance, only 29 specimens were recovered from level DBD 9, where *H. mahmoudii* was particularly scarce, even though six slides were prepared and exhaustively examined.

3.3.3.b. Scanning Electron Microscopy

Samples from 10 levels with abundant *H. mahmoudii* were studied in scanning electron microscopy (SEM), using a Hitachi 3000N at CEREGE, (Aix-En-Provence, France). I had difficulty obtaining specimens free of clay particles. This was partly resolved using the following method: 1) 0.06 g of shale was powdered; 2) the powder was then placed in a 50 ml solution of sodium metaphosphate and submitted to sonication for 1-2 minutes to disaggregate clay particles; 3) the suspension was diluted in 200 ml of water, and 4) filtered through a 8 μm Millipore membrane by means of vacuum filtration. To enhance cleaning, air was bubbled gently along the surface of the membrane; re-suspending the material for better filtration. 5) Once filtered, the membranes were fully

dried on a hot plate. 6) A central section of the membrane was cut and mounted on aluminum slabs. 7) Finally, the residue was sputter coated with gold/palladium alloy. Each 24 mm^2 sample was inspected at 600X; individual specimens were photographed at magnifications of 3,000 – 9000X.

3.3.4. Morphometric analysis

Quantitative analysis was conducted on the digital photographs obtained through light microscopy. Photographs were systematically taken for each specimen at three different focal points in order to illustrate: 1) the distal most surface of the proximal knob (proximal face), 2) the distal most surface of the distal knob (distal face) and 3) the main disc of the discoaster. Quantitative measurements were taken using software from Zeiss (AxioVision v. 3), and open source software (ImageJ, Abramoff et al., 2004).

Several morphologic characters were considered (Table 1). However, due to difficulties in obtaining a uniform method of measurement, some characters were eliminated from this study.

3.3.4.b. Measurements

Number of rays

The number of rays was counted in all specimens. Occasionally, rays were hidden under detrital particles. In such cases the number of rays was inferred from the number of lobes on the proximal knob.

Diameter of central disc:

The diameter of the central disc was calculated by doubling the longest radius measured from the center of the disc to the selected inter-ray area (Fig. 4). The measurements were made on proximal views because the convexity of the distal face would have resulted in inconsistent measurements. There was no ambiguity in measuring the radius of specimens in which the lobes of the proximal knob did not reach the periphery of the central disc. Particular attention was given to measure the periphery of the central disc and not the tips of the knob in specimens in which the lobes reached the periphery.

Diameter of the proximal knob:

For each proximal knob I measured: 1) the radius of the best-preserved and best-oriented lobe from center to the tip, and 2) the radius of the depression in the center of each knob (Fig. 3). From this, the total diameter of the knob and the average length of the free-standing part of each lobe was calculated (Fig. 4). The diameter of the proximal knob is the diameter at the most proximal part of the knob (at the contact with the central disc) (Fig. 3; plate 1, 3, 4) .

Diameter of the distal knob:

For each distal knob I measured the radius from the center to the tip of the best-preserved lobe and then calculated the diameter of the knob (Fig. 4). The diameter of the proximal knob is the diameter of the knob at its most distal end (the furthest from the central disc), as this is when it is most noticeable (plates 2, 3, 4).

3.3.4.c. Treatment of data

Statistical analysis

The mean, standard deviation (1σ), range, and 95% confidence intervals were calculated (Table 2) and plotted (Fig. 7) for each measured morphologic character. The distributions in ray number are illustrated as a bar graph (Fig. 6). Distributions of the measured and calculated characters are present as a violin-plot, a representation of data in a format combining boxplots with superimposed probability density curves (kernel density estimation; Fig. 8). A multivariate analysis of variance (MANOVA) and pairwise Hotelling's T^2 test were performed to test the variance between levels (5% significance level). Additionally, a comparison based on morphologic groups (see below) between the levels is done through a canonical variates analysis. All statistical computations were performed using the PAST software v. 2.17c (Hammer et al., 2001) and Rstudio with packages *MASS* (Venables, 2012) and *psych* (Revelle, 2013).. Graphs were drawn in Rstudio using the *ggplot2* package (Wickham, 2009).

Variability

The coefficient of variation (CV) was calculated as a measure of variability (Fig.7). The CV is defined as the ratio:

$$\frac{\text{standard deviation}}{\text{sample mean}} \times 100$$

This is a measure of variability relative to the sample mean and is an estimate of the variation in a population. Increased dispersion around the sample mean yields a large coefficient.

3.4. Results

The results presented here are for the DBH–DBD composite section (CS; see caption Fig. 5).

The MANOVA performed to test the variance between samples indicates statistically significant difference between the levels (Wilk's $\lambda = 0.1605$, df: 120, 5494; $F = 13.42$; $p < 0.01$). Pairwise Hotelling's T test to outline these differences (Table 3) indicates that levels CS 3 and CS 4 are the most similar ($p=0.83$).

3.4.1. Number of rays

Five- and six-rayed morphotypes occur throughout the section, but at different distributions (Fig. 6). The seven-rayed morphotype occurs consistently, albeit in low numbers, throughout the lower part of the section (levels CS 0 to CS 4). Above this, it occurs irregularly up to level CS 8.5, being absent in levels CS 2.5 and CS 6, the frequency of the seven-rayed morphotype ranges between 10 % and 23% in the lower part of the section (between CS 0.14 and CS 1.5 and at much lower frequency between 2% and 6%) in the upper part of the section (between CS 2 and CS 8.5). The six-rayed morphotype is the most abundant, ranging throughout the section with frequency between 50% and 80%. The five-rayed morphotype is most common between level DBD 1 m and DBH 9 m, with a frequency varying between 38% and 47%. The five-rayed morphotype occurs infrequently near the base of the section, except for level CS 0.4 where it represents 50% of the morphotype composition. In addition, the five-rayed morphotype decreases in frequency towards the top of the section, except at level CS 10.5 where it is more abundant than the six-rayed type.

3.4.2. Ø of the central disc

The diameter varies little throughout the section with increased variability occurring mostly in its lower part (Fig. 7a). The diameter varies between maximum of 9.22 µm at CS 0 and a minimum of 2.67 µm at CS 8.5. A steady decrease (~2.15 µm) in the range of size (5.35 µm to 3.20 µm) occurs between CS 0.4 and CS 2.5. Above this the range steadily increases up to CS 8.5, where it reaches 4.27 µm. A minimum range of 2.40 µm was recorded at CS 9.5, representing a size decrease of ~1.87 µm between CS 8.5 and CS 9.5. However, a range 4.02 µm marks the top of the section at CS 10.5.

The mean diameter of the central disc also varies little, from a maximum of 6.50 µm (n = 47) at DBH 5.14, to a minimum of 4.65 µm (n = 53) at CS 9.5, which represents a decrease of ~1.85 µm (Fig. 7a). There is a progressive decrease of ~ 1.77 µm (from 6.50 µm to 4.73 µm) between levels CS 0.14 and CS 2.5, followed by an increase of ~0.88 µm at level CS 3 (5.52 µm). Between levels CS 3 and CS 5, mean size decreases (by ~0.7 µm) to 4.82 µm. Between levels CS 5 and CS 8.5 the mean size is unchanged to CS 9.5, there is a decrease (of ~0.61µm) to 4.55 µm, which is followed by an increase to 5.22 µm (~0.67 µm) at the top, CS 10.5.

Density distributions and boxplots for the central disc are mostly symmetrical and unimodal (Figure 8a). However, plots for levels CS 0.14 and CS 0.4 are flatter showing increased variability, with standard deviations of 1σ = 1.24 µm and 1σ = 1.33 µm, respectively. From CS 0.4 to CS 2.5 the amount of deviation decreases to a minimum

(1σ = 0.67 μm) and remains constant up to level CS 5. The amount of deviation (1σ = 1.06 μm) increases between levels CS 5 and CS 8.5. Calculated variability is low (CV < 10%) and varies between 20.53 % (CS 8.5) and 13.56% (CS 9.5) (Fig. 9a).

3.4.3. Ø of the proximal knob

There is significant variability in the diameter of the proximal knob (Fig. 7b). Variability is found elevated from the base of the section up to level CS 2.2. Diameter size varies considerably from a maximum of 9.60 μm at CS 0.4 to a minimum of 1.15 μm at level CS 2.2. In the lowest part of the section the spread in size varies from 3.9 μm at CS 0 to 7.68 μm at CS 0.4. There is a sizable decrease (~4.11 μm) to a minimum range of 3.29 μm between levels CS 2.2 and CS 3 followed by a steady increase (~2.81 μm) in the magnitude reaching 6.10 μm at level CS 5. The magnitude in size drops ~2 μm at levels CS 6 and CS 6.5 (4.26 and 4.06 μm, respectively) and then increases again to 6.42 μm at level CS 8.5. At the top of the section, CS 10.5, the spread is 4.32 μm representing a decrease of ~2.06 μm between CS 9.5 and CS 10.5.

The mean diameter of the proximal knob exhibits considerable variability (Fig. 7b). Mean diameter varies from a minimum of 3.2 μm at level CS 0 to a maximum of 6.41 μm at CS 8.5. Between the lowest three levels, there is an increase of ~2.21 μm from 3.20 μm (at CS 0) to 5.41 μm (at CS 0.4). This is followed by a large decrease of ~2.04 μm to a mean value of 3.85 μm at level CS 1.15. Between levels CS 1.15 and CS 2.2, the mean diameter progressively increases by ~1.79 μm, reaching 5.64 μm at CS 2.2. Variability in the mean diameter is low between levels CS 2.5 and CS 6.5, although

steadily increasing (by ~ 1.18 μm) from 5.55 μm to 6.73 μm. A decrease of ~1.22 μm occurs at the top of the section, between levels CS 6.5 (6.73 μm) and CS 9.5 (5.51 μm), followed by a small increase (~0.44 μm) to 5.95 μm at CS 10.5.

The variability in the magnitude of the distributions of the proximal knob is high between levels CS 0 and CS 2.2. The distributions in these levels are non-symmetrical and display multimodality (Fig. 8b), with large deviations (1σ = 1.63 μm at CS 0.14; 2.25 μm at CS 0.4; 1.63 μm at CS 1.15; 1.64 μm at CS 1.5; 1.69 μm at CS 2; and 1.96 μm at CS 2.2). Between levels CS 2.5 and CS 9.5 distributions are symmetrical, unimodal, and the amount of deviation decreases (1σ = 0.82 μm to 1.10 μm).

The coefficient of variation (CV) also shows high variability in the proximal knob. Amounts of variability range between 13.76 % at level CS3 to a maximum of 42.31% at level CS 1.15 (Fig. 9b). Elevated variability (>25%) occurs in the lower portion of the section between levels CS 0 and CS 2.2. From level CS 1.15 to CS 3 there is a progressive 28.75% decrease in variability. Above level CS 3, variability on the knob diameter is low (<25%).

3.4.4. Ø of the proximal knob depression

The diameter of the proximal knob depression exhibits mostly low variability (CV <~25%, Fig. 9c) throughout the composite section. Levels of elevated variability (>25%) occur principally in the lower part of the section, except at levels CS 6.5 (26.0.9%) and CS 10.5 (26.36%).

The depression varies from a maximum diameter of 4.27 μm at CS 0.4 to a minimum diameter of 0.84 μm at CS 1.15 (Fig. 7c). From the base of the section to level CS 0.4 the magnitude in size increases (by ~1.81 μm) from 1.48 to 3.29 μm, and is followed by a decrease (of ~1.26 μm) from 3.29 μm to 2.03 μm between levels CS 0.4 and CS 1.5. A second, small increase (~0.41 μm) follows this at level CS 2.2 (2.44 μm). A second decrease in spread (by ~0.83 μm) occurs between levels CS 2.2 and CS 2.5, from 2.44 μm to 1.61 μm. The spread in size fluctuates little above this level, increasing (by ~0.81 μm) to 2.47 μm at CS 8.5. A small decrease ~1.0 μm occurs near the top of the section.

The mean depression varies in diameter from a minimum of 1.88 μm at CS 1.15 to a maximum of 2.61 μm at CS 3 (Fig. 7c). Between the lowest two levels there is a small increase (~ 0.31 μm) from 2.31 μm at CS 0.14 to 2.62 μm at CS 0.4. This is followed by a decrease (~0.74 μm) up to level CS 1.15 (1.88 μm). The mean diameter remains constant between this latter level and CS 2.5, and increases (~0.41 μm) slightly between CS 2.5 and CS 3. Means vary little between this level and the top of the section (CS 10.5). The distribution in diameter is symmetrical throughout the levels, with exception the lowest levels (Fig. 8c). These distributions are flatter, bimodal, with increased deviation (1σ = 0.62 μm at CS 0.14 and 0.77 μm at CS 0.4).

3.4.5. Length of proximal knob lobes:

Lengths of proximal lobes are only highly variable in the lower portion of the composite section (Fig. 9d). They vary considerably in size from a minimum of 0.04

μm at CS 1.15 to a maximum of 3.52 μm at CS 8.5 (Fig. 7d). Between levels CS 0 and CS 2.2, the spread in size varies from 1.34 μm to 2.95 μm. The magnitude decreases to 1.48 μm at level CS 3. Between levels CS 3 and CS 8.5 the spread fluctuates slightly, but generally increases from 1.48 to 2.95 μm (~ 1.4 μm). A decrease of ~1 μm occurs at the top of the section (1.85 μm at CS 10.5).

The mean length of the proximal lobes varies from a minimum of 0.56 μm at level CS 0 to a maximum of 2.56 μm at level CS 6.5 (Fig. 7d). It increases by 0.89 μm, from 0.56 μm at CS 0 to 1.45 μm at CS 0.4, and then decreases (by 0.64 μm) to 0.99 μm at level CS 1.15. There is a steady progressive increase (of ~1.57 μm) between 0.99 to 2.56 μm from CS 1.15 to CS 6.5. Above this, the mean length of the lobes decreases slightly ~0.5 μm between CS 8.5 and CS 9.5 before a final increase to 2.33 μm at CS 10.5.

Distributions in the length of the lobes are mostly symmetrical in the upper part of the section (Fig. 8d). But, between levels CS 0.14 and CS 2.2, the distributions are flat, display bimodality, and have increased deviation (1σ = 0.65 to 0.80 μm). This is followed by a decrease in deviation between levels CS 2.5 and CS 10.5 (1σ = 0.35 to 0.42 μm).

In the lower part of the section, from CS 0 to CS 2.2, the lobes exhibit substantial variability (>50%, Figure 9d). Variability is highest at level CS 1.15 (70.55%). Between levels CS 2.2 and CS 2.5, the amounts of variability decrease to 27.07%.

Minimum variability occurs at level CS 3 ~20.41%. Variability increases only slightly above this level, only reaching at 27.22% in level CS 9.5.

3.4.6. Ø of distal knob:

Variability is very low in the total diameter of the distal knob throughout the section (Fig. 9e). Diameters vary in size from a maximum of 8 μm at CS 0.4 to a minimum of 1.92 μm at CS 2.5. The spread is largest in the lower part of the section, varying between 5.08 μm at CS 0.4 and 2.81 at CS 2.2. The diameter remains stable between levels CS 3 and CS 10.5.

The mean diameter changes little throughout the section, from a minimum of 4.31 μm at level CS 0 to a maximum of 4.8 μm at level CS 0.4 (Fig. 7e). With the exception of level CS 0, the distribution of the diameter are mostly symmetrical and unimodal (Fig. 8e). Standard deviation decreases steadily up section (1σ = 0.65 μm at CS 0, 1σ = 0.61 μm at CS 10.5). Variability remains low (CV <20%), ranging from 22.04% at CS 0 to 9.89% at level CS 6 (Fig. 9e).

3.5. Discussion

3.5.1. Evolutionary patterns in H. mahmoudii

My study shows that the morphologic evolution of *H. mahmoudii* during its life span (370 kyr) includes an initial episode of high variability lasting ~83 kyr after which the morphology varied little. This is particularly well documented by the diameter of the proximal knob and the length of its lobes (Fig 9a, 9d).

During the first 83 kyr variability on the diameter of the proximal knob was noticeably high (>40% between levels CS 0.14 m and CS 1.5 m) as illustrated by the amplitude of the coefficient of variation in Figure 8. The mean diameter of the knob fluctuated, increasing (2.21μm) at first from levels CS 0 m to CS 0.4, then decreasing (1.56 μm) at level CS 1.15. The magnitudes of the distribution are broadest and bimodal at these levels. From level CS 1.15 to CS 2, the mean diameter increases in size, Hotelling's tests shows no significant difference between adjacent stratigraphic levels ($p > 0.05$, Table 3) and both size and the shape of the distribution decrease and become unimodal.

There was little change in the coefficient of variation values during the next 287 kyr. With values remaining considerably low (13-20%). The mean diameter of the knob was stable and the shape distributions are symmetrical and unimodal (Fig. 7).

3.5.2. Morphologic fixation in H. mahmoudii

The patterns described here compare well with evolutionary patterns that have been documented in unicellular organisms, planktonic foraminifera (Malmgren et al., 1983; Wei and Kennett, 1988; Malmgren and Kučera, 1996; Kučera and Malmgren, 1998), radiolarian (Kellogg, 1975; Kellogg and Hays, 1975; Lazarus 1983), diatoms (Sorhannus et al., 1988), and animals, including ostracods (Reyment, 1985), bryozoans (Jackson and Cheetham, 1999), and Cephalochordates (McHargue, 1982). In these

organisms, initiation of speciation was accompanied by high variance between ancestor and descendant, followed by morphological stasis in the descendant. For instance, Malgrem and Kucera (1996) have shown that morphologic transition occurred rapidly (~10 kyr) in the *Sphaeroidinella seminulina* to *S. dehiscens* lineage and was accompanied by increased variability expressed as strong morphologic fluctuations in the mean size of the test and the supplementary apertures, after which morphology quickly stabilized. In their study of the planktonic foraminifera *Globorotalia plesiotumida* - *G. tumida* lineage, Malmgren et al. (1983) showed that both taxa exhibited stasis of size and shape for several millions of years prior (*G. plesiotumida*) and after (*G. tumida*) intense morphologic variability that marked the accelerated (~600 kyr) phyletic change across the Miocene-Pliocene boundary. In the studies reinterpreted by Gould (1977) of radiolarian lineages (Kellogg, 1975; Kellogg and Hays, 1975), levels of variance reaching 20% were measured. The patterns described in these works correspond to that expected from the model of "punctuated" evolution (Eldredge and Gould, 1972) where speciation is a rapid phenomenon accompanied by high morphologic variance followed by morphologic stasis.

The pattern of morphologic change described here in *H. mahmoudii* fits well with the above studies of planktonic organisms and with the punctuated anagenesis model. For the first ~83 kyr the species exhibited morphologic variance of up to 75% and this was followed by morphologic stasis during which variance did not exceed 20% until the species' extinction. Unlike previous studies that have addressed the whole ancestor-descendant transition, I cannot document the ancestor of *H. mahmoudii*. It is unknown,

and it is a well-known fact that the paleontological records of speciation events in the coccolithophores are the exceptions. In as much as the episode of high variance was associated with the FAD of the species, and despite my inability to document the complete ancestor–descendant transition in this speciation event, I interpret my record as corresponding to the evolutionary history of *H. mahmoudii* (rather than to an unusual episode of strong morphologic variability during the life span of the species), and document morphologic fixation in the species following an episode of high variability.

3.5.2. Modalities of fixation in H. mahmoudii

The transition from high morphologic variability to low variability (i.e., fixation) occurs over a short interval of ~40 kyr and is preceded by a progressive decrease in the amplitude from 75% at level CS1.5 to 25% in level CS 2.5. During this short interval variability on the diameter of the proximal knob is extremely low. With the exception of the distal knob that exhibits low variability throughout the range of the species, all other measured variables also reach a minimum in variability at level CS 3.0. This level may represent a short episode of stabilizing selection leading to morphologic stability, as described by Lieberman (1996) and by Cheetham and Jackson (1995).

The initial, 83 kyr episode of high variability is marked by the occurrence of morphotypes typical of *H. mahmoudii* together with atypical morphotypes. The latter differ from the type only by the morphology of the proximal knob which exhibits in them different stages of completion of the lobes. There is a morphologic continuum from forms without lobes to forms with partially formed lobes to the forms with typical

well formed lobes (Fig. 10, Plates 4 and 5). These atypical forms have significance because their abundance decreases with time at the same time as the abundance of the typical morphotype increases, although these decrease/increase are not linear.

The first two canonical variates show a clear distinction between the typical (TY) and atypical (ATY) forms, explaining 82% of the variance observed in the data. The first CVA axis characterizes the disparity in the proximal knob (Fig. 11). Although they are distinct separate, the TY and ATY forms overlap slightly, which indicates a morphologic continuum in the symmetry of the knob. This also reflects the difficulty in assigning some specimens to either group.

Scatterplots establish the relationship between the measured variables in the TY and ATY forms. In most comparisons, the two groups plot separately (Fig. 12 a-c). There is a small positive correlation between the distal and proximal knobs in both TY and ATY forms ($R^2 = 0.176$ and 0.09, respectively). In the TY forms, the central disc shows strong positive correlations with the other main features and clusters as a main group. The ATY forms are united as a cluster of points that always plots separately. They are smaller and there is little or no correlation of the variables analyzed here with the diameter of the central disc (the total diameter of *H. mahmoudii* was not measured in this study; see above. Instead I measured the diameter of the central disc, which has low variability CV).

The TY and ATY co-occur in the lower part of the section up to CS 2.2. However, ATY is more frequent between CS0 and CS 1.5 (Fig. 13). The bimodal distributions in samples CS 0.14 to CS 2.2 results from the co-existence of the ATY and TY forms (Fig. 7). The occurrence and abundance of ATY forms at these levels explain the increased variability because their morphology is more variable. This is seen also in the fact that variability decreases up to level CS 3 in concert with the decrease in frequency of ATY forms. The latter are almost absent above level CS 3, occurring only sporadically (2 or 3 specimens), possibly as a morphologic remnant or as result of reworking. Nevertheless, the morphology of the proximal knob fixates at level CS3 (~ 105.7 kyr after the FAD of the taxon); above it the knob remains stable.

3.5.3. Mode and Tempo of evolution in the microplankton

Evolution through growth in variance (Gould, 1988) may be the dominant mode of evolution in the coccolithophores. Laboratory experiments on calcareous nannoplankton have revealed their high sensitivity and adaptability to environmental perturbations, such as changes in light intensity and duration, in temperature, nutrient availability and pH levels. The life cycle of coccolithophores is so fast (12- 60 hour) that a response to a perturbation can be immediate. This has been demonstrated in laboratory experiments (Paasche, 1968; Paasche and Klaveness, 1970; Iglesias-Rodriguez, 2008; Mueller et al., 2001; Gibbs, 2013), where a response is expressed within days from one (asexual) generation to the next .

The high variability that characterizes the early life span of a species may represent a strategy for handling abiotic and biotic stresses. Although most studies have attempted at linking speciation with a specific environmental parameter, most commonly temperature (for the planktonic foraminifera Wei and Kennett, 1988; Kučera and Malmgren 1998; Radiolarians, Lazarus 1995), successive generations of individuals during speciation are exposed to constant changes in a host of environmental parameters. In the case of unicellular eukaryotes such as coccolithophores, the changes occur on a scale of a few days. In these circumstances, it is advantageous for populations to be highly adaptable to an ever-changing environment. Perturbations are answered by adaptively increasing the envelope of possible morphologies in the following generation. Prolonged periods of biotic and abiotic perturbations would prolong the period of variability over multiple generations. The persistence of a perturbation over sufficient time would then lead to directional speciation by forcing selection of a particular morphology whereas a return to pre-perturbation conditions may collapse the envelope of variability on a new form. In the long term (over 100 kyr), these changes may appear unidirectional, but in the short term of a few days, the changes are non linear.

Fixation and morphologic stasis may imply the predominance of stabilizing selection (Hansen and Houle, 2004). However, in the case of *H. mahmoudii* the adaptive selective pressure is not understood. The increased variability presented during the early range of *H. mahmoudii* may resonate the response to a recovering ocean post-PETM.

3.5.4. Adaptive morphology

Although the underlying source for stabilizing selection and fixation on the proximal knob is not understood, the significance of the strongly lobated proximal knob in TY may tell us about the predominance of symbiotic relationships in this plankton group. Increase in the coccolith surface area through enlargement of a concavo-convex knob directly expands the physical space between the coccosphere and the cell, the cavities delineated between the lobes of the proximal knob allowing for more exchange with the surrounding environment. If, as discussed in Aubry 2009 and Aubry et al. 2011 (see also previous chapter), coccoliths serve as particle collectors or as anchors for diazotrophic bacteria, there is great selective advantage to the morphological fixation of the typical morphotype. Its strongly lobated proximal knob creates a series of deep pockets that may be advantageous for particle storage or even bacterial housing. These deep pockets, being on the proximal surface would allow for maximum exchange with a symbiont. A possible reason for the fixation of a complex knob may thus be a morphological adaptation to mixotrophy.

3.6. Conclusions

Through a quantitative morphometric analysis, I show for the first time microevolutionary pattern of morphologic fixation and stasis occurs in the coccolithophores. This is well documented in other fossil lineages, and represents a classic example of punctuated evolution. Morphologic variability of several variables (diameter, number of arms, size of knob, i.al.) of the coccolith *Helio-discoaster mahmoudii* is documented, and I show that significant variability concerns only the

proximal knob of the discoaster. High variability characterizes the first 83 kyr of the life span of the species, after which the morphology is fixated. During this early episode a continuum of morphostructural "completeness" of the knob occurs, being indicative of high variance anagenesis. As for most coccolithophore species the ancestor of *H. mahmoudii* is unknown, but I take this variance anagenesis as revealing of the mode of speciation in the species. I suggest that speciation occurs through a broad envelope of morphologic variability, after which high variability characters quickly stabilize, hinting at a shift in selective pressure. The nature of the fixation of a larger knob may be indicative of a physiological adaptation to mixotrophy. My study supports the finding of other studies that speciation in planktonic organisms involves extremely high variability prior to morphologic fixation.

3.7. References

Allegret and Ortiz, 2013. Uppermost Cretaceous to lowermost Eocene benthic foraminifera of the Dababiya Corehole: Stratigraphy, vol. 9, pp. 267–277

Abramoff, M., Magelhaes, P., and Ram, S., 2004, Image processing with ImageJ: Biophotonics international, v. 11, no. 7, p. 36–42.

Arnold, A., and Fristrup, K., 1982, The theory of evolution by natural selection: a hierarchical expansion: Paleobiology, v. 8, no. 2, p. 113–129.

Aubry, M.-P., *Cenozoic coccolithophores: Discoasterales*. New York: Micropaleontology Press. Atlas of Micropaleontology series, 3 volumes, (in press).

Aubry, M.-P., Ouda, K., and Dupuis, C., 2007, The Global Standard Stratotype-section and Point (GSSP) for the base of the Eocene Series …: Episodes.

Benton, M.J., and Pearson, P.N., 2001, Speciation in the fossil record: Trends in Ecology & Evolution, v. 16, no. 7, p. 405–411.

Berggren, W. A., & Pearson, P. N., 2005. A revised tropical to subtropical Paleogene planktonic foraminiferal zonation. The Journal of Foraminiferal Research, 35(4), 279-298.

Brand, L. E., 1994. Physiological ecology of marine coccolithophores. *Coccolithophores. Cambridge University Press, Cambridge*, 39-49.

Bown, P.R., 1998, Calcareous Nannofossil Biostratigraphy (British Micropalaeontological Society Publications Series) (P. R. Bown, Ed.): Springer.

Cheetham, A.H., and Jackson, J.B.C., 1995, Process from Pattern: Tests for Selection Versus Random Change in Punctuated Bryozoan Speciation (D. H. Erwin & R. L. Anstey, Eds.): Columbia University Press, New York.

Dupuis, C., Aubry, M.-P., Steurbaut, E., Berggren, W.A., Ouda, K., Magioncalda, R., Cramer, B., Kent, D.V., Speijer, R., and Heilmann-Clausen, C., 2003, The Dababiya Quarry Section: Lithostratigraphy, clay mineralogy, geochemistry and paleontology: Micropaleontology, v. 49, no. Suppl_1, p. 41.

Eldredge, N., and Gould, S.J., 1972, Punctuated equilibria: an alternative to phyletic gradualism: Models in paleobiology, v. 82, p. 115.

Frada, M., Probert, I., Allen, M.J., Wilson, W.H., and de Vargas, C., 2008, The "Cheshire Cat" escape strategy of the coccolithophore Emiliania huxleyi in response to viral infection.: Proceedings of the National Academy of Science, v. 105, no. 41, p. 15944–15949, doi: 10.1073/pnas.0807707105.

Gibbs, S.J., Poulton, A.J., Bown, P.R., Daniels, C.J., Hopkins, J., Young, J.R., Jones, H.L., Thiemann, G.J., O'Dea, S.A., and Newsam, C., 2013, Species-specific growth response of coccolithophores to Palaeocene--Eocene environmental change: Nature Geoscience, v. 6, no. 3, p. 1–5, doi: 10.1038/ngeo1719.

Gould, S.J., 1988, Trends as changes in variance: a new slant on progress and directionality in evolution: Journal of Paleontology, p. 319–329.

Hammer, Ø., Harper, D.A.T., Ryan, P.D., 2009. PAST: Paleontological Statistics Software Package for Education and Data Analysis, Version 1.94. Palaeontol. Electron., 4, p. 9.

Hansen, T.F., and Houle, D., 2004, Evolvability, stabilizing selection, and the problem of stasis: Phenotypic integration. Oxford University Press, Oxford,, p. 130–150.

Hull, P.M., and Norris, R.D., 2009, Evidence for abrupt speciation in a classic case of gradual evolution.: Proceedings of the National Academy of Science, v. 106, no. 50, p. 21224–21229, doi: 10.1073/pnas.0902887106.

Iglesias-Rodriguez, M.D., Halloran, P.R., Rickaby, R.E.M., Hall, I.R., Colmenero-Hidalgo, E., Gittins, J.R., Green, D.R.H., Tyrrell, T., Gibbs, S.J., Dassow, von, P., Rehm, E., Armbrust, E.V., and Boessenkool, K.P., 2008, Phytoplankton Calcification in a High-CO2 World: Science (New York, NY), v. 320, no. 5874, p. 336–340, doi: 10.1126/science.1154122.

Jackson, J., and Cheetham, A., 1999, Tempo and mode of speciation in the sea: Trends in Ecology & Evolution, v. 14, no. 2, p. 72–77.

Kellogg, D.E., 1975, The role of phyletic change in the evolution of Pseudocubus vema (Radiolaria): Paleobiology, v. 1, no. 4, p. 359–370.

Kellogg, D.E., and Hays, J.D., 1975, Microevolutionary patterns in late Cenozoic radiolaria: Paleobiology,, p. 150–160.

Kučera, M., and Malmgren, B.A., 1998, Differences between evolution of mean form and evolution of new morphotypes: an example from Late Cretaceous planktonic foraminifera: Paleobiology, v. 24, no. 1, p. 49–63.

Lazarus, D., 1983, Speciation in pelagic protista and its study in the planktonic microfossil record: a review: Paleobiology, v. 9, no. 4, p. 327–340.

Lazarus, D., Hilbrecht, H., Spencer-Cervato, C., and Thierstein, H.R., 1995, Sympatric speciation and phyletic change in Globorotalia truncatulinoides: Paleobiology, v. 21, no. 1, p. 28–51.

Lieberman, B., 1996, An evaluation of stabilizing selection as a mechanism for stasis: Palaeogeography.

Malmgren, B., Berggren, W.A., and Lohmann, G., 1983, Evidence for punctuated gradualism in the Late Neogene Globorotalia tumida lineage of planktonic foraminifera: Paleobiology, v. 9, no. 4, p. 377–389.

Malmgren, B.A., and Kennett, J.P., 1981, Phyletic gradualism in a Late Cenozoic planktonic foraminiferal lineage; DSDP Site 284, southwest Pacific: Paleobiology, v. 7, no. 2, p. 230–240.

Malmgren, B.A., and Kučera, M., 1996, Evolutionary changes in supplementary apertural characteristics of the late Neogene Sphaeroidinella dehiscens lineage (planktonic foraminifera): PALAIOS.

Mchargue, T.R., 1982, Ontogeny, phylogeny, and apparatus reconstruction of the conodont genus *Histiodella,* Joins Fm., Arbuckle Mountains, Oklahoma: Journal of Paleontology, v. 56, p. 1410-1433.

McIntyre, A., & Bé, A. W., 1967. Modern coccolithophoridae of the Atlantic Ocean—I. Placoliths and cyrtoliths. In *Deep Sea Research and Oceanographic Abstracts* (Vol. 14, No. 5, pp. 561-597). Elsevier.

Paasche, E., 1968. Marine Plankton Algae Grown with Light-Dark Cycles. *Physiologia plantarum*, *21*(1), 66-77.

Paasche, E., & Klaveness, D. (1970). A physiological comparison of coccolith-forming and naked cells of Coccolithus huxleyi. *Archiv für Mikrobiologie*, *73*(2), 143-152.

Pearson, P.N., Olsson, R.K., Huber, B.T., Hemleben, C and Berggren, W.A. (Eds.), Atlas of Eocene Planktonic Foraminifera, Cushman Foundation Special Publication, 41: 257-326.

Revelle, W., 2013. psych: Procedures for Personality and Psychological Research, Northwestern University, Evanston, Illinois, USA, http://CRAN.R-project.org/package=psych Version = 1.3.2.

Reyment, R.A., 1985, Phenotypic evolution in a lineage of the Eocene ostracod *Echinocythereis:* Paleobiology, v. 11, p. 174-194.

RStudio, 2012. RStudio: Integrated development environment for R (Version 0.97.551) [Computer software]. Boston, MA. Available from http://www.rstudio.org/

Sorhannus, U., Fenster, E.J., Burckle, L.H., And Hoffman, A, 1988, Cladogenetic and anagenetic changes in the morphology of *Rhizosolenia praebergonii* Mukhina: Historical Biology, v. 1, p. 185-205.

Wei, K., and Kennett, J., 1988, Phyletic gradualism and punctuated equilibrium in the late Neogene planktonic foraminiferal clade Globoconella: Paleobiology,, p. 345–363.

Venables, W. N. & Ripley, B. D., 2002. Modern Applied Statistics with S. Fourth Edition. Springer, New York. ISBN 0-387-95457-0

Wickham, H. ggplot2, 2009. elegant graphics for data analysis. Springer New York,

3.8. Figure captions

Figure 1.
Model of various microevolutionary trends on morphology. Morphologic stasis; Anagenesis through high variance (i.e. random walk); Anagenesis with low variance (directional trend). Arrow points to morphologic fixation. Shaded box represents proposed condition presented in this study.

Figure 2.
Map of Egypt. Location of the Dababiya quarry

Figure 3.
Graphical representations of morphostructure, for orientation of the discoaster see Aubry (in press). (a) proximal face, (b) distal face, (c) ray, (d) cross section

Figure 5.
Construction of composite section**.** In Dupuis et al. (2003) a composite of the two sections is constructed based on the correlation between three distinct pink layers. Dupuis et al. (2003) determined that the top of section DBH (9 m) is corresponds to section DBD at 7m. There is some disagreement with this correlation. A biostratographic study of planktonic foraminiferal by Kh. Ouda (personal communication) correlates the two sections (3 m overlap): 1) DBD 0.0 m (the base of DBD) corresponds to DBH 5.75 m; 2) DBD 1.0 m corresponds to DBH 6.5 m; 3) DBD 2.0 m corresponds DBH 7.5 m; 4) DBD 3.0 m is between levels DBH 8.5 m and DBH 9 m. My quantitative analysis of *H. mahmoudii* validates the latter composite section. I determine that DBD 3.0 m is approximately equivalent to DBH 8 m and that the base of DBD (0.0 m) is approximate to level DBH 6 m (since pk2 is not represent in DBD, see Dupuis et al. 2003), and that the top of the DBH (9 m) is approximate to DBD 4 m.

Figure 4.
Measured and calculated size variables. All measurements (when it applies) were taken from the center of each specimen: (1) radius of proximal knob; (2) radius of central disc; (3) radius of proximal knob depression; (4) radius distal knob. Abbreviations: PrK - Diameter of proximal knob; CD -Diameter of central disc; CDp - Diameter of proximal knob depression; LL –Lobe of length; DsK - Diameter of distal knob. Light microscope (1,600X).

Figure 6.
Graphical distribution of number of rays

Figure 7.
Stratigraphic distribution of measured variables. Dot - Mean size; dark grey – 1 standard deviation (1σ); light grey - range; bar - 95% confidence intervals. The depression of the proximal knob and the lengths of the lobes show a similar bottleneck pattern at CS3.0 as is seen in the diameter of the proximal knob. It consists of 1) early increased variability followed by 2) decreasing to a stable level. Both the lobes and the

depression are main morphologic characters of the proximal knob. The high variability exhibited by the lengths of the lobes implies that variability in the proximal knob is linked to variability in the lobes.

Figure 8.
Violin-plots and boxplots of measured characters. Black dots – outliers

Figure 9.
Distribution of variability calculated as a coefficient of variation (CV). Dot – CV; bar – 90% confidence interval. Three episodes of microevolution: 1) initial high variability (CV, 40% - 70%) over a stratigraphic range of 2.35 m lasting ~83 kyr; 2) A decrease to minimum CV (19%) over 1.15 m, this represents ~40 kyr; 3) A thick 7m interval of sustained low CV (<25%) representing ~240kyr.

Figure 10.
Typical (TY) and atypical (ATY) forms of *H. mahmoudii.* All the specimens were re-examined for these morphologic characters ("incomplete" lobes) on the proximal knob. Every specimen was assigned to either TY or ATY form. Any specimen with at least one lobe not reaching the periphery was considered "incomplete" and marked as a ATY. TY are considered "complete". To simplify, since ATY consists of 181 specimens, it was not further subdivided. Both morphotypes are present in light and scanning electron microscopy. ATY differs from TY (holotype) by its asymmetrically lobated proximal knob. In TY forms, the proximal knob is lobated radially and symmetrically; each lobe extends slightly beyond the periphery of the central disc. In ATY forms, the majority of the lobes do not reach the periphery of the central disc. Instead, the proximal knob appears "incomplete", the lobes varying in length around the knob. ATY represents a spectrum of "completeness"; from lobes being completely absent to almost completely formed (all but one lobe reaching the periphery of the central disc). In specimens without lobes, the shape of the knob appears as a central stem. In the light microscope, the stem of the knob is strongly delineated, being either circular or polygonal at the distal end. In specimens with short, non-uniform lobes unevenly distributed around the stem the lobes appear to flank the stem steeply as seen in the SEM. In these specimens, the stem is of small diameter (~2µm) and very prominent, appearing as slight protrusions around the well marked crest of the stem. In SEM faint shallow ridges are seen to run from the stem to the periphery of the central disc. Together they form a protolobe.

Figure 11.
Ordination of typical (TY) and atypical (ATY) forms calculated from the measured and calculated characters. The first canonical variates axes (CVA) jointly explain 95% of the observed variance between forms. The first CVA discriminates between the shapes of the proximal knob. Second and third CVA express overall size. The fourth CVA distinguishes morphotypes by the number of rays present. A, Ordination along the first two CVA. B, Ordination of the second and third CVA. C, Ordination along the first and third CVA. D, Ordination of first and fourth CVA. Color corresponds to forms; blue – TY; red – ATY.

Figure 12.
Scatter plots comparing the measured and calculated characters. Dark grey – TY; light grey – ATY.

Figure 13.
Stratigraphic distribution of TY and ATY forms

3.9. Table Captions

Table 1.
Criteria for the selection of morphologic characters measured

Table 2.
Descriptive statistics. Abbreviaitons: N= number of specimen; mean; sd – standard deviation; median, minimum; max – maximum; range; CV – coefficient of variation; skew – skewness; kurtosis; se – standard error. PrK - Diameter of proximal knob; CD - Diameter of central disc; CDp - Diameter of proximal knob depression; LL –Lobe of lenght; DsK - Diameter of distal knob.

Table 3.
MANOVA and post hoc Hotelling's pairwise comparisons. A. all samples in the stratigraphic sequence; B. Comparison of TY form; C. comparison of ATY form

3.10. Plate Captions

Plate 1.
Scanning electron micrographs (SEM) of proximal face (TY form)

Plate 2.
SEMs of distal face (TY form)

Plate 3.
TY form, light microscope images of (1,600X). A –proximal face; B- distal face. Scale bars = 5 μm

Plate 4.
Scanning electron micrographs (SEM) of proximal face (ATY form)

Plate 5.
ATY form, light microscope images (1,600X). A –proximal face; B- distal face. Scale bars = 5 μm

Figure 1

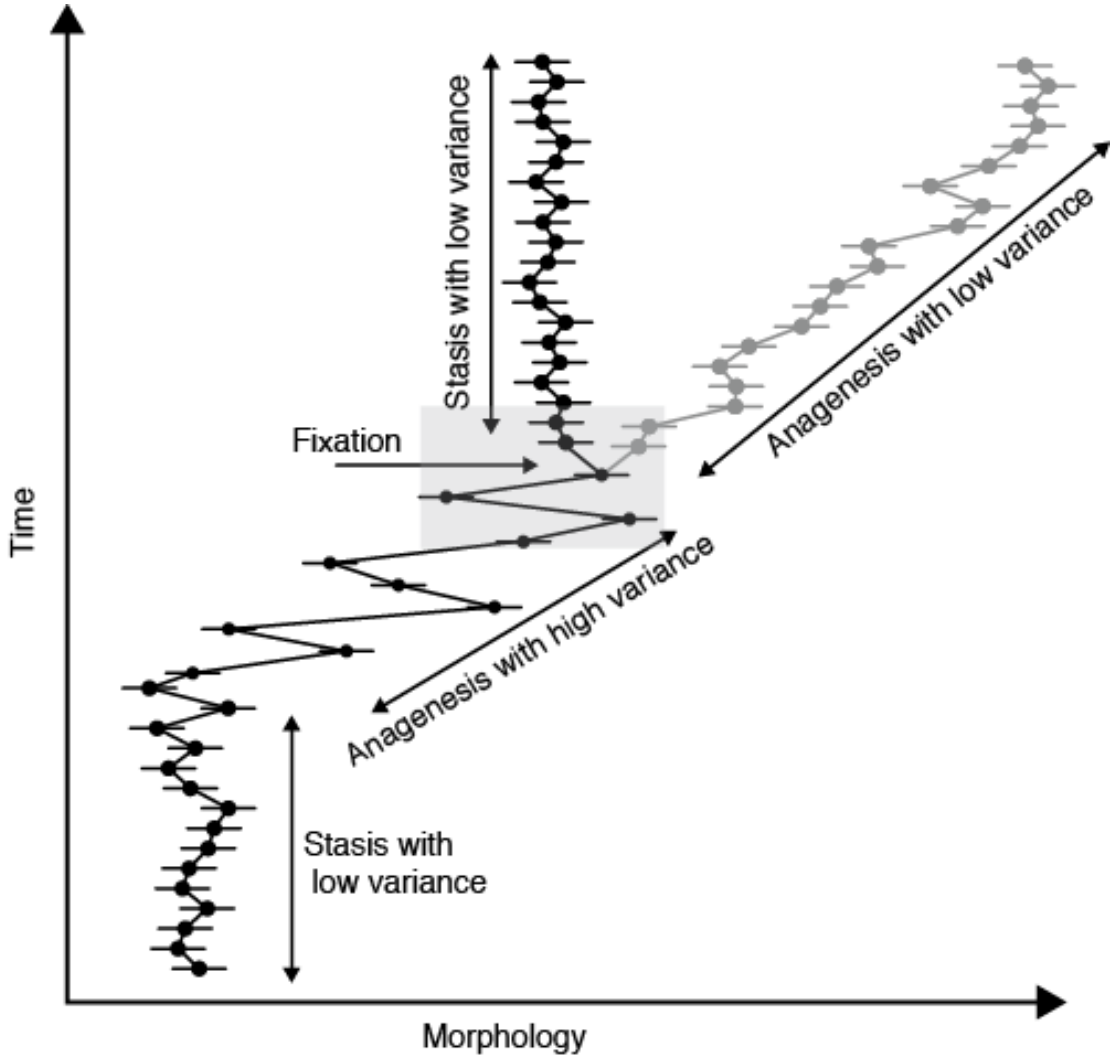
Time
Morphology
Stasis with low variance
Fixation
Anagenesis with low variance
Anagenesis with high variance
Stasis with
low variance

Figure 2.

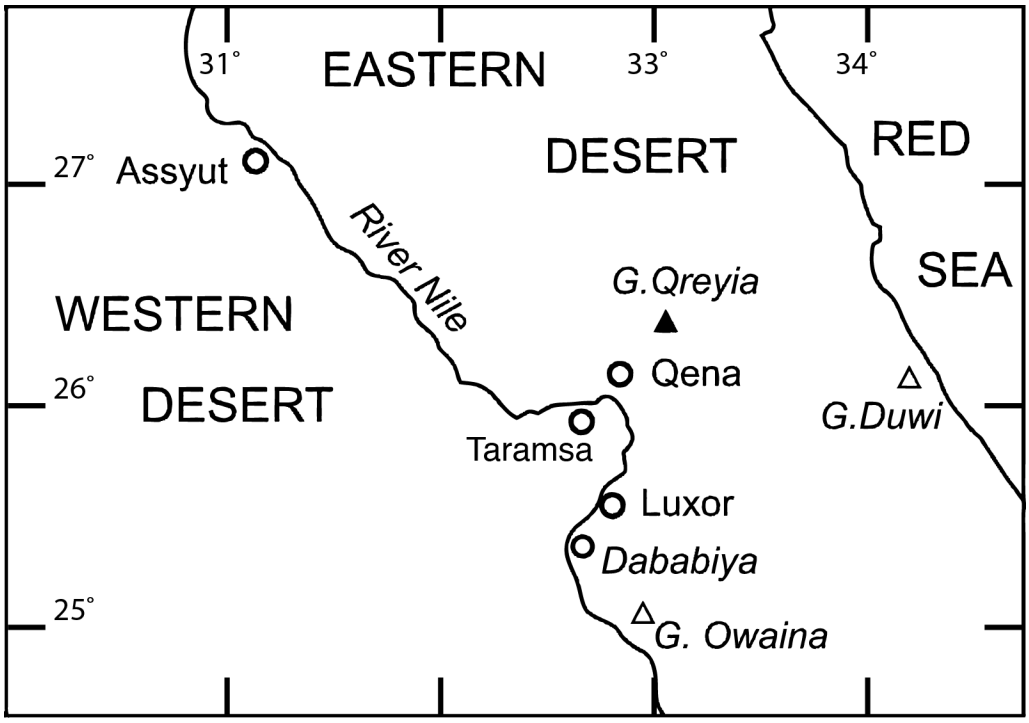
31°
EASTERN
33°
34°
DESERT
RED
SEA
27°
Assyut
River Nile
G.Qreyia
WESTERN
DESERT
26°
Qena
G.Duwi
Taramsa
Luxor
Dababiya
25°
G. Owaina

Figure 3.

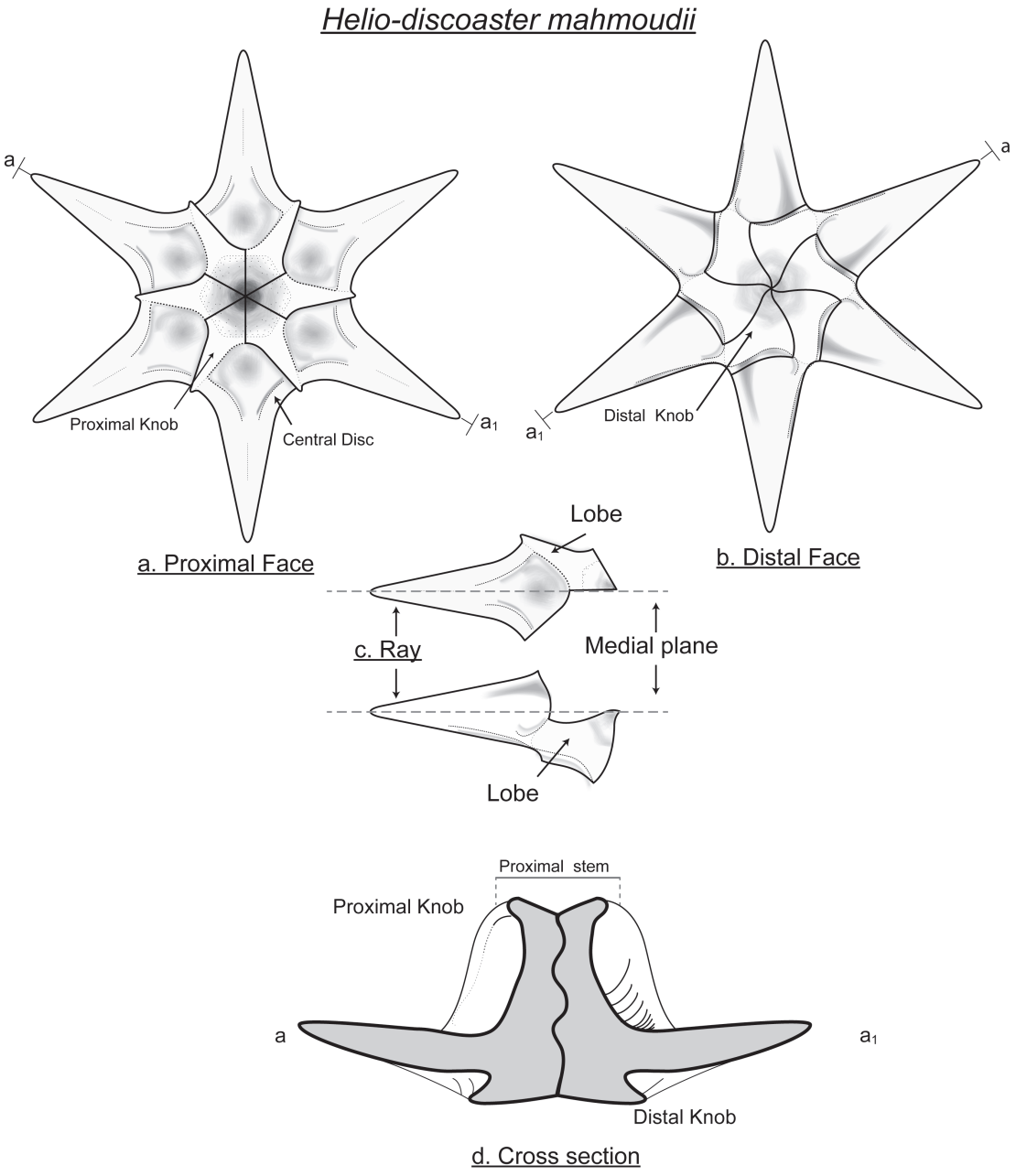
Helio-discoaster mahmoudii
a
a1
Proximal Knob
Central Disc
a. Proximal Face
a
a1
Distal Knob
b. Distal Face
Lobe
c. Ray
Medial plane
Lobe
Proximal stem
Proximal Knob
a
a1
Distal Knob
d. Cross section

Figure 4.

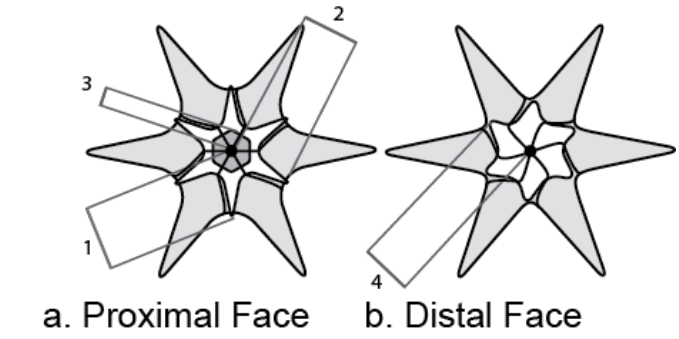

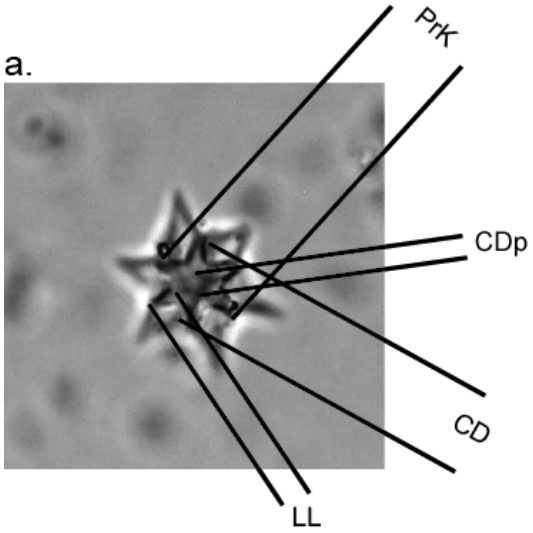

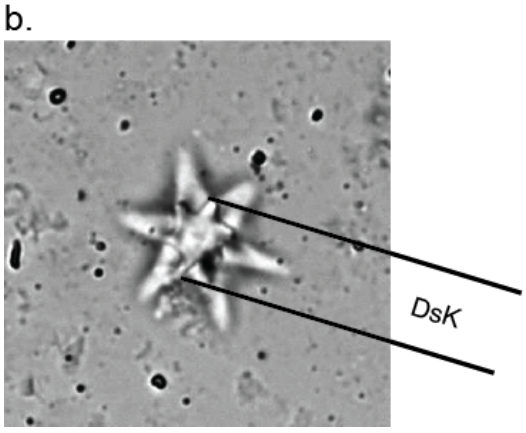

Figure 5.

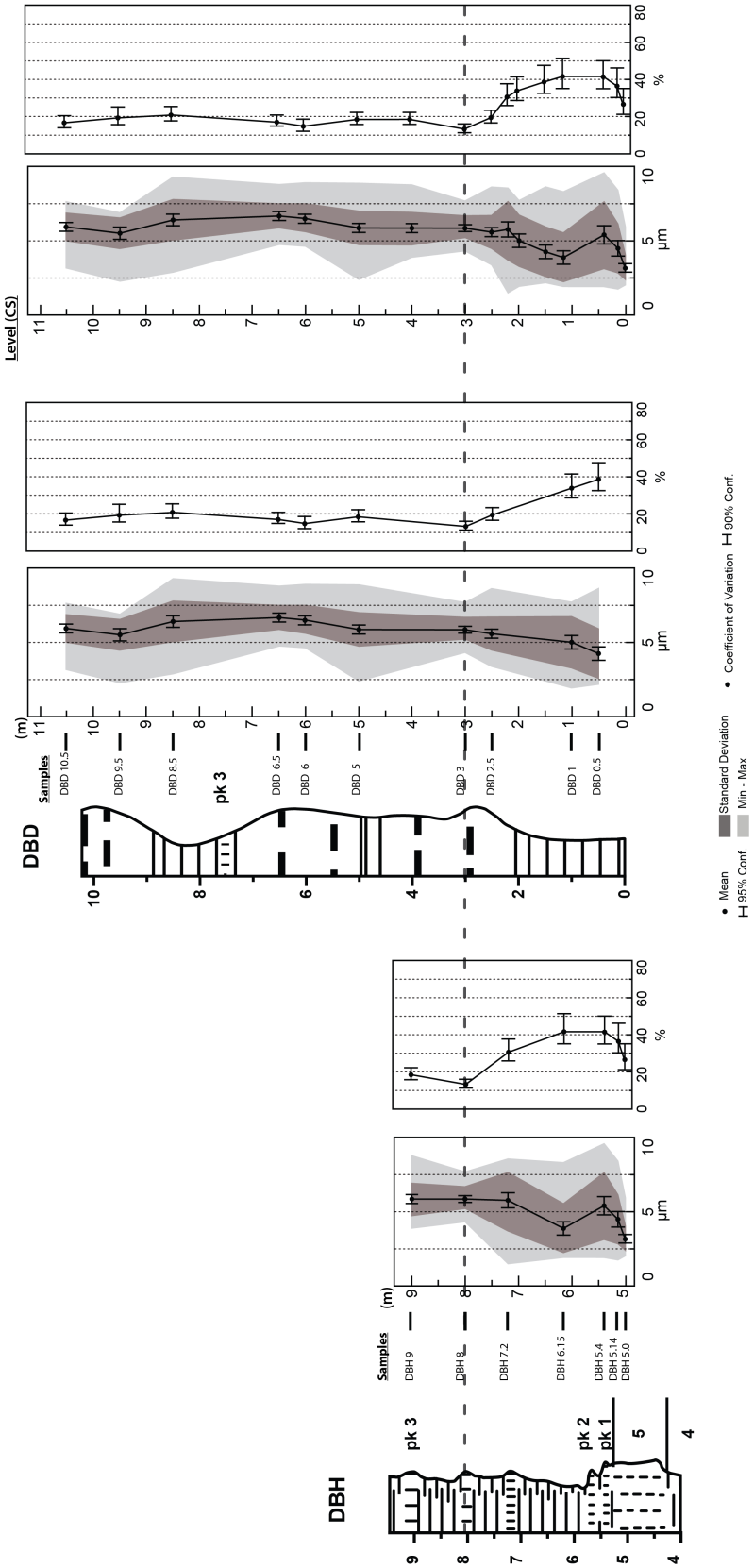
Level (CS)
Samples
DBD 10.5
DBD 9.5
DBD 8.5
DBD 6.5
DBD 6
DBD 5
DBD 3
DBD 2.5
DBD 1
DBD 0.5
DBD
pk 3
(m)
µm
%
Mean
95% Conf.
Standard Deviation
Min - Max
Coefficient of Variation
90% Conf.
DBH
pk 3
pk 2
pk 1
DBH 9
DBH 8
DBH 7.2
DBH 6.15
DBH 5.4
DBH 5.14
DBH 5.0

Figure 6.

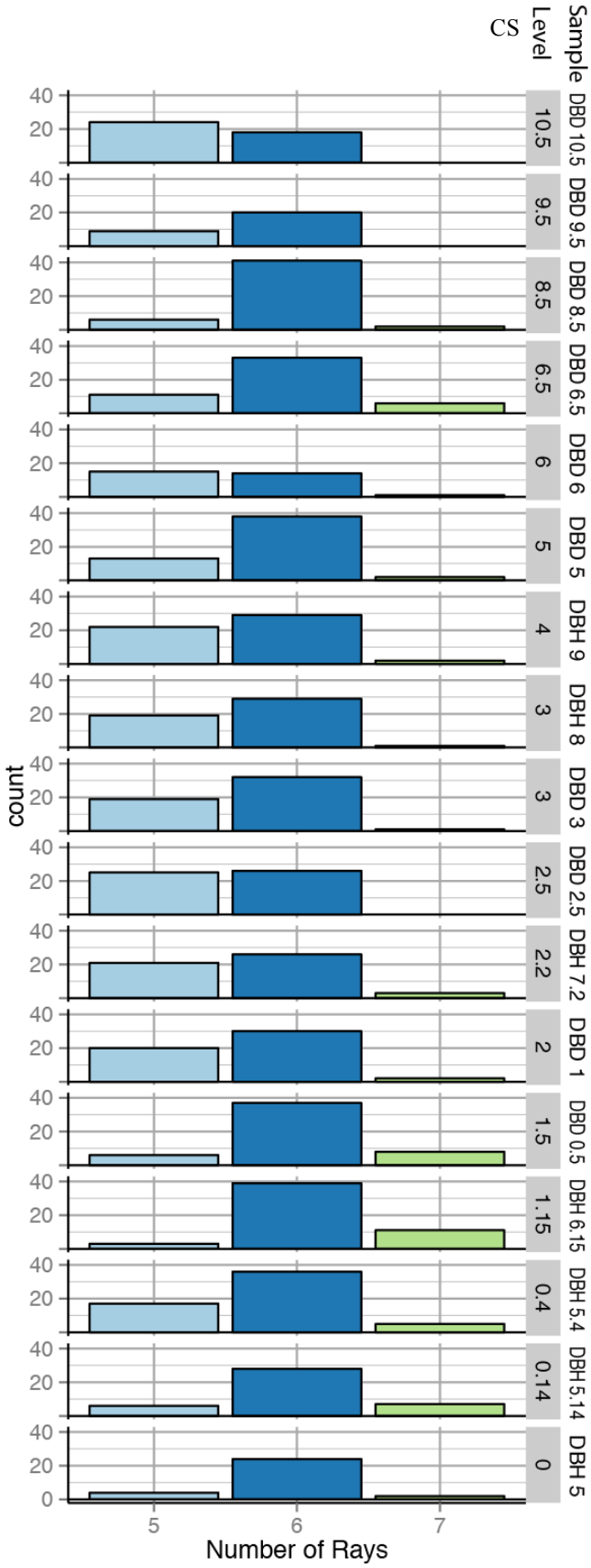
CS Level
Sample
DBD 10.5
DBD 9.5
DBD 8.5
DBD 6.5
DBD 6
DBD 5
DBH 9
DBH 8
DBD 3
DBD 2.5
DBH 7.2
DBD 1
DBD 0.5
DBH 6.15
DBH 5.4
DBH 5.14
DBH 5
count
Number of Rays

Figure 7.

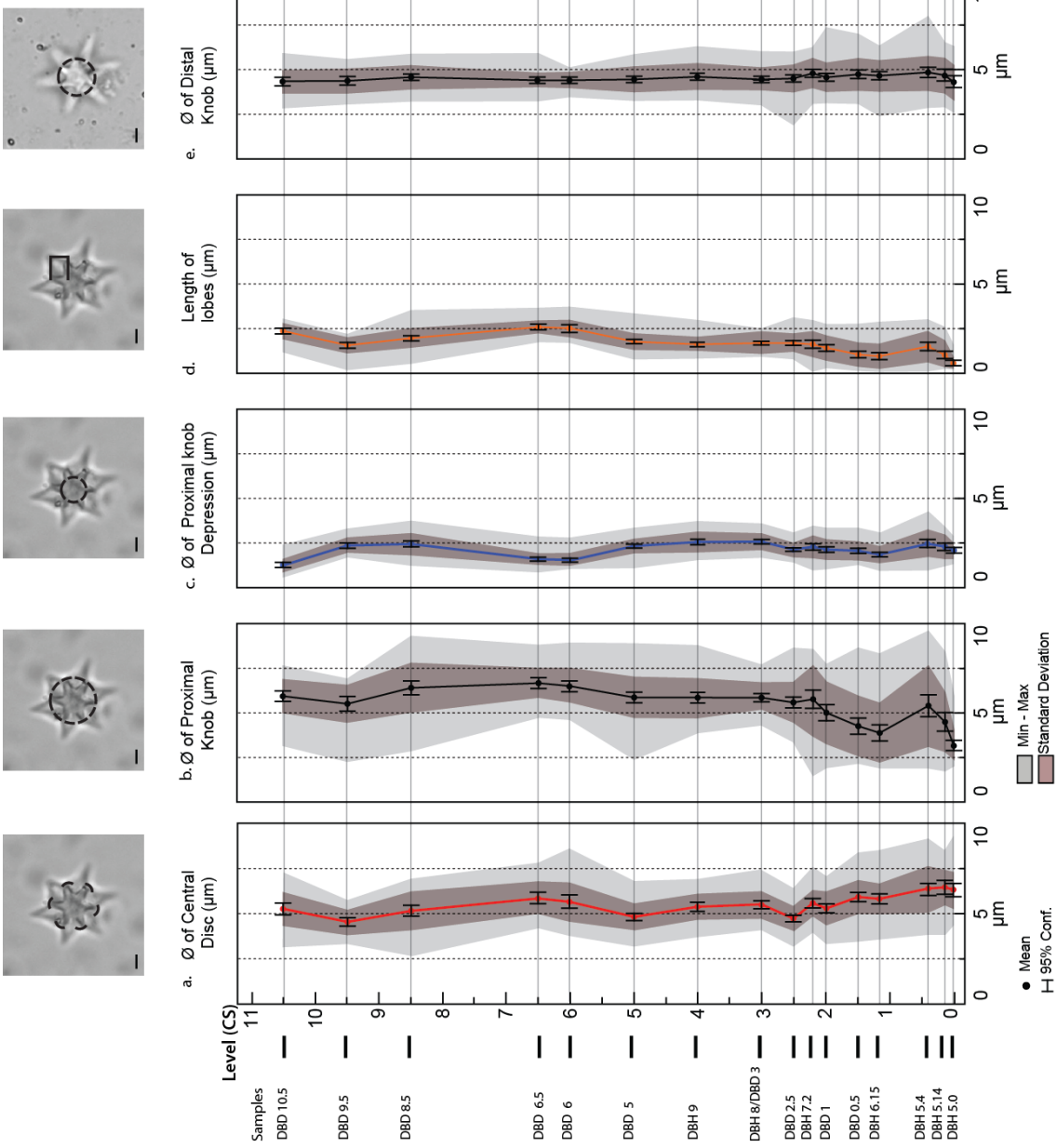
a. Ø of Central Disc (µm)
b. Ø of Proximal Knob (µm)
c. Ø of Proximal knob Depression (µm)
d. Length of lobes (µm)
e. Ø of Distal Knob (µm)
Level (CS)
Samples
DBD 10.5
DBD 9.5
DBD 8.5
DBD 6.5
DBD 6
DBD 5
DBH 9
DBH 8/DBD 3
DBD 2.5
DBH 7.2
DBD 1
DBD 0.5
DBH 6.15
DBH 5.4
DBH 5.14
DBH 5.0
Mean
95% Conf.
Min - Max
Standard Deviation
µm

Figure 8.

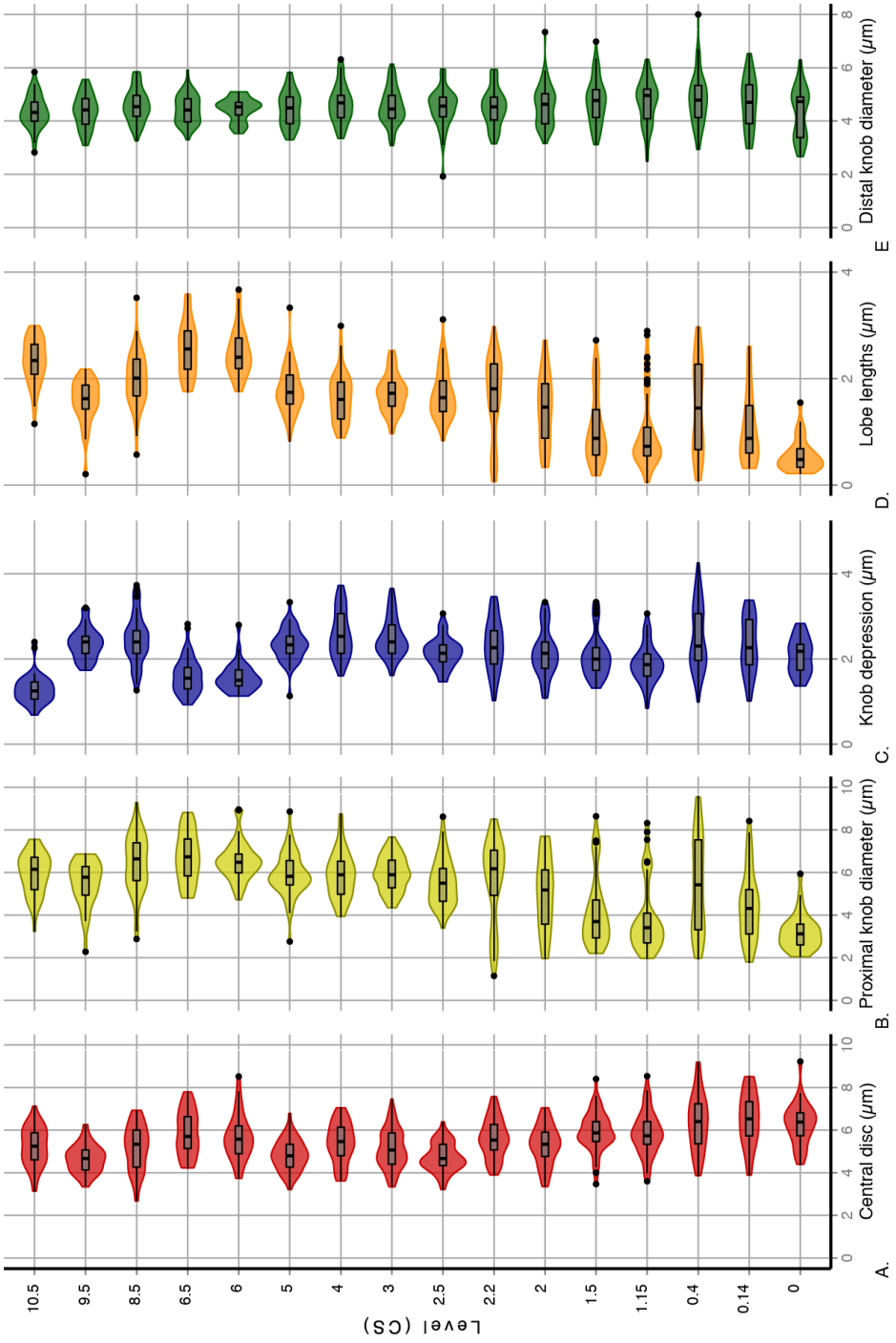
A.
Central disc (μm)
B.
Proximal knob diameter (μm)
C.
Knob depression (μm)
D.
Lobe lengths (μm)
E
Distal knob diameter (μm)
Level (CS)
10.5
9.5
8.5
6.5
6
5
4
3
2.5
2.2
2
1.5
1.15
0.4
0.14
0

Figure 9.

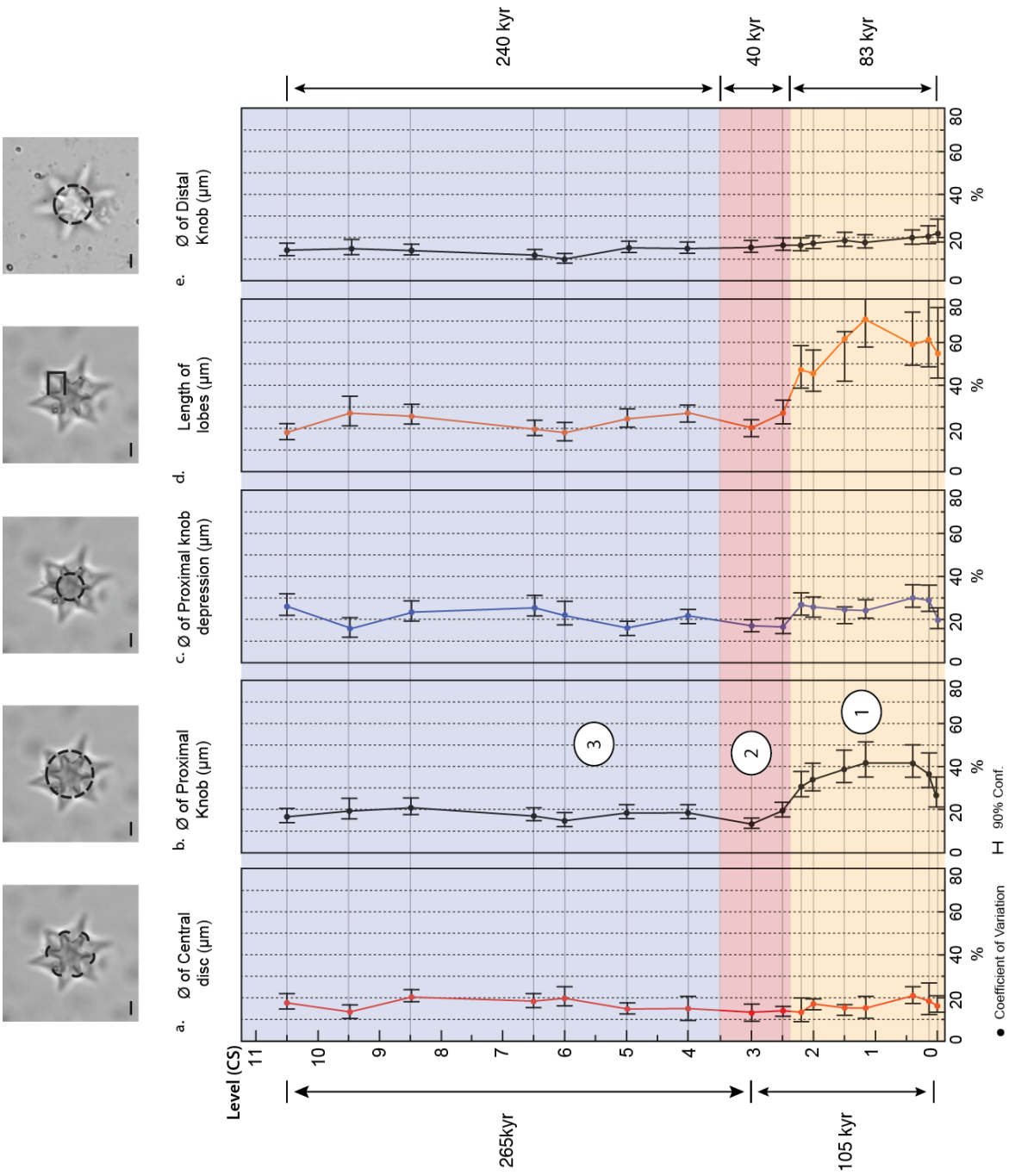
240 kyr
40 kyr
83 kyr
a. Ø of Central disc (µm)
b. Ø of Proximal Knob (µm)
c. Ø of Proximal knob depression (µm)
d. Length of lobes (µm)
e. Ø of Distal Knob (µm)
Level (CS)
265kyr
105 kyr
Coefficient of Variation
90% Conf.
%

Figure 10.

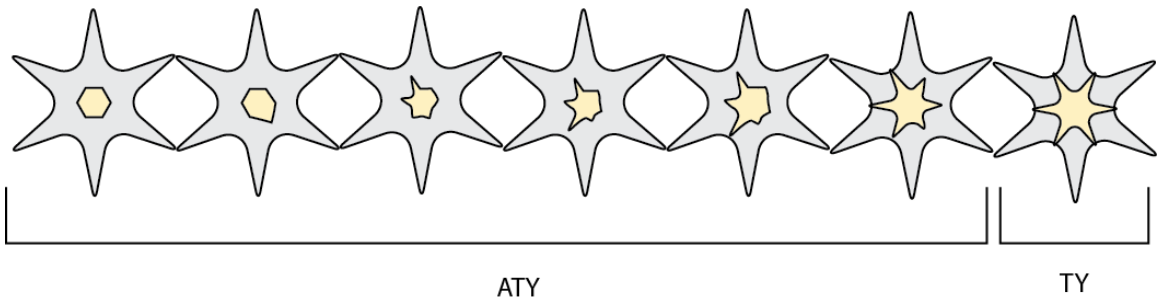

Figure 11.

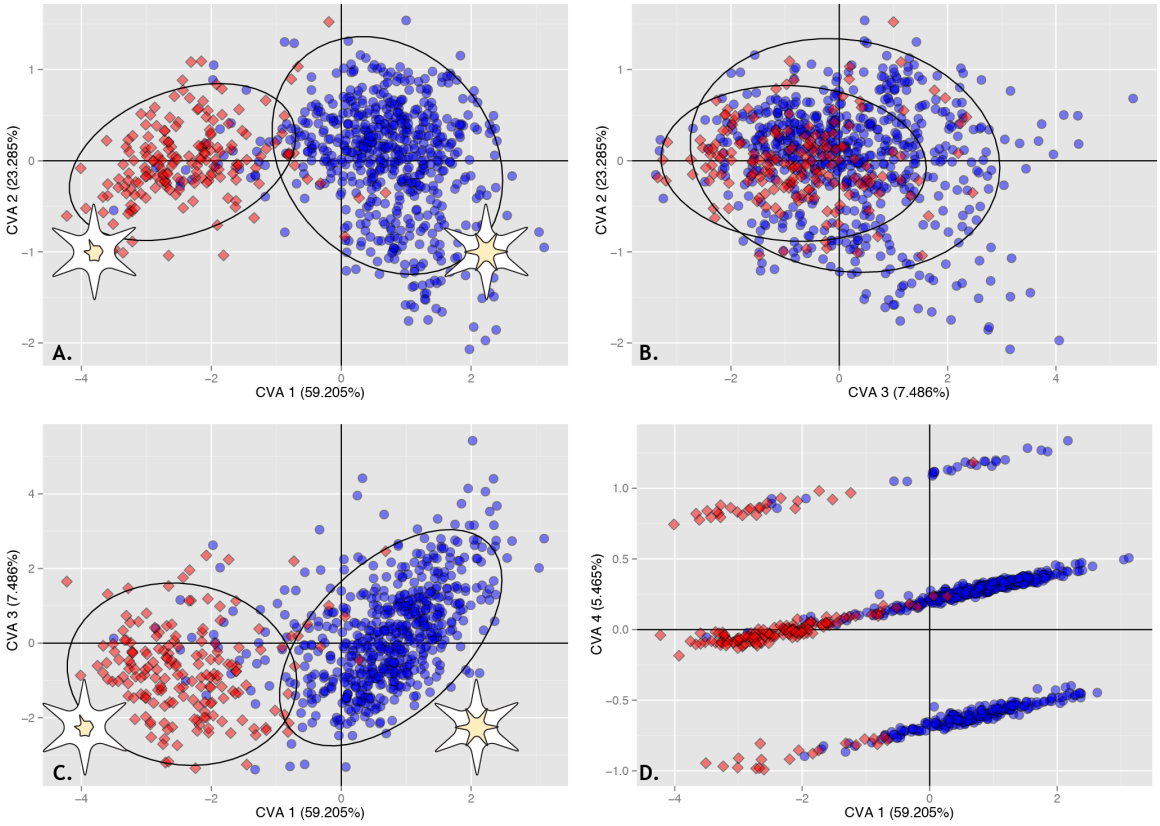

Figure 12.

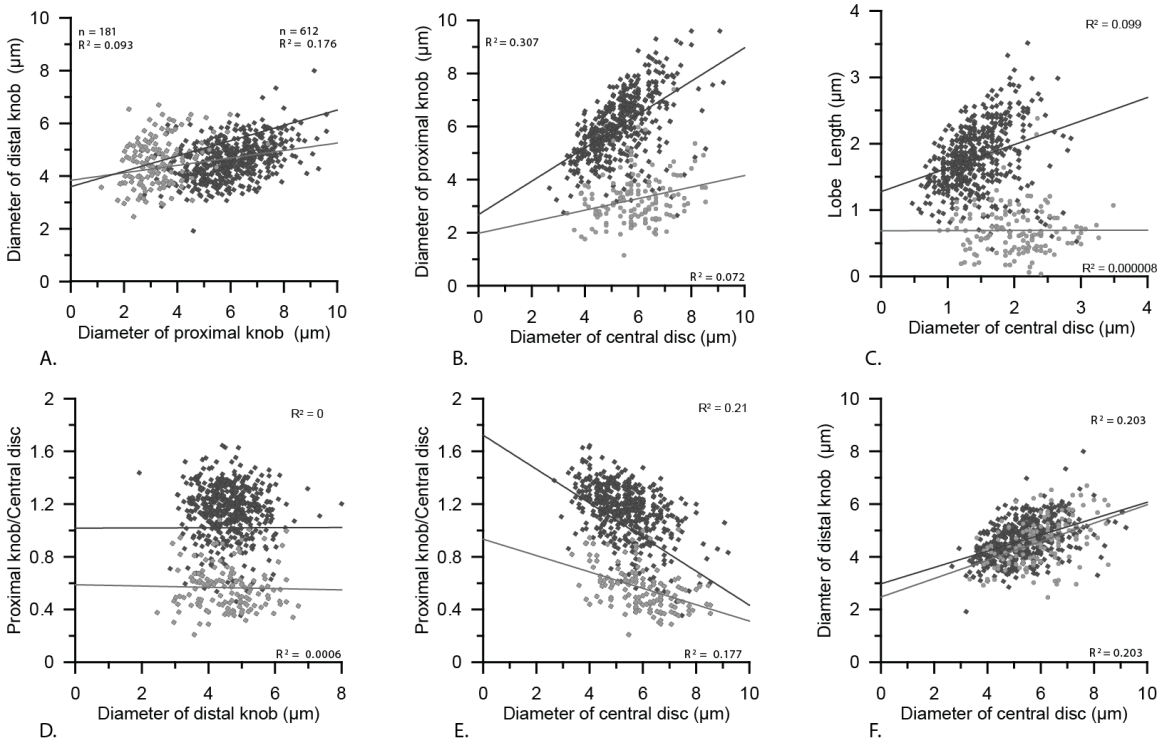
n = 181
R² = 0.093
n = 612
R² = 0.176
Diameter of distal knob (µm)
Diameter of proximal knob (µm)
A.
R² = 0.307
R² = 0.072
Diameter of proximal knob (µm)
Diameter of central disc (µm)
B.
R² = 0.099
R² = 0.000008
Lobe Length (µm)
Diameter of central disc (µm)
C.
R² = 0
R² = 0.0006
Proximal knob/Central disc
Diameter of distal knob (µm)
D.
R² = 0.21
R² = 0.177
Proximal knob/Central disc
Diameter of central disc (µm)
E.
R² = 0.203
R² = 0.203
Diamter of distal knob (µm)
Diameter of central disc (µm)
F.

Figure 13.

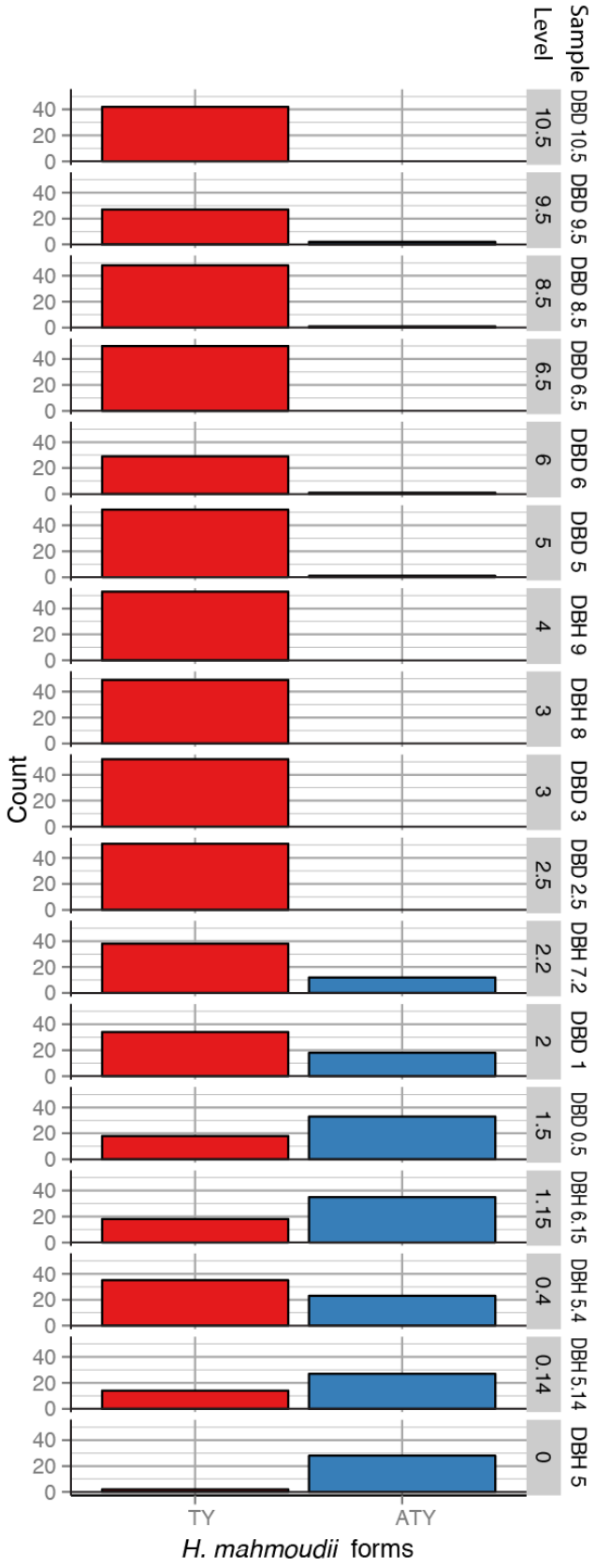
Sample
Level
DBD 10.5
10.5
DBD 9.5
9.5
DBD 8.5
8.5
DBD 6.5
6.5
DBD 6
6
DBD 5
5
DBH 9
4
DBH 8
3
DBD 3
3
DBD 2.5
2.5
DBH 7.2
2.2
DBD 1
2
DBD 0.5
1.5
DBH 6.15
1.15
DBH 5.4
0.4
DBH 5.14
0.14
DBH 5
0
Count
0
20
40
TY
ATY
H. mahmoudii forms

Table 1.

Morphologic Characters	Analyzed	Remarks
1) Number of rays	✓	Easily observed
2) Total diameter	No	Most rays were broken
3) Diameter of the central disc	✓	Measured from the inter-ray region
4) Thickness of the discoaster	No	Unreliable
5) Angle between rays	No	Difficult to determine due to perspective effect
6) Proximal knob		
6a) Ø of the knob	✓	Represents Ø of knob base
6b) Ø of the central depression	✓	Measured from the center
6c) lengths of the free portion of the lobes	✓	Calculated (6a-6b = 6c)
6d) angle between the lobes	No	Difficult due to perspective effect and modified by preservation
7) Distal knob		
7a) Ø of the knob	✓	Measured when knob is delineated
7b) Ø of the central depression	No	Not present in every specimen
7c) length of lobe	No	No free lobes

Table 2.

Sample		n	mean	sd	median	min	max	range	CV	skew	kurtosis	se
DBH 5.0	PrK	30	3.2	0.85	3.12	2.04	5.94	3.9	26.56	1.25	1.76	0.15
	CDp	30	2.07	0.42	2.18	1.36	2.84	1.48	20.29	0.09	-1.14	0.08
	CD	30	6.29	1.01	6.38	4.36	9.22	4.86	16.06	0.39	0.66	0.18
	LL	30	0.56	0.31	0.48	0.21	1.55	1.34	55.36	1.39	1.53	0.06
	DsK	30	4.31	0.95	4.73	2.64	6.32	3.68	22.04	-0.01	-1.18	0.17
DBH 5.14	PrK	41	4.44	1.63	4.32	1.76	8.42	6.66	36.71	0.55	-0.41	0.26
	CDp	41	2.31	0.66	2.27	1	3.4	2.4	28.57	-0.08	-1.13	0.1
	CD	41	6.5	1.24	6.53	3.87	8.53	4.66	19.08	-0.21	-0.83	0.19
	LL	41	1.06	0.65	0.88	0.31	2.61	2.3	61.32	0.89	-0.28	0.1
	DsK	41	4.7	0.97	4.7	2.96	6.54	3.58	20.64	-0.12	-1.01	0.15
DBH 5.4	PrK	58	5.41	2.25	5.42	1.92	9.6	7.68	41.59	0.21	-1.28	0.3
	CDp	58	2.51	0.76	2.3	0.98	4.27	3.29	30.28	0.32	-0.91	0.1
	CD	58	6.35	1.31	6.4	3.85	9.2	5.35	20.63	0.1	-0.66	0.17
	LL	58	1.45	0.86	1.45	0.07	2.99	2.92	59.31	0.12	-1.39	0.11
	DsK	58	4.8	0.96	4.78	2.92	8	5.08	20.00	0.59	0.86	0.13
DBH 6.15	PrK	53	3.85	1.63	3.41	1.94	8.32	6.38	42.34	1.19	0.28	0.22
	CDp	53	1.88	0.45	1.87	0.84	3.07	2.23	23.94	0.35	0.21	0.06
	CD	53	5.85	1.02	5.73	3.6	8.53	4.93	17.44	0.21	0.02	0.14
	LL	53	0.99	0.7	0.73	0.04	2.89	2.86	70.71	1.2	0.43	0.1
	DsK	53	4.7	0.83	4.96	2.46	6.34	3.88	17.66	-0.47	-0.12	0.11
DBH 7.2	PrK	50	5.64	1.96	6.17	1.15	8.54	7.4	34.75	-0.73	-0.66	0.28
	CDp	50	2.32	0.61	2.27	1.03	3.47	2.44	26.29	-0.06	-0.76	0.09
	CD	50	5.61	0.92	5.53	3.87	7.6	3.73	16.40	0.11	-0.74	0.13
	LL	50	1.66	0.79	1.81	0.06	2.98	2.92	47.59	-0.61	-0.78	0.11
	DsK	50	4.52	0.7	4.53	3.13	5.95	2.81	15.49	0.15	-0.55	0.1
DBH 8	PrK	49	6.06	0.82	6.01	4.4	7.69	3.29	13.53	-0.18	-0.79	0.12
	CDp	49	2.61	0.44	2.53	1.73	3.6	1.87	16.86	0.38	-0.7	0.06
	CD	49	5.52	0.77	5.6	4.13	7.47	3.33	13.95	0.36	-0.56	0.11
	LL	49	1.73	0.35	1.72	1.05	2.53	1.48	20.23	0.26	-0.53	0.05
	DsK	49	4.66	0.72	4.59	3.07	6.03	2.96	15.45	0.09	-0.76	0.1
DBH 9	PrK	53	5.87	1.1	5.9	3.91	8.78	4.87	18.74	0.42	-0.1	0.15
	CDp	53	2.59	0.56	2.53	1.6	3.73	2.13	21.62	0.37	-0.93	0.08
	CD	53	5.4	0.93	5.47	3.6	7.07	3.47	17.22	-0.2	-0.92	0.13
	LL	53	1.64	0.45	1.61	0.88	2.99	2.11	27.44	0.52	0.22	0.06
	DsK	53	4.63	0.7	4.68	3.34	6.31	2.97	15.12	0.36	-0.43	0.1
DBD 0.5	PrK	51	4.18	1.64	3.7	2.18	8.64	6.46	39.23	1.07	0.08	0.23
	CDp	51	2.07	0.51	2	1.31	3.33	2.03	24.64	0.93	0.26	0.07
	CD	51	5.94	0.92	5.87	3.47	8.4	4.93	15.49	-0.1	0.53	0.13
	LL	51	1.05	0.65	0.88	0.17	2.72	2.55	61.90	0.88	-0.38	0.09
	DsK	51	4.74	0.86	4.77	3.11	6.98	3.87	18.14	0.28	-0.34	0.12
DBD 1	PrK	52	5	1.69	5.18	1.94	7.72	5.78	33.80	-0.1	-1.08	0.23
	CDp	52	2.14	0.55	2.13	1.07	3.33	2.27	25.70	0.33	-0.46	0.08
	CD	52	5.31	0.92	5.33	3.33	7.07	3.73	17.33	-0.2	-0.63	0.13
	LL	52	1.43	0.65	1.46	0.33	2.73	2.4	45.45	0.04	-0.99	0.09
	DsK	52	4.57	0.77	4.62	3.15	7.34	4.19	16.85	0.77	1.34	0.11
DBD 2.5	PrK	51	5.55	1.1	5.5	3.38	8.62	5.24	19.82	0.59	-0.11	0.15
	CDp	51	2.14	0.35	2.13	1.45	3.07	1.61	16.36	0.23	-0.04	0.05
	CD	51	4.73	0.67	4.67	3.2	6.4	3.2	14.16	0.19	-0.35	0.09
	LL	51	1.7	0.46	1.64	0.82	3.11	2.29	27.06	0.74	0.28	0.06
	DsK	51	4.5	0.72	4.56	1.92	5.96	4.04	16.00	-0.77	1.91	0.1
DBD 3	PrK	52	5.86	0.82	5.88	4.32	7.69	3.37	13.99	0.19	-0.77	0.11
	CDp	52	2.4	0.46	2.27	1.6	3.67	2.07	19.17	1.02	0.72	0.06
	CD	52	4.75	0.87	4.67	3.33	7.07	3.73	18.32	0.58	-0.29	0.12
	LL	52	1.73	0.36	1.73	0.96	2.49	1.53	20.81	0.18	-0.35	0.05
	DsK	52	4.45	0.63	4.43	3.26	6.14	2.88	14.16	0.32	-0.02	0.09
DBD 5	PrK	53	5.9	1.01	5.82	2.76	8.86	6.1	17.12	0.01	1.33	0.14
	CDp	53	2.34	0.38	2.33	1.13	3.33	2.2	16.24	-0.18	0.93	0.05
	CD	53	4.82	0.72	4.8	3.2	6.8	3.6	14.94	0.21	-0.19	0.1
	LL	53	1.78	0.43	1.74	0.81	3.33	2.52	24.16	0.69	1.52	0.06
	DsK	53	4.45	0.66	4.49	3.28	5.84	2.56	14.83	0.14	-0.88	0.09
DBD 6	PrK	30	6.55	0.95	6.48	4.7	8.96	4.26	14.50	0.69	0.65	0.17
	CDp	30	1.57	0.34	1.5	1.12	2.8	1.68	21.66	1.59	3.29	0.06
	CD	30	5.66	1.09	5.57	3.72	8.52	4.8	19.26	0.59	0.19	0.2
	LL	30	2.49	0.45	2.4	1.75	3.67	1.92	18.07	0.75	0.16	0.08
	DsK	30	4.45	0.44	4.53	3.52	5.1	1.58	9.89	-0.44	-0.78	0.08
DBD 6.5	PrK	50	6.73	1.17	6.73	4.78	8.84	4.06	17.38	0.04	-1.13	0.17
	CDp	50	1.61	0.42	1.55	0.92	2.82	1.9	26.09	0.77	0.44	0.06
	CD	50	5.87	1.03	5.7	4.2	7.82	3.62	17.55	0.1	-1.18	0.15
	LL	50	2.56	0.51	2.56	1.74	3.6	1.86	19.92	0.3	-0.81	0.07
	DsK	50	4.43	0.54	4.41	3.28	5.92	2.64	12.19	0.25	-0.44	0.08
DBD 8.5	PrK	49	6.41	1.35	6.64	2.88	9.3	6.42	21.06	-0.42	-0.05	0.19
	CDp	49	2.46	0.57	2.4	1.27	3.73	2.47	23.17	0.19	-0.39	0.08
	CD	49	5.16	1.06	5.33	2.67	6.93	4.27	20.54	-0.3	-0.74	0.15
	LL	49	1.97	0.5	2.01	0.57	3.52	2.94	25.38	0.07	1.09	0.07
	DsK	49	4.58	0.62	4.54	3.24	5.86	2.62	13.54	0.2	-0.55	0.09
DBD 9.5	PrK	29	5.51	1.08	5.78	2.28	6.9	4.62	19.60	-1.03	0.78	0.2
	CDp	29	2.37	0.37	2.4	1.73	3.2	1.47	15.61	0.44	-0.33	0.07
	CD	29	4.65	0.65	4.67	3.33	6.27	2.94	13.98	0.28	-0.24	0.12
	LL	29	1.57	0.43	1.62	0.21	2.18	1.98	27.39	-1.17	1.55	0.08
	DsK	29	4.37	0.63	4.42	3.08	5.56	2.48	14.42	-0.09	-0.83	0.12
DBD 10.5	PrK	42	5.95	0.98	6.15	3.22	7.58	4.36	16.47	-0.5	-0.24	0.15
	CDp	42	1.29	0.34	1.25	0.68	2.4	1.72	26.36	1.16	2.31	0.05
	CD	42	5.23	0.91	5.24	3.12	7.14	4.02	17.40	-0.19	-0.64	0.14
	LL	42	2.33	0.42	2.34	1.15	3	1.85	18.03	-0.57	-0.12	0.07
	DsK	42	4.36	0.61	4.32	2.82	5.84	3.02	13.99	0.02	-0.01	0.09

Table 3.

A. All characters and Level

Overall: Wilk's λ = 0.1605; d.f. 120. 5494; F=13.42; p<0.0001

Level	CS 0	CS 0.14	CS 0.4	CS 1.15	CS 1.5	CS 1	CS 2.2	CS 2.5	CS 3	CS 4	CS 5	CS 6	CS 6.5	CS 8.5	CS 9.5	CS 10.5
CS 0	1.00	**0.01**	<	<	<	<	<	<	<	<	<	<	<	<	<	<
CS 0.14		1.00	0.07	<	<	<	<	<	<	<	<	<	<	<	<	<
CS 0.4			1.00	<	<	<	**0.01**	<	<	<	<	<	<	<	<	<
CS 1.15				1.00	0.43	<	<	<	<	<	<	<	<	<	<	<
CS 1.5					1.00	**0.01**	<	<	<	<	<	<	<	<	<	<
CS 1						1.00	0.34	<	**0.01**	**0.01**	<	<	<	<	<	<
CS 2.2							1.00	<	0.12	0.09	<	<	<	<	<	<
CS 2.5								1.00	<	<	<	<	<	<	<	<
CS 3									1.00	0.83	0.38	<	<	**0.03**	0.40	<
CS 4										1.00	<	<	<	<	**0.02**	<
CS 5											1.00	<	<	0.09	0.19	<
CS 6												1.00	**0.04**	<	<	**0.04**
CS 6.5													1.00	<	<	<
CS 8.5														1.00	**0.01**	<
CS 9.5															1.00	<
CS 10.5																1.00

B. TY forms and Level

Overall: Wilk's λ = 0.2344; d.f. 75. 2840; F = 13.39; p < 0.0001

Level	CS 0	CS 0.14	CS 0.4	CS 1.15	CS 1.5	CS 1	CS 2.2	CS 2.5	CS 3	CS 4	CS 5	CS 6	CS 6.5	CS 8.5	CS 9.5	CS 10.5
CS 0	1.00	0.81	0.37	0.35	0.14	**0.01**	**0.01**	<	<	<	<	<	<	<	<	<
CS 0.14		1.00	0.15	0.06	**0.01**	<	<	<	<	<	<	<	<	<	<	<
CS 0.4			1.00	**0.01**	**0.01**	<	<	<	<	<	<	<	<	<	<	<
CS 1.15				1.00	0.33	**0.01**	**0.02**	<	<	<	<	<	<	<	<	<
CS 1.5					1.00	0.87	0.17	**0.01**	0.18	0.46	<	<	<	**0.02**	<	<
CS 1						1.00	0.08	0.05	0.42	0.19	**0.01**	<	<	**0.03**	**0.01**	<
CS 2.2							1.00	<	<	**0.01**	<	<	<	**0.04**	<	<
CS 2.5								1.00	<	<	<	<	<	<	<	<
CS 3									1.00	0.09	<	<	<	<	0.27	<
CS 4										1.00	<	<	<	<	**0.01**	<
CS 5											1.00	<	<	0.08	0.27	<
CS 6												1.00	0.94	<	<	**0.02**
CS 6.5													1.00	<	<	<
CS 8.5														1.00	**0.04**	<
CS 9.5															1.00	<
CS 10.5																1.00

C. ATY and Level

Overall: Wilk's λ= 0.6826; d.f. = 35. 700; F = 1.903; p= 0.001

Level	CS 0	CS 0.14	CS 0.4	CS 1.15	CS 1	CS 2.2	CS 2.5	CS 9.5
CS 0	1.00	0.10	0.29	<	<	<	<	0.18
CS 0.14		1.00	0.27	**0.02**	**0.02**	0.08	0.27	0.73
CS 0.4			1.00	**0.04**	0.22	0.53	0.28	0.69
CS 1.15				1.00	0.47	0.28	0.61	0.25
CS 1					1.00	0.19	0.10	0.06
CS 2.2						1.00	0.54	0.58
CS 2.5							1.00	0.89
CS 9.5								1.00

Plate 1.

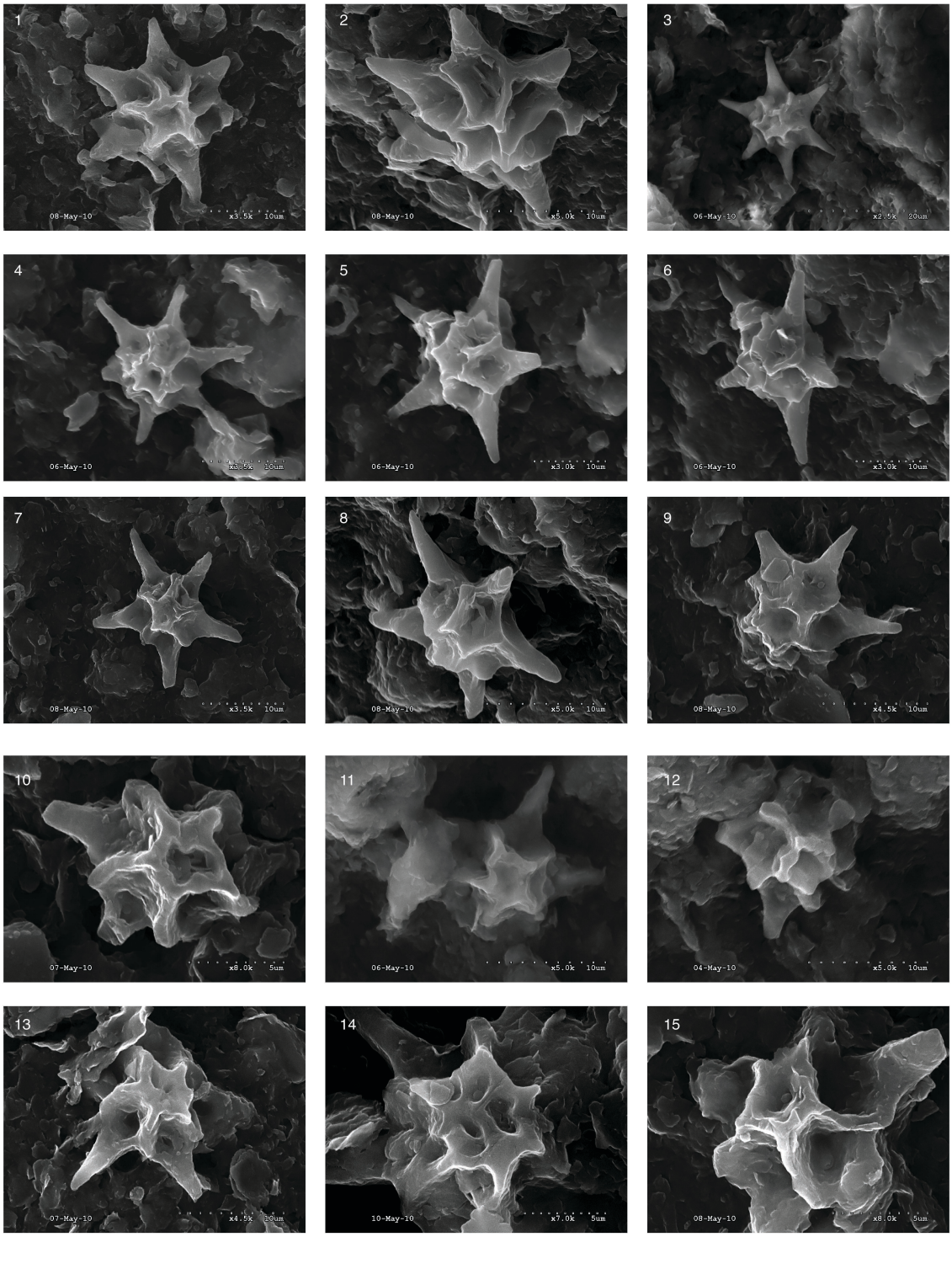
1
08-May-10 x3.5k 10um
2
08-May-10 x5.0k 10um
3
06-May-10 x2.5k 20um
4
06-May-10 x3.5k 10um
5
06-May-10 x3.0k 10um
6
06-May-10 x3.0k 10um
7
08-May-10 x3.5k 10um
8
08-May-10 x5.0k 10um
9
08-May-10 x4.5k 10um
10
07-May-10 x8.0k 5um
11
06-May-10 x5.0k 10um
12
04-May-10 x5.0k 10um
13
07-May-10 x4.5k 10um
14
10-May-10 x7.0k 5um
15
08-May-10 x8.0k 5um

Plate 2.

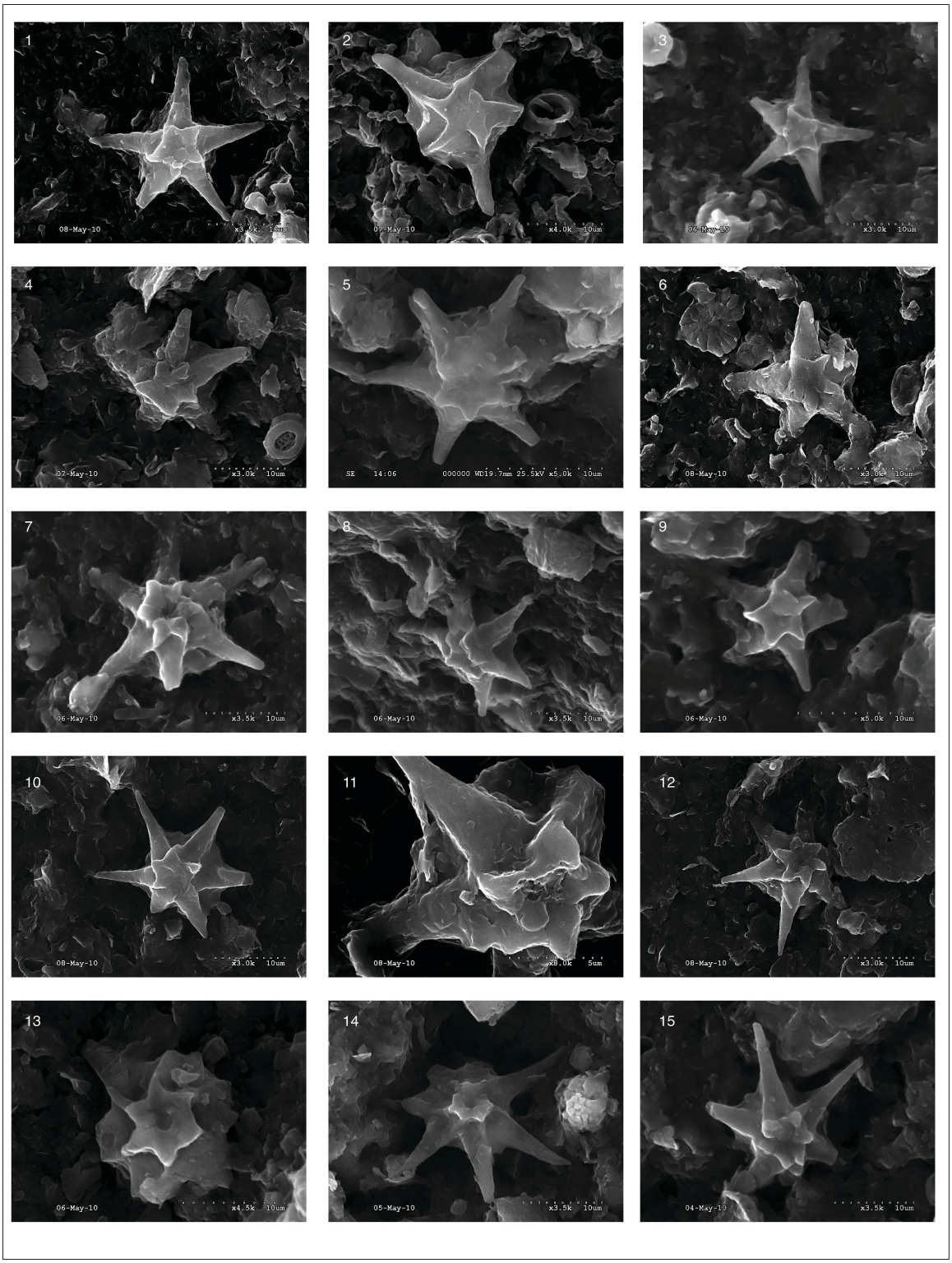
1
08-May-10
2
07-May-10
3
4
07-May-10
5
6
08-May-10
7
06-May-10
8
06-May-10
9
06-May-10
10
08-May-10
11
08-May-10
12
08-May-10
13
06-May-10
14
05-May-10
15
04-May-10

Plate 3.

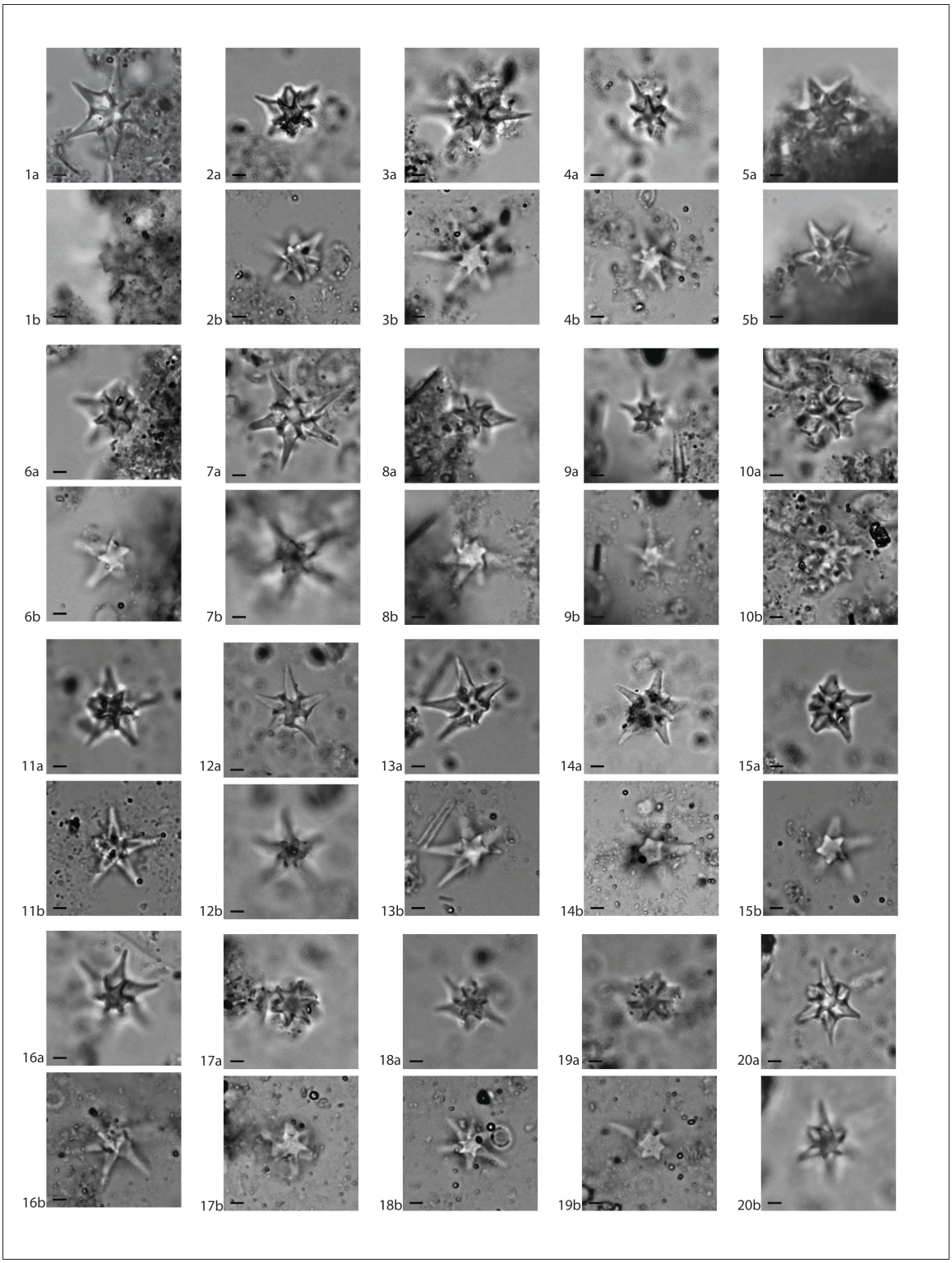
1a
2a
3a
4a
5a
1b
2b
3b
4b
5b
6a
7a
8a
9a
10a
6b
7b
8b
9b
10b
11a
12a
13a
14a
15a
11b
12b
13b
14b
15b
16a
17a
18a
19a
20a
16b
17b
18b
19b
20b

Plate 4.

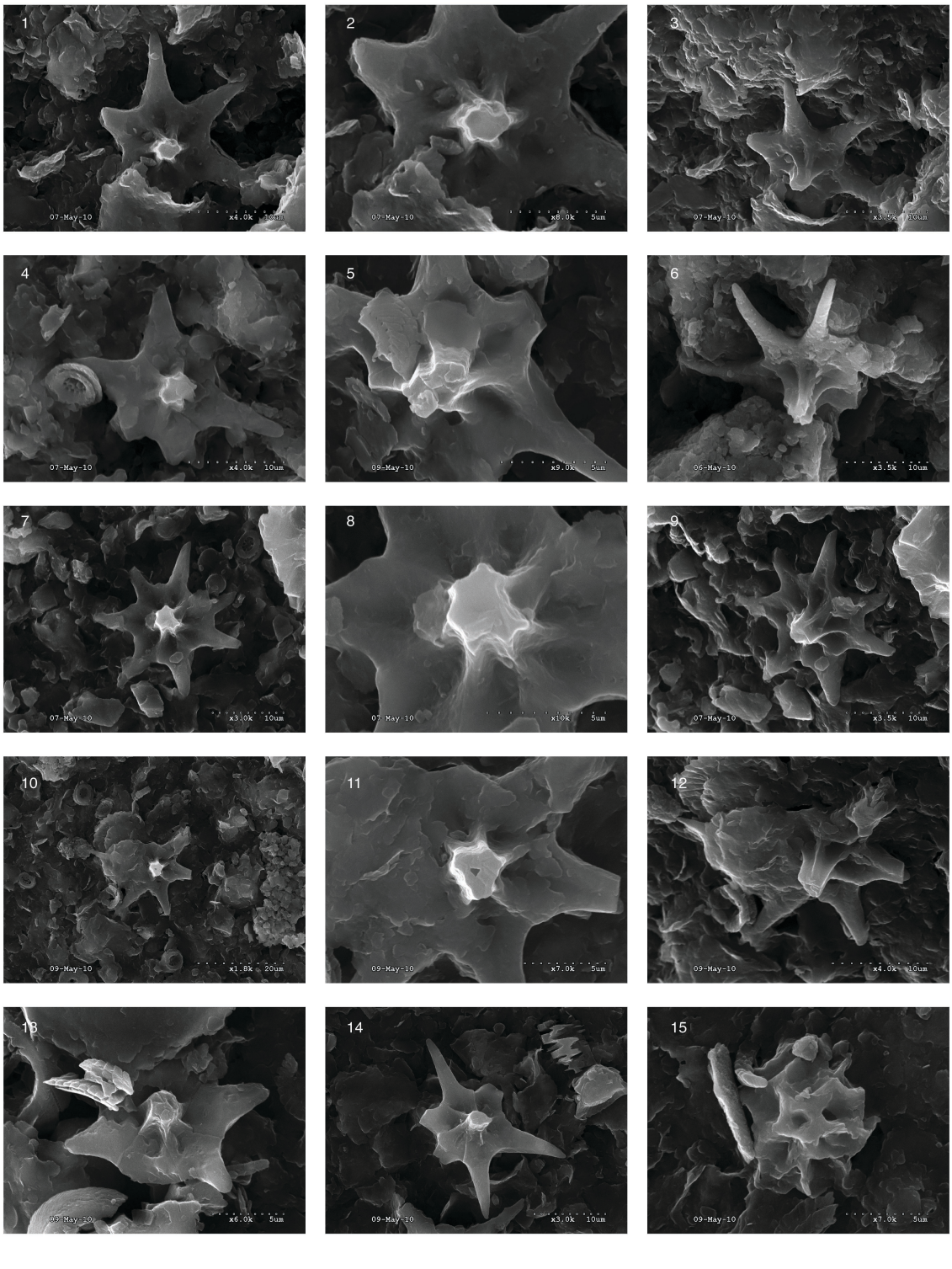
1
07-May-10 x4.0k 10um
2
07-May-10 x8.0k 5um
3
07-May-10 x3.5k 10um
4
07-May-10 x4.0k 10um
5
09-May-10 x9.0k 5um
6
06-May-10 x3.5k 10um
7
07-May-10 x3.0k 10um
8
07 May 10 x10k 5um
9
07-May-10 x3.5k 10um
10
09-May-10 x1.8k 20um
11
09-May-10 x7.0k 5um
12
09-May-10 x4.0k 10um
13
09-May-10 x6.0k 5um
14
09-May-10 x3.0k 10um
15
09-May-10 x7.0k 5um

Plate 5.

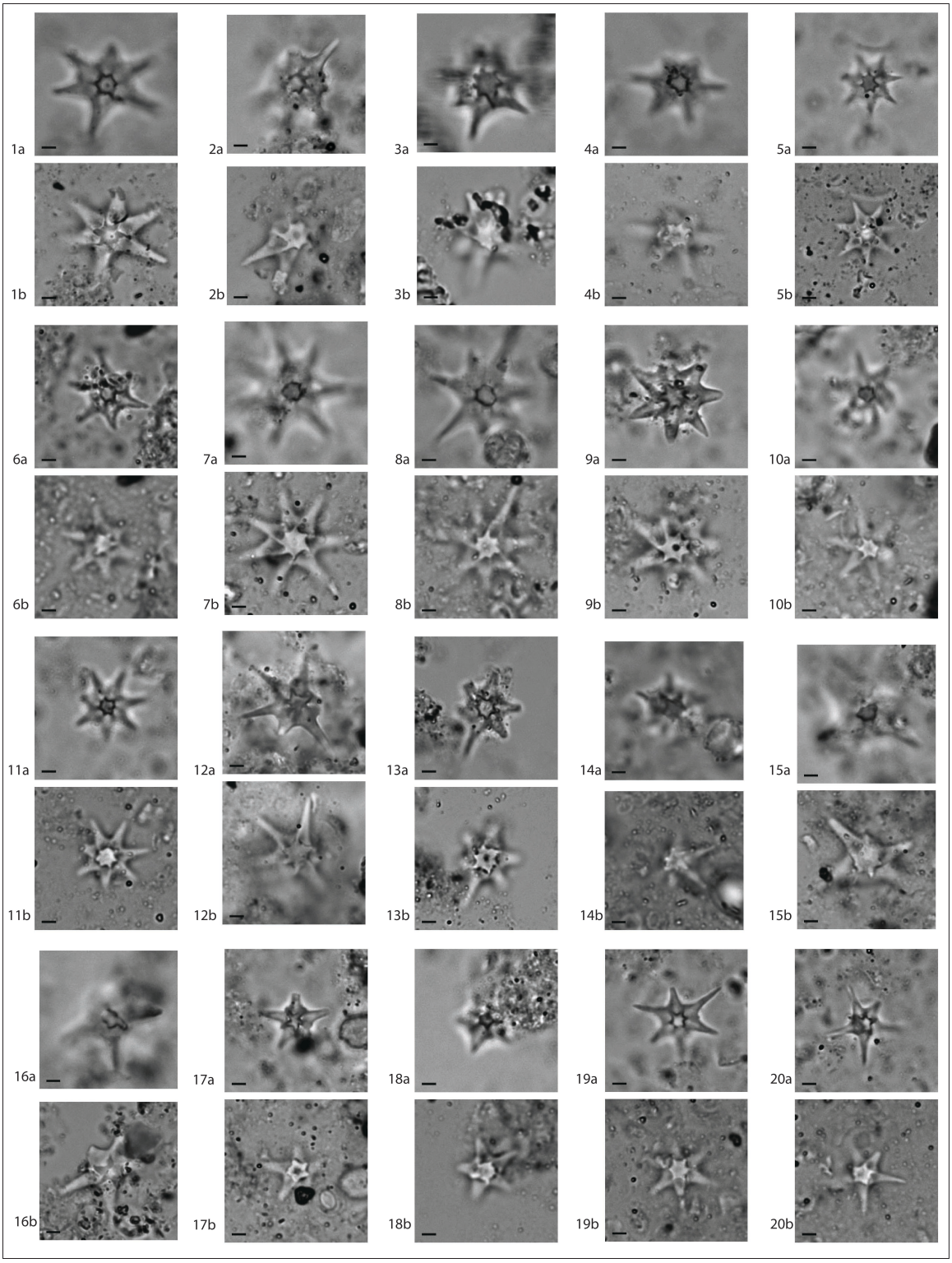
1a
2a
3a
4a
5a
1b
2b
3b
4b
5b
6a
7a
8a
9a
10a
6b
7b
8b
9b
10b
11a
12a
13a
14a
15a
11b
12b
13b
14b
15b
16a
17a
18a
19a
20a
16b
17b
18b
19b
20b

Chapter 4

Microevolutionary patterns in the Tribrachiatus lineage:

A case of punctuated anagenesis

4.1 Abstract

I have conducted a detailed morphometric analysis on the early Eocene calcareous nannoplankton *Tribrachiatus* lineage using outline-based and landmark-based geometric morphometric analyses, as well as traditional morphometrics. One of the only undeniable and uninterrupted lineages in coccolithophores, this lineage consists of three successive species that have evolved through a rotation of two stacked equilateral triplets. In this study I examined the transition from the hexaradiate form *T. bramlettei* (the stem species) to the asymmetric hexaradiate form *T. contortus,* as recorded at North Atlantic DSDP Site 550 over a thin stratigraphic interval (0.5 m) representing a few thousand years. Digitized images of coccoliths encountered in twenty seven samples from a 6 m thick interval (representing 180 kyr) were analyzed. The dynamics of speciation in the *T. bramlettei* - *T. contortus* evolutionary transition involves: 1) the sudden appearance, within 15 kyr (= sample resolution), of a wide diversity of morphotypes that are intermediate between *T. bramlettei* and *T. contortus,* together with typical forms of *T. bramlettei*; 2) 19 kyr later, the appearance, among intermediates and *T. bramlettei*, of typical morphotypes of *T. contortus*, and 3); 54 kyr later, the extinction (LAD) of *T. bramlettei* . There is thus a substantial overlap between ancestor and descendant. With time, the frequency of the *T. bramlettei* morphotype decreased, whereas that of the *T. contortus* morphotype increased and the intermediate forms became increasingly similar

to *T. contortus* and less similar to *T. bramlettei*. The spectrum of intermediate forms is such that shapes that would be assigned to *T. contortus* in the early part of the transition would be assigned to *T. bramlettei* in the late stage of the transition. The evolutionary pattern seen in the *Tribrachiatus* lineage exhibits the characteristics of punctuated anagenesis.

4.2. Introduction

One of the major questions today in evolutionary studies is how speciation occurs - its tempo and mode of change. In the fossil record, morphological changes reflect speciation events, and different patterns of speciation (gradual vs. punctuated) have been described in different marine fossil groups. In particular, marine plankton have shown speciation through both gradual evolution (Benton and Pearson, 2001; Malmgren and Kennett, 1981) and also abrupt morphologic breaks interrupting morphologic stasis (Malmgren and Kučera, 1996). In marine invertebrates common patterns of both stasis and anagenesis have been illustrated (Pachut and Anstey, 2012). Malmgren et. al. (1983) introduced a model that incorporated the stasis of punctuated evolution with the gradual linear transformation of anagenesis, for which they adopted the term punctuated gradualism. They showed that speciation results from the combined effects of gradual (non-lineage breaking) evolution preceded and succeeded by morphologic stasis. The new model was initially received with disagreement (Bookstein, 1987; MacLeod, 1991), but recent studies of speciation modeling (Hunt, 2006; Hunt, 2008; Hunt and Carrano, 2010; Hunt, 2012) have reignited the discussion, including a new way of interpreting this speciation pattern (Hull and Norris, 2009). Of particular interest is the pattern of increased morphologic variability preceding morphologic stability, which was discussed in Chapter 3.

Since the species of marine protists have very rapid evolutionary rates they constitute an ideal source for evolutionary studies. In particular, marine sediments allow us to retrace the microevolutionary steps that occurred through time, allowing the determination of the modes and tempo of speciation. The marine fossil record also contains the evidence for rapidly changing past environments and for shifting past biodiversity, both of which potentially acted as forcing agents on natural selection. Their documentation help determine the leading cause(s) of speciation and explain morphologic change during speciation.

A complete marine fossil record presents a hidden problem; although the presence of morphologically similar transitional forms is instrumental in establishing phylogenies (Pearson. 1997), it also makes the delineation of the initiation of speciation and that of a first evolutionary appearance (first appearance datum; FAD) of species more difficult to determine. This has been a main theme in studies of phylogeny in planktonic foraminifera, i.e., the difficulty in determining the point along an evolving lineage when specimens represent a different species (Aze et al., 2011). A detailed morphometric analysis is a potential solution to this problem. However, in as much as speciation events are rarely unambiguous, few studies have attempted to illustrate the underlining microevolutionary patterns (Kellogg, 1975; Kellogg and Hays, 1975; Malmgren and Kennett, 1981; McHargue, 1982; Lazarus 1983 ; Malmgren and Berggren 1983; Arnold, 1983; Reyment, 1985; Sorhannus et al., 1988; Wei and Kennett, 1988; Lazarus 1995; Malmgren and Kucera 1996; Kučera and Malmgren 1998; Jackson and Cheetham 1999,

Benton and Pearson, 2001; Chapter 3, this work). In addition, identification of cryptic (in which two morphologically similar species represent different genotypes) adds new complexity to the mechanism of speciation (de Vargas et al., 1999; Hull and Norris, 2009).

Detailed morphometric studies of coccoliths (including those in the two previous chapters) describe and interpret coccolith morphology through a basic kit of measurable characters (length, width, height, ellipticity, dimensions of central units, surface area, angles, and counting). These traditional metrics are quite appropriate when applied to highly geometric forms (i.e., placoliths, caneoliths, umbelloliths, and pentaliths sensu Aubry, 1998, 2009, 2013). However, morphometric analysis has limitations; the results are abstract and do not described quantitatively the complex characters that are easily described qualitatively. Geometric morphometrics, on the other hand, is a type of quantitative statistical analysis of shapes, based on Cartesian coordinates, that separates shape from the overall size, rotation and position. It provides analytical techniques to visualize and comprehensively compare shapes and shape differences and transformations between individuals. Geometric morphometrics has been applied to a variety of multidisciplinary fields as distinct as biomedical research and geology (sedimentology). It is most commonly applied to biology and paleontology, fields that were founded based on the qualitative description of taxa. The use of quantitative methods was developed to improve the ability to describe small morphologic variations indicative of a response to selective (abiotic or biotic) pressures. Geometric

morphometrics is well designed for describing evolutionary and ontogenetic processes because they emphasize accurate description of shapes and their transformation.

The technique of eigenshape analysis was developed by Lohmann (1983) and was immediately applied to a biogeographic study of the planktonic foraminifera *Globorotalia truncatulinoides* (Lohmann and Malmgren, 1983) and to a study of microevolution during speciation in the *G. tumida* lineage (Malmgren et al., 1983). Except for Lohmann's brief application of the method to the coccolith *Eu-discoaster challengeri* (Lohmann, 1983), eigenshape analysis or any other geometric morphometric analysis has not been applied to the coccolithophores. Garratt and Swan (1991) used a Fast Fourier Transform (FTT) to analyze morphology. They computed an elliptical template from 5 manually positioning coordinate points along the axes of three Mesozoic coccolith species. Grey-scaled images were scanned for elliptical and circular shapes using the template producing a power spectrum from the changing grey-levels (representing the coccolith structure). The power spectra are then analyzed through FTT, which is not a true outline-based analysis. Other studies on the marine protists have applied geometric morphometric techniques to problems of macroevolution, phylogeny and paleogeobiography (Quillévéré et al., 2000, 2008, 2009, 2011; Morard et al., 2009).

I examine here the rapid (~73 kyr) microevolutionary (morphologic) transition from *T. bramlettei* to *T. contortus* which occurred at ~ 53.93 Ma as part of the evolution of the early Eocene *Tribrachiatus* lineage. This lineage is one of the few indisputable lineages of coccolithophores (as strongly expressed as that of the mid-Miocene planktonic

foraminifera *Globigerinoides trilobus* to *Orbulina universa* transition). I analyze the morphological variability during this evolutionary transition through a combination of traditional morphometrics and through the coordinate-point variant of extended eigenshape analysis, which is a relative warps analysis applied to curve data (MacLeod, 2001). I show that transitional speciation is marked by a rapid morphologic shift that includes increasing variability, and that once the next species is established in the sequence variability decreases. This supports the finding (Chapter 3, this work) that fixation of the morphology of the species *Heliodiscoaster mahmoudii* follows high morphologic variability associated with the FAD of the species. In that study it was not possible to document the full speciation event because the ancestor of *H. mahmoudii* is unknown. The present study documents fixation of the ancestor *T. bramlettei*, followed by high morphological variability during the *bramlettei-contortus* transition. Fixation of the morphology of *T. contortus* requires further documentation, and work is currently in progress to this end.

4.3. Morphology of the species

The genus *Tribrachiatus* Shamrai 1963 is inferred here to be a coccolithophore of an Order Incertae Sedis of the Haptophytes, following Aubry (2014). It is known only from its coccoliths, each a single crystal of calcite modified in the form of two superposed equilateral triplets. Each triplet is triradiate with roughly regularly spaced arms (they form angles of 120° ± 5°). The two superposed triplets are arranged at angles that are species characteristic (see Aubry, 2014). The lineage is marked by the rotation of the triplets with respect to each other so that an hexaradiate species with the arms of the triplets essentially arranged symmetrically at 60° angles (*T. bramlettei*) evolve into an hexaradiate species with

asymmetrically arranged arms forming angles of 40 to 50° and 70 to 80° (*T. contortus*) to forms that are triradiate with evenly spaced arms. (*T. orthostylus*) (Fig. 1). Only the first step in this lineage is considered here (Fig. 1).

4.3.1. Tribrachiatus bramlettei Brönniman and Stradner 1960

This is the stem species of the lineage. The upper (UT) and lower (LT) triplets are symmetrically superposed with evenly distributed arms (~60º angle). In the (arbitrary) standard position, a tip of the UT point to 0° (i.e., parallel to the y-axis; Fig. 2, Pl. 1). In this position, the corresponding ray of the LT points to 180º. This configuration occurs only in *T. bramlettei*. Each arm is labeled A through F in a clockwise order. Arms A, C, and E belong to the UT; arms B, D, and F belong to the LT.

4.3.2. Tribrachiatus contortus Stradner 1959

The next taxon in the lineage, is a form that shows some degree of central flattening and twisting of the arms between the triplets. Arms are asymmetrically arranged into couplets (i.e. A-B, B-C, C-D, D-E, E-F, F-A) with alternating lesser (LA) and greater (GA) angle displacement, typical ~40º to ~70º respectively (Fig. 2, Pl. 1).

4.4. Material and Procedure

4.4.1 Material

The *Tribrachiatus* lineage is well represented at DSDP Site 550 on Goban Ridge in the North Atlantic Ocean (Fig. 3) where it occurs from ~408 mbsf to ~ 366 mbsf (Aubry et

al., 1996). At this site the ranges of the four species of *Tribrachiatus* were documented. *Tribrachiatus bramlettei* is the oldest species, ranging between 408 mbsf and 372 mbsf; *T. digitalis* co-occurs with it between 383 mbsf and 378 mbsf. The range of *T. contortus* between 373 mbsf and 361 mbsf overlaps slightly with that of the upper range of *T. bramlettei*. Finally, the range of *T. orthostylus*, with a lowest occurrence (LO) at 366 mbsf, overlaps over 5 m with the upper range of *T. contortus*. Because of a recovery gap between 373.06 and 372.66 mbsf, the exact location of the LO of *T. digitalis* in the section is unknown, and the transition between *T. bramlettei* and *T. digitalis* was not recovered. In contrast, the overlaps of occurrence from *T. bramlettei* to *T. contortus* and from *T. contortus* to *T. orthostylus* were well recovered and documented between 372 mbsf and 373 mbsf, and 366 mbsf and 361 mbsf, respectively (Aubry et al., 1996).

For this study, I focus on the transition between the first occurrence of *T. contortus* (372.86 ± 0.3 mbsf) and the last occurrence of *T. bramlettei* (371.95 ± 0.3 mbsf). I sampled the 6 m thick interval between 375.38 and 369.36 mbsf at a stratigraphic resolution of 30 cm, and took 7 additional samples between 371.56 and 373.26 mbsf (resulting in a stratigraphic resolution of 10 cm for this interval) to better document the evolutionary transition. Standard smear slides were prepared and systematically surveyed using a Zeiss Axioplan2 at magnification 600X. Initially the first 300 specimens encountered in the slide were photographed at different focal planes (see procedure below) for morphometric analysis. This, however, was extremely time consuming (one month/sample) so that the number of photographed specimens was reduced to 100 (thus reducing analysis time to about one week per sample). In total, 2719 specimens were

photographed and 13,600 photographs were taken. Videos were also used to enhance analysis.

4.4.2 Procedures

4.4.2.a. Image acquisition and preparation

All specimens were photographed in bright-field at a magnification of 1,600X. To standardize measurements for morphometric analyses all specimens were oriented in the standard position. Due to the nature of the material, traditional micrographs capturing fully focused specimen were problematic. Since specimens are physically and optically thick along the optical axis, standard microscope technique of modifying the in-depth focus by adjusting the condenser aperture reduced resolution and increased airy diffraction patterns (producing dark hallows around specimen). This made quantitative treatment difficult. To reduce analytical errors produced from airy diffraction the following procedure was developed to produce ideal micrographs for quantitative treatment: (1) the aperture diaphragm in the condenser was adjusted to a wider opening. This increases resolution to produce a sharper image, increases light intensity, reduces contrast and in-depth focus; (2) Since in-depth focus becomes narrower, a series of 3 to 6 images were prepared as a z-stack for each specimen, from the highest focal plane (most proximal to viewer) to the lowest focal plane (most distal: see Fig 4.); (3) Images were merged in Adobe Photoshop CS5 Extended through the statistical stacking feature by the maximum and/or mean stacking mode. The final micrographs provide extended depth of field and higher resolution. Figure 5 displays the effectiveness of this technique in

removing airy diffraction patterns when imaging thick specimen as compared to the standard approach (via the aperture; Plate 1).

4.4.2.b. Traditional Morphometrics

In the main study by Romein (1979), the primary character considered of importance were the angles between the arms of the triplets. A similar analysis is conducted here. Angles were measured, beginning with arm A and working clockwise, each angle (A-B, B-C, C-D, D-E, E-F, F-A) was recorded (Fig. 2). Two sets of angles were identified, the lesser angles (LA: A-B, C-D and E-F) and the greater angles (GA: B-C, D-F and F-A). Arm lengths were not considered in this study for two reasons: 1) there is still uncertainty about the significance of the taxonomic criterion of arm length (Bybell and Self-Trail, 1994; Bybell and Self-Trail, 1997; Angori and Monechi, 1996; Salis et al., 2000; Aubry et al., 2000) as mentioned above, and 2) in many specimens the tips of the arms are broken. I also measured diameters using the technique of 3-point circles. Points were placed in the inter-arm regions (Fig. 2). The greater diameter was traced between arms A-B, C-D, and E-F), and the lesser diameter between B-C, D-E, and F-A (Fig. 2). Both diameters are clearly distinct in *T.* contortus because the points to connect are well separated. In *T. bramlettei*, the diameter tends to intersect or overlap because the points determining the two circles are close to one another. For specimens of this species, placement of the 3-points was inferred based on the orientation of the specimen.

4.4.2.c. Statistical Analysis

The mean lesser angle (LA) and greater angle (GA) was calculated, respectively, for each specimen. Coefficients of variation for LA and GA were calculated for each stratigraphic level (Table 1). This was performed to determine if rotational change between the two angles is uniform.

4.4.2.d. Outline-based geometric morphometrics

In order to expand on the traditional morphometric approach previously used by Romein (1979), I conducted a complementary shape analysis through geometric morphometry.

The shapes of *T. bramlettei and T. contortus* were quantified through a combination of digitized outlines and landmarks (Fig. 2). Shape was studied through the comparison of morphologically equivalent characters using landmarks (Bookstein et al., 1978; Bookstein, 1989). Ideally this would be recording "homologous points" on the specimens, if such a thing exists (Bookstein, 1997), this is not the case with the *Tribrachiatus* coccoliths. Being radially symmetrical and displaying reflective symmetry, they lack clear homologous features. As explained above, the arms were matched arbitrarily because there is no natural orientation to them based on some distinct criterion. Eigenshape outline analysis (Lohmann, 1983) is one of these methods. It was selected for this study, because it is ideal for describing complex shapes and complex morphological change such as those that involved in the transition from *T. bramlettei* to *T. contortus*. In eigenshape outline analysis, shapes are defined by outlines. Outlines are constructed from line segments linked by Cartesian points. In standard eigenshape analysis, outlines are then processed though a shape function to define the outline data as

functions of the net angular change between all points along the outline (Zahn and Roskies, 1972). This procedure normalizes and aligns the coordinate data by removing size and rotation. Comparison between shapes is accomplished by matching outlines through rotation to a position of maximum correlation between points. Eigenshape analysis was first modified by Macleod (1999), who extended the technique to include landmarks that break outlines into homologous segments and also allows for shape analysis of sub-feature through open outlines. Modified again by Macleod (2001), Coordinate-Point Extended Eigenshape Analysis (CP-EES) aligns outlines and landmarks through the landmark-based procedure of Procrustes generalized least-squares superimposition (Rohlf and Slice, 1990), then applies a singular value decomposition to a covariance matrix of the aligned specimens; this is mathematically equivalent to a relative warps analysis of landmark data, thus unifying the two main geometric morphometric techniques. CP-EES is used for this study because it allows easy and effective shape description, which is expressed as deviations from the mean shape.

Following the procedures as described by Lohmann (1983) and Macleod (1999; and 2001), outlines were collected for the 2,719 specimens. Because we are dealing with a large dataset, Rohlf's TPS software (tpsDig2, 2013; tpsUtil, 2013) was favored for outline digitation. The software is capable of rapid edge detection. This feature, however, was found to be problematic, partly due to the translucent nature of calcite crystals, but also due to detritus or other nannofossils commonly scattered on and around each specimen. The edge detection feature in tpsDig2 failed to distinguish between the interior and exterior of most specimens and also between them and adjacent detrital

particles. Additional image processing was required to perform this procedure. Segmentation of each specimen into a binary image was achieved through Photoshop's quick select tool. This allows for the rapid and accurate selection of specimens by hand and also for quick alterations of the selected specimens. Selected specimens are converted into a binary mask and saved. These binary images are now easily recognized by tpsDigs2 (Fig. 6). Outlines were collected on these with the following two parameters. Each outline begins at the tip of arm A in standard position. Outlines proceed clockwise around the specimen. For each specimen between 800 and 1000 Cartesian coordinates were assigned depending on its size. Six landmarks were placed in clockwise order at the base of each furrow (or interray area) between each arm, breaking the outline into six segments. The resulting tps files were then read into Mathematica (version 9, Wolfram Research Inc.) and processed using the Coordinate-point Eigenshape notebooks developed by Jonathan Krieger (CPES Step 1: split and interpolate the outlines, version 1.1, 2009; Step 2: Procrustes superposition, version 1.3, 2009; Step 3: Singular value decomposition and models, version 1.4, 2010; Step 4: scatterplots, version 1.4, 2009). Linear interpolation reduced the number of points to100 equally spaced points per line segment (total of 600 points per specimen). This number was found to accurately describe the shapes. The first thirty eigenshape axes were visualized as a series of shape models. Scores for the first fifteen coordinate point eigenshapes explain 95% of the observed variance in shape. However, upon further examination of the shape models, variance observed in models ES4 – ES14 (with the exception of ES 8, 9 and15) described broken or uneven arms, as well as specimens which, when photographed, were slightly tilted along their z-axis (similar to a dreidel at rest). For each stratigraphic section, mean

values were computed for specimen scores along the first three CPEES axes (describing 58.46% of the observed variance) and plotted along with histograms to compare the shapes and the shape change through the section.

4.5. Results

4.5.1. Lesser Angle

The LA shows fairly low variability within each sample (Fig. 9). The average LA decreases up core from 58º at 375.38 mbsf to 42º at 369.36 mbsf (Fig. 7a). In the lower part of the section, from 375.38 to 373.06 mbsf, the angle is stable (55º - 59º). There is a significant, but poorly documented (because of a core gap) 5º decrease between 373.06 and 372.66 mbsf, from 54.13º to 48.86º. From this level (372.66 mbsf) to 371.76 mbsf there is a progressive ~5º decrease in LA to 44º. Above this level, the LA decreases only slightly, ~2º, from 44º to 42º at level 369.36 mbsf. The distributions in LA are mostly symmetrical and unimodal (Fig. 8). Ignoring the few outliers which are present in some samples, the spread in the distribution expands up core from ~10º (between 375.38 and 373.06 mbsf), to ~20º (between 372.66 and 371.46 mbsf), to ~25º (370.86 and 371.16 mbsf). The spread decreases back to ~15º at the top of the section between 370.56 and 369.36 mbsf.

Variability, as calculated by coefficient of variation, is very low (1 to 4 %) in the lower 2 m of the core, from 375.38 to 373.26 mbsf (Fig. 9a). The CV doubles at 373.16 mbsf to 8% and remains between 6 and 10% up to 371.46 mbsf. A short jump of increase in variability occurs between 371.16 and 370.86 mbsf, from 13 and 11 % respectively. The CV decreases to between 6 and 8 % between 370.56 and 369.36 mbsf.

4.5.2 Greater Angle

Changes in the GA mean mirror changes in the LA. The GA increases by about 15º up core, from 62.5º at 375.38 mbsf to 77.6º at 369.36 mbsf (Fig. 10). From 375.38 to 373.06 mbsf GA increases slightly by ~ 4º (from 62º to 66º). A 5º increase occurs between 373.06 and 372.66 mbsf, from 66º to 71.3º. From 372.46 to 371.76 mbsf there is a progressive ~5º increase in the GA from 70º to 75º mbsf. The GA increases slightly (~2º) from this level to 369.36 mbsf where it reaches ~78º. Distributions in the GA are symmetrical and unimodal (Fig. 11). The main spread in the samples increases up core from ~10º (between 375.38 and 373.06 mbsf), to ~20º (between 372.66 and 371.46 mbsf), to ~25º (370.86 and 371.16 mbsf). The spread decreases back to ~15º at the top of the section between 370.56 and 369.36 mbsf.

Variability in the greater angle is very low (CV = 1 to 3 %) in the lower 2 m of the core, from 375.38 to 373.26 mbsf (Fig. 12). The CV increases to 6% at 373.16 mbsf and remains between 6 and 10% up to 371.96 mbsf. The CV progressively decreases from 7 and 4% between 371.16 and 369.36 mbsf.

4.5.3. Coordinate-point Extended Eigenshape Analysis

The first CP-eigenshape axis (ES 1, 45.35% of shape variance; table 2) describes the amount of rotational symmetry between the upper triplet (UT) and the lower triplet (LT) (Fig. 13). Low scores on ES1 are highly rotated, asymmetrical forms with shallow furrows between the arms with LA. This form is akin to well-established *T. contortus*. Conversely, high scores along ES 1 describe strongly symmetrical forms with furrows

between each arm of equal depths, characterizing *T. bramlettei*.

The second CP-eigenshape (ES 2, 13.12 % of shape variance) is associated with the lengths of the arms and the depths of the furrows (Fig. 13). Low scores along this axis indicate very short-armed forms with very shallow bifurcations between the arms. Positive scores along this axis have deep furrows with long arms.

The third CP-eigenshape (ES 3, 7.94% of shape variance) is associated with increased variability between the angles of similar arm couplets (i.e. increased variability between A-B, C-D and E-F). A low score indicates similar angles between equivalent arm couplets within a group (all LA couplets vs. all GA couplets). A high score indicates asymmetry regarding the distribution of angles between similar couplets.

Although increasing CP-eigenshapes actually describe lowering shape variance, it is often the case that, although representing a small overall contribution to shape variation, "small" morphologic variation may be biologically important. They may be identified through CPEES. A select few shapes are worth describing. The eighth (ES 8, 2.34% of shape variance) is similar to ES 3 but rotated and exhibits less variation. The ninth CP-eigenshape (ES 9, 2.08% of shape variance) describes a dextral and sinistral geometry present along the arm lengths of the UT and LT, respectively. A low score indicates forms with slightly counterclockwise curving arms. A high score shows forms with a slight clockwise curvature. The fifteenth CP-eigenshape (ES 15, 0.69% of shape variance) illustrates a difference along the furrows of the LA. Forms with a low score

have slender arms with wide and shallow furrows, as if web-like. High scores represent forms with wider arms and narrow furrows. The twenty-ninth CP-eigenshape (ES 29, 0.12 % of shape variance) describes another geometric shape in which arms show a small amount of bending. A low score indicates forms in which the A-B, C-D and E-F couplets show some inward lateral bending. The curvatures of the arms with high scores display outward lateral bending.

4.6. Discussion

4.6.1. Evolutionary pattern from T. bramlettei to T. contortus

In this study, the combination of traditional morphometrics and outline analysis (CP-EES) reveals a complete morphologic replacement of *T. bramlettei* by *T. contortus.* This evolutionary transition occurs over a thin 2.4 m interval from 372.66 to 370.26 mbsf (Fig. 14 and 15), assuming a constant sedimentation rate of ~3.7 cm/kyr (see age-depth plot Fig. 1b), this represents ~ 73 kyr and is almost twice as long as the ~40 kyr computed from the FAD of *T. contortus* to the LAD of *T. bramlettei* by Aubry et al. (1996). In the lower six samples from 375.38 to 373.06 mbsf (2.32 m), spanning ~ 68 kyr, the CP-EES analysis reveals that only shapes characteristic of *T. bramlettei* occur (Pl. 1). Above these levels, shapes that are intermediate between *T. bramlettei* to *T. contortus* begin to appear (Figs. 14 and 15, Pl. 2). From 370.26 to 369.36 mbsf, shapes assignable to *T. contortus* prevail although intermediate shapes are still present in low numbers (Pl. 3). This is particularly well documented by the LA and GA measurements. The angle measurements show a more gradual transition, implying that the initiation of morphologic change occurs at slightly different times for different morphological characters.

Ordination of *Tribrachiatus* on its first two CP-eigenshapes (58.47% of observed variance, Fig. 16 and 17) shows clearly that *T. bramlettei* occupies a distinct position in morphospace during the earlier ~68 kyr. The shapes in this interval also show very low variability along ES 1(Fig. 16 and 17). Shape distinction between *T. bramlettei* and *T. contortus* is delineated through the center of the morphospace along the first eigenshape axis; this represents the mean sample shape. Along the first axis the mean sample shape (0.0) describes intermediate forms between *T. bramlettei* and *T. contortus*, more positive scores indicating *T. bramlettei* and negative scores representing *T. contortus*.

The distinction between *T. bramlettei* and *T. contortus* is also well demonstrated by the LA and GA measurements (Fig. 7 – 12). Both angles show a thin ~2.32 m interval from 375.58 to 373.26 mbsf (~42 kyr) of very low variability (CV = 1.26 % to 4.28%). The doubling in angle variability (CV = 8%) in the following sample (373.16 mbsf) indicates the first appearance of true intermediate forms. This is illuminated in figure 17 as the cluster of specimens migrates through the morphospace and begins to occupy the central space.

The main interval of evolutionary transition (372.66 to 370.26 mbsf) occurred between 53.914 Ma and 53.814 Ma (Fig.14 and 15). During this interval the spread in eigenscores increases indicating increasing shape variation (Fig. 15). This is evident as the cluster of specimens progressively shifts across the middle of the morphospace towards more negative values (Fig.17). Further, this is clearly demonstrated in figure 15 as group means along the ES 1 display strong negative directional trend. This shift is present as a

progressive ~5º decrease in the mean LA (Fig.7). This interval indicates a period of relatively high morphologic variability interpreted as the overlapping occurrences of *T. bramlettei* and *T. contortus* with a spectrum of intermediate forms. In the uppermost intervals, from 370.06 to 369.36 mbsf, the clusters of specimen (Fig.17) shift mostly to the negative morphospace, indicating that shapes belonging to true *T. bramlettei* are no longer present. However, several specimen still plot in the middle of the morphospace, indicating that intermediate forms between *T. bramlettei* and *T. contortus* are still present, suggesting that the complete morphologic transition has not be captured in my record. (Analyses are already in progress to extend my record and capture the full transition).

In summary, the dynamics of speciation in the *T. bramlettei*-*T. contortus* evolutionary transition involves the following; 1) within 15 kyr (=sample resolution), the sudden appearance of a wide diversity of morphotypes that are intermediate between *T. bramlettei* and *T. contortus* together with typical of *T. bramlettei*; 2) 19 kyr later, the appearance, among intermediates and *T. bramlettei*, of typical morphotypes of *T. contortus*; and 3) 54 kyr later, the extinction (LAD) of *T. bramlettei* . There is thus a substantial overlap between ancestor and descendant. With time, the frequency of the *T. bramlettei* morphotype decreased whereas that of the *T. contortus* morphotype increased at the same time as the intermediate forms became increasingly similar to *T. contortus* and less similar to *T. bramlettei*. The spectrum of intermediate forms is such that shapes that would be assigned to *T. contortus* in the early part of the transition would be assigned to *T. bramlettei* in the late stage of the transition.

4.6.2. Comparison with record of speciation in other coccolithophores

To my knowledge, there is only one previous study of speciation among coccolithophores, that is the speciation of *Heliodiscoaster mahmoudii* (Chapter 3, this volume). Yet, I was unable to show the whole ancestor-descendant transition in that speciation because the ancestor has not been identified to date. In *H. mahmoudii* I was able to determine that two thirds of the life span of the species was characterized by morphologic fixation/stability, whereas the first third of it was characterized by high morphologic variability. The degree of variability in the *T. bramlettei* to *T. contortus* transition is much less than in the *H. mahmoudii.* In the former it increases from 2 - 3 % in *T. bramlettei* to 6 - 8% during the transition, peaking at 14% (just at the level of the LAD of *T. bramlettei*) whereas in *H. mahmoudii* variability reached as much as 70%. This implies that the degree of variability changes considerably between speciation events.

I can predict from this that not all speciation events in the coccolithophores are alike. However, in *H. mahmoudii* as in the *Tribrachiatus* species morphologic fixation occurs prior and after the speciation event. It is interesting to note that the duration of the episode of high morphological instability is of the same order of magnitude in the two cases (>83 kyr in *H. mahmoudii*, see Chapter 3; 73 kyr in the *Tb-Tc* transition).

4.6.3. Comparison with record of speciation in planktonic foraminifera

A similar dynamic of speciation to that discussed here was described by Malmgren et al. (1983) for the *G. plesiotumida* to *G. tumida* transition, with morphologic fixation of the ancestor and the descendant separated by a short interval of high morphologic variability. However, the duration of the event was several orders of magnitude greater than in the *T. bramlettei* to *T. contortus* transition (600 kyr vs. 73 kyr).

Malmgren et al. (1983) adopted the term "punctuated gradualism" because the amount of time represented by the episode of high variability represented more than 1% of the total life span of the descendant, and also because there was no cladogenesis involved. Eldredge and Gould (1972) defined punctuated equilibrium as speciation occurring over an episode shorter than 1% of the life span of the descendant. In *G. plesiotumida* to *G. tumida* lineage, the transition represents >12% of the life span of *G. tumida.* In the *Tribrachiatus* lineage, the *T. bramlettei* to *T. contortus* transition represents more than 22% of the life span of *T. contortus* (= 325 kyr), Therefore I present here a case analogous to that presented by Malmgren et al. (1983) of punctuated gradualism, or of punctuated anagenesis as subsequently renamed by Gould (1985).

Hull and Norris (2009) reexamined the *G. plesiotumida —G. tumida* lineage and concluded that the intermediate morphotypes between the two species actually represented pseudo-cryptic species. I do not see evidence for pseudo-cryptic speciation in my data.

As a note: Malmgren et al. calculated that speciation involved 600,000 generations, based on yearly sexual reproduction of the planktonic foraminifera. Based on culture of extant species, the coccolithophore reproduce mostly asexually, at a rate of cell divisions every 12 to 60 hours depending on species (Brand, 1994). Based on environmental observations it is inferred that they reproduce sexually once or twice a year (as a response to stress). *Tribrachiatus* is an extinct genus, but for the sake of discussion it can be assumed that mitosis occurred every 60 h (larger taxa reproducing less often), and that meiosis occurred twice a year. Assuming these conditions, 73 kyr would correspond to 146,000 sexual generations and >10.5 $x10^6$ asexual generations.

4.6.4. Stratigraphic implication

The results presented here show that the FAD of *T. contortus* is recorded at 372.66 mbsf and the LAD of *T. bramlettei* at 370.06 mbsf, separated by ~2.4 m –thick stratigraphic interval and representing a duration of ~73 kyr. These results support those of Aubry et al. (1996) at this site, who located the FAD of *T. contortus* between 372.64 and 373.08 mbsf and the LAD of *T. bramlettei* between 371.73 and 372.17 mbsf. In contrast they are in conflict with the biostratigraphic interpretation by Raffi et al. (2005) of the lower Eocene stratigraphy at Site 550. Using semi-quantitative counting techniques these authors placed the FAD of *T. contortus* between 386.49 and 382.49 mbsf, which is at least 10 m below the level where the FAD of the species is placed here (Fig.18). As I document, beyond doubt, the speciation of *T. contortus* from *T. bramlettei*, it is impossible that *T. contortus* could naturally occur at stratigraphic levels older than its FAD. Raffi et al.'s record of the species below 372.66 mbsf may be due to contamination or it may reflect

taxonomic misidentification (i.e., confusion with *T. digitalis*). In any case, the results presented here support the introduction of Subzone NP10d by Aubry (1996).

4.7. Conclusions

I present here the first comprehensive geometric morphometric analysis performed on a coccolithophore species, based on the measurements of >2,200 specimens occurring over a 6 m stratigraphic interval. The early Eocene speciation of the species *Tribrachiatus contortus* from *T. bramlettei* is described using a combination of traditional morphometric techniques and coordinate-point extended eigenshape analysis (CP-EES). I show that the transition between both species lasted ~ 73 kyr and involved high morphologic variability. Morphologic fixation of the shape of *T. bramlettei* prior to the speciation event is evident. Only the early stage of morphologic fixation of the shape of *T. contortus* is documented here, but further documentation is in progress. It is clear that the distinctive *T. contortus* shape arose from a pool of intermediate shapes between parent and daughter species. The modalities of speciation described here compare well with those described among planktonic foraminifera. The *T. bramlettei*-*T. contortus* evolutionary transition represents a remarkable case of Punctuated Anagenesis.

4.8. References

Arnold, A., and Fristrup, K., 1982, The theory of evolution by natural selection: a hierarchical expansion: Paleobiology, v. 8, no. 2, p. 113–129.

Angori, E., and Monechi, S., 1996, High-resolution calcareous nannofossil biostratigraphy across the Paleocene/Eocene boundary at Caravaca (southern Spain): Israel J. Earth Sci, v. 44, p. 197–206.

Aubry, M.-P., Berggren, W.A., Stott, L., and Sinha, A., 1996, The upper Paleocene-lower Eocene stratigraphic record and the Paleocene-Eocene boundary carbon isotope excursion: implications for geochronology: Geological Society London Special Publications, v. 101, no. 1, p. 353–380, doi: 10.1144/GSL.SP.1996.101.01.18.

Aubry, M.-P., Requirand, C., and Cook, J., 2000, The Rhomboaster-Tribrachiatus lineage: A remarkable succession of events from 55.5 to 53.2 Ma: GFF, v. 122, no. 1, p. 15–18.

Aze, T., Ezard, T.H.G., Purvis, A., Coxall, H.K., Stewart, D.R.M., Wade, B.S., and Pearson, P.N., 2011, A phylogeny of Cenozoic macroperforate planktonic foraminifera from fossil data: Biological Reviews, v. 86, no. 4, p. 900–927, doi: 10.1111/j.1469-185X.2011.00178.x.

Benton, M.J., and Pearson, P.N., 2001, Speciation in the fossil record: Trends in Ecology & Evolution, v. 16, no. 7, p. 405–411.

Bookstein, F.L., 1997, Landmark methods for forms without landmarks: localizing group differences in outline shape: Medical Image Analysis, v. 1, p. 225–243.

Bookstein, F.L., 1989, Principal warps: Thin-plate splines and the decomposition of deformations: Pattern Analysis and Machine Intelligence, IEEE Transactions on, v. 11, no. 6, p. 567–585.

Bookstein, F.L., 1987, Random walk and the existence of evolutionary rates: Paleobiology, v. 13, no. 4, p. 446–464.

Bookstein, F.L., Gingerich, P.D., and Kluge, A.G., 1978, Hierarchical linear modeling of the tempo and mode of evolution: Paleobiology,, p. 120–134.

Bybell, L.M., and Self-Trail, J.M., 1994, Evolutionary, Biostratigraphic, and Taxonomic Study of Calcareous Nannofossils from a Continuous Paleocene-Eocene Boundary Section in New Jersey:.

Bybell, L.M., and Self-Trail, J.M., 1997, Late Paleocene and early Eocene calcareous nannofossils from three boreholes in an onshore-offshore transect from New Jersey to the Atlantic continental rise: Proceedings of the Ocean Drilling Program, Scientific Results, v. 156, p. 91–110.

de Vargas, C., Norris, R.D., Zaninetti, L., Gibb, S.W., and Pawlowski, J., 1999,

Molecular evidence of cryptic speciation in planktonic foraminifers and their relation to oceanic provinces.: Proceedings of the National Academy of Science, v. 96, no. 6, p. 2864–2868, doi: 10.1073/pnas.96.6.2864.

Garratt, J., and A. Swan., 1991, Morphological data from coccolith images.: Nannoplankton Research, Proceedings of the Fourth INA Conference, Prague. Vol. 1, pp. 11-34

Gould, S.J., 1985, The paradox of the first tier: an agenda for paleobiology: Paleobiology,, p. 2–12.

Hull, P.M., and Norris, R.D., 2009, Evidence for abrupt speciation in a classic case of gradual evolution.: Proceedings of the National Academy of Science, v. 106, no. 50, p. 21224–21229, doi: 10.1073/pnas.0902887106.

Hunt, G., 2006, Fitting and comparing models of phyletic evolution: random walks and beyond: Paleobiology, v. 32, no. 4, p. 578–601.

Hunt, G., 2008, Gradual or pulsed evolution: when should punctuational explanations be preferred?: Journal Information, v. 34, no. 3.

Hunt, G., 2012, Measuring rates of phenotypic evolution and the inseparability of tempo and mode: Paleobiology, v. 38, no. 3, p. 351–373, doi: 10.5061/dryad.c1m60s84.

Hunt, G., and Carrano, M.T., 2010, Models and methods for analyzing phenotypic evolution in lineages and clades, *in* Alroy, J. and Hunt, G. eds., Quantitative Methods in Paleobiology, The Paleontological Society Papers, The Paleotological Society, p. 245–269.

Jackson, J., and Cheetham, A., 1999, Tempo and mode of speciation in the sea: Trends in Ecology & Evolution, v. 14, no. 2, p. 72–77.

Kellogg, D.E., 1975, The role of phyletic change in the evolution of Pseudocubus vema (Radiolaria): Paleobiology, v. 1, no. 4, p. 359–370.

Kellogg, D.E., and Hays, J.D., 1975, Microevolutionary patterns in late Cenozoic radiolaria: Paleobiology,, p. 150–160.

Krieger, J.D. 2013., Coordinate point Extended Eigenshape v. 1.4 (personal communication).

Kučera, M., and Malmgren, B.A., 1998, Differences between evolution of mean form and evolution of new morphotypes: an example from Late Cretaceous planktonic foraminifera: Paleobiology, v. 24, no. 1, p. 49–63.

Lazarus, D., 1983, Speciation in pelagic protista and its study in the planktonic microfossil record: a review: Paleobiology, v. 9, no. 4, p. 327–340.

Lazarus, D., Hilbrecht, H., Spencer-Cervato, C., and Thierstein, H.R., 1995, Sympatric speciation and phyletic change in Globorotalia truncatulinoides: Paleobiology, v. 21, no. 1, p. 28–51.

Lohmann, G., 1983, Eigenshape analysis of microfossils: a general morphometric procedure for describing changes in shape: Mathematical Geology, v. 15, no. 6, p. 659–672.

Lohmann, G., and Malmgren, B.A., 1983, Equatorward migration of Globorotalia truncatulinoides ecophenotypes through the Late Pleistocene: Gradual evolution or ocean change?: Paleobiology, v. 9, no. 4, p. 414–421.

MacLeod, N., 1999, Generalizing and extending the eigenshape method of shape space visualization and analysis: Paleobiology,, p. 107–138.

MacLeod, N., 2001, Landmarks, localization, and the use of morphometrics in phylogenetic analysis: Topics in geobiology, v. 19, p. 197–234.

MacLeod, N., 1991, Punctuated Anagenesis and the Importance of Stratigraphy to Paleobiology: Paleobiology, v. 17, no. 2, p. 167–188.

Malmgren, B.A., and Kennett, J.P., 1981, Phyletic gradualism in a Late Cenozoic planktonic foraminiferal lineage; DSDP Site 284, southwest Pacific: Paleobiology, v. 7, no. 2, p. 230–240.

Malmgren, B.A., and Kučera, M., 1996, Evolutionary changes in supplementary apertural characteristics of the late Neogene Sphaeroidinella dehiscens lineage (planktonic foraminifera): PALAIOS.

Malmgren, B.A., Berggren, W.A., and Lohmann, G., 1983, Evidence for punctuated gradualism in the Late Neogene Globorotalia tumida lineage of planktonic foraminifera: Paleobiology, v. 9, no. 4, p. 377–389.

Mchargue, T.R., 1982, Ontogeny, phylogeny, and apparatus reconstruction of the conodont genus Histiodella, Joins Fm., Arbuckle Mountains, Oklahoma: Journal of Paleontology, v. 56, p. 1410-1433.

Morard, R., Quillévéré, F., Escarguel, G., Ujiié, Y., de Garidel-Thoron, T., Norris, R.D., and de Vargas, C., 2009, Morphological recognition of cryptic species in the planktonic foraminifer Orbulina universa: Marine Micropaleontology, v. 71, no. 3-4, p. 148–165, doi: 10.1016/j.marmicro.2009.03.001.

Pachut, J.F., and Anstey, R.L., 2012, Rates of anagenetic evolution and selection intensity in Middle and Upper Ordovician species of the bryozoan genus Peronopora: Paleobiology, v. 38, no. 3, p. 403–423, doi: 10.5061/dryad.jm3bs78v.

Quillévéré, F., Morard, R., Escarguel, G., Douady, C.J., Ujiié, Y., de Garidel-Thoron, T., and de Vargas, C., 2011, Global scale same-specimen morpho-genetic analysis of

Truncorotalia truncatulinoides: A perspective on the morphological species concept in planktonic foraminifera: Palaeogeography, Palaeoclimatology, Palaeoecology,, p. 1–11, doi: 10.1016/j.palaeo.2011.03.013.

Quillévéré, F., Norris, R.D., Berggren, W.A., and Aubry, M.-P., 2000, 59.2 Ma and 56.5 Ma: Two significant moments in the evolution of acarininids (planktonic foraminifera): GFF, "Early Paleogene Warm Climates and Biosphere Dynamics," v. 122, p. 131–132.

Quillévéré, F., Norris, R.D., Kroon, D., and Wilson, P.A., 2008, Transient ocean warming and shifts in carbon reservoirs during the early Danian: Earth and Planetary Science Letters, v. 265, no. 3-4, p. 600–615.

Quillévéré, F., Norris, R.D., Moussa, I., and Berggren, W.A., 2009, Role of photosymbiosis and biogeography in the diversification of early Paleogene acarininids (planktonic foraminifera):.

Raffi, I., Backman, J., and Pälike, H., 2005, Changes in calcareous nannofossil assemblages across the Paleocene/Eocene transition from the paleo-equatorial Pacific Ocean: Palaeogeography, Palaeoclimatology, Palaeoecology, v. 226, no. 1-2, p. 93–126, doi: 10.1016/j.palaeo.2005.05.006.

Reyment, R.A., 1985, Phenotypic evolution in a lineage of the Eocene ostracod Echinocythereis: Paleobiology, v. 11, p. 174-194.

Rohlf, F.J. tpsDig 2013:. http://life.bio.sunysb.edu/morph/

Rohlf, F.J. TPSUTIL.2013:. http://life.bio.sunysb.edu/morph/

Rohlf, F.J., and Slice, D., 1990, Extensions of the Procrustes method for the optimal superimposition of landmarks: Systematic Biology, v. 39, no. 1, p. 40–59.

Romein, A.J.T., 1979, Lineages in early Paleogene calcareous nannoplankton: Utrecht Micropaleontological Bulletins, v. 22.

Salis, von, K., Monechi, S., Bybell, L.M., Self-Trail, J.M., and Young, J.R., 2000, Remarks on the calcareous nannofossil markers Rhomboaster and Tribrachiatus around the Paleocene/Eocene boundary: GFF, v. 122, no. 1, p. 138–140.

Sorhannus, U., Fenster, E.J., Burckle, L.H., And Hoffman, A, 1988, Cladogenetic and anagenetic changes in the morphology of *Rhizosolenia praebergonii* Mukhina: Historical Biology, v. 1, p. 185-205.

Wei, K., and Kennett, J., 1988, Phyletic gradualism and punctuated equilibrium in the late Neogene planktonic foraminiferal clade Globoconella: Paleobiology,, p. 345–363.

Zahn, C.T., and Roskies, R.Z., 1972, Fourier Descriptors for Plane Closed Curves:

Computers, IEEE Transactions on,, no. 3, p. 269–281, doi: 10.1109/TC.1972.5008949.

4.9. Figure Captions

Figure 1.
A) The biostratigraphic range of the *Tribrachiatus* lineage at Site 550 (modified from Raffi et al., 2005). The evolutionary interpretation of the lineage as described by Romein (1979) is illustrated on the right. The *Tribrachiatus* lineage consists of three species, from oldest to youngest (1). *T. bramlettei*, (2) *T. contortus* and (3) *T. orthostylus.* The evolutionary transition involves rotation of the hexaradiate (six-rayed) form to produce a triradiated (3-rayed) form with intermediate morphotypes found between the taxa.
B) Age-Depth plot for Site 550. Estimated ages from Aubry et al. 1996: 1) FAD of *T. contortus* at ~373 mbsf and 53.93 Ma; 2) LAD of *T. bramlettei* ~372 mbsf and 53.89 Ma; 3) FAD *T. orthostylus* ~366 mbsf and 53.64 Ma. A sedimentation rate of ~3.7cm/ky is computed.

Figure 2.
Illustrated schematic for both *T. bramlettei* and *T. contortus* specimen oriented in standard position for measurement purposes. Outlines were digitized clockwise beginning from the tip of arm A. Landmarks, represented by colored dots, were placed clockwise beginning with the A-B inter-ray region. Blue dots represent position from which the 3-point greater diameter is measured. Pink dots represent position from which the 3-point lesser diameter is measured.

Figure 3.
Location of Leg 80 drill sites. From Deep Sea Drilling Project Initial Reports Volume 80 (pg. 251)

Figure 4.
Procedure for producing stacked images (extended depth of field). For each specimen three photographs were taken at different focal points. A composite image was constructed for the purpose of outline analysis through the maximum statistics script in Photoshop CS5. PR = proximal focus, CT = central focus, DS = distal focus, CP = composite figure.

Figure 5.
Comparison of stacked images vs. standard micrographs. Standard micrograph composed by adjusting aperture in stage condenser to increase focal depth. Increased focal depth increases airy disk diffraction, decreasing quality of image

Figure 6.
A) Example of processed binary image. B) Outline made through tpsDIG's automatic feature. Line segments broken by 6 landmarks. Each segment composed of 100 evenly space interpolated points. Each outline starts from tip of arm A. C) Comparison with mean shape produced though CPEE Mathematica notebook.

Figure 7.

A) Stratigraphic distribution mean lesser angles. B) Chronology mean lesser angles. Dot = Mean value; bar = 95% confidence interval

Figure 8.
Frequency distributions of lesser angle in stratigraphic section.

Figure 9.
A) Coefficient of variation for lesser angle in stratigraphic section. B) Coefficient of variation for lesser angle in chronologic sequence. Yellow region represents period of transition between *T. bramlettei* and *T. contortus*. bar = 95% confidence interval

Figure 10.
Chronology of mean greater angle measurements

Figure 11.
Frequency distribution of greater angles in stratigraphic section.

Figure 12.
Coefficient of variation for greater angle in chronologic sequence. Yellow region represents period of transition between *T. bramlettei* and *T. contortus*. bar = 95% confidence interval

Figure 13.
Shape Models. Shape change for the first ten eigenshapes, plus ES 15 and ES 29. Each eigenshapes shows the range of shapes along the axis. ES1= 47.35% of total variance, ES2 = 12.56% of total variance, ES3 = 7.26% of total variance, ES4 = 5.99% of total variance, ES5 4.02% of total variance.
Note: For eigenshapes 2, there is debate about this form: it has been argued by Angori and Monechi (1996) as being a short armed morphotype of *T. bramlettei*. Conversely, it has also been assigned as an independent species by Bybel and Self-trail (1996; Bybell and Self-Trail, 1997)

Figure 14.
Frequency distribution ES1 (lesser angle) in stratigraphic of section. Red line represent position of mean shape. FAD of *T. contortus* and LAD of *T. bramlettei* as interpreted by the modal shift of the distribution crossing the mean shape (red) line

Figure 15.
Stratigraphic distribution of mean shape along ES1. Dot = Group mean; bar = 95% confidence interval. Shape models illustrate the dominant shape in the section. Bright yellow = True *T. bramlettei*, Dark Yellow = early intermediate form, Grey = Intermediate form, Red = True *T. contortus*

Figure 16.
Ordination of ES1 and ES2, represents 48% of total variance observed. A) Shape plane shows the relative positions of the *T. bramlettei*, *T. contortus*, and intermediate form in

morphospace as the described by the first two ES axis. Bright yellow = True *T. bramlettei*, Dark Yellow = early intermediate form, Grey = Intermediate form, Red = True *T. contortus.* B) Shape models superimposed by group mean shape positions. This shows the shapes being represented by the data. C) All specimen plotted in the morphospace. Shows actual shaped represented by the data. Morphospace divided into three regions; Yellow = T. bramlettei space, Grey = Intermediate form space, Red = T. contortus space.

Figure 17.
Ordination of ES1 and ES2, with specimen separated by stratigraphic levels. This shows how the specimen change shape up section. Morphologic fixation (stasis) observable in lower 2 m as displayed by unmoving cluster of points.

Figure 18.
Comparison of the *Tribrachiatus* lineage biostratigraphic range at Site 550 from Raffi et al., 2005).

4.10. Table Captions

Table 1.
Summary of measured angles. LA = Lesser angles, GA = Greater angles, CV = Coefficient of variation

Table 2.
Summary of coordinate point extended eigenshape analysis. Eigenvalues and percentages of variance explained by the first 15 eigenshapes

4.10. Plate Captions

Plate 1. Typical *Tribrachiatus bramlettei.* (1-8) Sample 550-31-1 38-39 cm; (9) Sample 550-31-1 8-9 cm; (10-15) Sample 550-30-6 111-112 cm. Mean stacked images at 1,600X, bar = 5 μm

Plate 2. *T. bramlettei – T. contortus* intermediate forms. (1-5) Sample 550-30-5 96-97 cm; (6) Sample 550-30-5 86-87 cm; (7-9) Sample 550-30-4 86-87 cm; (10-15) Sample 550-30-5 46-47 cm; Mean stacked images at 1,600X, bar = 5 μm

Plate 3. Typical *Tribrachiatus contortus.* (1-3) Sample 550-30-3 87-88 cm; (4-6) Sample 550-30-3 116-117 cm; (7-9) Sample 550-30-3 147-148 cm; (10-12) Sample 550-30-4 06-07 cm; (13-15) Sample 550-30-4 26-27 cm; Mean stacked images at 1,600X, bar = 5 μm

Figure 1.

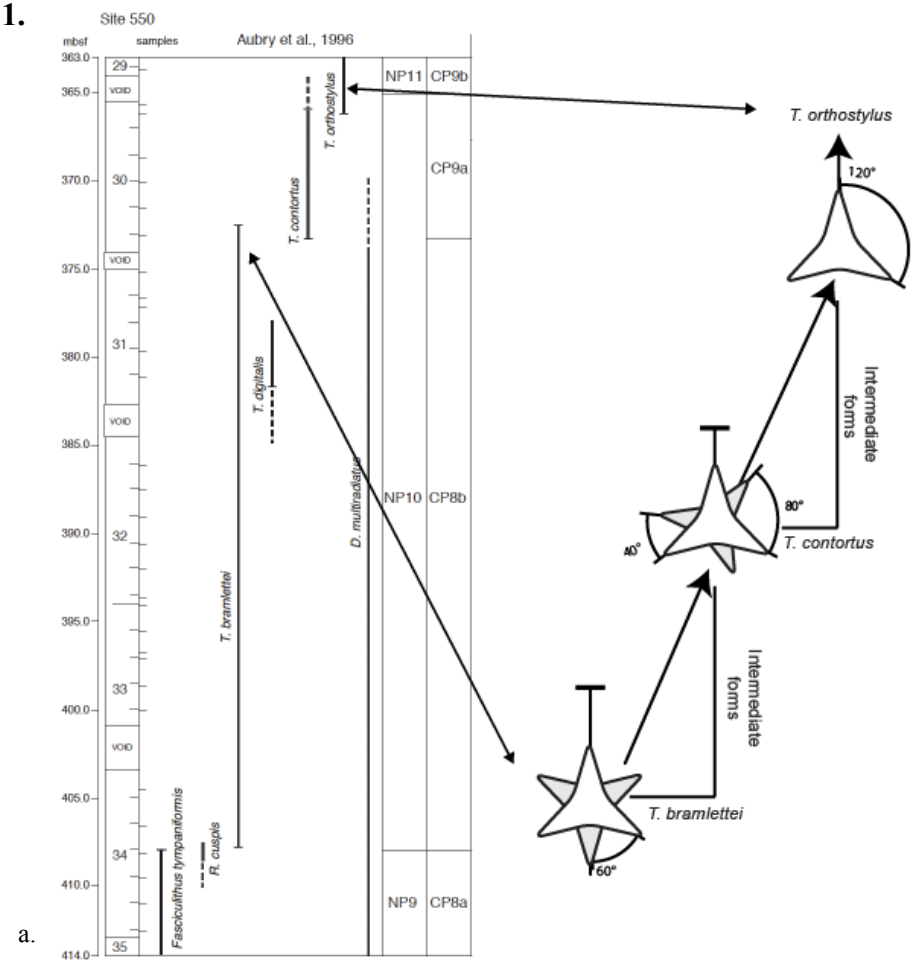
Site 550
mbsf
samples
Aubry et al., 1996
NP11
CP9b
CP9a
NP10
CP8b
NP9
CP8a
T. orthostylus
T. contortus
T. digitalis
T. bramlettei
D. multiradiatus
Fasciculithus tympaniformis
R. cuspis
VOID
T. orthostylus
120°
Intermediate forms
80°
40°
T. contortus
Intermediate forms
T. bramlettei
60°

a.

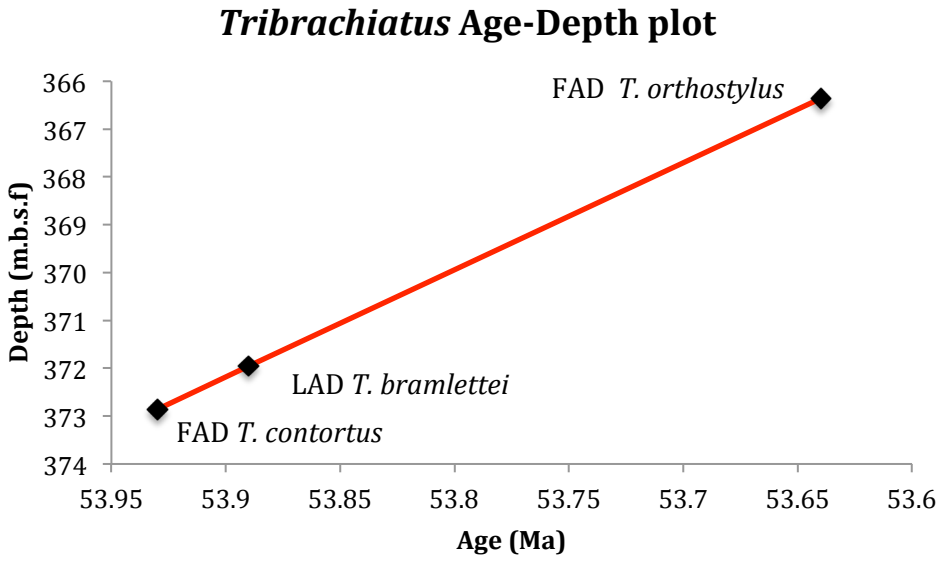
Tribrachiatus Age-Depth plot
Depth (m.b.s.f)
366
367
368
369
370
371
372
373
374
FAD *T. orthostylus*
LAD *T. bramlettei*
FAD *T. contortus*
53.95
53.9
53.85
53.8
53.75
53.7
53.65
53.6
Age (Ma)

b.

Figure 2.

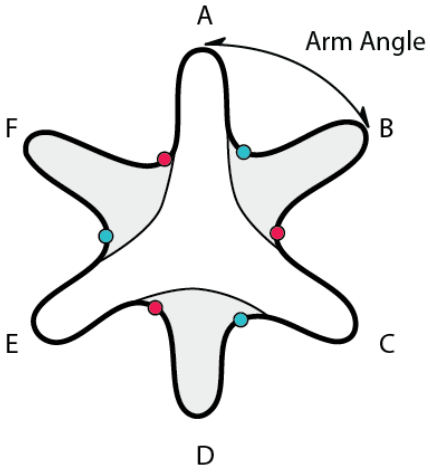

T. bramlettei

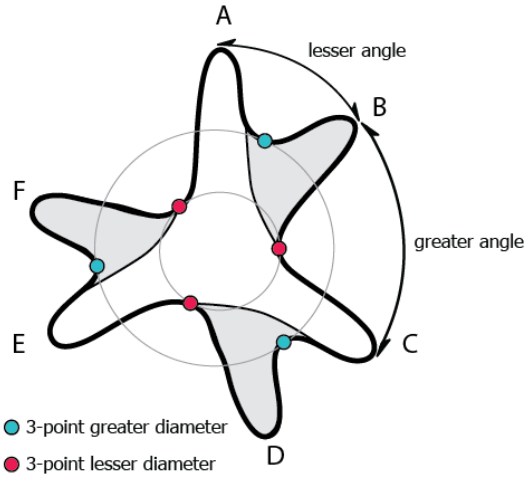

T. contortus

Figure 3.

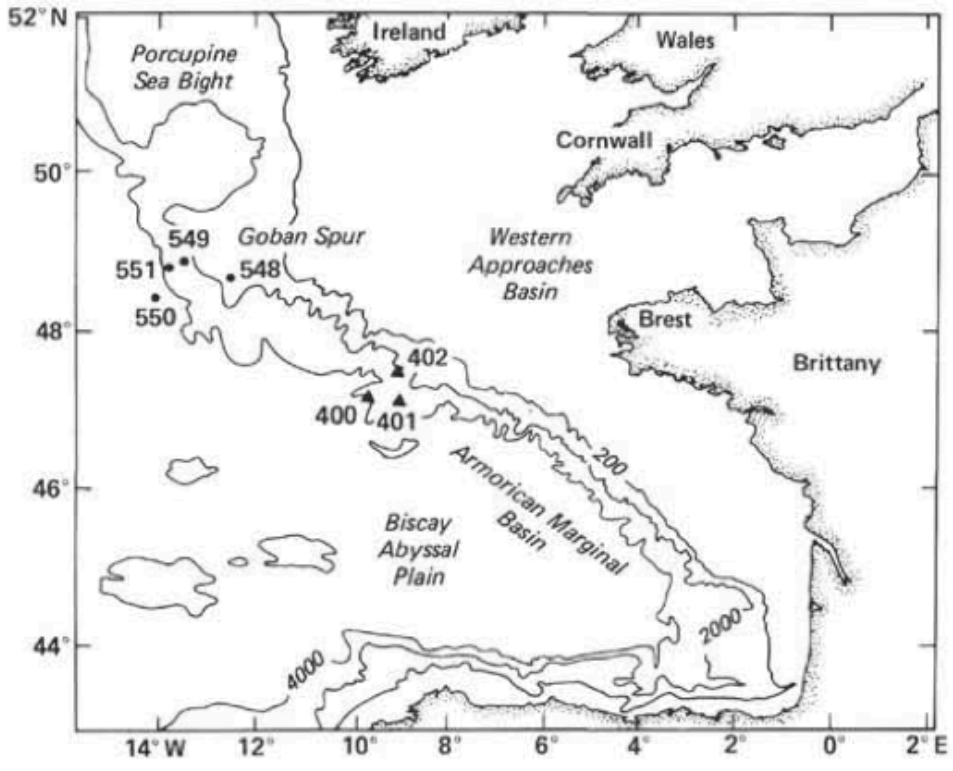
52° N
50°
48°
46°
44°
14° W
12°
10°
8°
6°
4°
2°
0°
2° E
Ireland
Wales
Cornwall
Porcupine
Sea Bight
Goban Spur
549
548
551
550
Western
Approaches
Basin
Brest
Brittany
402
400
401
200
Armorican Marginal
Basin
Biscay
Abyssal
Plain
2000
4000

Figure 4.

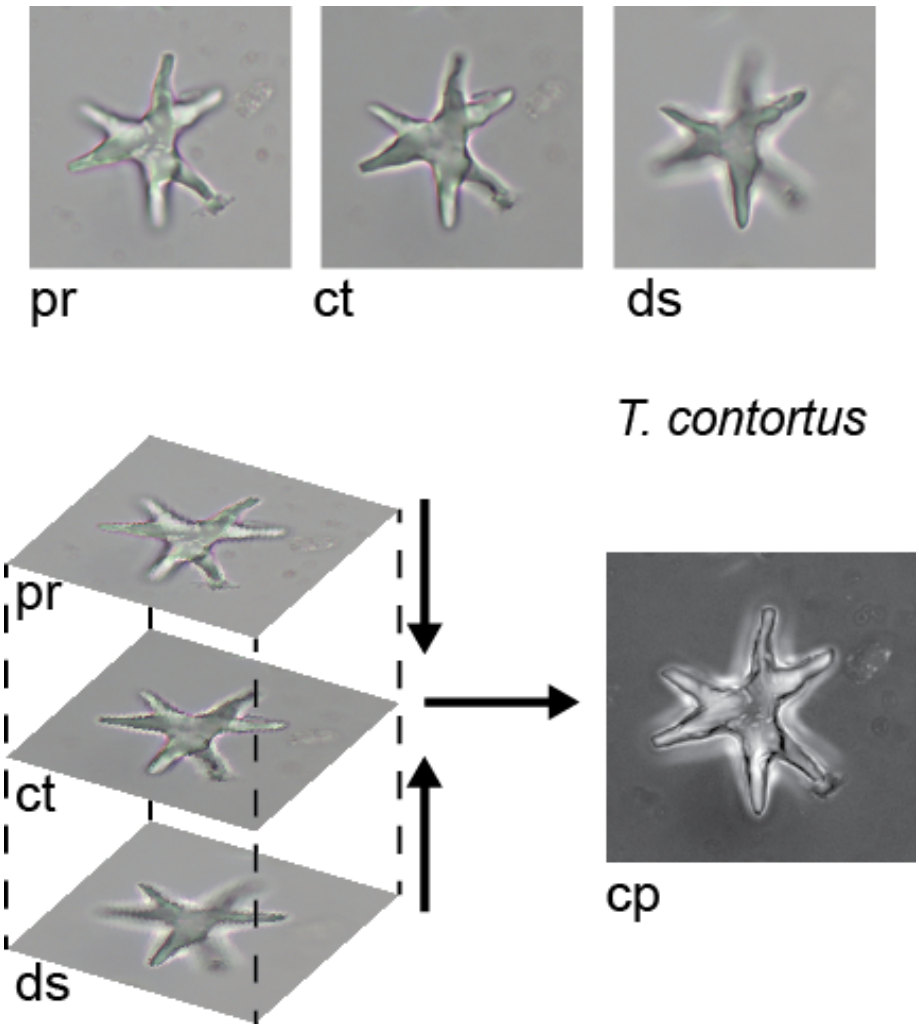

Figure 5.

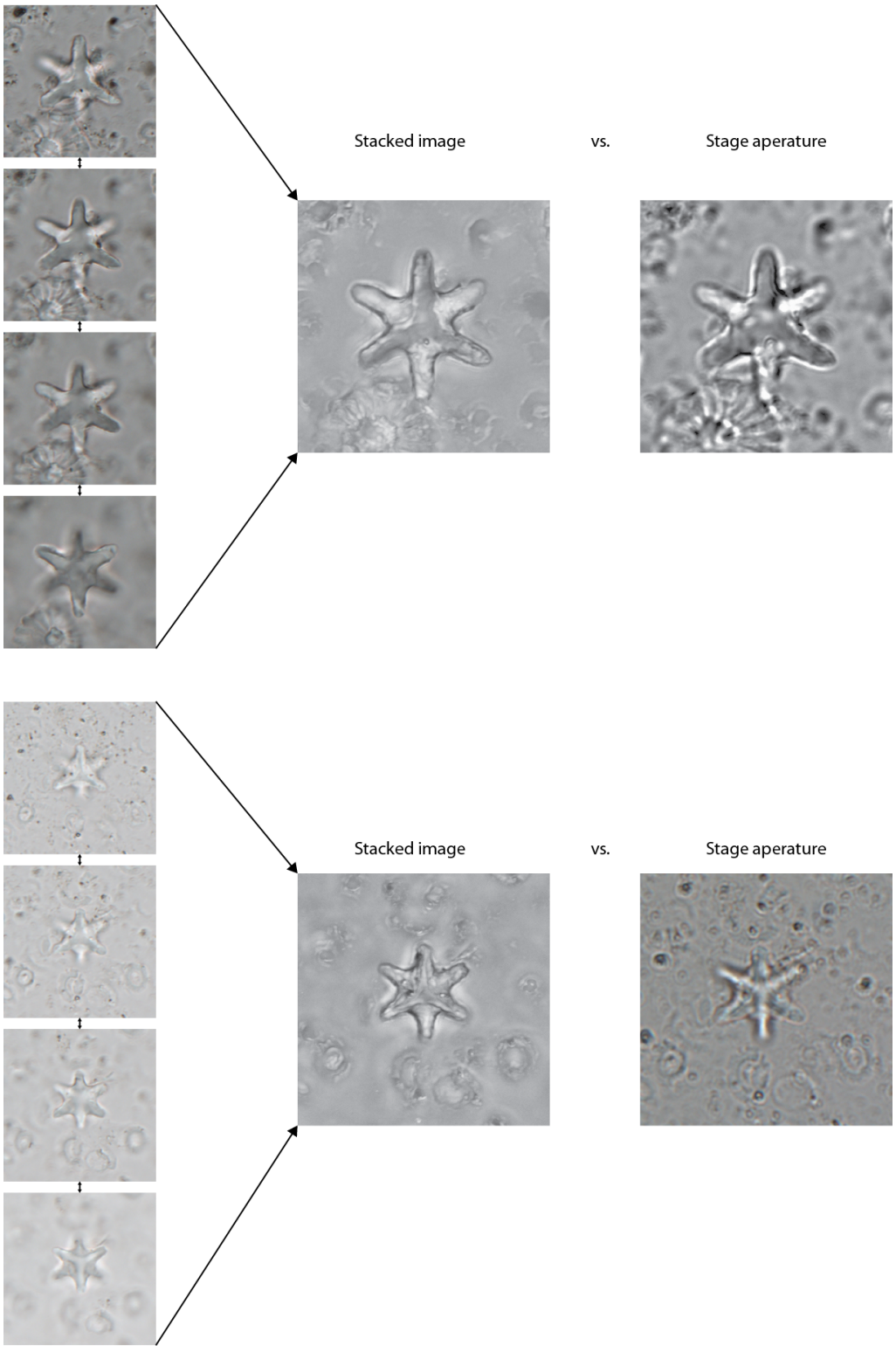
Stacked image
vs.
Stage aperature
Stacked image
vs.
Stage aperature

Figure 6.

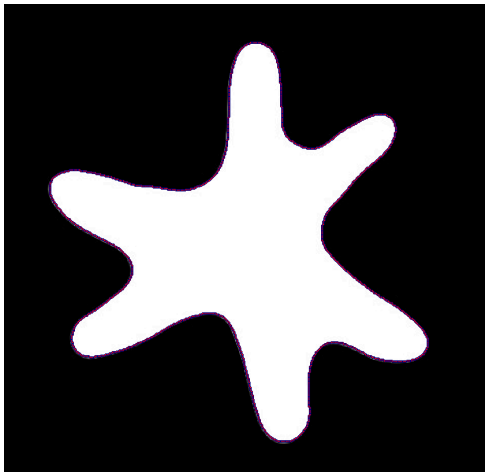

a.

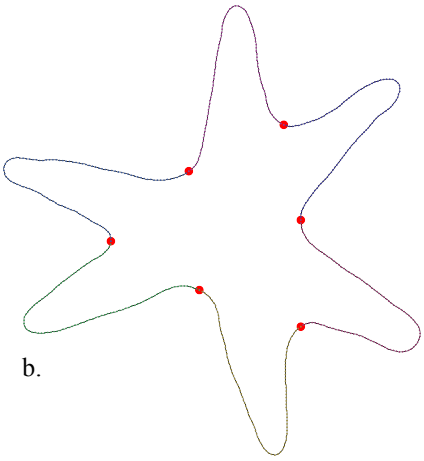

b.

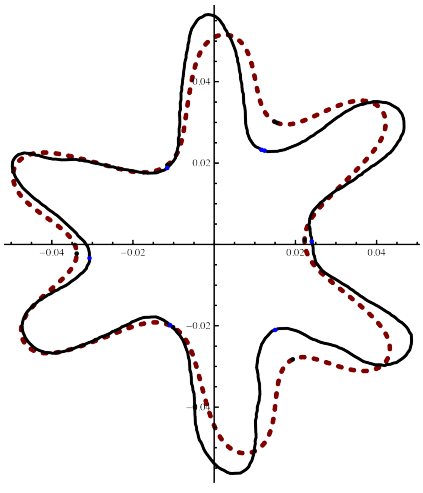

c.

Figure 7.

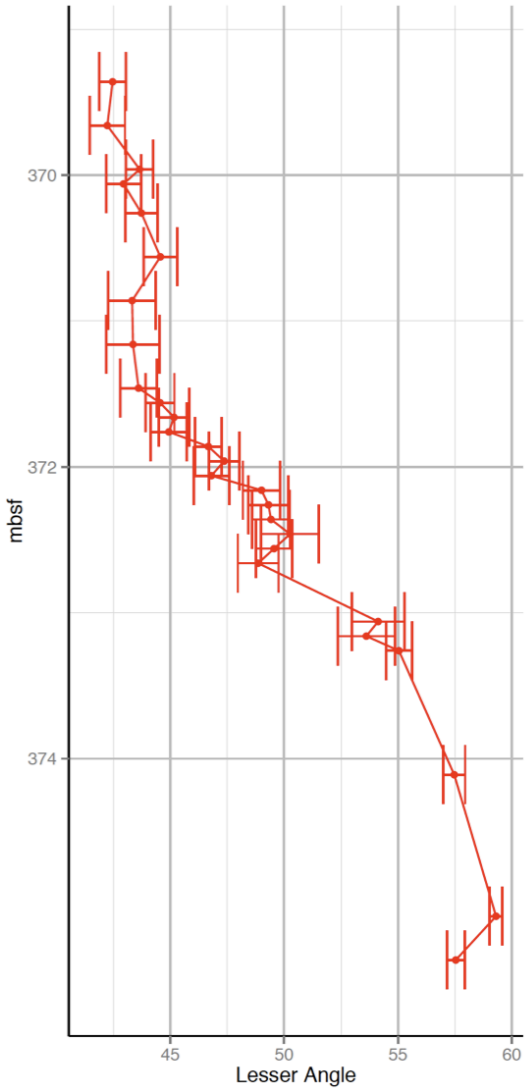
370
372
374
mbsf
45
50
55
60
Lesser Angle

a.

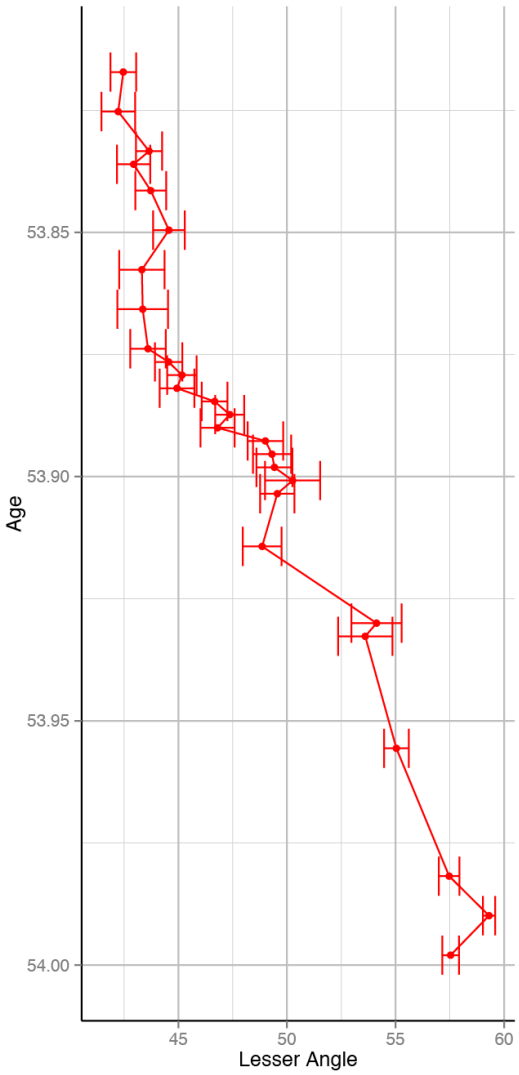
53.85
53.90
53.95
54.00
Age
45
50
55
60
Lesser Angle

b.

Figure 8.

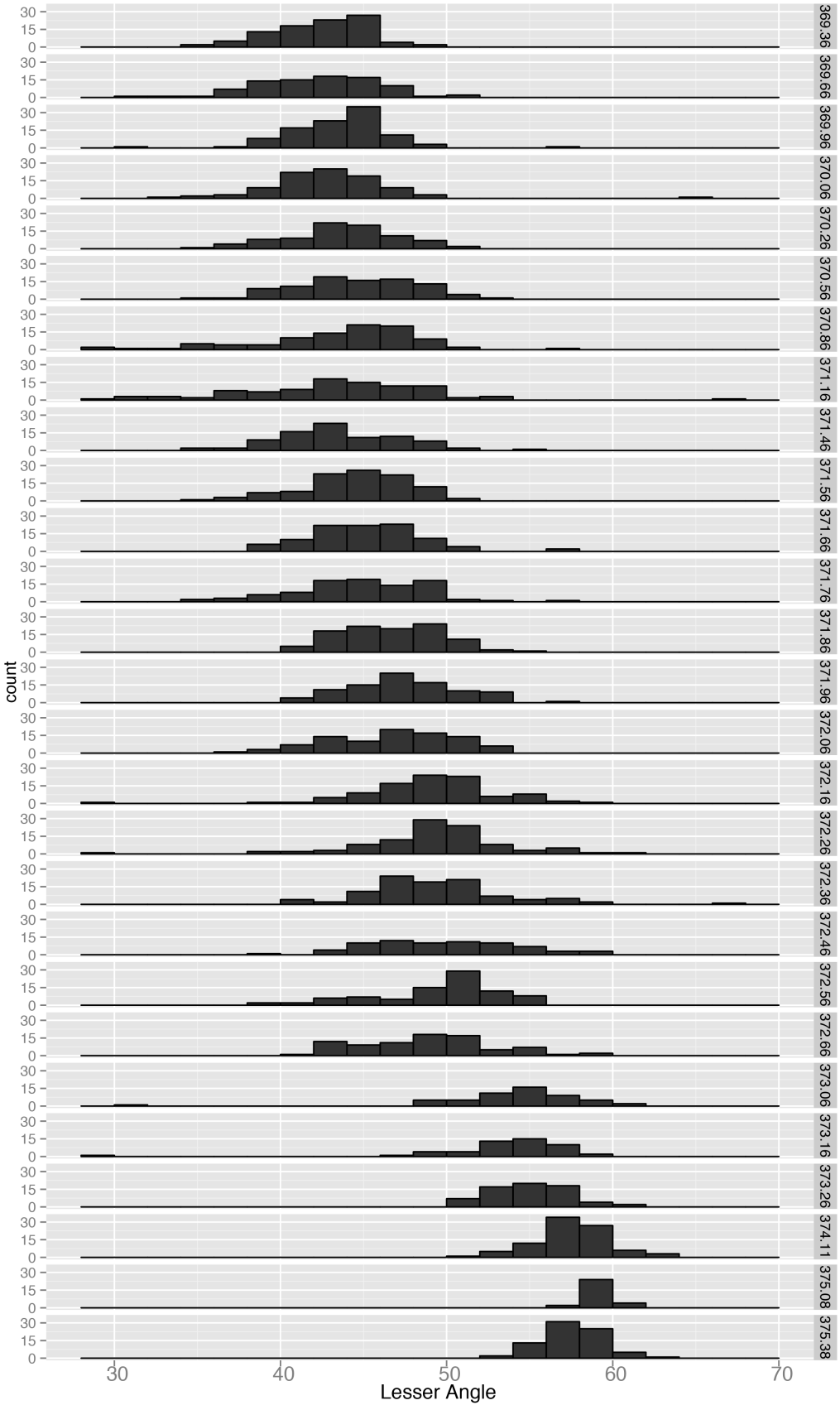
count
Lesser Angle
30
40
50
60
70
0
15
30
369.36
369.66
369.96
370.06
370.26
370.56
370.86
371.16
371.46
371.56
371.66
371.76
371.86
371.96
372.06
372.16
372.26
372.36
372.46
372.56
372.66
373.06
373.16
373.26
374.11
375.08
375.38

Figure 9.

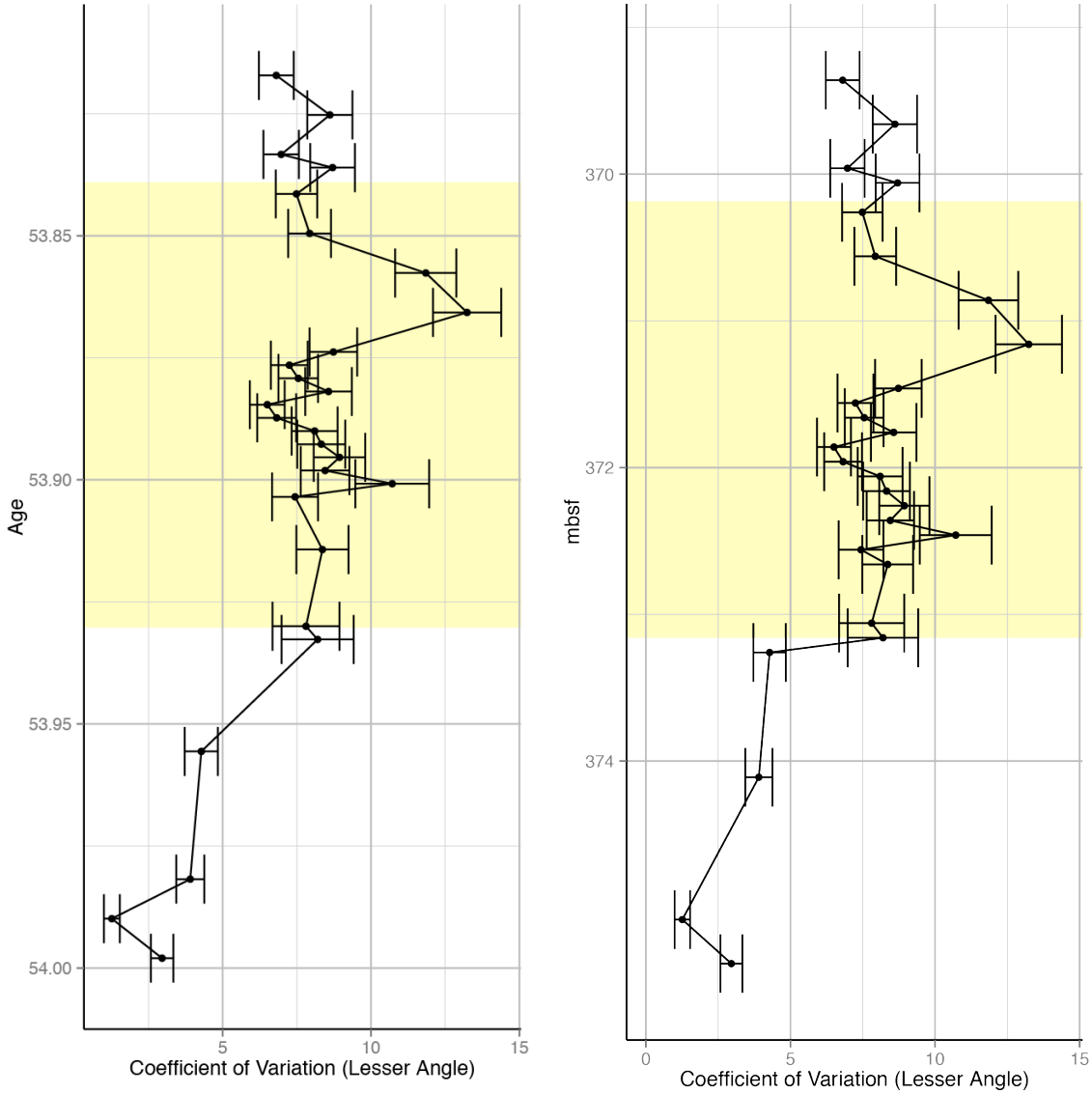
Age
53.85
53.90
53.95
54.00
5
10
15
Coefficient of Variation (Lesser Angle)
mbsf
370
372
374
0
5
10
15
Coefficient of Variation (Lesser Angle)

a. b.

Figure 10.

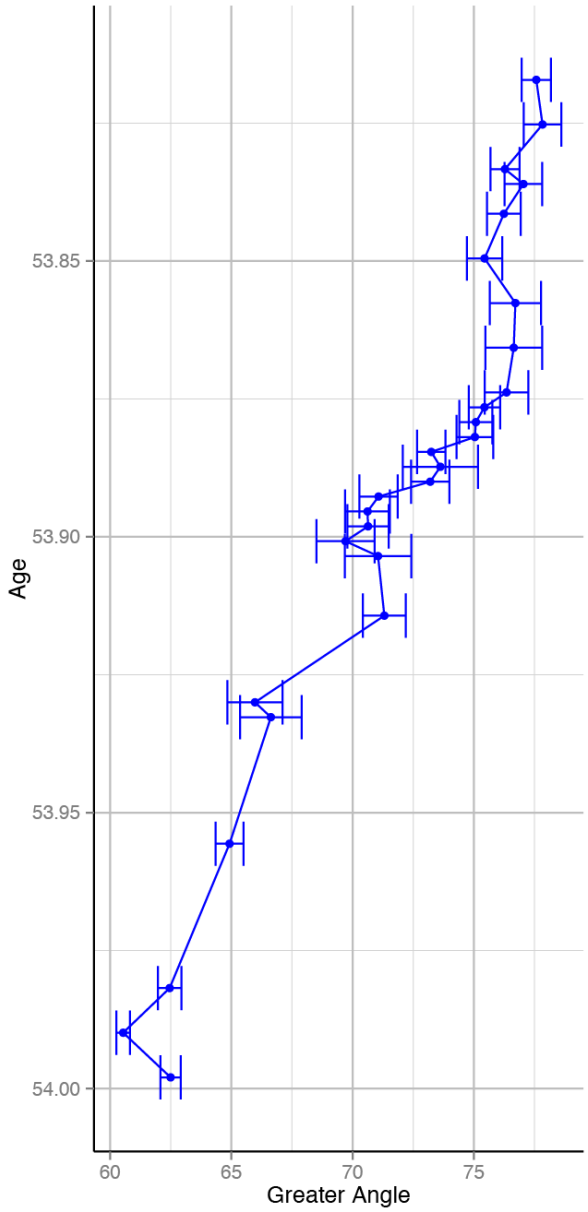

Figure 11.

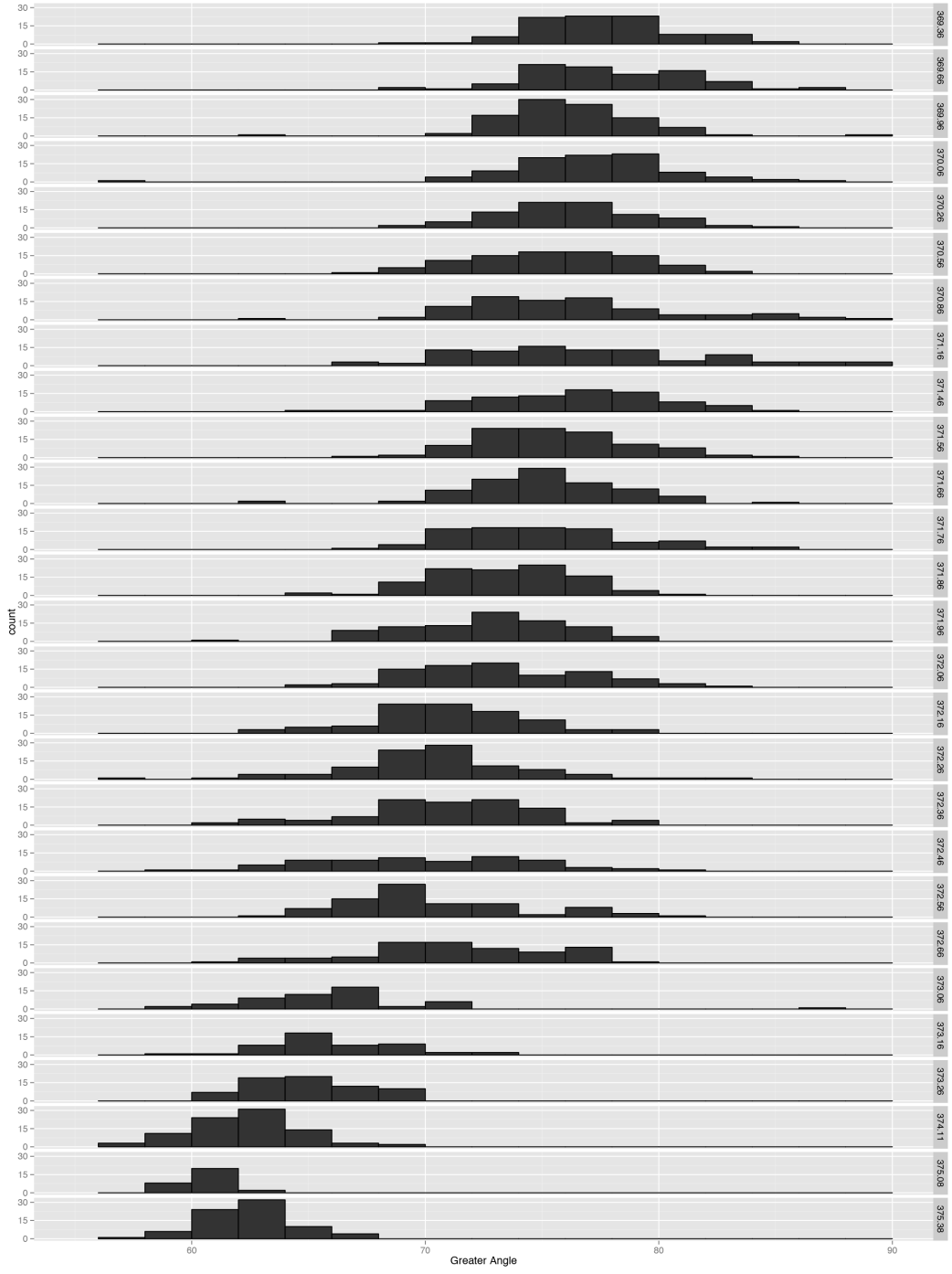
count
Greater Angle
60
70
80
90
0
15
30
369.36
369.66
369.96
370.06
370.26
370.56
370.86
371.16
371.46
371.56
371.66
371.76
371.86
371.96
372.06
372.16
372.26
372.36
372.46
372.56
372.66
373.06
373.16
373.26
374.11
375.08
375.38

Figure 12.

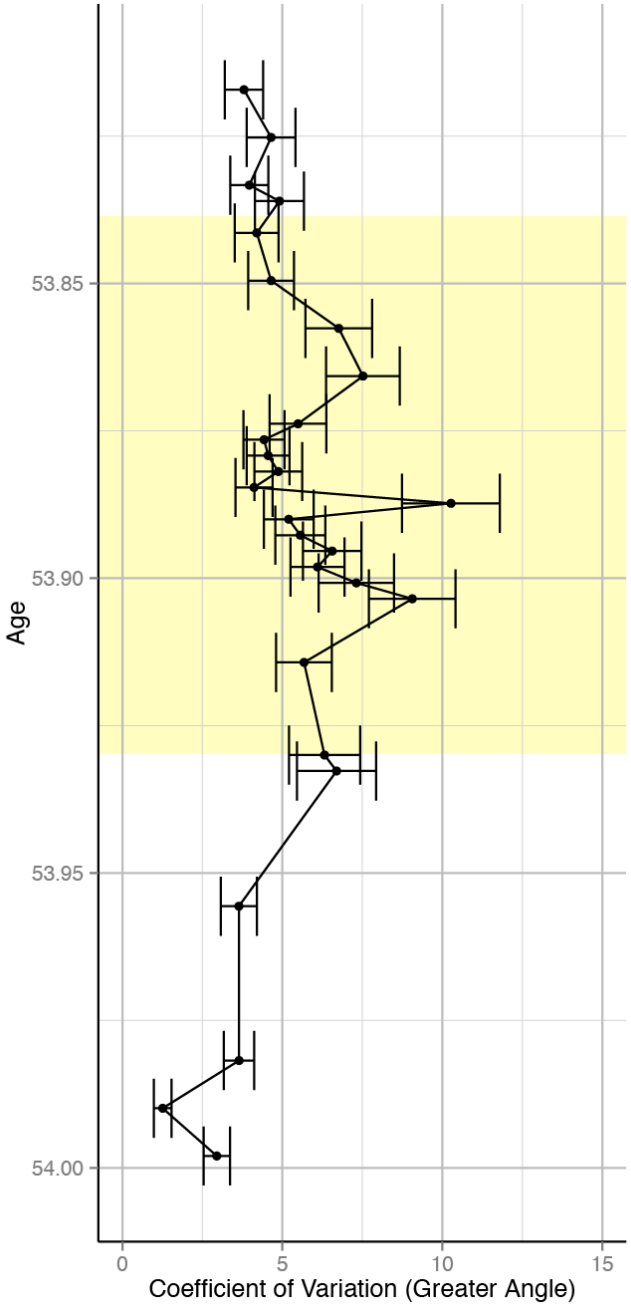
53.85
53.90
53.95
54.00
Age
0
5
10
15
Coefficient of Variation (Greater Angle)

Figure 13.

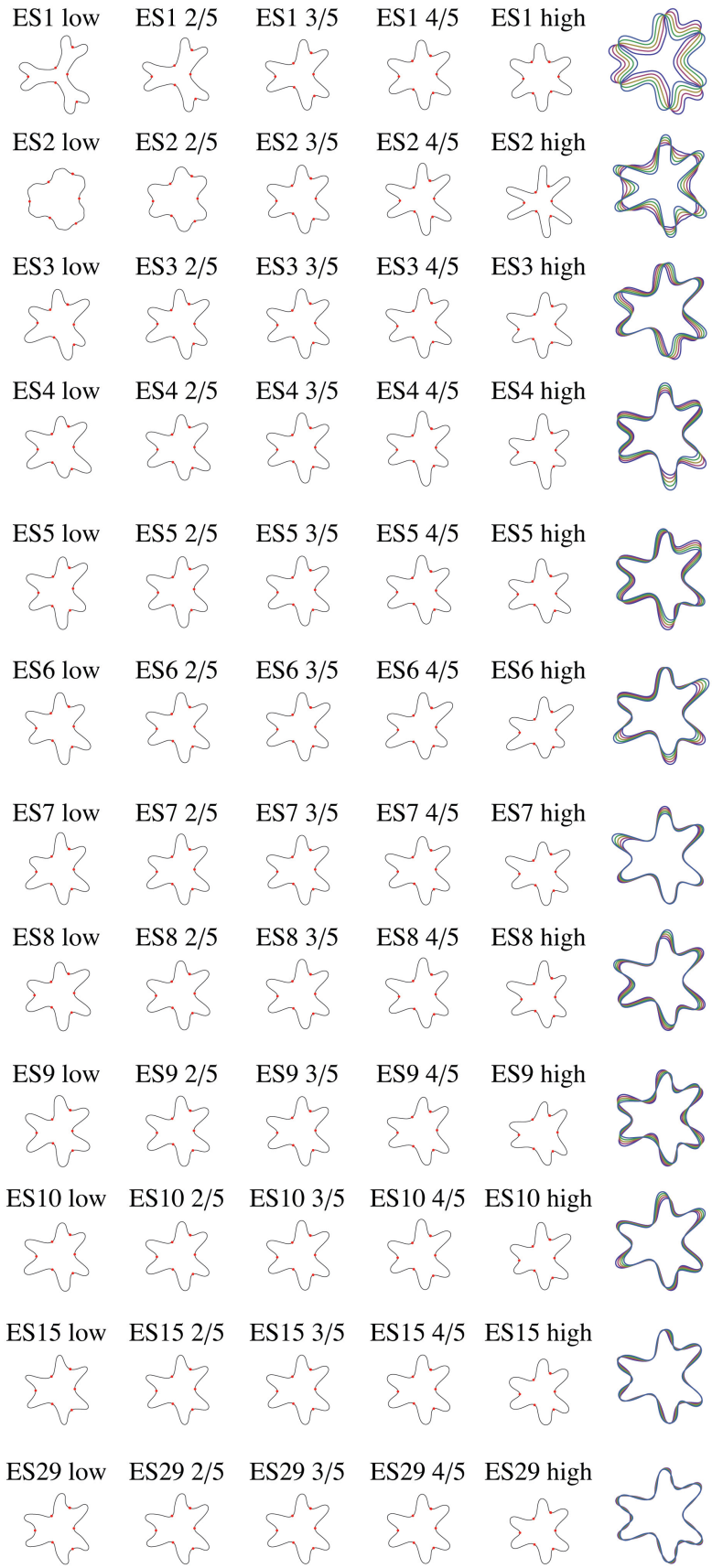
ES1 low
ES1 2/5
ES1 3/5
ES1 4/5
ES1 high
ES2 low
ES2 2/5
ES2 3/5
ES2 4/5
ES2 high
ES3 low
ES3 2/5
ES3 3/5
ES3 4/5
ES3 high
ES4 low
ES4 2/5
ES4 3/5
ES4 4/5
ES4 high
ES5 low
ES5 2/5
ES5 3/5
ES5 4/5
ES5 high
ES6 low
ES6 2/5
ES6 3/5
ES6 4/5
ES6 high
ES7 low
ES7 2/5
ES7 3/5
ES7 4/5
ES7 high
ES8 low
ES8 2/5
ES8 3/5
ES8 4/5
ES8 high
ES9 low
ES9 2/5
ES9 3/5
ES9 4/5
ES9 high
ES10 low
ES10 2/5
ES10 3/5
ES10 4/5
ES10 high
ES15 low
ES15 2/5
ES15 3/5
ES15 4/5
ES15 high
ES29 low
ES29 2/5
ES29 3/5
ES29 4/5
ES29 high

Figure 14.

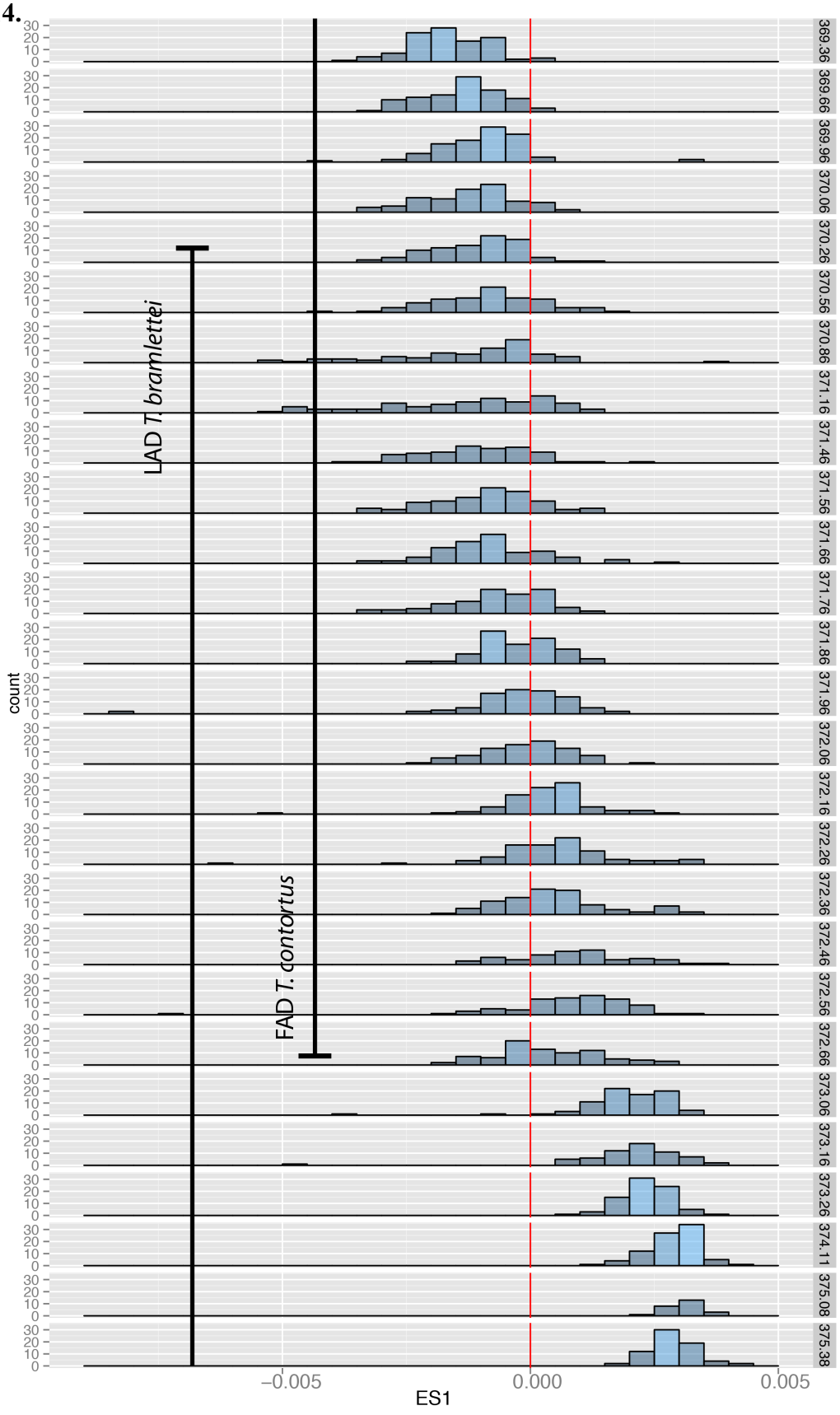
LAD T. bramlettei
FAD T. contortus
count
ES1
−0.005
0.000
0.005
369.36
369.66
369.96
370.06
370.26
370.56
370.86
371.16
371.46
371.56
371.66
371.76
371.86
371.96
372.06
372.16
372.26
372.36
372.46
372.56
372.66
373.06
373.16
373.26
374.11
375.08
375.38

Figure 15.

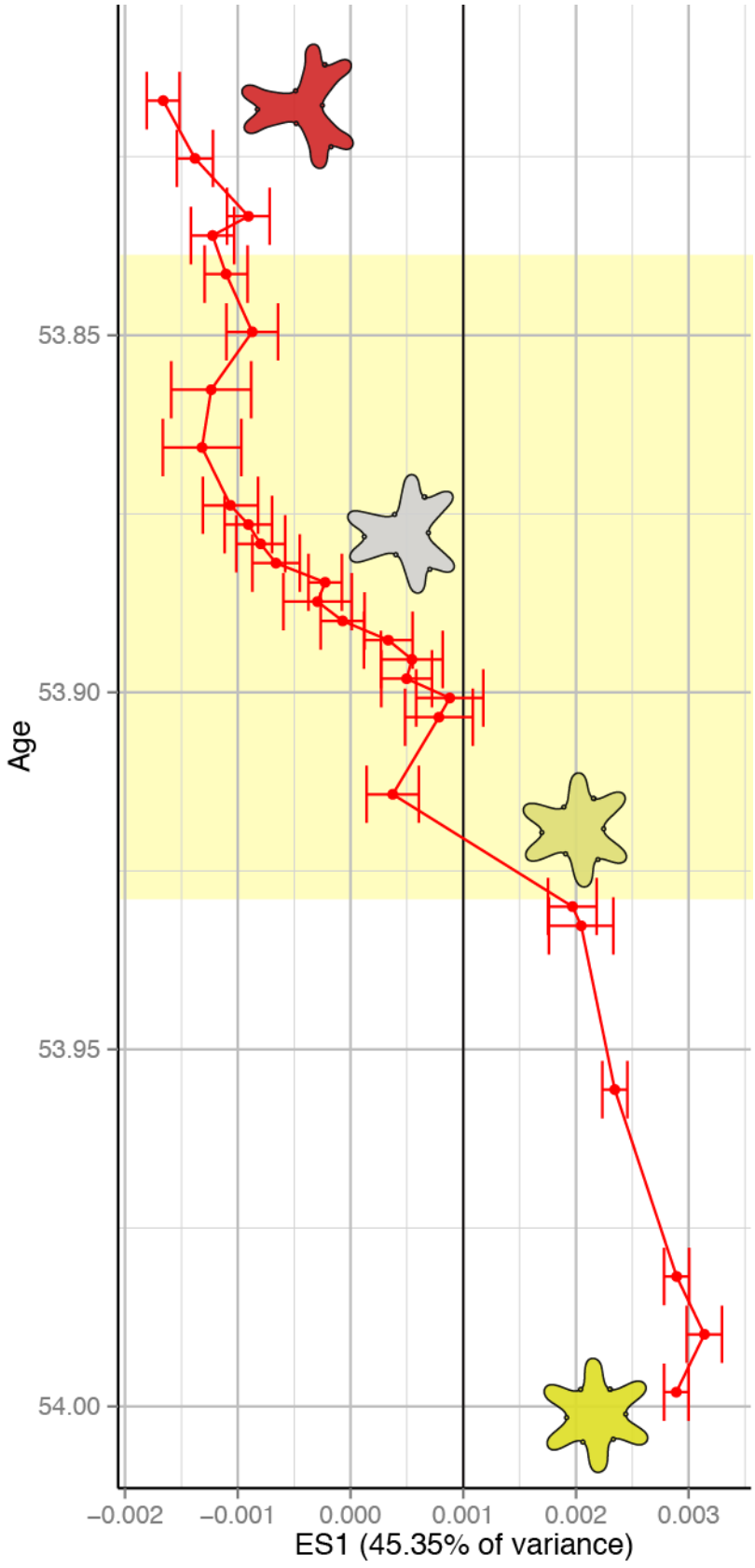
53.85
53.90
53.95
54.00
Age
−0.002
−0.001
0.000
0.001
0.002
0.003
ES1 (45.35% of variance)

Figure 16.

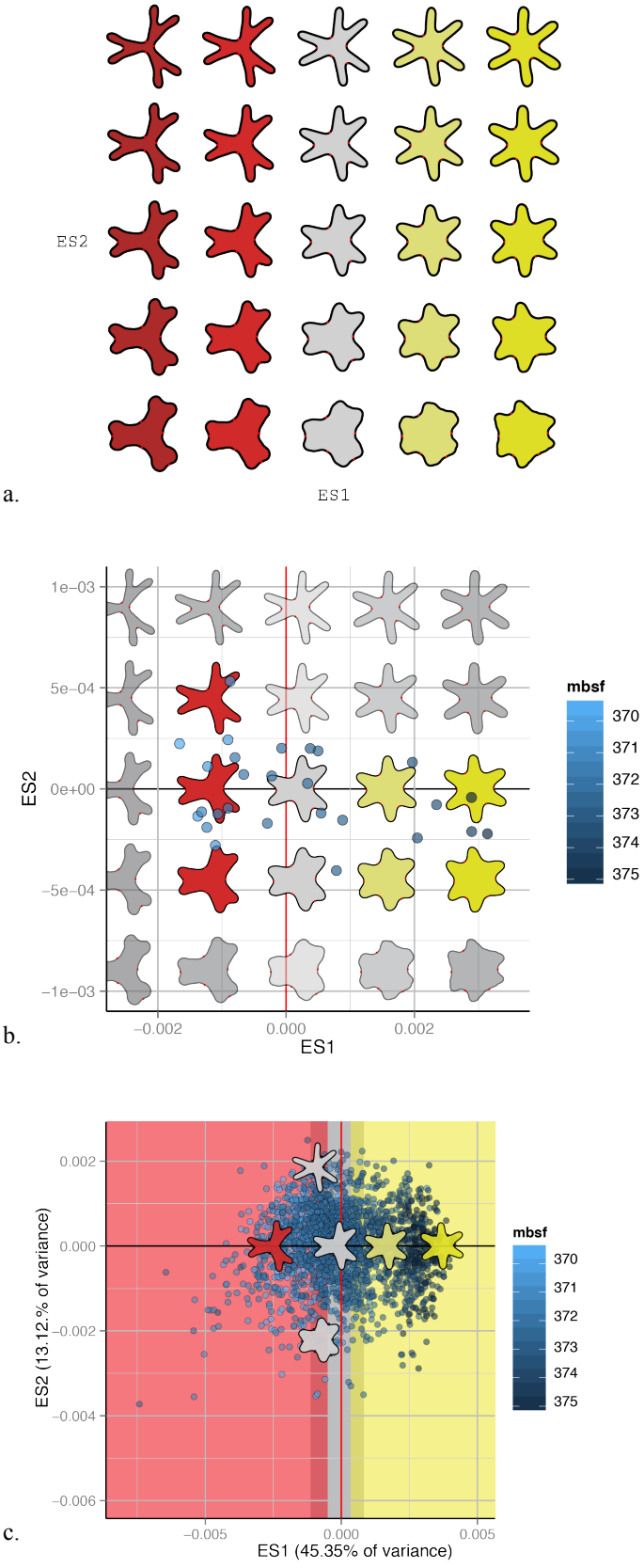
ES2
ES1
a.
1e−03
5e−04
0e+00
−5e−04
−1e−03
−0.002
0.000
0.002
ES2
ES1
b.
mbsf
370
371
372
373
374
375
0.002
0.000
−0.002
−0.004
−0.006
ES2 (13.12.% of variance)
−0.005
0.000
0.005
ES1 (45.35% of variance)
c.
mbsf
370
371
372
373
374
375

Figure 17.

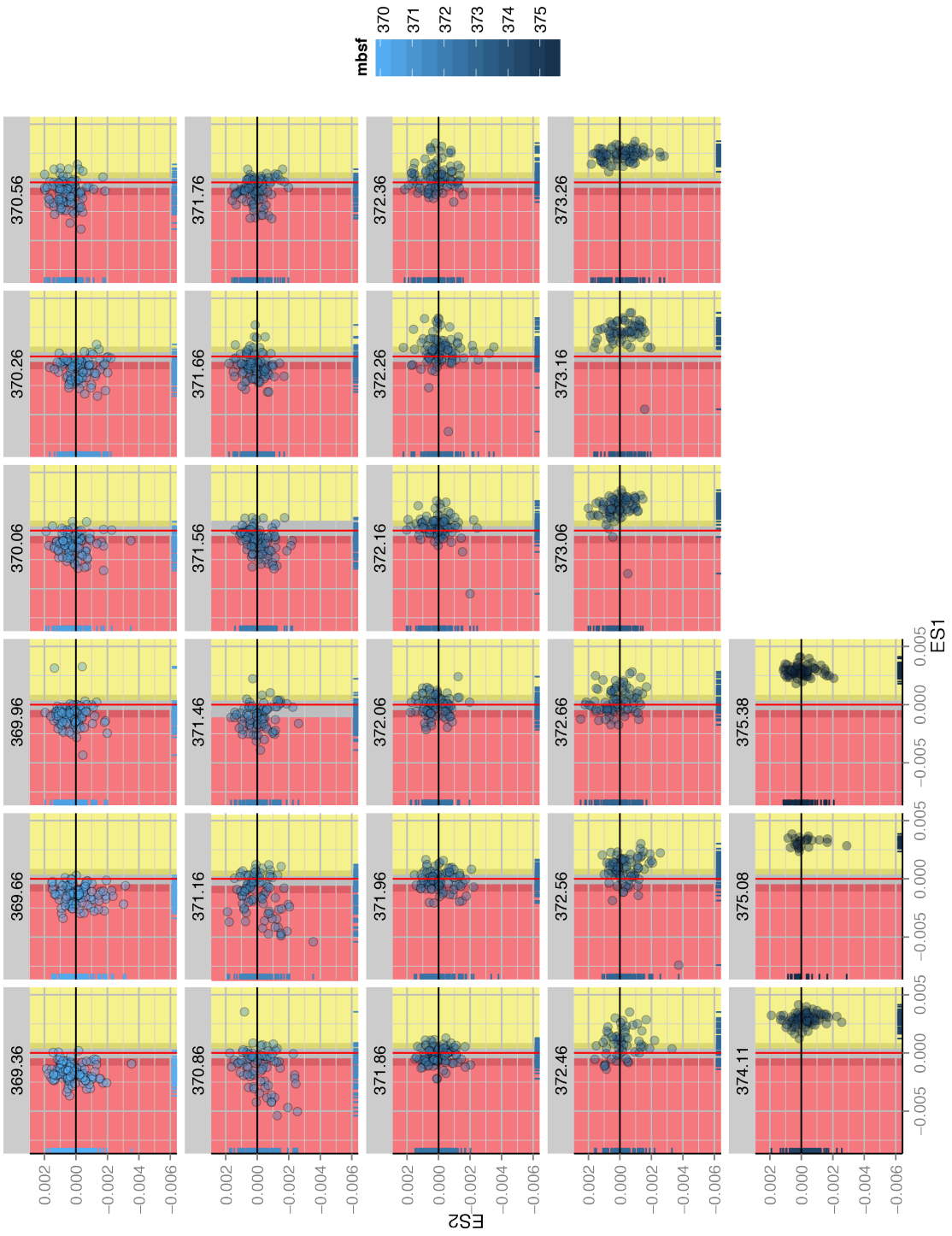
mbsf
370
371
372
373
374
375
370.56
371.76
372.36
373.26
370.26
371.66
372.26
373.16
370.06
371.56
372.16
373.06
369.96
371.46
372.06
372.66
375.38
369.66
371.16
371.96
372.56
375.08
369.36
370.86
371.86
372.46
374.11
0.002
0.000
−0.002
−0.004
−0.006
ES2
ES1
0.005
0.000
−0.005

Figure 18.

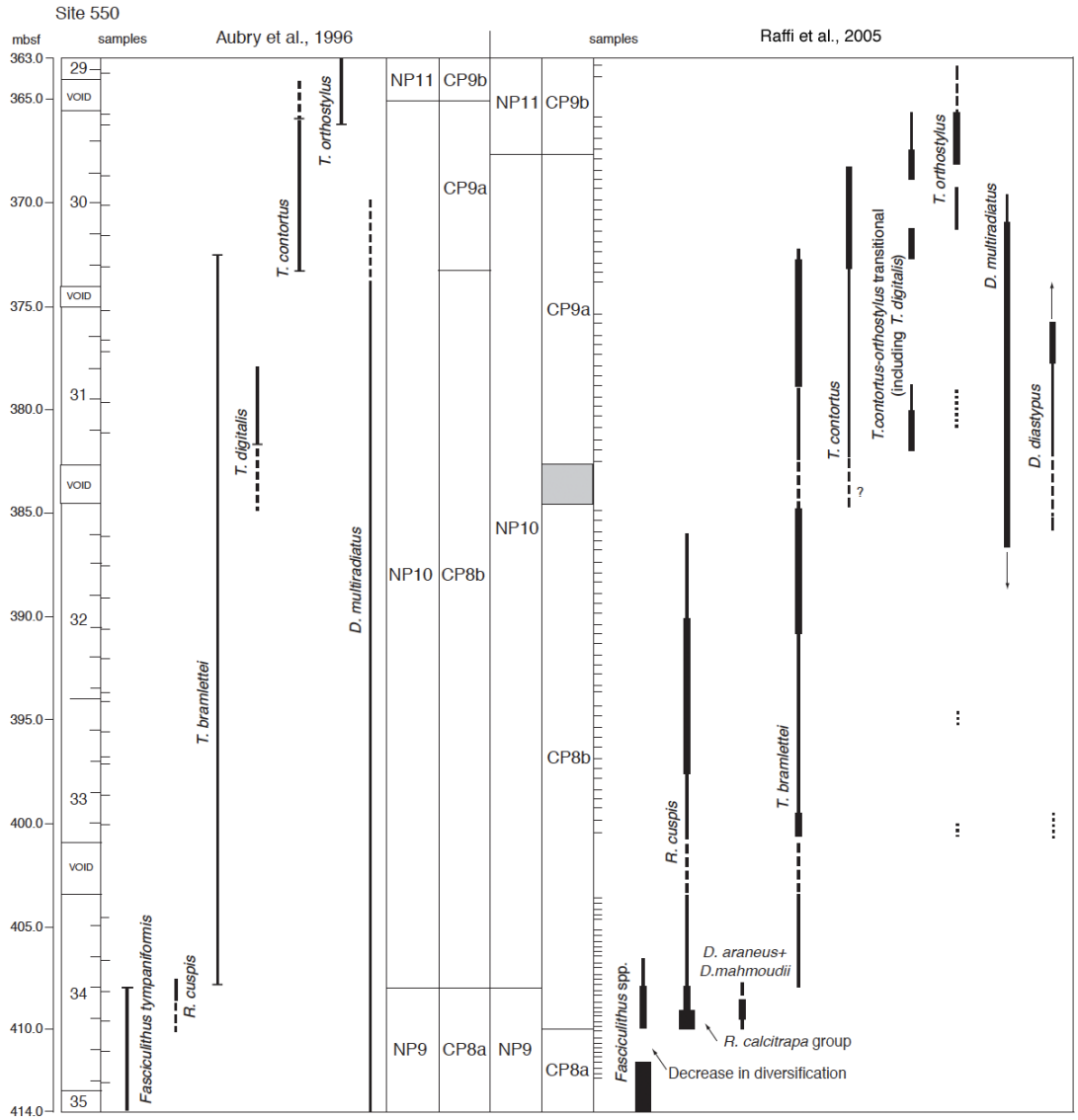
Site 550
mbsf
samples
Aubry et al., 1996
samples
Raffi et al., 2005
363.0
365.0
370.0
375.0
380.0
385.0
390.0
395.0
400.0
405.0
410.0
414.0
29
VOID
30
VOID
31
VOID
32
33
VOID
34
35
Fasciculithus tympaniformis
R. cuspis
T. bramlettei
T. digitalis
T. contortus
T. orthostylus
D. multiradiatus
NP11
NP10
NP9
CP9b
CP9a
CP8b
CP8a
Fasciculithus spp.
R. cuspis
T. bramlettei
T. contortus
?
T.contortus-orthostylus transitional
(including T. digitalis)
T. orthostylus
D. multiradiatus
D. diastypus
D. araneus+
D.mahmoudii
R. calcitrapa group
Decrease in diversification

Table1

mbsf	Age	Mean LA	STDev LA	Mean GA	STDev GA	CV LA	CV GA
369.36	53.82	42.46	2.89	77.57	2.95	6.81	3.80
369.66	53.83	42.23	3.64	77.83	3.62	8.61	4.65
369.96	53.83	43.65	3.04	76.28	3.03	6.97	3.97
370.06	53.84	42.94	3.74	77.04	3.78	8.71	4.91
370.26	53.84	43.73	3.27	76.24	3.20	7.49	4.20
370.56	53.85	44.57	3.54	75.44	3.51	7.93	4.65
370.86	53.86	43.32	5.13	76.71	5.19	11.85	6.76
371.16	53.87	43.36	5.74	76.64	5.76	13.24	7.52
371.46	53.87	43.60	3.81	76.35	4.19	8.73	5.49
371.56	53.88	44.55	3.23	75.44	3.34	7.25	4.43
371.66	53.88	45.16	3.41	75.08	3.42	7.55	4.56
371.76	53.88	44.94	3.85	75.04	3.66	8.57	4.87
371.86	53.88	46.67	3.04	73.24	3.01	6.51	4.11
371.96	53.89	47.37	3.23	73.62	7.56	6.82	10.27
372.06	53.89	46.81	3.79	73.20	3.81	8.10	5.20
372.16	53.89	49.01	4.08	71.07	3.95	8.32	5.56
372.26	53.90	49.31	4.41	70.62	4.63	8.94	6.56
372.36	53.90	49.42	4.18	70.64	4.31	8.45	6.10
372.46	53.90	50.26	5.39	69.71	5.10	10.72	7.31
372.56	53.90	49.56	3.69	71.05	6.44	7.44	9.06
372.66	53.91	48.86	4.09	71.31	4.05	8.36	5.68
373.06	53.93	54.13	4.23	65.97	4.17	7.81	6.32
373.16	53.93	53.61	4.40	66.63	4.46	8.20	6.69
373.26	53.96	55.04	2.36	64.93	2.36	4.28	3.64
374.11	53.98	57.47	2.25	62.46	2.28	3.91	3.65
375.08	53.99	59.31	0.75	60.54	0.76	1.26	1.26
375.38	54.00	57.54	1.70	62.50	1.84	2.96	2.95

Table 2

	eigenvalues	total variance (percent)	cumulative variance (percent)
ES1	0.00659317	47.34699863	47.34699863
ES2	0.001752709	12.58658998	59.93358861
ES3	0.001010307	7.255232358	67.18882096
ES4	0.000834522	5.992886403	73.18170737
ES5	0.000559765	4.019795408	77.20150277
ES6	0.000472056	3.389938554	80.59144133
ES7	0.000374234	2.687456751	83.27889808
ES8	0.000319457	2.294093644	85.57299172
ES9	0.000283423	2.035320073	87.6083118
ES10	0.000262198	1.88290173	89.49121353
ES11	0.000209243	1.502622004	90.99383553
ES12	0.000174862	1.25572486	92.24956039
ES13	0.000123848	0.889377566	93.13893796
ES14	0.000111955	0.803974521	93.94291248
ES15	9.51494E-05	0.683289	94.62620148
ES16	8.81141E-05	0.63276667	95.25896815
ES17	8.09728E-05	0.581483751	95.8404519
ES18	6.30345E-05	0.452664756	96.29311665
ES19	5.99762E-05	0.430702367	96.72381902
ES20	5.0285E-05	0.361107819	97.08492684
ES21	4.40675E-05	0.31645859	97.40138543
ES22	4.26232E-05	0.306086489	97.70747192
ES23	2.86794E-05	0.205953262	97.91342518
ES24	2.55543E-05	0.183511326	98.09693651
ES25	2.41402E-05	0.173356097	98.2702926
ES26	2.20635E-05	0.158443175	98.42873578
ES27	2.09553E-05	0.150484342	98.57922012
ES28	2.01631E-05	0.144795393	98.72401551
ES29	1.61265E-05	0.115807849	98.83982336
ES30	1.19593E-05	0.085882325	98.92570569

Plate 1

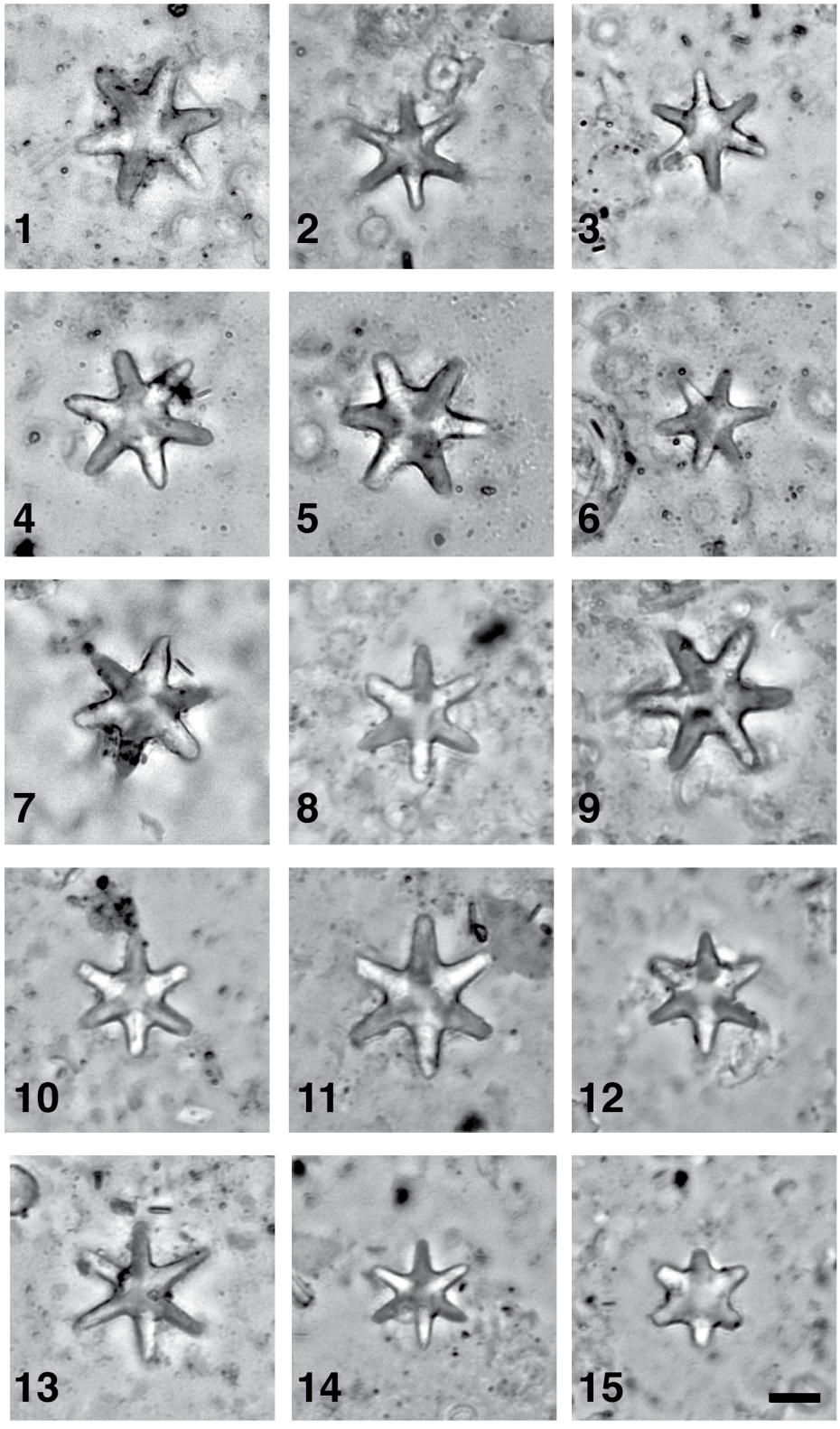

Plate 2

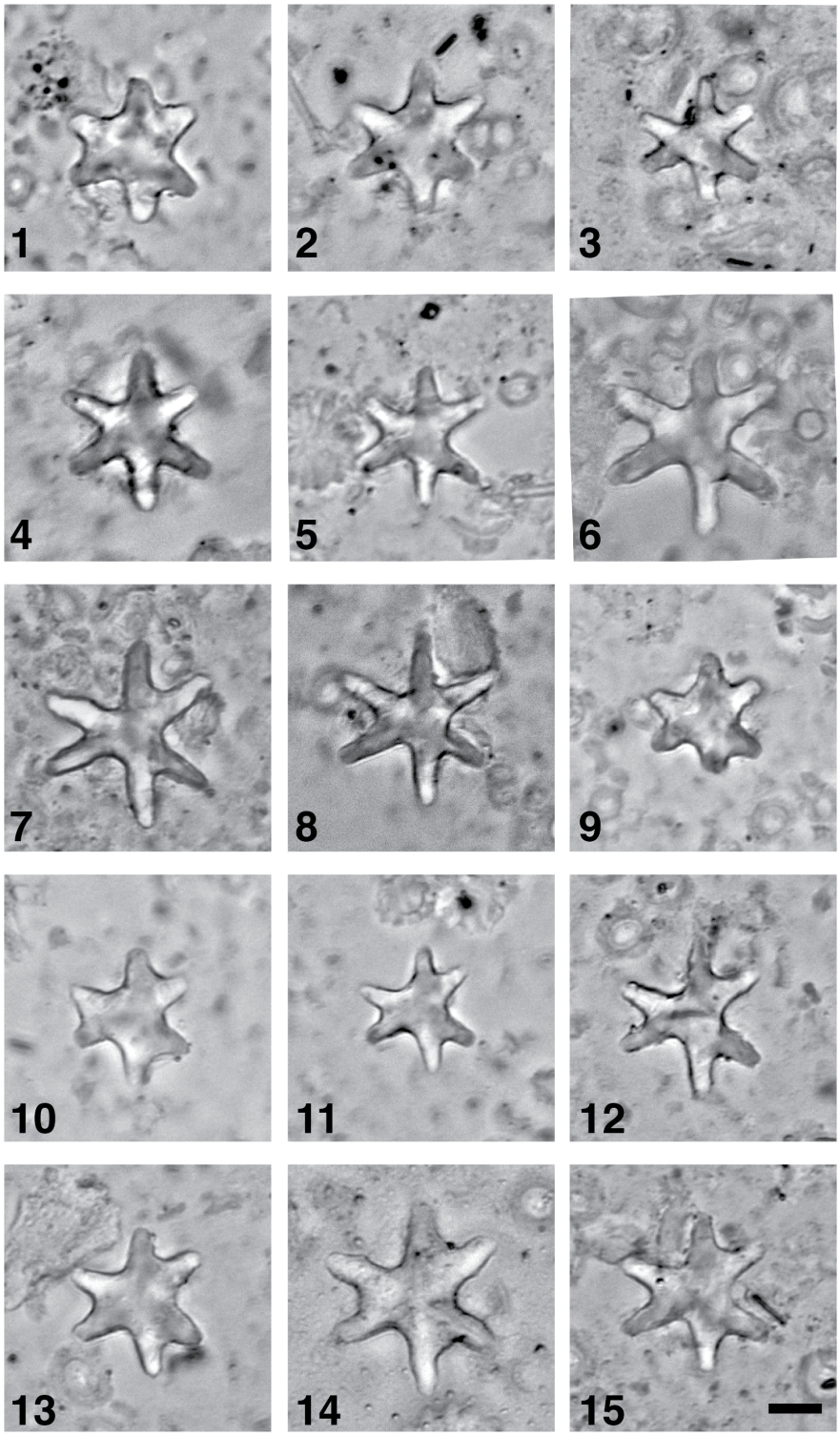

Plate 3